Understanding the role of Rab GTPases in plant immunity

Thesis submitted to the University of East Anglia for the degree of Doctor of Philosophy

Jelle Ludolf Postma

The Sainsbury Laboratory

John Innes Centre

Norwich, UK

July 2018

ABSTRACT

Plants employ cell-surface localized receptor-like kinase (RLK) and receptor-like protein (RLP)-type pattern recognition receptors to monitor their surroundings for the presence of infectious pathogens. RLPs interact with the SUPPRESSOR OF BIR1-1 (SOBIR1) RLK for stability and signaling, but it is unclear how signaling is activated. Here, I reveal that the SERK3 RLK is recruited to the tomato Cf-4 RLP upon activation by the *Cladosporium fulvum* effector Avr4, followed by Cf-4-SOBIR1 co-internalization into late endosomes/multivesicular bodies (LE/MVBs). This extends known RLK-type early activation mechanisms and subcellular localization changes to RLP-SOBIR1-based detection systems, pointing at a widely generalisable mechanism for receptor turnover. Secretory and endocytic membrane trafficking pathways underlie the potentiation and execution of defence. Membrane-associated Rab GTPases are critical regulators of specific pathways, and accumulate at pathogen infection sites, yet their roles in immunity are poorly understood. Here, proteomic analysis of the secretory ARA5/RABD2a complex upon elicitation with bacterial flagellin revealed increased secretion of several uncharacterized RLKs and modules of cell-surface based chemical defences. Comparison between proteomic changes on ARA5/RABD2a and the endocytic ARA7/RABF2b points at flagellin-induced turnover of cell-surface proteins that monitor cell wall integrity and function in processes involving reactive oxygen species. ARA7/RABF2b concentrated under bacterial infection sites, and upon flagellin elicitation recruited the atypical resistance proteins TIR-NBS3 (TN3) and HOMOLOG OF RPW8 4 (HR4). TN3 and HR4 were required for immunity against non-adapted powdery mildew and could be monitoring Rab GTPase-mediated endosomal activity in plant defence.

ACKNOWLEDGEMENTS

Firstly, Silke, I owe you an enormous thank you.

You offered me the choice of joining your lab, to continue and deliver on a promising lead, and to explore new, Humboldt-style projects that turned out to be hugely interesting too. I am struck by the many opportunities you gave me, which allowed me to develop myself as a scientist in the best possible manner, and you were there when times were tough. Thanks!

I would like to sincerely thank my supervisory committee members for helping me navigate the scary but thrilling world of science, by being involved and available when it mattered. Jonathan, Christine, Jan, Hannah. This mind is eternally indebted to you.

Thank you Matthieu for your continued guidance at critical points during the project, I felt you connected me to home.

I extend my thanks to the examiners, who spend valuable time on critically evaluating the academic end product of the project. Thank you, profs. Birch, Downie.

Finally, I would like to acknowledge all former lab colleagues and office mates, and shoutout to my SR-lab PhD buddies - the other two Js - Jenna and Janina. Cheers also to Sara, Will and Jess who overlapped with me.

CONTENTS

GLOSSARY

ARA7	Arabidopsis Rab GTPase 7
BAK1	BRI1-ASSOCIATED KINASE 1
BIFC	Bimolecular fluorescence complementation
BIR1	BAK1-INTERACTING RECEPTOR-LIKE KINASE 1
Cf-4	*Cladosporium fulvum* resistance-4
CNL	Coiled-coil NLR
DAMP	Damage-associated molecular pattern
ER	Endoplasmic reticulum
EV	Extracellular vesicle
FLS2	FLAGELLIN-SENSITIVE 2
GO	Gene ontology
GTP	Guanosine tri-phosphate
HR	Hypersensitive response
HR4	HOMOLOG OF RPW8.2 4
ILV	Intraluminal vesicle
IP	Immunoprecipitation
KD	Kinase-dead
LE/MVB	Late endosome/multivesicular body
LRR	Leucine-rich repeat
MAMP	Microbe-associated molecular pattern
MS	Mass-spectrometry
NLR	Nucleotide-binding leucine-rich repeat containing protein
PM	Plasma membrane
PRR	Pattern recognition receptor
RLK	Receptor-like kinase
RLP	Receptor-like protein
RPW8	RESISTANCE TO POWDERY MILDEW 8
SERK	SOMATIC EMBRYOGENESIS RECEPTOR KINASE
SOBIR1	SUPPRESSOR OF BIR1-1
TGN/EE	*trans*-Golgi network/early endosome
TN3	TIR-NBS 3
TNL	Toll/interleukin-1 receptor NLR
TRV	Tobacco rattle virus
YFP	Yellow fluorescent protein

CHAPTER 1

GENERAL INTRODUCTION

This chapter contains edited portions from the following published works to which I contributed:

(1) "Avr4 promotes Cf-4 receptor-like protein association with the BAK1/SERK3 receptor-like kinase to initiate receptor endocytosis and plant immunity"

Jelle Postma, Thomas W. H. Liebrand, Guozhi Bi, Alexandre Evrard, Ruby R. Bye, Malick Mbengue, Hannah Kuhn, Matthieu H. A. J. Joosten, Silke Robatzek

New Phytologist (2016) doi: 10.1111/nph.13802

(2) "A Moving View: Subcellular Trafficking Processes in Pattern Recognition Receptor-Triggered Plant Immunity"

Sara Ben Khaled, Jelle Postma, Silke Robatzek.

Annual Review of Phytopathology (2015) doi: 10.1146/annurev-phyto-080614-120347

1.1 - Plants and microbes

Plants exist in ecosystems shared with a diversity of other organisms, with which they continuously interact (Austin and Ballaré, 2014). Microbes populate the phyllosphere and rhizosphere, and can engage in mutualistic, commensal, or pathogenic interactions with the plant host (Rosado et al., 2018). Most agronomically important microbial plant symbionts are found to be filamentous fungi, oomycetes, or bacteria (Dean et al., 2012; Mansfield et al., 2012; Kamoun et al., 2015). Besides engaging in crucial mutualistic symbioses with arbuscular mycorrhizal fungi or rhizobacteria, plants are under constant threat of microbial pathogens which depend on plants for access to nutrients in order to complete their life cycle, at the expense of plant biological fitness. Plants are resistant to most pathogens, but can be infected by lineages that have adapted to particular hosts through co-evolution, or by pathogens that have developed strategies to circumvent defenses of a broad range of hosts (Garcia-Guzman and Morales, 2007).

Upon coming into physcial contact with the host epidermis, pathogens encounter pre-formed structural defenses, such as the waxy cuticle and the cell wall, which consists of a rigid, highly interlinked polysaccharide matrix (Serrano et al., 2014; Underwood, 2012). Spores of filamentous fungal and oomycete pathogens germinate and produce an initial germ tube which may grow into

an appressorium, or may form hyphae that grow across the surface and invade natural openings such as stomata or wounds. The appressorium is a structurally reinforced hyphal bulb, which builds up to high fluid pressures and projects a penetration peg that breaches the host cell wall, upon which an intimate interaction between fungal invasion structures and the host plasma membrane (PM) is established (Szabo and Bushnell, 2001; Whisson et al., 2016). At this site, an elaborate molecular exchange takes place, where pathogen effectors accumulate in the extracellular space and translocate into the host cell to modify its physiology and suppress defenses.

Foliar bacterial pathogens broadly seek to access the intracellular space of the host apoplast, and can enter through natural openings such as stomata or wounds. Like filamentous pathogens, bacteria concentrate their efforts on specific locations at the host cell surface. Instead of breaching the cell wall and establishing close membrane contact, they extend needle-like modified pili that reach the host cell membrane and pierce it, forming a channel through which effector molecules are inserted into the host cytoplasm, where they modulate host processes in order to facilitate bacterial infection (Melotto and Kunkel, 2013). Recent studies have shown that the bacterial pathogens *Pseudomonas syringae* pv. *tomato* (*Pto*) DC3000 which is the causative agent of bacterial speck disease, as well as *Agrobacterium tumefaciens* which causes crown gall disease, translocate effectors into the host cell in a non-homogenous manner. Using small fluorescent probes that allow tagged effector molecules to pass through secretion systems, effectors were shown to accumulate in the host cytoplasm coinciding with bacterial positions at the cell surface (Li et al., 2014; Li and Pan, 2017; Park et al., 2017).

1.2 - Cell-surface based surveillance by pattern recognition receptors

In addition to pre-formed structural defenses, the plasma membrane of host cells is decorated with pattern recognition receptors (PRRs), that have specific binding affinity to a broad range of extracellular microbe-associated molecular patterns (MAMPs) that signify the presence of “non-self” microbial intruders, or danger-associated molecular patterns (DAMPs) that are “self” or “modified-self” molecules which are formed extracellularly, or are secreted in response to stress (Choi and Klessig, 2016; Monaghan and Zipfel, 2012). Most PRRs consist of transmembrane (TM) proteins that present an extracellular leucine-rich repeat (LRR) containing domain that confers recognition specificity, but can also contain extracellular carbohydrate-binding LysM or lectin domains that mediate pattern detection instead (Boutrot and Zipfel, 2017).

1.3 - Receptor-like kinases in immunity

Broadly, two classes of PRRs are distinguished, based on the presence of an intracellular kinase domain on receptor-like kinases (RLKs), or a short cytosolic non-kinase tail present in receptor-like proteins (RLPs (Wu and Zhou, 2013). Known RLK-type PRRs include CHITIN-ELICITOR RECEPTOR KINASE 1 (CERK1) and LYSM-CONTAINING RECEPTOR-LIKE KINASE 5 (LYK5), which cooperatively bind the fungal MAMP chitin, LIPOOLIGOSACCHARIDE-SPECIFIC REDUCED ELICITATION (LORE) mediating recognition of bacterial lipopolysaccharides, FLAGELLIN-SENSING 2 (FLS2) that binds the bacterial flagellin-derived 22 amino acid epitope flg22, and EF-TU RECEPTOR (EFR) that binds the bacterial Elongation Factor-Tu (EF-Tu)-derived 18 amino acid epitope elf18 (Cao et al., 2014; Ranf et al., 2015; Boller and Felix, 2009). In addition, RLK-type PRRs can function in perceiving DAMPs, such as the PEP1 RECEPTOR 1 and 2 (PEPR1, PEPR2) which bind the secreted peptide pep1, and WALL-ASSOCIATED KINASE 1 (WAK1) which detects cell-wall derived oligogalacturonide DAMPs (Kohorn and Kohorn, 2012; Tang and Zhou, 2016).

FLS2 serves as a model PRR, of which the events following flg22 perception and receptor activation are well characterized. Upon binding flg22, FLS2 recruits the co-receptor BRASSINOSTEROID INSENSITIVE 1 (BRI1)-ASSOCIATED RECEPTOR KINASE/SOMATIC EMBRYOGENESIS RECEPTOR KINASE 3 (BAK1/SERK3) and engages in transphosphorylation events. SERK-member engagement is shared with the developmental brassinosteroid receptor BRI1, but results in different outputs (Roux et al., 2011; Schwessinger et al., 2011; Chinchilla et al., 2009). The receptor-like cytoplasmic kinase (RLCK) BOTRYTIS-INDUCED KINASE (BIK1) that interacts with FLS2 pre-activation, is phosphorylated and released from the receptor complex, and subsequently phosphorylates the membrane-localized NADPH-oxidase RESPIRATORY BURST OXIDASE HOMOLOGUE D (RBOHD) which results in the production of extracellular reactive oxygen species (ROS; (Kadota et al., 2014). Additionally, FLS2 activation results in the sequential phosphorylation of MITOGEN-ASSOCIATED PROTEIN KINASES (MAPKs) in a MAPK cascade, that positively regulates the expression of defense-related genes and confers resistance to pathogens (Rasmussen et al., 2012). Furthermore, FLS2 activation is coupled to the production and downstream signaling of the phytohormones salicylic acid (SA) and ethylene, which is a hallmark of defense activation in response to biotrophic pathogens (Zipfel et al., 2004). FLS2 activation can be regulated at the receptor complex level by BAK1-INTERACTING RECEPTOR-LIKE KINASE 2 and 3 (BIR2, BIR3), which bind to BAK1/SERK3 and inhibit its interaction with FLS2 (Halter et al., 2014; Imkampe et al., 2017). Additionally, heterotrimeric G-proteins and protein phosphatases interact with BIK1 and control its phosphorylation status (Liang et al., 2016).

1.4 - Receptor-like proteins in immunity

LRR-RLP-type PRRs perceive highly diverse extracellular patterns, including MAMPs that are not associated with specialized virulence factors, such as *Phytophthora* elicitins detected by the solanaceous ELICITIN RESPONSE (ELR), bacterial cold-shock protein epitope csp22 detected by both *Nicotiana benthamiana* RECEPTOR-LIKE PROTEIN REQUIRED FOR CSP22 RESPONSIVENESS (CSPR) and Arabidopsis RLP23, and Cuscuta factor secreted by the parasitic plant *Cuscuta reflexa,* which is detected by tomato CUSCUTA RECEPTOR 1 (CuRe1; (Domazakis et al., 2018; Du et al., 2015; Saur et al., 2016; Hegenauer et al., 2016).

RLPs also perceive apoplastic enzymatic virulence factors such as the *P. sojae* glycosyl hydrolse XEG1 detected by *N. benthamiana* Response to XEG1 (RXEG1), ethylene-inducing fungal xylanases detected by tomato EIX-RESPONDING 2 (EIX2), and fungal endopolygalacturonases detected by Arabidopsis RESPONSIVENESS TO BOTRYTIS POLYGALACTURONASES1 (RBPG1)/RLP42 (Wang et al., 2018; Ron, 2004). In addition, RLPs function in detecting pathogen secreted effectors, such as tomato Ve1 that detects *Verticillium dahliae* Avirulence on Ve1 tomato (Ave1), as well as RLPs from the well-studied model pathosystem *Cladosporium fulvum*/tomato, with tomato Cf-2 that detects effects of the Avr2 effector on the apoplastic protease Required for *C. fulvum* Resistance 3 (RCR3), Cf-9 that detects the Avr9 effector which requires the presence of a yet-unidentified high-affinity binding site (HABS) at the cell surface, and Cf-4 that detects the apoplastic effector Avr4 which protects fungal chitin against the activity of apoplastic chitinases (Jonge et al., 2012; Dixon et al., 1996; Van der Hoorn, 2001; Takken et al., 1999).

RLPs interact with the RLK SUPPRESSOR OF BIR1-1 (SOBIR1), which is necessary for accumulation and signaling of the majority of tested RLPs (Liebrand et al., 2014). SOBIR1 was previously identified in a screen for suppressors of the spurious cell death phenotype in *bir1-1* mutants, and was recently found to engage with BAK1/SERK3 to trigger cell death (Gao et al., 2009; Domínguez-Ferreras et al., 2015). Based on biochemical studies, SOBIR1-BAK1/SERK3 heterodimerization and cell death activation can be inhibited by the RLK BIR1, which reminisces of the role for BIR2 and BIR3 in preventing heterodimerization and signal activation of FLS2 with BAK1/SERK3 (Liu et al., 2016).

Evidence is mounting that RLP-SOBIR1 pairs also depend on recruitment of SERK members in order to initiate signaling. Genetically, SERK1 has previously been implicated in Cf-4 mediated resistance, as well as SERK3 for Ve1 and RLP30 resistance (Fradin et al., 2011). Recent biochemical studies show that RLP-SOBIR1 two-component-receptor modules that contain for example ELR, RLP23, NBRXEG1, Cf-4 or Cf-9 physically recruit SERK members in order to activate down stream signaling, converging the RLP pathway onto known RLK signal acivation pathways at the PM (Chapter 3; (Du et al., 2015; Albert et al., 2015; Wang et al., 2018; Postma et

al., 2016). The outputs of RLP-based receptor systems are similar to known RLK outputs, but often include the induction of a hypersensitive response (HR), which manifests as cell death in expressing tissue. Additionally, MAPK activation, ethylene and SA production, as well as ROS production are coupled to RLP activation (Stulemeijer et al., 2007; Thomas et al., 2000; Brading et al., 2000).

1.5 - Intracellular surveillance by NLRs

In addition to cell-surface perception of extracellular MAMPs, plants employ intracellular detection platforms that recognize the presence of pathogen-borne effectors. These consist of nucleotide-binding (NB) domain and LRR-containing (NLR) proteins, which are among the most rapidly evolving gene families in plants (Wu et al., 2017). Broadly, two classes of NLRs are defined, that are distinguished based on the presence of an N-terminal TOLL/INTERLEUKIN1 RECEPTOR (TIR) or coiled coil (CC) domain, grouping them in TIR-NLRs (TNLs) and CC-NLRs (CNLs) (El Kasmi and Nishimura, 2016). They can directly bind effectors, or bind to effector targets (guardees) and monitor their integrity, triggering immune signaling upon effector modification of self molecules. In addition, they can contain non-canonical integrated domains that replicate patterns found on *bona fide* effector targets. Thus, NLRs can probe for the presence of effectors without physically associating to the effector target (Sarris et al., 2016; Ellis, 2016).

NLR activation is coupled with a conformational change from the ADP-bound “off-state” to the ATP-bound “on-state”, and can require homodimerization through TIR or CC domains. Activation is further hallmarked by signaling through the major determinants ENHANCED DISEASE SUSCEPTIBILITY 1 (EDS1), commonly associated with TNL signaling, and NON-RACE-SPECIFIC DISEASE RESISTANCE 1 (NDR1), which is associated with CNL signaling. EDS1 furthermore interacts with and PHYTOALEXIN DEFICIENT 4 (PAD4) and SENESCENCE-ASSOCIATED GENE 101 (SAG101), both necessary for defense activation which is coupled to the production of SA (El Kasmi and Nishimura, 2016; Li et al., 2015). Often, NLR-activation results in cell death, but this does not fully correlate with their capacity to mediate resistance (Greenberg et al., 2000).

TNLs can be truncated, and exist as functional TIR, TIR-NBS (TN) or TIR-unknown (TX) proteins. Arabidopsis encodes 21 *TN* genes, which are spread throughout the genome and cluster together with genes encoding full-length NLRs, with which they are thought to function in heteromultimeric complexes as a general mechanism (Nandety et al., 2013). TN proteins have the capacity to induce cell death and resistance through canonical EDS1/PAD4 defense activation modules.

NLRs can function together in multimeric complexes, as exemplified by Arabidopsis RESISTANT TO P. SYRINGAE 4 (RPS4) and RESISTANT TO RALSTONIA SOLANACEARUM 1 (RRS1), which form heteromultimers that include NLR homodimers and EDS1 and PAD4 (Cesari et al., 2014; Williams et al., 2014). More extremely, the recently emerging “sensor-helper” model, present in asterids, reveals the functional dependency of multiple sensor-NLRs, that detect unrelated effectors, on a limited number of helper-NLRs. Sensor-NLR clades are highly diversified, while helper-NLR clades are conserved, which points at an evolutionary flexible system that allows for rapid adaptation to novel effectors while maintaining common signaling output (Wu et al., 2017, 2018).

1.6 - RPW8-type resistance proteins

In Arabidopsis, such a network may be echoed. A small number of ACTIVATED DISEASE RESISTANCE 1 (ADR1) family of CNLs is required for the defense activation of multiple sensor-TNLs, that detect functionally unrelated effectors. ADR1 encodes an atypical CNL, in which the CC-domain in its entirety is homologous to full-length RESISTANCE TO POWDERY MILDEW 8 (RPW8) (Bonardi et al., 2011; Collier et al., 2011; Dong et al., 2016). The *RPW8* locus is present in Arabidopsis ecotype Col-0 (Colombia), but was originally identified in ecotype Ms-0 (Moscow), where it encodes the homologs *RPW8.1* and *RPW8.2*, of which both confer broad-spectrum resistance to adapted powdery mildews when expressed in Col-0 (Xiao et al., 2005). So-defined CC-RPW8 (CC_R) domains are additionally found in the family of tobacco helper-NLR N-REQUIREMENT GENE 1 (NRG1), and overexpression of individual CC_R-domains of ADR1-like and NRG1-like proteins is associated with the induction of cell death (Collier et al., 2011; Peart et al., 2005).

In Ms-0, *RPW8.2* encodes a TM-CC protein, which is membrane associated, carried on secretory vesicles to the haustoria of powdery mildews, and there promotes cell wall apposition, localized ROS production, the initiation of cell death and associated resistance (Kim et al., 2014). RPW8.2 membrane targeting is required for its function in promoting cell death and in conferring post-penetration resistance against all tested powdery mildew strains (Wang et al., 2013). Initiation of RPW8-based defense signaling is dependent on EDS1, PAD4 and NDR1, and is dependent on SA signaling (Xiao et al., 2005).

Col-0 encodes four genes on the *RPW8* locus which consist of *HOMOLOG OF RPW8.2 1* through *4* (*HR1-4*). *HR3* is most similar to *RPW8.2* and *RPW8.1*, and all RPW8 homologs in Col-0 and Ms-0 are thought to derive from a *HR3*-like ancestral gene (Zhong and Cheng, 2016). Out of HR1-4, it was recently found that upon *p35S*-driven overexpression in Arabidopsis, only HR3 triggered necrotic cell death at resting state, but HR1-3 conferred resistance to the adapted powdery mildew *Golovinomyces cichoracearum* (Berkey et al., 2017). C-terminally fluorescently

tagged HR1 and HR3 localized to the PM, HR2 surrounded chloroplasts, and HR4 could not be detected in Arabidopsis, but localized to punctae and the cytoplasm in *N. benthamiana* transient expression. Upon *G. cichoracearum* infection, only HR3 accumulated under the attempted penetration site, but at later time points, all homologs enriched around haustoria. Specifically, HR4 was found to localize to punctate structures at *G. cichoracearum* haustoria in transiently expressing *N. benthamiana* epidermal cells (Berkey et al., 2017).

1.7 - Plant subcellular trafficking and Rab GTPases

The ability for spatial reorganisation of cellular components provides an essential platform through which to prepare and execute defences. Pre-formed cell walls are produced by cellulose synthases, which are translocated from inside the cell to the cell surface where they deposit cell wall polymers to build initial barriers (Kumar and Turner, 2015; Zhang et al., 2016). Upon infection by pathogens that concentrate their efforts at small regions on the cell surface, induced structural defenses such as the location-specific formation of callose-rich cell wall appositions in the form of papillae, depend on the focal accumulation of callose synthases, which are retrieved from their default location and concentrate at the pathogen contact site (Ellinger and Voigt, 2014).

Plant cells achieve spatial reorganisation through employing membrane trafficking (**fig. 1.1**). Bounding membranes of, among others, the endoplasmic reticulum (ER), Golgi or PM can produce membrane vesicles that carry membrane-associated and soluble cytosolic or lumenal cargoes through the cytoplasm to deliver them at other subcellular locales. This process starts by the induction of membrane curvature at the donor membrane through the recruitment of coat proteins such as COPI functioning in the Golgi, and clathrin, which performs this function at the PM. This is coupled to cargo sorting mediated by adaptor-proteins. Further membrane invagination, up to the point where scission is induced by proteins such as dynamin, and subsequent vesicle release into the cytoplasm. Upon trafficking through the cytosol, often mediated by interaction with actin or microtubule filaments, tethering factors link vesicles to the acceptor membrane, and upon closer approach, soluble N-ethylmaleimide-sensitive-factor attachment receptors (SNAREs) present on both membranes form multimeric complexes, and mediate membrane fusion which results in cargo delivery at the acceptor membrane (Bonifacino and Glick, 2004).

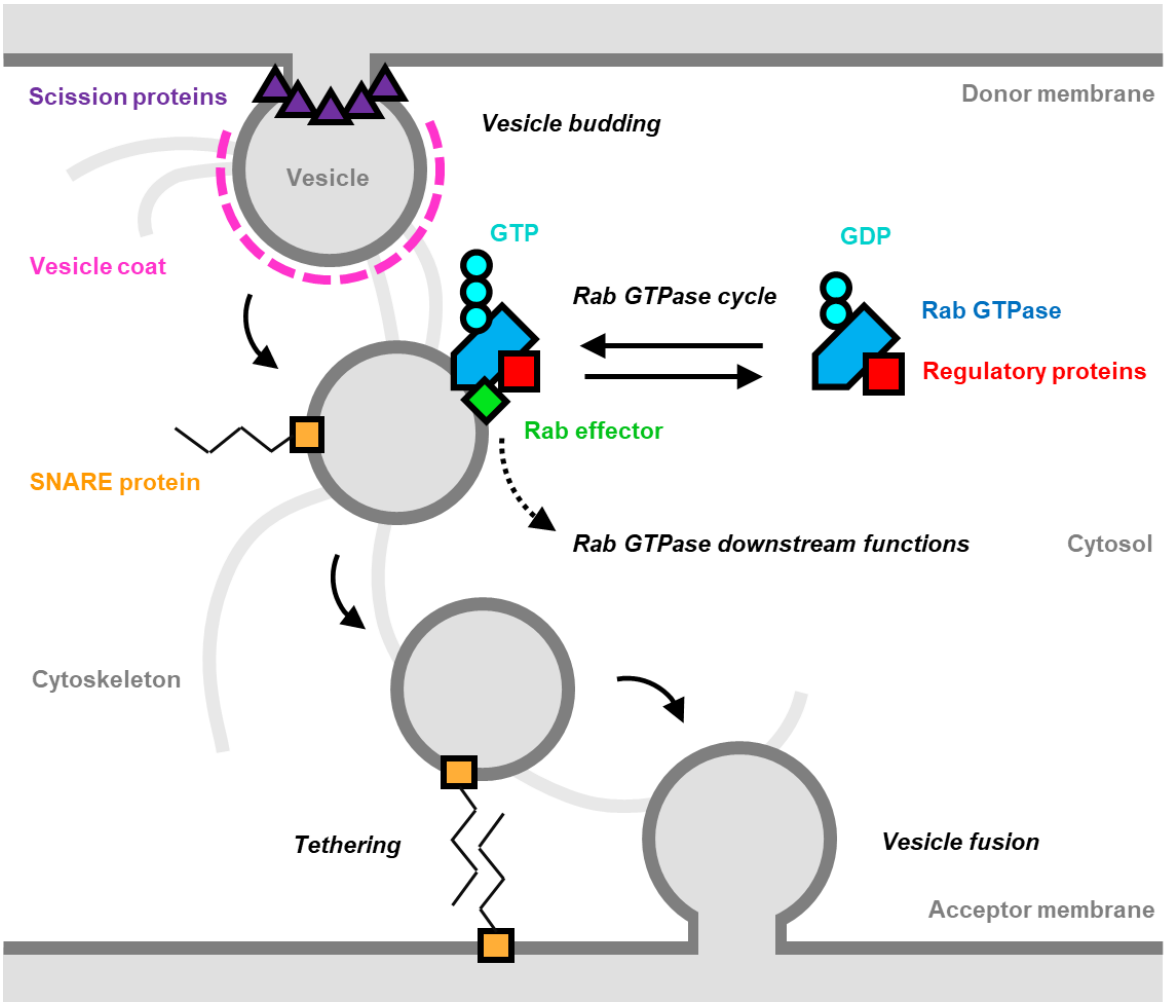

Figure 1.1. Schematic overview of membrane trafficking mechanisms, and association with Rab GTPases. At the cytosolic side of the donor membrane (top left), membrane invagination, recruitment of coat proteins and membrane scission generate a vesicle. Trafficking regulators such as SNARE proteins and Rab GTPases are present on the vesicle (middle), which associates with, and travels along the cytoskeleton. Rab GTPases cycle through a GDP-bound cytosolic state, and a GTP-bound membrane-associated state. At the membrane, upon GTP hydrolysis by the Rab GTPase, Rab effectors are activated and perform diverse downstream functions. Vesicles then tether and fuse with acceptor membranes, upon which their cargo is delivered (lower right).

Distinct subcellular trafficking pathways exist, which define specific routes between donor and acceptor membranes. Pathway-specific membrane-associated proteins govern the biochemical processes occurring on these membrane compartments, and can influence their fate. Among these are small membrane-associated G-proteins belonging to the Rab GTPase family . Arabidopsis encodes 57 Rab GTPases, which fall within 8 clades (RABA-H) that are grouped based on homology to mammalian clades (Woollard and Moore, 2008). Rab GTPases are small, lipid-modified molecular switches that shuttle between a membrane-associated, active GTP-bound state, and a cytosolic, inactive GDP-bound state. Cytosolic Rab GTPases interact with

GDP-dissociation inhibitors (GDIs) which cover the lipid group, thus preventing membrane association and nucleotide exchange (Saito and Ueda, 2009a). Rab GTPases engage with GDI-dissociation factors (GDFs) which remove GDIs and allow membrane association. In Arabidopsis, GDIs are represented by Prenylated Rab Acceptor (PRA)/Ypt-Interacting Proteins (Yip) (Alvim Kamei et al., 2008). Membrane-associated, GDP-bound Rab GTPases interact with Rab Guanine Exchange Factors (Rab GEFs), which promote GTP association. In their GTP-bound state, Rab GTPases are considered active, and engage with a diversity of associated proteins which are Rab effectors, and of which the activity can be regulated by their interacting Rab GTPases (Grosshans et al., 2006). Activity is ceased upon GTP hydrolysis, promoted by Rab GTPase-Activating Proteins (Rab GAPs), which leads to subsequent removal from the membrane (Saito and Ueda, 2009a).

1.8 - Secretory and endocytic pathways

The default secretory pathway (**fig. 1.2**) describes the membrane trafficking route taken by newly biosynthesized proteins, starting at the endoplasmic reticulum (ER), transitioning through *cis-, medial* and *trans*-Golgi cisternae, the *trans*-Golgi Network (TGN) which in plants also functions as the early endosome (EE), before being secreted to the PM (Rojo and Denecke, 2008; Foresti and Denecke, 2008). Rab GTPases in functioning in the early secretory pathway localize to the Golgi and TGN/EE, and fall within the subclades RabD1 (RABD1) and RabD2 (ARA5/RABD2a, RABD2b, and RABD2c (Pinheiro et al., 2009; Woollard and Moore, 2008). Constitutively GDP-bound mutants of ARA5/RABD2a exerted a dominant negative effect on traffic between the ER and Golgi, but in loss-of function mutations, showed considerable functional overlap with other RabD2 members (Pinheiro et al., 2009). Post-Golgi secretory processes occur between the TGN/EE and PM, function downstream of RabD, and are mediated by Rab GTPases in the RabA and RabE clades. While knowledge on the function of RabE proteins is limited, they localized to the Golgi, and dominant-negative fusions accumulated secretory markers in the Golgi (Speth et al., 2009; Mayers et al., 2017). The RabA clade is highly diversified in plants, with members that localize to the TGN/EE and mediate secretory traffic between the TGN/EE and PM, as well as between TGN/EE and the forming cell plate upon cytokinesis (Lunn et al., 2013; Asaoka et al., 2013; Feraru et al., 2012).

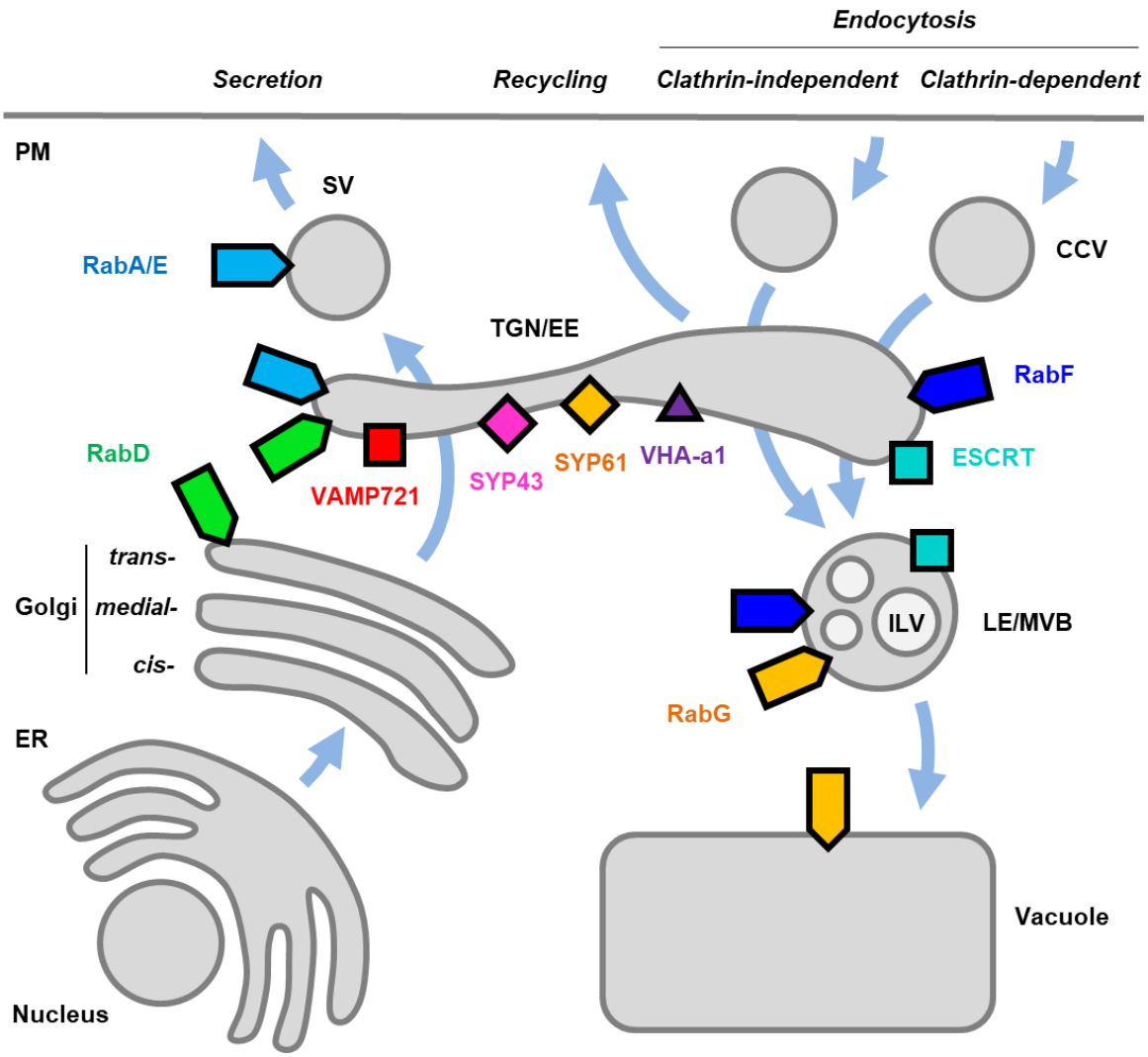

Figure 1.2. Schematic overview of membrane trafficking pathways in plants. Newly synthesized secreted proteins originate at the endoplasmatic reticulum (ER, lower left), and travel through the Golgi apparatus, encountering *cis*-, *medial*- and *trans*-Golgi compartments successively. Mediated by RabD and RabA/E-type GTPases, they are transferred into the *trans*-Golgi network/early endosome (TGN/EE, middle), from where they are delivered to the plasma membrane (PM) by secretory vesicles (SV). The TGN/EE consists of a domain, or population, that is VAMP721 and RabA-positive and has secretory activity, as well as a domain or population that is SYP43, SYP61 and VHA-a1 positive, which exhibits both endocytic and secretory activity. Retrieval of PM-localized cargoes occurs through clathrin-dependent endocytosis (top right) by means of clathrin-coated vesicles (CCVs), or by clathrin-independent endocytosis. Endocytosed cargoes traffic through the TGN/EE which, under control of the ESCRT complex, generates late endosomes/multivesicular bodies (LE/MVB) containing cargo-carrying intraluminal vesicles (ILVs). LE/MVBs associate with RabF and RabG-type GTPases, which govern its maturation and delivery to the vacuole (lower right), into which ILVs and their cargoes are released. Arrows indicate trafficking directionality of secreted and endocytosed cargoes.

The endocytic pathway (**fig. 1.2**) originates at the PM, where T-PLATE/clathrin-dependent and clathrin-independent endocytosis internalize membrane localized cargoes which then accumulate in the TGN/EE (Paez Valencia et al., 2016). From here, cargoes can recycle back to the PM, or be targeted to late endosomes (LE)/multivesicular bodies (MVBs), which are thought to mature from the TGN/EE (Scheuring et al., 2011; Dettmer et al., 2006). LE/MVB maturation is coupled to the formation of intraluminal vesicles (ILVs) through the action of multimeric ENDOSOMAL SORTING COMPLEX REQUIRED FOR TRANSPORT (ESCRT) components, which are required for the endosomal sorting of endocytic cargoes that are targeted to the vacuole for degradation (Gao et al., 2017; Buono et al., 2017). Known Rab GTPases functioning along the endocytic pathway belong to the RabF clade with the close homologs RHA1/RABF2a and ARA7/RABF2b localizing to TGN/EE as well as LE/MVBs (Ueda et al., 2004), the plant-unique RabF protein ARA6/RABF1 localizing to LE/MVBs (Ueda et al., 2001), and RabG proteins that localize to the vacuolar membrane (Geldner et al., 2009). During endosomal maturation, LE/MVBs undergo RabF to RabG conversion, through the action of the LE/MVB localized RabF effectors SAND/MONENSIN SENSITIVITY 1 (SAND/MON1) and CALCIUM CAFFEINE ZINC SENSITIVITY 1 (CCZ1), which are bona-fide ARA7 effectors and function in complex as the GEF for RabG proteins (Cui et al., 2014a; Singh et al., 2014a). Interestingly, it has recently been shown that the ER actively participates in facilitating endocytic processes. ER-PM-contact site-localized VAMP-ASSOCIATED PROTEIN 27 (VAP27) proteins associated with clathrin and endocytic membranes, and positively regulated endocytic activity (Stefano et al., 2018). Furthermore, LE/MVBs physically associate with the ER, which influences their distribution and streaming, with overexpression of ER-localized structural proteins that affect ER morphology also leading to abberant localizations of LE/MVB-dependent endosomal cargoes (Stefano et al., 2015).

1.9 - Trafficking pathways share the *trans*-Golgi network/early endosome

Both secretory and endocytic traffic pass through the TGN/EE, yet cargoes of these pathways can be transported to their destinations in a pathway-specific manner. The TGN/EE is not one homogenous compartment, but can be subdivided into separate populations based on multiple criteria (Gendre et al., 2015). Firstly, TGN/EE compartments can mature from *trans*-Golgi cisternae, which is supported by the observation of Golgi-associated (GA) and Golgi-independent (GI) populations of TGN/EE, when marked by the TGN/EE-resident SNARE SYNTAXIN OF PLANTS 43 (SYP43; (Uemura et al., 2014). In agreement with this, upon chemical disruption, some TGN/EE compartments recover in a partially Golgi-independent manner, pointing at partialy Golgi-independent origins, potentially of endocytic origin (Ito et al., 2017). Secondly, two populations of TGN/EE can be distinguished, based on the presence of RABA2a, RABA1b and VAMP721 and high amounts of clathrin, which mark a population with secretion and PM-

recycling, or the presence of SYP61, SYP43 and VHA-a1, and secretory vesicle clusters, which mark a populations that is associated with both secretory and endocytic traffic (Gendre et al., 2015; LaMontagne and Heese, 2017). The precise compartmentalization and dynamics of TGN/EE are as of yet poorly understood, but recent advances in subcellular fractionation, proteomics and lipidomics have begun to shed light on mechanisms of cargo sorting at this major trafficking hub (Wattelet-Boyer et al., 2016).

1.10 - Functions of the secretory pathway in immunity

The secretory pathway plays an important role in delivering PRRs to the cell surface, potentiating cells for the detection of extracellular patterns. Newly synthesized PRRs first localize to the ER, where they are processed and folded into their correct structures. This requires the ER quality control (ERQC) machinery that, when impaired, cause the accumulation of EFR in this organelle (Farid et al., 2013; Häweker et al., 2010; Li et al., 2009; Lu et al., 2009; Nekrasov et al., 2009). Consequently, loss-of-function mutants in ERQC components are insensitive to elf18 and show enhanced susceptibility to bacterial infection (Häweker et al., 2010). PRRs carry a typical N-terminal signal peptide that directs the receptors for ER export to enter the secretory pathway. FLS2 associates with ER-resident RETICULON-LIKE PROTEINS GROUP B (RTNLB) 1 and 2, which in loss-of-function mutants caused FLS2 accumulation at the ER (Lee et al., 2011). Similarly, Cf-4 interacts with ERQC machinery, and upon genetic interference with the ERQC components CALRETICULIN 3a (CRT3a) and HSP70-interacting BiP chaperones, Cf-4 accumulated, but was incorrectly glycosylated and affected in its capacity to mount HR upon Avr4 treatment (Liebrand et al., 2012).

A distinct member of the RabA clade, RABA1b has been implicated in transport of FLS2 to the PM (Choi et al., 2013). Co-expression of dominant-negative (DN) RABA1b and FLS2 in *N. benthamiana* significantly reduced FLS2 PM localization, while FLS2 accumulated in small cytosolic vesicles. As DN-RABA1b expression caused morphological changes to SYP61-marked TGN/EE, this suggests that RABA1b is involved in transport of FLS2 from the TGN/EE to the PM.

The secretory pathway also responds to activation of immunity. Upon treatment with the MAMPs flg22 or fungal xylanase, the PM-localized secretory pathway SNARE proteins PEN1/SYP121, SYP122 and SYP132 are rapidly phosphorylated (Kalde et al., 2007; Benschop et al., 2007). Furthermore, treatment with the central defense hormone SA leads to transcriptional changes that depend on the SA-receptor NON-EXPRESSOR OF PATHOGENESIS-RELATED (PR) GENES 1 (NPR1), and include upregulation of *PR*-genes which encode for secreted antimicrobial proteins (Wang et al., 2005). SA and NPR1-dependent transcriptional reprogramming also includes the upregulation of ERQC components and secretory pathway genes that are required for the secretion of PR proteins (Wang et al., 2005). SA-induced secretory trafficking also seems

to be engaged in PRR delivery to the PM. SA upregulates expression and PM-accumulation of the PRRs FLS2, EFR and CERK1, as well as BAK1/SERK3 (Tateda et al., 2015). This is dependent on the ER-localized ACCELERATED CELL DEATH 6 (ACD6), a membrane-associated protein involved in positive feedback regulation with SA. ACD6 forms complexes with FLS2 and ER-chaperones, possibly to facilitate the folding and delivery of FLS2 under SA-inducing conditions (Zhang et al., 2014b).

A client of upregulated secretion upon SA-signaling is PR-1, which is a cysteine-rich protein that accumulates in the extracellular space to high levels upon pathogen challenge (van Loon, 1975; Van Loon and Van Strien, 1999). It exerts antimicrobial effects through binding and sequestering sterols from pathogen membranes (Gamir et al., 2017). Upon fluorescent tagging, it localizes to ER and Golgi, and is dependent on canonical secretory processes to be exported (Watanabe et al., 2013; Pečenková et al., 2017). PR-1 secretion is negatively affected by the Golgi-resident SNARE MEMBRIN-12 (MEMB12), which promotes retrograde Golgi-ER traffic, and is itself negatively regulated by RNA-interference upon infection by *Pto* DC3000, supporting a role for the Golgi in PR-1 secretion and immunity (Zhang et al., 2011b). Post-Golgi secretion of PR-1 requires the TGN/EE localized ubiquitin E3 ligase KEEP ON GOING (KEG) which when mutated causes PR-1 to accumulate in the vacuole (Gu and Innes, 2012), and requires the PM-localized SNARE SYP132, which forms complexes with the TGN/EE-localized secretory SNAREs VESICLE-ASSOCIATED MEMBRANE PROTEIN 721 (VAMP721) and VAMP722 that are involved in TGN/EE-PM transport (Kalde et al., 2007).

In addition to potentiating the PM with detection capacity and facilitating the secretion of antimicrobial proteins, the secretory pathway is involved in the execution of cell-surface based immune responses. The PM-localized SNARE PEN1/SYP121 engages with VAMP721/722 and the cytosolic SNARE SNAP33, which have resting state functions in default secretion, to promote pre-penetration resistance and formation of the callose-rich papilla upon pathogen challenge (Kwon et al., 2008; Assaad et al., 2004). Furthermore, upon powdery mildew attempted penetration, formation of the papilla co-incides with focal accumulation of the callose synthase POWDERY MILDEW RESISTANT 4 (PMR4)/GLUCAN SYNTHASE-LIKE 5 (GSL5), which is necessary for pathogen-induced callose deposition (Ellinger et al., 2013). Interestingly, overexpression of the secretory Rab GTPase RABA4c results in enhanced PMR4-dependent callose deposition and resistance to the adapted powdery mildew *Golovinomyces oronti* (Ellinger et al., 2014a). RABA4c and PMR4 interact *in vivo*, and because PMR4-dependent enhanced callose deposition depends on the activation status of RABA4c, PMR4 is considered to be its Rab effector. Upon infection with *Pto* DC3000, Golgi and PM-localized RABE1d focally accumulated at the cell periphery, suggesting the plant engages in the cell-surface concentration of secretory processes also in response to bacteria (Speth et al., 2009). Indeed, expression of a permanently

GTP-bound constitutive-active (CA) RABE1d conferred increased resistance against *Pto* DC3000, coupled with enhanced secretion of PR-1.

1.11 - Functions of the endocytic pathway in immunity

Internalization and late endosomal sorting, which pass cargoes from the PM through the TGN/EE and LE/MVB, also contribute to plant immunity. Mutants affected in genes coding for the endocytic coat protein CLATHRIN HEAVY CHAIN (CHC) and dynamin-related proteins (DRPs), which are homologs of mammalian dynamins that mediate vesicle scission, are impaired in endocytic uptake, and show enhanced susceptibility to *Pto* DC3000 (Collings et al., 2008; Smith et al., 2014; Mbengue et al., 2016). Similarly, infection success of *Pto* DC3000, as well as the adapted oomycete pathogen *Hyaloperonospora arabidopsidis* (*Hpa*) is enhanced in *vps28-2* and *vps37*-1, which are loss-of function mutants in ESCRT subunits that mediate cargo sorting into LE/MVBs (Lu et al., 2012; Spallek et al., 2013; Scheuring et al., 2011). Thus, endocytic uptake and correct endosomal cargo sorting are required to mount a successful defense response.

Upon ligand stimulation, cell-surface lcoalized PRRs such as FLS2, EFR and PEPR1 translocate into endosomes in a clathrin-dependent manner (Ortiz-Morea et al., 2016; Mbengue et al., 2016; Robatzek et al., 2006). At resting state, FLS2 recycles between the PM and TGN/EE as evidenced by chemical inhibition of TGN/EE-PM transport using Brefeldin-A (Beck et al., 2012b). Upon activation, FLS2 is sorted into LE/MVBs in a BAK1/SERK3-dependent manner, as evidenced by co-localization with FM4-64 and endosomal Rab GTPases ARA7 and ARA6 (Beck et al., 2012b). Endosomal accumulation of FLS2 occurs in a transient manner, with a maximum of FLS2 endosomes at ca. 1 h after activation, and is thought to underlie its vacuolar delivery and subsequent degradation (Beck et al., 2012b; Choi et al., 2013).

Similarly, the tomato RLP EIX2 resides at the PM, and after activation with xylanase, it shows increased localization at endosomes that are marked by the LE/MVB marker FYVE (Sharfman et al., 2011). In agreement, chemical interference of late endosomal trafficking and disruption of the actin cytoskeleton reduces EIX2 endocytosis (Bar and Avni, 2009a). EPS15 homology domain 2 (EHD2) has been implicated in decreasing the bundling of actin filaments and impairs endocytosis of EIX2 upon overexpression (Bar and Avni, 2009a, 2009b). This correlates with a reduction in xylanase-triggered HR, ethylene production and *PR1* gene expression, and is consistent with reduced xylanase-induced HR upon chemical disruption of actin (Bar and Avni, 2009a). Interestingly, although actin is required for endocytosis of activated FLS2, EHD2 does not seem to affect flg22-induced *PR1* gene expression, but can interfere with Cf-4 and Cf-9 mediated HR (Bar and Avni, 2009b). However, whether EHD2 also inhibits Cf-4 endocytosis, and not FLS2 endocytosis, remains to be demonstrated. This could be related to EHD2 associating with RLPs but not RLKs, as there is evidence that EHD2 interacts with SlEix2 through its coiled-coil domain.

1.12 - Connections between the endocytic pathway and cell-surface delivery

Initial contact between the pathogen and the plant cell is associated with the recruitment and focal accumulation of diverse subcellular components. These responses are especially well-studied in the context of infection by filamentous pathogens, and include the formation to a callose-rich papilla (Voigt, 2014), local immobilization of mitochondria, peroxisomes, clustering of ER and accumulation of endomembrane compartments of endocytic nature (Nielsen et al., 2012; Griffis et al., 2014; Fuchs et al., 2015b; Nielsen et al., 2017b). Indeed, in electron microscopy studies, LE/MVBs have been shown to fuse with the PM under pathogen contact sites, which is thought to be coupled to the release of ILVs which are then considered extracellular vesicles (EVs; (An et al., 2006).

In concert with this, upon attempted penetration, the plant upregulates the local production of toxic metabolites, among which those derived from indole-3-glucosinolate precursors (Bednarek et al., 2009; Clay et al., 2009). Enzymes functioning early in the pathway that converts indole-3-glucosinolates such as those belonging to the CYTOCHROME P81 (CYP81) family have been observed at the ER, while final conversion steps are mediated by myrosinases among which is PENETRATION 2 (PEN2) that localizes to mitochondria and peroxisomes (Fuchs et al., 2015b). The PM-localized ABC-transporter PEN3 focally accumulates at the site of attempted penetration, and is thought to export the toxic metabolites thus produced, concentrating chemical defenses at the biologically relevant location (Stein et al., 2006; Underwood and Somerville, 2008, 2013). PEN3 focal accumulation is thought to be mediated by endocytic uptake from the PM, and fusion of LE/MVBs at the cell surface in an unconventional secretion process, but conclusive evidence for this is lacking (Underwood et al., 2017). In addition, the PM-localized SNARE PEN1/SYP121 focally accumulates, and is found in the extracellular space at fungal invasion sites, possibly mediated by LE/MVB redirection as well (Assaad et al., 2004; Nielsen et al., 2012). Yet, LE/MVB-dependent extracellular accumulation of PEN1 is not thought to be required for its biological function. While a PEN1 function in regulating the dynamics of callose deposition, which is underpinned by default secretory processes, has been demonstrated (Assaad et al., 2004), it can form complexes with the LE/MVB-localized snare VAMP727, suggesting potential involvement in unconventional secretion (Ebine et al., 2012).

PEN3 focal accumulation is insensitive to chemical disruption of TGN/EE-dependent recycling and default secretory processes (Underwood and Somerville, 2013), providing further evidence for its intermediary translocation into LE/MVBs before arriving at the PM. This echoes the LE/MVB sorting of FLS2 upon activation, which also did not depend on TGN/EE-based secretion or recycling as tested upon chemical disruption (Beck et al., 2012b). Interestingly, PEN3 focal accumulation can be triggered in the absence of pathogens upon MAMP treatment with flg22 and chitin, independent of protein biosynthesis (Underwood and Somerville, 2013). Using fluorescent

fusions, PEN3 can be observed to accumulate at endosomal compartments at time points preceding its cell-surface accumulation (Underwood et al., 2017).

1.13 - Involvement of Rab GTPases in pathogen-targeted traffic

While both secretory and endocytic traffic can participate in the delivery of defence components to the PM and extracellular space, the roles for Rab GTPases on these trafficking pathways are poorly understood. Yet, Rab GTPases accumulate at the pathogen interface, suggesting their involvement. ARA6-positive LE/MVBs accumulate under attempted penetration sites, and around haustoria of the powdery mildew *Blumeria graminis* f.sp. *hordei* (*Bgh*; (Nielsen et al., 2012). Interestingly, at resting state, ARA6 has been shown to induce SNARE-complex formation between the LE/MVB-localized VAMP727 and PM-localized SYP121/PEN1, pointing at a non-canonical role for this plant-unique Rab GTPase (Ebine et al., 2011b).

Upon penetration, haustoria of fungal *G. orontii* and the oomycete pathogen *Phytophthora infestans* are surrounded by both ARA7 and ARA6, and LE/MVB-dependent cargoes such as activated FLS2 accumulate in the extrahaustorial matrix of *P. infestans* (Inada et al., 2016; Bozkurt et al., 2015). Furthermore, RABG3c localized around *P. infestans* haustoria (Bozkurt et al., 2015). RabG clade proteins are normally localized to the vacuolar membrane, and are involved in vacuolar delivery of RabF compartments (Geldner et al., 2009; Singh et al., 2014b). Taken together, these data suggest that Rab-GTPase dependent cargo delivery occurs at pathogen interfaces.

All RabF GTPases, RHA1, ARA7 and ARA6, share a common activator in the Rab GEF VACUOLAR PROTEIN SORTING 9a (VPS9a; (Goh et al., 2007). ARA7 and ARA6 localize to the host-derived extrahaustorial membrane (EHM) of the adapted mildew *G. orontii*, but VPS9a is conspicuously excluded from this location (Inada et al., 2016). This suggests pathogen-mediated manipulation of EHM composition, and could suggest active interference with Rab GTPase-mediated processes through targeting their regulatory complex. Indeed, *G. orontii* effector candidates have been predicted to interact with PRA1 Rab GTPase-regulatory proteins (Mukhtar et al., 2011; Weßling et al., 2014). In studies using the nonadapted *Bgh* on Arabidopsis, VPS9a mutants showed an increased penetration success, as well as decreased callose apposition at pathogen interfaces (Nielsen et al., 2017b). It is therefore thought that VPS9a/RabF pathways contribute to both pre- and postpenetration resistance to nonadapted pathogens.

LE/MVBs have been proposed to generate EVs through cell-surface delivery and secretion of ILVs, based on electron microscopy studies (An et al., 2006). This hypothesis is further supported by the observation that *Pto* DC3000-infection stimulates the biogenesis of LE/MVBs and the occurrence of EV-like vesicles in the paramural space, which was dependent on regulators of LE/MVB biosynthesis (Wang et al., 2014, 2015). Correspondingly, apoplastic purifications of

Arabidopsis contained EVs which share high proteomic identity to published LE/MVB proteomes (Rutter and Innes, 2017b). Their occurrence is upregulated upon both SA treatment and infection with *Pto* DC3000, and they carry biotic-stress related proteins such as PEN1/SYP121, PEN3 and indole-3-glucosinolate metabolic enzymes (Rutter and Innes, 2017b). More recently, in studies using the necrotrophic fungus *Botrytis cinerea*, ARA6 clusters were observed under attempted penetration sites, coupled to the increased delivery of EVs that were shown to carry micro-RNAs with fungal targets, pointing at a role for EVs in *trans*-kingdom delivery of plant-borne defense components which thus accumulate inside the pathogen (Cai et al., 2018). While taken together, the above observations point at critical roles for endosomal Rab GTPase-regulated trafficking pathways in executing defense, it remains to be shown how changes in Rab GTPase activation status and subsequent activation of their downstream Rab-effectors contribute to immunity.

1.14 - Trafficking is subject to effector manipulation and host surveillance

Because trafficking processes are of fundamental importance to the preparation and execution of plant immunity, to pathogens that seek to circumvent host defenses they would make great effector targets. Indeed, large scale yeast-2-hybrid (Y2H) screens that probed Arabidopsis host protein interactions with a panel of *G. orontii, Hpa* and *Pto* DC3000 effectors have yielded predicted interactions between pathogen effectors and trafficking regulators that include coat proteins, Rab GTPase regulatory proteins, motor proteins and cytoskeletal elements in both secretory and endocytic traffic (Mukhtar et al., 2011; Weßling et al., 2014). Furthermore, individual effectors have been specifically shown to target trafficking components during infection, such as *Phytophthora* AVR3a which targets dynamin-dependent endocytic processes and can accumulate at host endosomes (Chaparro-Garcia et al., 2015; Engelhardt et al., 2012), AVR1 which targets secretory EXOCYST tethering factors (Du et al., 2015), and AvrBlb2, which inhibits the secretion of host-borne proteases and thus confers increased virulence (Bozkurt et al., 2011). Similarly, *Pseudomonas* effectors of unknown composition suppress PEN3 focal accumulation, and HopM1 targets the TGN/EE localized trafficking regulator HOPM1 INTERACTOR 7/BREFELDIN-A VISUALISED ENDOCYTIC TRAFFICKING DEFECTIVE 1 (MIN7/BEN1), suppresses secretion of PR-1 and callose deposition, and thus confers enhanced bacterial virulence (Nomura et al., 2006, 2011).

Conversely, in plants, connections between trafficking processes and NLR-mediated immunity exist. Interference with subcellular trafficking processes can result in cell-death associated defences. Firstly, the *pen1/syp121 syp122* double mutant of closely homologous SNAREs exhibits a lesion-mimic phenotype with programmed cell death (Zhang et al., 2008). This can be rescued by mutations in NLR genes. Secondly, the HR-like cell death in the *accelerated cell death 11* (*acd11*) mutant, and HR induced by NLR-mediated immunity, are suppressed by loss-of-function in LAZARUS 1 (LAZ1), whose protein partially localizes to endosomes (Malinovsky et

al., 2010). Thirdly, NLR-associated immunity prevents degradation of MIN7/BEN1 by HopM1. Finally, the secretory tethering factor EXO70B1, interacts with SNARE-protein SNAP33 and the TN-type NLR TIR-NBS2 (TN2) *in planta*. *Exo70b1* mutants exhibit a sponteneous HR-like cell death, and an increased resistance to powdery mildews, both phenotypes fully dependent on TN2 (Zhao et al., 2015; Liu et al., 2017). This suggests that EXO70B1 or a dependent pathway is guarded by TN2. These observations support the concept that molecular components that regulate subcellular transport are monitored by NLRs and thus, when absent, trigger the induction of strong defense responses. It is noteworthy that NLR signaling increases SA levels, and SA in turn exerts regulation on secretory and endocytic trafficking processes (Du et al., 2013; Wang et al., 2005).

1.15 - Concluding remarks

Taken together, plant subcellular trafficking is interlinked with the immune system, and contributes to host defenses at multiple stages of pathogen infection. This includes building pre-existing cell surface barriers, maintaining cell surface-based detection capacity, and employing transport pathways to recruit defense components to regions of pathogen contact in a timely manner. Pathogens deliver effectors to manipulate the underlying trafficking pathways, and plants employ sensors to monitor their integrity. Rab GTPases localize and function on these pathways, and are required for full immunity, yet their precise contributions to defense are poorly understood, which warrants further investigation.

1.16 - Thesis aims

Signal initiation of RLK-type PRRs that detect MAMPs in Arabidopsis is well understood, and involves ligand-induced heterodimerization with BAK1/SERK3, activation of the PM-localized receptor complex, and subsequent ligand-induced internalization of the PRR which is then sorted for degradation through RabF-positive compartments (Ben Khaled et al., 2015). Cf-4 represents an RLP-type PRR that functions in effector-detection in tomato, and unlike RLK-type PRRs, besides genetic evidence for a role of SERK1, no direct involvement in Cf-mediated immunity of SERK members has been reported to date (Fradin et al., 2011). Instead, Cf-RLPs interact with the RLK SOBIR1 for stability and signaling capacity, independent of the presence of their ligands (Liebrand et al., 2013). *C. fulvum* infection is confined to the apoplast, and correspondingly, secretes effectors that accumulate there (Joosten and de Wit, 1999; Stergiopoulos and de Wit, 2009). This suggests that Cf proteins function at the PM, but their exact subcellular localization has remained unclear.

In order to elucidate the subcellular localization and signal activation mechanisms of SOBIR1-dependent RLPs, I aimed to:

- Reveal the subcellular localization of Cf-4
- Reveal the subcellular localization of constitutively interacting Cf-4-SOBIR1 complexes
- Probe for ligand-induced subcellular localization dynamics of Cf-4 upon activation by Avr4
- Investigate the requirements for SERK members in Cf-dependent receptor outputs and immunity

Secondly, besides carrying ligand-activated PRRs, endosomal Rab GTPases and associated compartments dynamically respond to pathogen infection and contribute to the delivery of defense cargoes at pathogen contact sites (Cai et al., 2018; Nielsen et al., 2017b). Equally, Rab GTPases along the secretory pathway have been shown to govern delivery and activation of cell-surface localized defense cargoes (Ellinger et al., 2014b; Choi et al., 2013). Yet, most studies have been performed in the context of infection by filamentous pathogens, and defence-induced cargo changes along Rab GTPase mediated pathways, or changes in proteins associating with the Rab GTPases themselves have not been mapped in a comprehensive way.

In order to gain insight into the dynamics of the secretory pathway marked by ARA5 and the endocytic pathway marked by ARA7 upon bacterial infection, as well as into MAMP-induced proteomic changes in the proteomes interacting with these Rab GTPases, I sought to:

- Investigate localization changes of ARA7 and ARA5 upon bacterial infection
- Reveal changes in ARA7 and ARA5-associated proteins after flg22-stimulus
- Identify flg22-responsive ARA7-interacting proteins which are defence-related
- Further characterize a subset of flg22-responsive ARA7 interacting defence-related proteins for roles in immunity

CHAPTER 2

EXPERIMENTAL PROCEDURES

2.1 - Plant materials

2.1.1 - Plant lines used in this study

Species		Genotype	Source
Arabidopsis thaliana	Col-0		
	Col-0	*pUB::YFP-ARA5*	Geldner et al., 2009
	Col-0	*pUB::YFP-ARA7*	Geldner et al., 2009
	Col-0	*pUB::RFP-ARA7*	Dettmer et al., 2006
	Col-0	*pUB::YFP-ARA5 x pUB::RFP-ARA7*	Generated, cross
	Col-0	*fls2*	Zipfel et al., 2004
	Col-0	*tn3*	SALK_018440.56.00
	Col-0	*hr4*	SALK_208828
	Col-0	*tn3 / pUB::TN3-GFP*	Generated, transformation
	Col-0	*hr4 / pUB::HR4-GFP*	Generated, transformation
	Col-0	*pUB::TN3-GFP*	Generated, transformation
	Col-0	*pUB::HR4-GFP*	Generated, transformation
Nicotiana tabacum	Samsun		
Nicotiana benthamiana	Domin.		
	Domin.	*p35S::Cf-4*	Liebrand et al., 2013
	Domin.	*p35S::Cf-4-GFP*	Postma et al., 2016
Solanum lycopersicum	Moneymaker	*Cf-0*	Dixon et al., 1996
	Moneymaker	*Cf-4*	Wulff et al., 2004

2.1.2 - Growth of Arabidopsis on soil

Arabidopsis thaliana seeds were germinated on soil (Levington F2 peat, 4 mm grit, Exemptor insecticide) and grown under 80 % humidity and 20 °C. Seedlings were transplanted to individual 4 cm x 4 cm pots. For plants used in experiments, a short-day regime of 10 hours light / 14 hours dark was used. For propagation and crossings, a long-day regime of 16 hours light / 8 hours dark was used.

2.1.3 - Growth of *Nicotiana benthamiana* on soil

Nicotiana benthamiana Domin. seeds were germinated on soil (Levington F2 peat, 4 mm grit) and kept under plastic foil at high humidity for 1 week. Seedlings were transplanted to individual 9 cm x 9 cm pots and grown under 80% humidity with a regime of 16 hours light / 8 hours dark. Plants were used at 2 weeks for virus-induced gene silencing, or 4-5 weeks for all other purposes.

2.1.4 - Growth of Arabidopsis in liquid media

For gas sterilisation, ca. 50 mg of Arabidopsis seeds in a paper bag were placed in a sealable chamber with a volume of ca. 10 L, alongside a beaker containing 200 mL commercial thick bleach (Parozone) to which 8 mL hydrochloric acid was added. The chamber was sealed and left in a fume hood overnight, after which the seed bag was retrieved and placed in a laminar flow hood to dry.

Under laminar flow, seeds were sown in resealable conical flasks containing 200 mL liquid MS medium supplemented with 1% (w/v) sucrose, without antibiotic selection. Flasks with seeds were stored at 4 °C overnight for vernalization, and then placed in a 120 rpm shaker for an incubation time of 8 days, growing at 22 °C under a light regime of 16 hours light / 8 hours dark.

2.1.5 - Generation of Arabidopsis protoplasts

Protoplasts were obtained from soil-grown plants at ca. 4-5 weeks of age using the tape sandwich method based on Sheen et al., 2002 . Fully grown leaves were sandwiched in between strips of masking tape, and the lower epidermis was removed by separating the tape. Tape strips containing the leaves were then placed face-down into a petri dish containing enzyme solution (1.5% cellulase (Onuzuka R10, Yakult BIC2224), 0.4% macerozyme (R10, Apollo Scientific cat. BIM0481), 0.1% BSA (Sigma cat. A-6793), 0.4 M mannitol, 20 mM KCl, 20 mM MES pH 5.7, 10 mM $CaCl_2$) and the digestion was allowed to continue for 1.5 hours at room temperature. Protoplasts were recovered by filtration through 40 mm nylon mesh, centrifugation at 100 x *g* for 2 min at 4 °C and resuspension in W5 buffer (154 mM NaCl, 125 mM $CaCl_2$, 5 mM KCl, 2 mM MES pH 5.7).

2.1.6 - Crossing of Arabidopsis

Arabidopsis plants were grown in long-day conditions for 5-8 weeks until inflorescences started appearing. Mature flowers with fully developed anthers on donor inflorescences of both parents were opened using tweezers. Closed buds on recipient inflorescences of

both parents were also opened using tweezers. Cross-pollination was achieved by separating the donor flower from the inflorescence using tweezers, and physically rubbing it onto the opened recipient flower for several seconds. Pollinated buds were marked using colored tape and plants were returned to long-day conditions. Seeds were harvested from pollinated siliques, and selected by germination on MS media with appropriate antibiotics.

2.2 - Transformation and transfection systems

2.2.1 - Generation of Arabidopsis transgenic plants

Arabidopsis was transformed using the floral dipping method (Bent, 2006) using *Agrobacterium tumefaciens* strain GV3101. Transformations were performed by Matthew Smoker and Jodie Pike (The Sainsbury Laboratory, Norwich, UK). Transformants were selected by germination on soil, growing for 1 week under short day conditions and spray application of phosphinothricin (PPT)/BASTA herbicide (Melford cat. P0159). At 2 weeks of age, survivors were transplanted into invidual 4 cm x 4 cm pots and recovered for 1 additional week. Confocal microscopy was used to confirm expression of fluorescent proteins, and T1 plants were used for experiments and propagation.

2.2.2 - Transfection of Arabidopsis by particle bombardment

Adult leaf tissue was subjected to particle bombardment for transient expression of fluorescent tagged proteins. Purified plasmid DNA (2 µg) was coated onto 125 µg gold particles (⌀ = 1.0 µm) using 1 M $CaCl_2$ and 20 mM spermidine, and washed with 100 % ethanol. Three separated Arabidopsis leaves were placed on solid Murashige and Skoog (MS) medium adaxial side up, and petioles making contact with the medium. A pressurized helium-based particle delivery system (Bio-Rad Biolistics PDS-1000) was used to deliver gold particles into distal leaf tissue at optimized pressure (1100 or 900 psi) and height. Transfected leaves on MS were incubated on a bench top at room temperature overnight, and a scalpel was used to prepare tissue for microscopic analysis.

2.2.3 - Arabidopsis protoplast transfection

Protoplasts were transfected using poly-ethylene glycol (PEG). Briefly, 100-150 µg plasmid DNA was added to a 2 mL suspension of ca. 5 x 10^5 protoplasts mL^{-1} in MMg buffer (4 mM MES pH 5.7, 0.4 M mannitol, 15 mM $MgCl_2$). Then, 2 mL PEG buffer (40% v/v PEG4000 (Sigma cat. 81240), 0.4 M mannitol, 0.2 M $CaCl_2$) was mixed in, and the transfection was allowed to continue for 10 minutes at room temperature. After one wash

with excess W5 buffer, pellets were resuspended in 2 mL W5 buffer and kept at room temperature overnight. On day 2, protoplasts were used for confocal microscopy or excess liquid was removed and protoplasts were flash-frozen in liquid nitrogen in preparation for protein extraction.

2.2.4 - *Agrobacterium tumefaciens* mediated transformation of *N. benthamiana*

A. tumefaciens strains GV3101 and GV3101 carrying the helper plasmid PMP90RK were grown for 2-3 days under appropriate selection at 28 °C in 10 mL liquid L-medium shaking at 120 rpm, or on solid L-medium 1 % agarose plates without shaking. Liquid cultures were spun down at 3000 x *g* for 5 minutes, and pellets were resuspended in dH_2O. From plates, bacteria were harvested using a spatula and resuspended in distilled water (dH_2O). Bacteria were washed 1 x with dH_2O and dilutions were adjusted to OD_{600} = 0.3 for each strain, in preparation for (co-)infiltration. Acetosyringone was added to a final dilution of 250 µM, and bacterial suspensions were syringe-infiltrated in *N. benthamiana* leaves.

2.2.5 - Virus-induced gene silencing in *N. benthamiana*

Tobacco rattle virus (TRV)-mediated VIGS in *N. benthamiana* was performed as follows. *A. tumefaciens* GV3101 carrying *TRV-RNA1* (pYL155) at OD_{600} = 0.4 and GV3101 carrying *TRV-RNA2* (pYL279) containing the respective target sequence at OD_{600} = 0.2 were co-infiltrated in leaves of 2-week old *N. benthamiana* plants. *TRV-RNA1* alone, or *TRV-RNA2::GUS* (Tameling and Baulcombe, 2007) was used as a control. At 4-5 weeks of age, plants were used for further analysis.

2.3 - DNA techniques and molecular cloning

2.3.1 - Primers used in this study

Name	Sequence	nt	Purpose
Cf-9-TOPO-F	CACCATGGATTGTGTAAAACTTGTA	25	Cf-9 TOPO cloning
Cf-9-nostop-R	ATATCTTTTCTTGTGCTTTTTC	22	
BAK1-TOPO-F	CACCATGGAACGAAGATTAATGATC	25	BAK1 TOPO cloning
BAK1-TOPO-R	TTATCTTGGACCCGAGGGGTATTC	24	
TN3-Ftopo	CACCATGGCTGCATCTACTTCTTCT	25	AT1G66090 / TIR-NBS 3 cloning
TN3-Rnostop	TACAAAATCAGCCAGAGACAC	21	
HR4-Ftopo	CACCATGCCGATTGCTGAGCTTGCT	25	AT3G50480 / HR4 cloning
HR4-Rnostop	TTTATTATGCTTTTCAGATAT	21	
FLOT1a-CDNA-F	TTGGGCGAAAAGTCCAAATTAAATCAAA	28	FLOT1 cDNA-specific amplification
FLOT1a-CDNA-R	CACAAGTAAACGACCAAACCATGCCACT	28	
FLOT-Ftopo	CACCATGTTCAAAGTTGCAAGAGCG	25	AT5G25250 / FLOT1 cloning
FLOT-Rstop	TTAGCTGCGAGTCACTTGCTTC	22	
PUB-GW-F	TGATTACGAATTCGAGCTCGG	21	amplify cassette from pUB-DEST
PUB-GW-R	GGCCCGACGTCGCATGCCTGC	21	
F-LP	GAAACTTCGATTGGGGAAGAC	23	SALK_018440.56.00.x (tn3) g.typing
F-RP	GTGGCAAAGCTTATGGTGAAG	23	
J-LP2	GGGATCGAATCGGTAAGCTC	20	SALK_208828 (hr4) g.typing
J-RP2	GGCTTAGATGATGGGCCTTA	20	
YFPn-F	GTGACCACCCTGGGCTACGG	20	sequencing pAM-PAT YFPc/n fusion
YFPc-F	CATTTGGAGAAGGACCTCGAG	21	
YFPn-R	GGCGGACTTGAAGAAGTCGT	20	
YFPc-R	GTCACGAACTCCAGCAGGAC	20	
M13-F	GTAAAACGACGGCCAG	16	sequencing pENTR and pGEM-T
M13-R	CAGGAAACAGCTATGAC	17	
GFP-R	CGAGGGTGGGCCAGGGCACGGG	22	sequencing binary vectors
RFP-R	CAGCTTGATGTCGGTCTTGTAGGCG	25	sequencing binary vectors

2.3.2 – Plasmids used in this study

(see next page)

Name	Vector	Origin
p35S:Cf-4-eGFP	pBIN-KS	Liebrand et al., 2012
p35S:SlSOBIR1-eGFP	pBIN-KS	Liebrand et al., 2013
p35S:SlSOBIR1-like-eGFP	pBIN-KS	Liebrand et al., 2013
p35S:AtSOBIR1-eGFP	pBIN-KS	Liebrand et al., 2013
p35S:SlSOBIR1-mCherry	pAM-PAT	Postma et al., 2016
p35S:AtSOBIR1-mCherry	pAM-PAT	Postma 2016 NPhyt
p35S:SlSOBIR1-HA	pGWB14	Postma 2016 NPhyt
p35S:AtSOBIR1-10Myc	pGWB20	Liebrand et al., 2013
p35S:AtSOBIR1-RD/N-10Myc	pGWB20	Liebrand et al., 2013
p35S:SlSERK3-10Myc	pGWB20	Postma et al., 2016
pFLS2:FLS2-GFP	pCAMBIA2300	Robatezek et al., 2006
pUB:BAK1-KD	pUB-GW	Postma et al., 2016
pUB:TN3-eGFP	pUB-GW-eGFP	Present study
pUB:TN3-mRFP	pUB-GW-mRFP	Present study
pGEM-T-pUB:TN3-eGFP	pGEM-T Easy	Present study
pUB:HR4-eGFP	pUB-GW-eGFP	Present study
pUB:eGFP-FLOT1	pUB-eGFP-GW	Present study
p35S:Avr4	pMOG1048	van der Hoorn et al. 2000
p35S:YFPc-ARA7/RABF2b	pAM-PAT	Present study
p35S:YFPn-ARA7/RABF2b	pAM-PAT	Present study
p35S:TN3-YFPc	pAM-PAT	Present study
p35S:TN3-YFPn	pAM-PAT	Present study
p35S:ARA6/RabF1-YFPc	pAM-PAT	Present study
p35S:YFPc-ARA5/RABD2a	pAM-PAT	Michaela Kopischke
p35S:YFPc-RABG3b	pAM-PAT	Michaela Kopischke
p35S:Cf-4-YFPc	pAM-PAT	Postma et al., 2016
p35S:Cf-4-YFPn	pAM-PAT	Postma et al., 2016
p35S:SlSOBIR1-YFPc	pAM-PAT	Postma et al., 2016
p35S:SlSOBIR1-YFPn	pAM-PAT	Postma et al., 2016
p35S:SlSOBIR1-like-YFPc	pAM-PAT	Postma et al., 2016
p35S:SlSOBIR1-like-YFPn	pAM-PAT	Postma et al., 2016
p35S:AtSOBIR1-YFPc	pAM-PAT	Postma et al., 2016
p35S:AtSOBIR1-YFPn	pAM-PAT	Postma et al., 2016
p35S:FLS2-YFPc	pAM-PAT	Frei dit Frey et al., 2012
p35S:FLS2-YFPn	pAM-PAT	Frei dit Frey et al., 2012
pUB:mCherry-ARA7/RabF2b	pNIGEL	Geldner et al., 2009
pUB:mCherry-MEMB12	pNIGEL	Geldner et al., 2009
pUB:mCherry-ARA5/RABD2a	pNIGEL	Geldner et al., 2009
pUB:eYFP-ARA5/RABD2a	pNIGEL	Geldner et al., 2009
p35S:ARA6/RABF1-RFP	pHTS13	Ueda et al., 2004
pUB:VHAa1-RFP	pUBQ10	Dettmer et al., 2006
p35S:ACA8-mCherry		Postma et al., 2016
Px-RK (peroxisome)	pBIN20	Nelson et al., 2007
Mt-RK (mitochondrion)	pBIN20	Nelson et al., 2007
RxD460V	pB1	Bendahmane et al., 2002
BAX	p30B-TMV	Lacombe et al., 1999
TRV-RNA2:GUS	pyl156-TRV2	Temeling et al., 2007
TRV-RNA2:Cf-4	pyl156-TRV2	Liebrand et al., 2013
TRV-RNA2:NbSOBIR1/NbSOBIR1-like	pyl156-TRV2	Liebrand et al., 2012
TRV-RNA1	pyl156-TRV1	Liu et al., 2007
TRV-RNA2:NbSERK3a/b	pyl156-TRV2	Heese et al., 2007

2.3.3 - DNA extraction for Arabidopsis genotyping

Genomic DNA (gDNA) extractions were performed using a rough preparation method. From each plant at ca. 2-3 weeks of age, a leaf disc of ca. 0.25 cm^2 was obtained using cork borer. Tissue was submerged in 400 µL pre-heated extraction buffer (200 mM Tris pH 7.5, 250 mM NaCl, 25 mM EDTA, 0.5% SDS) and incubated at 65 °C for 20-30 minutes. Debris was removed by centrifugation at 16.000 x *g* for 10 minutes, and supernatant was transferred to a new tube. Equal volumes of pre-cooled isopropanol were added and incubated for 5 minutes at room temperature. Precipitated gDNA was pelleted by centrifugation at 16.000 x *g* for 15 minutes. gDNA was washed once with 70% EtOH and resuspended in water.

2.3.4 - Polymerase Chain Reaction for Arabidopsis genotyping

Polymerase chain reactions (PCR) were performed on newly acquired SALK mutant lines to test for the presence and homozygosity of T-DNA insertions. 20 µL Taq polymerase reactions were set up, containing 2 µL of gDNA samples prepared as above. Per mutant plant, two reactions were set up. Forward and reverse primers flanking the predicted T-DNA insertion site were used to test for the presence of the wildtype sequence. To test for the presence of the SALK pBIN-pROK2 T-DNA insertion, insertion-specific primer LBb1.3 was used in combination with a forward or reverse flanking primer, depending on the predicted orientation of the T-DNA insertion. PCRs were ran for 32 cycles with an elongation time of 2 minutes, and 10 µL of the samples was used for ethidium bromide agarose gel electrophoresis.

2.3.5 - RNA extraction and cDNA-preparation

Arabidopsis and *N. benthamiana* RNA was extracted using the RNeasy Plant Mini kit (QiaGen cat. 74904) and eluted in 50 µL RNAse-free water. In both cases, ca. 1 cm^2 tissue was used, and Arabidopsis was treated with flg22 by leaf infiltration 3 hours prior to extraction. DNA was digested using a Turbo DNA-free kit (Ambion cat. AM1907), and RNA concentrations were measured using a NanoDrop 8000 spectrophotometer (ThermoFisher cat. ND-8000-GL) and up to 2 µg per reaction was used for cDNA synthesis using SuperScript III reverse transcriptase (ThermoFisher cat. 18080093) in the presence of RNAse Out (ThermoFisher cat. 10777019). cDNA was stored at -20 °C.

2.3.6 - Cloning and colony PCR

PCR was used to clone gene fragments using Phusion High Fidelity polymerase (New England Biolabs cat. M0530S), or to test the presence or absence of sequences using

Taq polymerase produced in the lab by heterologous expression in *E. coli*. Reactions contained 1x Phusion Buffer or Taq buffer (New England Biolabs cat. M0273S), 0.5 mM dNTP, 5 U/µL Phusion polymerase, 0.1 volume of lab-produced Taq polymerase, 10 µM primer DNA, and a variable concentration of input DNA. Reactions were performed in 200 µL PCR strips in a thermal cycler (G-Storm cat. GS4) with a default cycle number of 30 and annealing temperature of 56 °C, both subject to optimization for each experiment. Cloning (Phusion) and genotyping (Taq) reactions were set up to run 5 initial cycles with a lower annealing temperature of 50 °C. Colony PCRs (cPCR), on bacterial cells picked from colonies with a pipette tip, were preceded by a 5 minutes 90 °C melting step to release template DNA into the reaction.

2.3.7 - Gateway entry cloning

Desired gene fragments were amplified using Phusion PCR from either cDNA, existing expression vectors, or bacterial cells carrying the template DNA. Forward primers were extended with the CACC sequence at the 5' end to allow directional cloning. Reverse primers omitted the stop codon when amplifying fragments for C-terminal fluorescent protein tagging. 50 µL Phusion PCRs were performed and 20-30 µL of the product was used for gel electrophoresis. Bands of the expected size were identified, excised using a scalpel and purified using a NucleoSpin gel and PCR clean-up kit (Macherey Nagel cat. 740609.50).

1-4 µL of pure PCR product was mixed with 1 µL pENTR/d-TOPO vector (Invitrogen K2400-20) and incubated for 1 hour at room temperature. The full ligation reaction was added to 30 µL chemocompetent *E. coli* DH5α cells, and heat-shock transformation was performed for 1 min at 42 °C. cPCR-identified positive colonies were grown in liquid culture, plasmids were purified using a NucleoSpin Plasmid Miniprep kit (Macherey Nagel cat. 740588.50) and sent for sequencing (GATC Biotech) with the universal M13F/R primers. Detected sequences were compared to expected sequences using web-hosted Clustal Omega Multiple Sequence Alignment (EMBL-EBI).

2.3.8 - Gateway binary vector generation

To transfer coding sequences from pENTR/d-TOPO into destination vectors, Gateway LR reactions were performed with LR Clonase II Enzyme mix (ThermoFisher cat. 11791020). Enzyme mix was thawed on ice from -80 °C, spun down briefly at 10.000 x *g,* and used in a downscaled LR reaction with 50-100 ng entry vector and 200-300 ng binary destination vector. The reaction was incubated overnight at room temperature, and transfected into chemocompetent *E. coli* cells.

Coding sequences were transferred into binary destination vectors containing the Arabidopsis ubiquitin-10 (UB) promoter (untagged, GFP, RFP; Grefen et al. 2010), pAM-PAT-based vectors with the Cauliflower Mosaic Virus 35S promoter (mCherry; unpublished, GenBank AY436765, provided by Ralph Panstruga), or pAM-PAT-based 35S vectors for bimolecular fluorescence complementation (BiFC, split-YFP) encoding fusions with the YFP N- and C-termini (YFPn, YFPc; Bernoux et al. 2008).

2.3.9 - Generation of protoplast expression vectors

In order to generate short backbone expression vectors for use in protoplast transfection, the pGEM-T Easy vector system (Promega cat. A1360) was used. pUB-driven binary vectors containing the desired expression cassettes were used as a template. Vector backbone-universal primers were designed to amplify the expression cassette including promoter, coding sequence, fluorescent protein sequence and terminator. The PCR products were ran on gel, and fragments of expected size were excised and purified. In preparation for mounting into pGEM-T Easy, a single-nucleotide adenine extension was added to the fragments in a 30 minute 80 °C reaction using Taq polymerase in the presence of $MgCl_2$ and dATP. 3 µL of the reaction product was supplemented with rapid ligation buffer, pGEM-T Easy linearized vector (Promega) and T4 DNA ligase (New England Biolabs cat. M0202S), and incubated for 1 hour at room temperature. The resulting ligation was mixed with 30 µL chemocompetent *E. coli* DH5α cells for transformation and selection. Colonies were selected based on IPTG/X-Gal blue-white selection, and successful ligation was confirmed by sequencing with universal M13 F/R primers.

2.3.10 - DNA gel electrophoresis

Gel electrophoresis was performed on 1 % agarose Tris/Borate/EDTA (TBE) gels. Samples were mixed with 0.1 volume of loading dye (50% glycerol, bromophenol blue) before loading 10 µL into gel slots, alongside a 2-log DNA size marker (New England Biolabs cat. N3200S). Electrophoresis was ran at 100 V for 30 minutes or until desired separation of ladder and/or fragments. Gel pictures were obtained using a Gel-Doc XR with UV-illumination (Bio-Rad cat. 1708195) and printed for documentation.

2.3.11 - *Escherichia coli* transformation

DNA plasmids were introduced into chemocompetent *Escherichia coli* DH5α cells using heat shock. Briefly, a 50 µL aliquot of cells was defrosted from -80 °C on ice and mixed with 0.5 µL purified plasmid (50-100 ng) in water. After 20 minutes incubation on ice, cells were subjected to heat shock at 42 °C for 1.5 minutes in a thermomixer (Eppendorf cat.

5355000038). Cells were cooled on ice for 1 minute, and 500 µL L-media was added, and allowed to recover for at least 1 hour at 37 °C and 120 rpm shaking. 50 µL and 450 µL were plated on L-agar plates with appropriate selection. 1 day after transformation, positive colonies were tested with cPCR.

2.3.12 - *Agrobacterium tumefaciens* transformation

Binary vectors were introduced into electrocompetent *Agrobacterium tumefaciens* GV3101 cells carrying helper plasmids pMP90 or pMP90RK (for PAM-PAT-based vectors and mCherry vector). 30 µL aliquots of cells were thawed on ice and mixed with 50-100 ng plasmid DNA. The mixture was transferred to a cuvette and transfected at 2.4 kV / 200 Ω using a Gene Pulser Xcell electroporation system (Bio-Rad cat. 1652666). Cells were recovered in 500 µL L-media for at least 2 hours at 28 °C and 120 rpm shaking. 50 µL and 450 µL were plated on L-agar plates with appropriate selection. 2-3 days after transformation, positive colonies were tested with cPCR.

2.4 - Protein biochemistry

2.4.1 - Protein purification from *N. benthamiana*

Samples from fully expanded mature leaves of *N. benthamiana* plants were obtained using a cork borer no. 3 (⌀ = 1 cm) and added to tubes with 2 steel beads (⌀ = 3.2 mm) and crude total protein extraction buffer (40 mM TRIS pH 7.5, 6 % SDS, 50 mM DTT, 0.5 mM PMSF, 50 % glycerol, bromophenol blue, 1 % plant protease inhibitor cocktail (Sigma cat. P9599)). Tissue was homogenized in a TissueLyser (MM200, Retsch) for 1 minute at 30 Hz. Tubes were centrifuged at 16000 x *g* for 20 minutes to pellet debris, and supernatant was transferred to a new tube, heated at 70 °C for 10 minutes and used in SDS-PAGE.

2.4.2 - Co-immunoprecipitation from *N. benthamiana*

Immunoprecipitation (IP) and co-IP experiments from *N. benthamiana* were performed with GFP-trap beads (ChromoTek cat. GFP-Trap_A) or Myc-trap beads (ChromoTek cat. Myc-trap_A). Briefly, tissue was flash-frozen in liquid nitrogen and homogenized with steel beads in a TissueLyser. 0.5 g powder was measured in tubes and suspended in 2 mL IP-buffer B (50 mM Tris pH 7.5, 150 mM NaCl, 5 % glycerol, 1 mM EDTA, 1 % IGEPAL/NP-40, 5 mM DTT, 1 % plant protease inhibitor cocktail (Sigma cat. P9599), 1 % phosphatase inhibitor cocktail 2 (Sigma cat. P5726), 1% phosphatase inhibitor cocktail 3 (Sigma cat. P0044) and 0.5 mM PMSF). Samples were gently mixed, filtered through miracloth (Merck Millipore cat. 475855), and centrifuged at 16000 x *g* for 30 min. 1.5 mL

cleared lysate was transferred to a Protein LoBind 1.5 mL tube and 20 µL IP bead slurry was added. IP was performed at 4 °C for 2.5 h rotating, and beads were washed three times with IP buffer B. Immunoprecipitated proteins were released in Laemmli buffer (50 mM Tris, 50% glycerol, 4% SDS, 1% plant protease inhibitor cocktail (Sigma cat. P9599), 1 M DTT, 0.5 mM PMSF, bromophenol blue) by heating for 10 min at 70 °C, and used for SDS-PAGE.

2.4.3 - Ligand treatment of Arabidopsis seedlings

Arabidopsis thaliana seedlings were flask-grown in 200 mL liquid medium for 8 days as described above, and treated with flg22 peptide or water control. For treatments, 1 mL of liquid medium was removed from the flask and used to resuspend a 30 µl stock of 10 mM flg22 peptide (aiming for a final treatment at a concentration of 1.5 µM) or 30 µL water as a control, upon which the resulting mixture was returned to the flask. Flasks were swirled by hand and placed in a vacuum chamber. Vacuum was created using a pump for 90 seconds, and released over the course of 3 minutes. Flasks were then returned to the growth chamber to shake at 120 rpm for 3 hours. Liquid media was poured off, seedlings were then rinsed with an excess of dH_2O once and retrieved from the flask onto tissue paper using a metal spoon. Seedlings were dabbed with tissue paper to remove excess liquid, wrapped in aluminium foil, flash-frozen in liquid nitrogen and either used immediately or stored at -80 °C for later use.

2.4.4 - Protein purification from Arabidopsis seedlings

Flash-frozen seedlings were ground into a powder by pestle and mortar, and 15 grams of powder was mixed with 70 mL IP-buffer A (HEPES-NaOH 100 mM pH 7.5, 10 mM EDTA, 10 mM EGTA, 7.5 mM KCl, 17.5 % Sucrose, 0.01 % NP40/IGEPAL, 10 mM DTT, 1 % plant protease inhibitor cocktail (Sigma cat. P9599)). The mixture was agitated for ca. 5-10 minutes at 4 °C, filtered through miracloth, and distributed equally across two 50 mL tubes (2 x ca. 35 mL). Filtrate was centrifuged at 5000 x *g* for 20 minutes at 4 °C to pellet remaining debris, and the clear lysate was transferred to 2 clean 50 mL tubes.

2.4.5 - Immunoprecipitation from Arabidopsis seedlings

To a total of 70 mL clear lysate, after removing 500 µL to use as ‘input’ sample, 60 µL of GFP-Trap bead slurry was added. The precipitation was allowed to continue for 2.5 hours under roll-shaking at 4 °C, and beads were recovered by centrifugation at 500 x *g* for 5 minutes. Beads were transferred to 1.5 mL Protein LoBind Tubes (Eppendorf cat. 0030108116) and sequentially washed with 5 x 1 mL IP buffer A, allowing equilibration of

3 minutes after each addition of fresh IP buffer A. Excess liquid was removed using a needled syringe, and samples were stored at -80 °C for later use.

2.4.6 – Protein extraction and immunoprecipitation from Arabidopsis protoplasts

Protoplasts were transfected overnight and harvested by centrifugation, removal of excess liquid and flash-freezing in liquid nitrogen. To a pellet of frozen protoplasts, 1.5 mL of pre-cooled complete IP buffer A (as used for Arabidopsis seedlings) was added, and tubes were gently inverted several times at 4 °C until completely resuspended. The homogenate was then centrifuged at 5000 x *g* for 20 minutes at 4 °C to pellet debris, and 1 mL of clear supernatant was transferred to a Protein LoBind tube. To the clear lysate, 20 µL of GFP-trap bead slurry was added, and the immunoprecipitation was performed as described above for Arabidopsis seedlings.

2.4.7 - SDS-PAGE/Western blot with pre-cast gradient and home made gels

In preparation for SDS-PAGE, clear lysates from protein extractions were mixed with equal volumes of 2x extraction buffer (100 mM Tris, 60% glycerol, 8 % SDS, 2 % plant protease inhibitors (Sigma cat. P9599), 1M DTT, 2% PMSF, bromophenol blue). To samples containing IP beads, 100 µL 1X Laemmli buffer was added. In both cases, samples were heated at 70 °C for 10 minutes, centrifuged at 500 x *g* for 1 minute, and loaded onto acrylamide gels.

For loading of IP samples used in mass spectrometry, 1 mm 4–20% acrylamide gradient Mini-PROTEAN TGX Precast Protein Gels (BioRad) were used. For all other samples, gels were prepared in two parts: stacking gel (4.5 % acrylamide, 0.15 M Tris, 0.1 % SDS, 0.5% APS, 0.5% TEMED) and running gel (10 % acrylamide, 0.35 M Tris, 0.1 % SDS, 0.5% APS, 0.5% TEMED). 20 µL of each sample was loaded onto 15-slots gels, 30-40 µL was loaded onto 10-slots gels.

Electrophoresis was performed at 80 V for 10 minutes, followed by 100-120 V until the green front escaped the gel and molecluar weight markers (PageRuler Plus prestained protein ladder, ThermoFisher cat. 26619) were sufficiently expanded. Proteins were then transferred to a PVDF membrane using semi-dry transfer (TransBlot transfer cell, Bio-Rad cat. 1703940) for 1 hour at 25 V, and blocked for at least 1 hour and up to 1 day using Tris-buffered saline (TBS, 50 mM Tris-Cl, pH 7.5. 150 mM NaCl) containing 0.1 % surfactant (Tween, polysorbate-20, Sigma cat. P1379) and 5% milk powder (Marvel UK, dried skimmed milk) at 4 °C.

2.4.8 - Antibody treatment of PVDF membranes

The PVDF membrane containing proteins was rinsed once in TBS-Tween 0.1% (TBST). Antibodies were premixed with TBST / 5% milk in the appropriate dilution factor, and applied to the membrane in a square petri dish. Antibody treatments proceeded for at least 1 hour subject to optimization. For primary/secondary antibody systems, the membrane was washed 3 x 10 minutes in TBST between antibodies. In all cases, after the final antibody treatment the membrane was washed 2 x 10 minutes with TBST and 1 x 10 minutes with TBS.

2.4.9 - Conjugated antibody signal detection

The membrane was transferred to a transparent plastic sheet and 500 µL substrate was applied. For horse radish peroxidase (HRP)-conjugated antibodies, Pierce ECL Western Blotting Substrate (ThermoFisher cat. 32106) or SuperSignal West Femto Maximum Sensitivity Substrate (ThermoFisher cat. 34095) was used, covered with a second plastic sheet, and incubated in the dark for 5 minutes. For alkaline-phosphatase (AP)-conjugated antibodies, CDP-Star substrate (ThermoFisher cat. T2304) was diluted 1:100 in AP-buffer (100 mM NaCl, 100 mM Tris, 50 mM $MgCl_2$, 1% Tween).

Excess substrate was dripped off the membrane, which was then sandwiched between clean plastic sheets, and signal was captured using light sensitive X-ray film (Fujifilm cat. Super RX) by incubation for variable, optimized periods of time. Light sensitive films were developed in a dark room, and digitized using an office USB scanner at 300 dots per inch. Finally, total proteins were stained using Ponceau S (Ponceau S 0.1% w/v, acetic acid 5%) and destained with dH_2O, or stained with InstantBlue (Expedeon cat. ISB1L) coommassie blue and destained in 20% methanol, 5 % acetic acid until bands of interest were clearly discernible.

2.5 - Mass spectrometry

2.5.1 - Tryptic digest from gradient gel fragments

Protein samples obtained by immunoprecipitation from Arabidopsis seedlings were run on pre-cast 4-20% gradient SDS-PAGE gels, allowing one free lane between samples to prevent cross-contamination. Gels were then stained using InstantBlue (Expedeon) Coomassie staining until a band at ca. 55 kDa, corresponding to the expected molecular weight of YFP-ARA5 / YFP-ARA7, was visible, and then destained using dH_2O. Using a scalpel, each lane containing proteins was excised and further cut into five individual samples: one narrow segment around the intense band at ca. 55 kDa, and four more

segments resulting from cutting the remaining gel material above and below ca. 55 kDa in halves. The five samples were assigned to 1.5 mL Eppendorf Protein LoBind tubes, then further mashed with a scalpel and stored at -20 °C or used immediately.

Gel samples were washed/destained twice with acetonitrile (AcN)/ammonium bicarbonate (ABC), and dried with 100% AcN for ca. 15 minutes. Disulfide bonds were reduced using 10 mM dithiotriol (DTT) in ABC for 30 min at 56 °C shaking. Cysteines were alkalized using 55 mM chloroacetamide in ABC for 30 minutes in the dark. Samples were washed (AcN/ABC) and dried (AcN), and 100 ng Trypsin (Promega) in 40 µL AcN/ABC was added to initiate tryptic digest. After ca. 5 min, 60 µL dH_2O was added to fully submerge samples, and the reaction was incubated overnight at 37 °C. Peptides were retrieved with three washes of 100 µL 5% formic acid / 50% AcN with 10 min sonication, and transferred to a new Protein LoBind tube.

2.5.2 - OrbiTrap Fusion run and spectral matching

LC-MS/MS analysis was performed using a hybrid Orbitrap Fusion mass spectrometer, fed by nanoflow UHPLC (ThermoScientific). Tryptic peptides were injected onto a reverse phase trap column connected to an analytical column (Acclaim Pepmap 100, ThermoScientific). They were eluted with a 9-50% gradient of acetonitrile across 50 minutes, followed by a 50-60% gradient over 30 min at a flow rate of 300 nL/min. MS events consisted of an initial full scan using the Orbitrap analyser, followed by a collision-induced dissociation and higher-energy collisional dissociation maximizing the chance to acquire ions. Orbitrap Fusion software settings were as follows: resolution = 120000, m/z range = 300-1800, maximal infusion time = 50 ms, and automatic gain control was set for target 200000 ions. The precursor dissociation events were driven by the data dependent algorithm function with dynamic exclusion 30 s after the collision is triggered. Only precursor ions with positive charge states 2-7 and intensity threshold greater than 10000 were selected for fragmentation.

Peak lists in the form of Mascot generic files (mgf files) were prepared from raw data using MS Convert (Proteowizard project) and sent to peptide match search on Mascot server v2.4.1 using Mascot Daemon (Matrix Science Ltd.). Peak lists were searched against protein databases including typical protomics contaminants such as keratin. Tryptic peptides with up to two possible miscleavages and charge states +2 to +4 were allowed in the search. Data were searched with a monoisotopic precursor and fragment ion mass tolerance of 10 ppm and 0.6 Da respectively. Mascot results were combined in Scaffold 4.4.0 (Proteome Software Inc.), filtered to retain proteins with PeptideProphet lower limit of 95% confidence, and ProteinProphet lower limit of 99% confidence. At least

2 identified peptides per protein were required. Results were exported to MS Excel (Microsoft Office).

2.5.3 - Filtering criteria to define proteomes

A Microsoft Excel table was exported from Scaffold 4 (version 4.3.4 20140611, ProteomeSoftware), listing all Arabidopsis proteins and their detected number of spectra in any replicate of any treatment or genotype (pUB::YFP-ARA5 (ARA5), pUB::YFP-ARA7 (ARA7), pUB::YFP (YFP); water, flg22; replicates 1,2,3), with a minimum ProteinProphet confidence score of 99% and with 2 or more associated detected spectra.

A base proteome for ARA7 under water treatment was defined as follows. 1) Quality control: a protein must be detected in >1 replicates of ARA7-water, and the total of combined spectra found across all 3 replicates must be >5. 2) Comparison to YFP control: The total of combined spectra of a protein in Y7-water must be >4 fold greater than the total of combined spectra in YFP-water. A base proteome for ARA5-water was defined in the same way.

A list of proteins upregulated in ARA7 purifications under flg22-treated conditions was defined by applying the above quality control and YFP-control comparisons, now to spectral counts in flg22-treated samples only. Then, for each protein, the total of combined spectra in ARA7-flg22 must be >2 fold greater than the total in ARA7-water. ARA5 was analyzed in the same way.

In order to allow the above calculations with total spectral values across all three replicates that are 0, an arbitrary value of 0.000001 was added to all total spectral values. Enrichment factors, eg. $\log_{10}$ (ARA7-water / YFP-water), were calculated to capture bait specificity and fold change ratio between treatments.

2.6 - Bioassays and bacteria

2.6.1 - Bacterial strains used in this study

Species	Genotype	Source
Agrobacterium tumefaciens:		
GV3101	PMP90	Holsters et al., 1980
GV3101	PMP90 RK	Holsters et al., 1980
Pseudomonas syringae:		
pv. *tomato* DC3000		Whalen et al., 1991
pv. *tomato* DC3000	*cor*	Melotto et al., 2006
pv. *tomato* DC3000	*hrcC*	Boch et al., 2002
pv. *tomato* DC3000	*hrcC / pTac::mCherry*	Sebastian Pfeilmeier
pv. *tomato* DC3000	*pTac::mCherry*	Sebastian Pfeilmeier
pv. *tomato* DC3000	AvrRpt2	Mudgett et al., 1999
pv. *tabaci*		Gasson, 1980

2.6.2 - *Pseudomonas* spray inoculation

Soil-grown Arabidopsis plants at 4-5 weeks of age were covered with transparent lids one day in advance. *Pseudomonas syringae* was grown on a plate with rifampicin and further appropriate selection at 2 days in advance, harvested using a spatula, spun down at 3000 x *g* for 10 minutes, washed once in 10 mM $MgCl_2$ and diluted to OD_{600}=0.2 (1 x 10^8 CFU mL^{-1}) in 10 mM $MgCl_2$. Prior to spray application, 0.04 % Silwet L77 (De Sangosse UK) was added to the bacterial suspension, and the mixture was transferred to a spray bottle. Bacteria were then inoculated onto Arabidopsis leaves by spraying the top and bottom of the leaves evenly. Plants were covered with transparent lids and grown for 3 days under normal conditions.

2.6.3 - *Pseudomonas* inoculation by infiltration and induced resistance pretreatment

Soil-grown Arabidopsis plants at 4-5 weeks of age were covered with transparent lids one day before inoculation. For induced resistance assays, on the same day three fully expanded leaves per plant were marked and infiltrated with 10 µM flg22 peptide (QRLSTGSRINSAKDDAAGLQIA, EzBiolabs) or a water control. *Pseudomonas syringae* was pregrown on plate with rifampicin and appropriate selection 2 days before inoculation, harvested using a spatula, washed once in water and diluted to OD_{600} = 0.0002 (1×10^5 cfu mL^{-1}). Bacteria were then syringe-infiltrated into the abaxial side of marked Arabidopsis leaves. Plants were covered with transparent lids and grown for 3 days under normal conditions.

2.6.4 - Quantifying bacterial proliferation in dilution series

Using a cork borer, ca. 0.75 cm^2 tissue was harvested from three leaves per plant and placed into 200 µL of $MgCl_2$ 10 mM together with two steel beads (⌀ = 3.2 mm). Tissue was homogenized at 30 Hz for 2 minutes using a TissueLyser (MM200, Retsch) and transferred into 96-wells plates. A dilution series using $MgCl_2$ 10 mM was set up, and 10 µL of dilution factors 10^{-1}, 10^{-2}, 10^{-3} and 10^{-4} were plated on square L-media plates supplemented with rifampicin and nystatin. After 24-48 hours of incubation at 28 °C, colony numbers in all dilution spots were counted by hand and data was analyzed in Microsoft Excel. Using data from the lowest dilution factor with individually discernible colonies, the number of colony forming units (CFU) per cm^2 of originally harvested leaf tissue was calculated and averaged over the number of plants used. Means were compared to each other using one-way ANOVA and labeled in significance grouping using a post-hoc Tukey's HSD test.

2.6.5 - Hypersensitive response assays in *N. benthamiana*

Cladosporium fulvum Avr4 and Avr2 were heterologously produced in *Pichia pastoris* and purified using the His-affinity tag (Dirk-Jan Valkenburg, Laboratory of Phytopathology, Wageningen UR, The Netherlands). *N. benthamiana* plants were subjected to VIGS at 2 weeks of age, and were used for hypersensitive response assays at 4-5 weeks of age. Purified effector proteins were infiltrated at 300 µM, or expressed through *A. tumefaciens* mediated transformation alongside positive controls RxD460V (Bendahmane et al., 2002) and BAX (Lacomme and Santa Cruz, 1999). HR phenotypes were recorded 3-6 days after infiltration.

2.7 - Light microscopy

2.7.1 - Confocal laser scanning microscopy

Confocal laser scanning microscopy (CLSM) was performed using a Leica SP5 upright microscope fitted with hybrid (HyD) detectors. Objectives used in this study are: 63 × 1.20 NA water immersion; 40 × 0.85 NA air; 20 × NA 0.50 air. For multi channel image acquisition, line sequential scanning and 3x line averaging was used. Z-stacks were acquired over 10 µm, in steps of 1 µm. Excitation and detection wavelengths were adjusted for each fluorophore.

The Leica Image Format (LIF) files were exported from the Leica Application Suite Advanced Fluorescence (LAS-AF, version 1.6.3 build 1163, Leica), processed in FIJI (FIJI Is Just ImageJ, versions from 2013-2018) and annotated in Microsoft Powerpoint.

2.7.2 – Fluorescent probes used in this study

Probe	Excitation (nm)	Detection (nm)
eGFP	488	495-540
eYFP	514	520-570
mRFP	561	570-630
mCherry	561	600-630
autofluorescence	-	700-800

2.7.3 - Automated high throughput spinning disc microscopy

Sample preparation and ligand treatment

Arabidopsis seedlings were grown on F2 soil for 14 days in a controlled environment chamber (CentiForce Fitotron SGC 120) at 22 °C and a regime of 12 hours light / 12 hours dark. Cotyledons were picked using tweezers and transferred adaxial side-up to the central 60 pins of a custom 96-pin rubber stamp (made by Simon Foster) using high-vacuum silicone grease as an adhesive (Sigma cat. Z273554-1EA).

An optical 96-wells plate (Greiner Bio-One cat. 655892) was prepared, adding 200 µL dH_2O to 30 wells left of centre, and 200 µL flg22 (10 µM) to 30 wells right of centre. The custom stamp with cotyledons was lowered into the optical plate, incubated bench-top at room temperature and used for high throughput confocal imaging at indicated time points (30, 90, 150 min).

Laser and acquisition settings

The Opera High Content Screening System (PerkinElmer) with a 40 × 0.90 NA water immersion objective was used for rapid image acquisition. For both GFP and YFP imaging, a solid state 488 nm laser at 4000 µW was used for excitation, and emission was captured between 502-577 nm. Images were captured with a CCD camera and an exposure time of 40 ms. For each cotyledon, z-stacks of 21 images were acquired at 5 locations successively. Cotyledons were scanned row-by-row, measuring 5 water treated wells and 5 flg22 treated wells in an alternating manner. Total acquisition time per optical plate was ca. 30 minutes.

Post processing

For automated spot detection, the resulting FLEX image files were processed using Single Channel Spot Detection v. 4.1 (by Ji Zhou, The Sainsbury Laboratory, Norwich, UK) for Acapella Studio (PerkinElmer, version 2.2.2.7338). Analysis was configured to require at least 70 % valid image area (less than 30 % dark area), a spot roundness of greater than 0.125 and a spot width-to-length ratio of greater than 0.425. The resulting annotations were visually inspected by taking an arbitrary sample of output images. Data was further processed in Microsoft Excel.

2.7.4 - Confocal microscopy in *N. benthamiana* tissues

Magnifications and focus stacking

For GFP localizations, GFP-RFP/mCherry colocalizations, and for GFP vesicle quantitation, the 63 × objective was used and z-stacks of 10 µm were obtained. For BiFC/split-YFP of vesicle localized signals, the 63 × objective was used and single images were obtained. For BiFC/split-YFP of plasma membrane localized reconstituted signal, pictures were taken with the 40 × objective to capture numerous cells per field of view.

Ligand treatments for receptor mediated endocytosis

100 µM of purified *C. fulvum* Avr4 or Avr2 dissolved in water were syringe-infiltrated into fully expanded mature *N. benthamiana* leaves. After 1 hour, 1 cm diameter leaf discs were obtained by cork borer and used for microscopic analysis. Stable expressing plants were treated at 4-5 weeks of age, and transiently expressing plants at 4-5 weeks of age were treated at 2 days after agroinfiltration.

Vesicle quantification

Images were acquired using 63 × magnification. The resulting LIF-files were processed using FIJI, and maximum projections of the combined GFP and autofluorescence channels were automatically generated using a custom macro (FileIO, by Ji Zhou). Spot quantification in z-projections was automated using adaptive intensity and color thresholding in EndoQuant v. 1.075 (by Ji Zhou) for Acapella Studio. The resulting annotations were visually inspected and data were processed in Microsoft Excel.

2.7.5 - Confocal microscopy in Arabidopsis tissues

Transgenic Arabidopsis plants were observed using the 63 × objective. Seedling cotyledons were picked using tweezers, and adult leaf tissue was obtained using a biopsy punch (⌀ = 2 mm). In both cases, abaxial sides were imaged. Transiently expressing protoplasts were transferred in a volume of 1 µL onto a microscope slide with reaction wells (Marienfeld cat. 1216521) and directly used for imaging. For particle bombardment, transfected cells were located through the binocular using a GFP filter cube at 20 × magnification, and images were acquired at 63 × magnification.

2.7.6 - Confocal imaging of focal accumulations

Introduction of bacteria

Pto DC3000 or Pto DC3000 *cor*, carrying a genomic insertion with constitutive promoter driven *pTac::mCherry* (generated by Sebastian Pfeilmeier) were grown on plate at 28 °C for 2 days, and incubated on bench top at room temperature for 1 day. Bacteria were harvested using a spatula, washed once with dH_2O, and resuspended at OD_{600} = 0.2. Bacterial suspensions were syringe-infiltrated into mature Arabidopsis leaves. Infiltrated plants were kept on bench top at room temperature for 5-6 hours, and samples were taken with a biopsy punch.

Image acquisition

For detailed, qualitative imaging of abaxial mesophyll, the Leica SP5 confocal microscope and 63 × magnification was used. Z-stacks were acquired starting from the epidermal equatorial plane up to 10-20 µm into the tissue, in steps of 1 µm. For image acquisition in preparation for quantification, single images of the first adaxial mesophyll layer at lower magnification of 20 × were acquired.

Quantification of focal accumulations with FIJI (script)

In order to quantify the number of focal accumulations per field of view, a custom macro for FIJI was written that applies the following functions to a series of 8-bit greyscale images: Gaussian blur (σ = 2 px), global threshold (grey value min. = 40, max. = 255), create mask, analyze particles (min. area = 20 px.), list number of particles. The results were further processed in Microsoft Excel. Mean values within experiments were statistically analysed using a Student's t-test comparing treatment to water.

CHAPTER 3

AVR4 PROMOTES CF-4 RECEPTOR-LIKE PROTEIN ASSOCIATION WITH THE BAK1/SERK3 RECEPTOR-LIKE KINASE TO INITIATE RECEPTOR ENDOCYTOSIS AND PLANT IMMUNITY

This chapter consists of an edited and expanded version of the following publication:

"Avr4 promotes Cf-4 receptor-like protein association with the BAK1/SERK3 receptor-like kinase to initiate receptor endocytosis and plant immunity"

Jelle Postma, Thomas W. H. Liebrand, Guozhi Bi, Alexandre Evrard, Ruby R. Bye, Malick Mbengue, Hannah Kuhn, Matthieu H. A. J. Joosten, Silke Robatzek

New Phytologist (2016) vol. 210, issue 2, p. 627-42, doi: 10.1111/nph.13802

The majority of the data are based on experiments performed by myself. Specific experimental contributions of co-authors are acknowledged in the main text as well as in figure legends.

RESULTS

3.1 - CF-4 AND SOBIR1 CO-INTERNALIZE UPON CF-4 ACTIVATION

3.1.1 - Cf-4 interacts with SOBIR1 at the plasma membrane

In order to study the dynamic subcellular localization of Cf-4 in antifungal immunity, I used the fluorescently tagged Cf-4-GFP construct which triggers a hypersensitive response in *N. benthamiana* upon perception of the *Cladosporium fulvum* effector Avr4 (**fig. S1;** Liebrand et al., 2012). I transiently expressed Cf-4-GFP with the plasma membrane marker Autoinhibitory Calcium ATPase 8 (ACA8, Frei dit Frey et al., 2012), and revealed by co-localization that Cf-4-GFP is present at the plasma membrane (**figs. 3.1, S2**), which corresponds to its predicted site of biological function in perceiving Avr4, which has been shown to be present in the apoplast (Joosten et al., 1994; van den Burg et al., 2006). In addition, the constitutive Cf-4-interacting RLK *Sl*SOBIR1 and its homologs *Sl*SOBIR1-like and *At*SOBIR1 also localized to the plasma membrane (**figs. 3.1-2, S2-4**), raising the possibility that Cf-4-SOBIR1 dimers are present at this location. To test for presence of Cf-4-SOBIR1 dimers, I co-expressed bimolecular fluorescence complementation (BiFC) fusion constructs of both, and revealed that Cf-4 and SOBIR1

reconstituted a signal at the PM as confirmed by colocalization with ACA8 (**fig. 3.1**). As a negative control, I co-expressed BiFC fusion constructs of *Sl*SOBIR1 and FLS2, and while both proteins could be expressed, they did not reconstitute a signal (**fig. S5**), corresponding to published data that SOBIR1 does not interact with RLK-type PRRs (Liebrand et al., 2013). Taken together, I conclude that Cf-4 and *Sl*SOBIR1 interact at the PM.

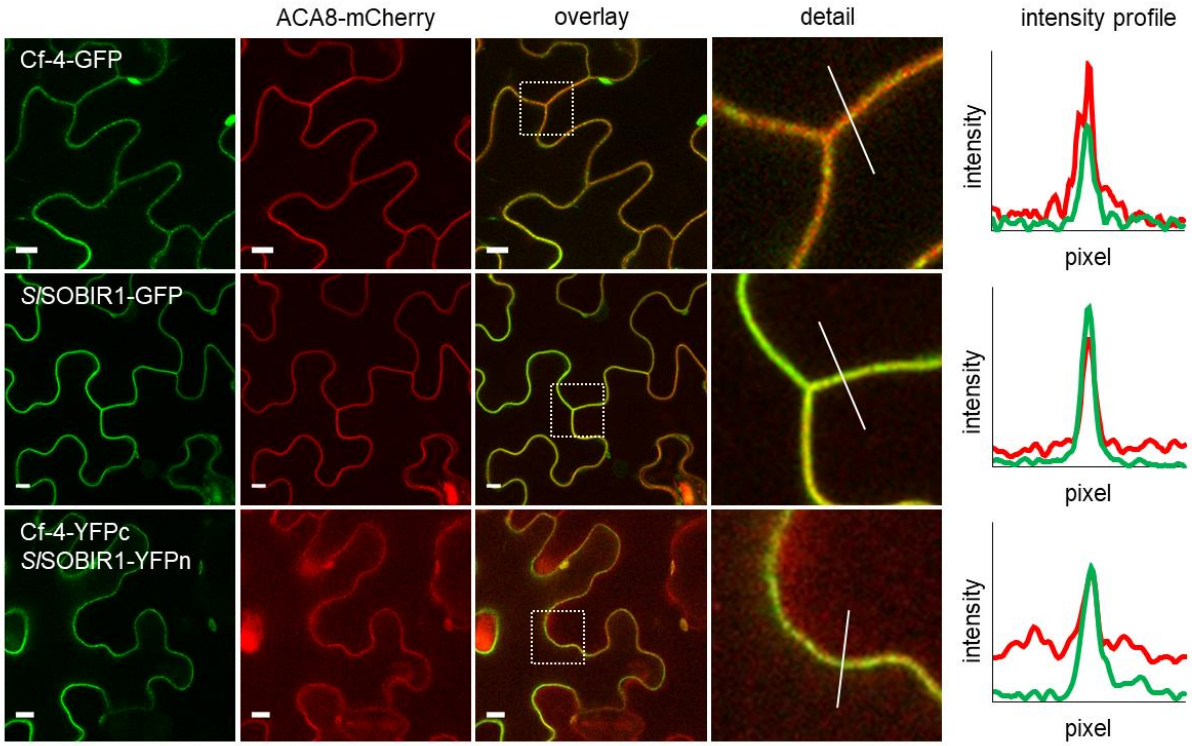

Fig. 3.1. Cf-4 and *Sl*SOBIR1 are present at the plasma membrane. Single z-plane confocal micrographs show *N. benthamiana* leaf epidermal cells transiently co-expressing the indicated Cf-4 and *Sl*SOBIR1 fusion proteins and plasma membrane-localized ACA8-mCherry. The first column of panels show GFP/YFP fluorescence, the second panels show mCherry fluorescence and the third column of panels depict the overlay images of the two fluorescence signals shown in the first and second panels. Overlay images indicate co-localization of the proteins fused to GFP or YFP and mCherry, as a yellow color is produced. Dashed squares in these images are shown as detailed pictures (magnified in the fourth column of panels). White lines in the detailed pictures indicate the regions of interest (ROIs) that correspond to the intensity profiles in the last column of panels. Intensity profiles indicate the grey-value of pixels across the ROI in the green and red channels, on a scale of 1-300. Images were taken at three days post infiltration (dpi) for Cf-4-GFP and *Sl*SOBIR1-GFP and at two dpi for BiFC of Cf-4, C-terminally fused to the C-terminal half of YFP (YFPc), with *Sl*SOBIR1 C-terminally fused to the N-terminal half of YFP (YFPn); scale bars = 10 µm.

3.1.2 - Avr4 triggers endocytosis of the Cf-4-SOBIR1 complex

Previously, *At*SOBIR1 has been shown to localize to FM4-64-positive vesicles, suggesting endosomal localization (Leslie et al., 2010b). To further probe the identify of SOBIR1-positive vesicles, I co-expressed the GFP-tagged tomato and Arabidopsis SOBIR1 homologs with a panel of RFP-tagged known endomembrane markers, which localize to Golgi (MEMB12), TGN/EE (VHA-a1), TGN/EE-LE/MVB (ARA7) and LE/MVB (ARA6). SOBIR1 punctae did not overlap with MEMB12 or VHA-a1, but did overlap with ARA7 and ARA6, confirming constitutive SOBIR1 localization to endosomes (**figs. 3.2, S3-4**).

Endosomal localization of cell surface receptors can be triggered by ligand perception (Mbengue et al., 2016; Ortiz-Morea et al., 2016; Beck et al., 2012b). Because Cf-4 interacted with SOBIR1 at the PM as shown in BiFC, and SOBIR1 constitutively localized to endosomes, I was prompted to test whether Cf-4 could also localize to endosomes upon activation by Avr4. To address this, I co-expressed Cf-4-GFP and *Sl*SOBIR1-mCherry in *N. benthamiana* and infiltrated the purified *C. fulvum* effector protein Avr4. I also infiltrated Avr2, which is not recognized by Cf-4, as a negative control. In untreated leaves, Cf-4-GFP localized to the PM, while *Sl*SOBIR1-mCherry localized to the PM and endosomes (**figs. 3.1, 3.3A**). Interestingly, Avr4 treatment triggered Cf-4-GFP localization to *Sl*SOBIR1-mCherry-positive vesicles, pointing at ligand-induced endocytosis (**figs. 3.3A, S6**). I could confirm the endosomal nature of Avr4-induced Cf-4-GFP compartments by co-localization with the LE/MVB-marker ARA6 (**fig. 3.3A**). Because Avr2 did not trigger internalization of Cf-4-GFP (**fig. 3.3A, S6**), I conclude that Cf-4 endocytosis is ligand-specific and dependent on receptor activation.

Because upon Avr4 treatment, Cf-4 and SOBIR1 localized at late endosomes, I hypothesized that they may be internalized in complex with each other. To investigate this, I co-expressed Cf-4 and SOBIR1 BiFC constructs, which reconstituted signal at the PM (**fig. 3.1**). Upon activation of Cf-4 by Avr4 treatment, but not upon Avr2 treatment, BiFC signal was also reconstituted at ARA6-positive LE/MVBs (**fig. 3.3B**), confirming ligand-induced endocytosis of the Cf-4-SOBIR1 heterodimer, which corresponds to Avr4-induced endosomal colocalization of Cf-4 and SOBIR1 (**fig. 3.3A**). Ligand-induced internalization of receptor heterodimers has been shown before for BRI1-BAK1/SERK3 in Arabidopsis protoplasts (Russinova, 2004). In contrast, upon co-expression of BiFC fusion constructs of FLS2 which revealed localization of homodimers to the PM, flg22-treatment could not induce internalization, suggesting the complex may be impaired in recruiting the BAK1/SERK3 co-receptor, which is required for ligand-induced FLS2 endocytosis (Chinchilla et al., 2007; Beck et al., 2012b).

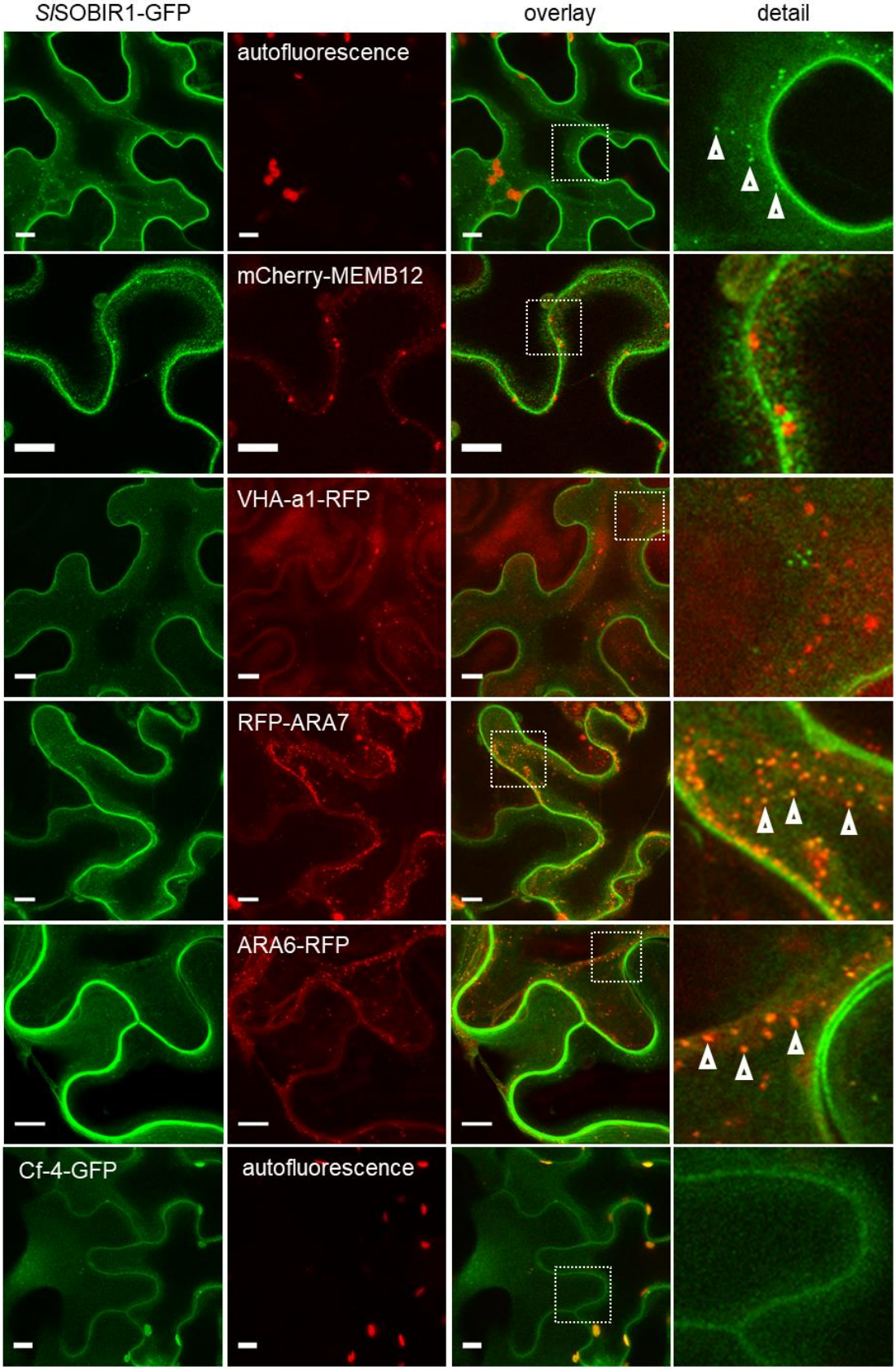
SlSOBIR1-GFP
autofluorescence
overlay
detail
mCherry-MEMB12
VHA-a1-RFP
RFP-ARA7
ARA6-RFP
Cf-4-GFP
autofluorescence

Fig. 3.2. *Sl*SOBIR1 constitutively localizes to endosomes. Maximum projections of confocal micrograph z-stacks show *N. benthamiana* leaf epidermal cells transiently expressing *Sl*SOBIR1-GFP or Cf-4-GFP (left panels), either without or with co-expression of the indicated organelle markers fused to mCherry/RFP (middle, left panels). Co-localization in the overlay images is depicted by the development of a yellow color (middle, right panels). Dashed squares in these images are shown as detail pictures (magnified in the right panels). Arrowheads in the detail pictures point at mobile vesicles in the upper right panel and indicate *Sl*SOBIR1 localization at endosomes in the two lower right panels. Images were taken at three dpi; scale bars = 10 µm.

3.1.3 - Cf-4 endocytosis requires functional BAK1/SERK3 and SOBIR1

Ligand-induced activation and endocytosis of FLS2 depends on BAK1/SERK3 (Beck et al., 2012b; Choi et al., 2013). Therefore, I hypothesized that ligand-induced endocytosis of Cf-4 shares the same requirement. To address this, in collaboration with Alexandre Evrard (The Sainsbury Laboratory, Norwich, UK), I used tobacco rattle virus (TRV)-based virus-induced gene silencing (VIGS) and knocked down the two endogenous tobacco *BAK1/SERK3* homologs *NbSERK3a/b* (Heese et al., 2007) and tested for the capacity for Avr4 to induce Cf-4-GFP endocytosis. Interstingly, upon Avr4 treatment, Cf-4-GFP endocytosis was reduced in *TRV::NbSERK3a/b* leaves as compared to *TRV*-control leaves (**figs. 3.4, S7**), while Cf-4-GFP accumulation levels were unaffected by *NbSERK3a/b* silencing (**fig. S7**). Upon *NbSERK3a/b* silencing, which did not affect the total number of ARA6 endosomes (**fig. 3.4**), transient co-expression of Arabidopsis BAK1/SERK3, could restore the capacity for Cf-4-GFP to internalize upon Avr4 treatment (**figs. 3.4, S7**). Cf-4-GFP internalization was dependent on the full functionality of BAK1/SERK3, as co-expression with the kinase-dead *AtBAK1-KD* could not restore Avr4-induced Cf-4-GFP accumulation at endosomes (**figs. 3.4, S7**). These data together provide evidence that both RLK and RLP-type cell-surface immune receptors share the functional requirement for the RLK BAK1/SERK3. Upon analysis by qRT-PCR, performed in collaboration with Ruby Bye (Laboratory of Phytopathology, Wageningen UR, The Netherlands), we could show that *TRV::NbSERK3a/b* silencing additionally co-silences a *NbSERK1* homolog, which indicates that Cf-4 endocytosis might additionally require SERK1.

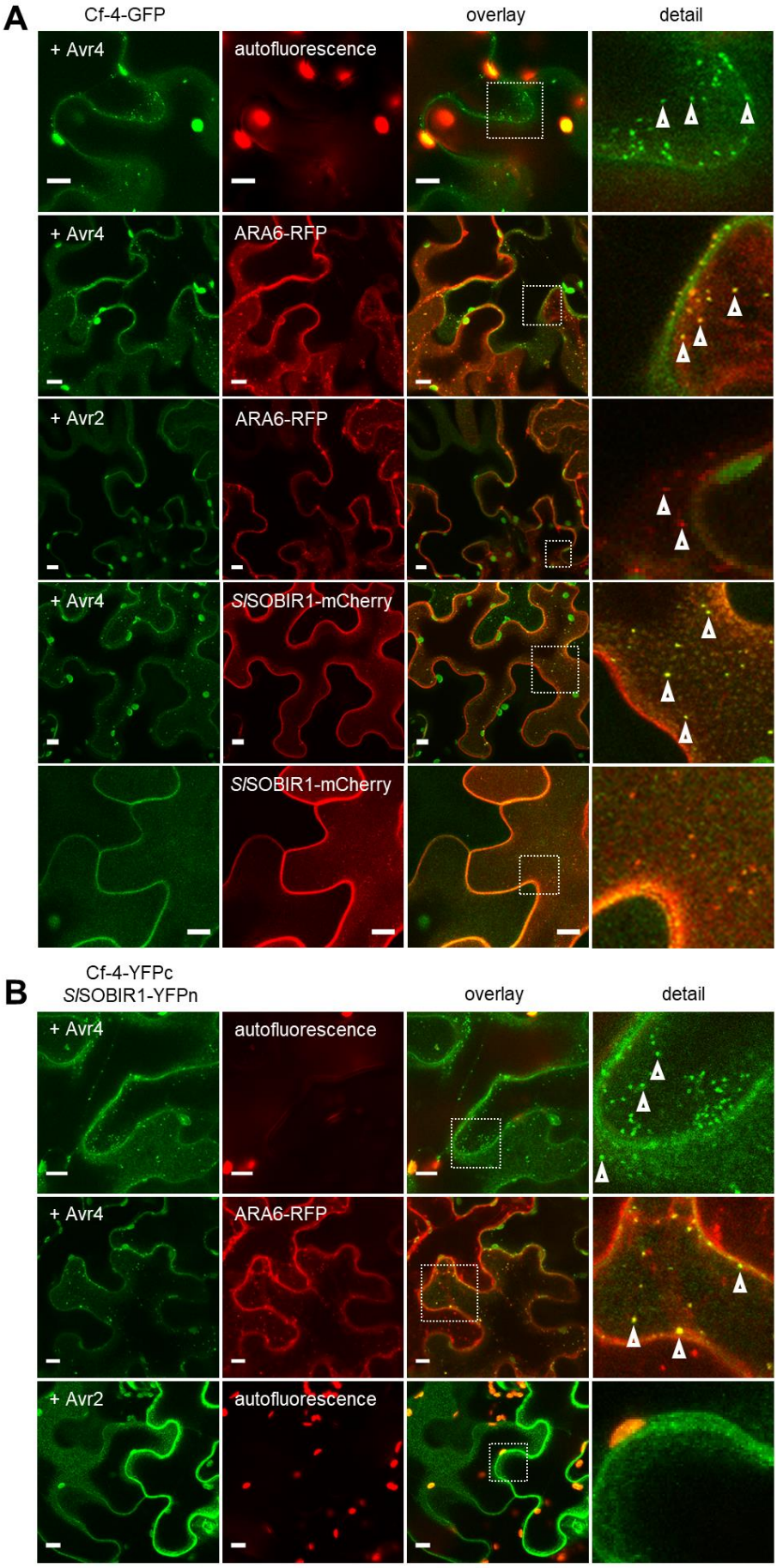
A
Cf-4-GFP
overlay
detail
+ Avr4
autofluorescence
+ Avr4
ARA6-RFP
+ Avr2
ARA6-RFP
+ Avr4
SlSOBIR1-mCherry
SlSOBIR1-mCherry
B
Cf-4-YFPc
SlSOBIR1-YFPn
overlay
detail
+ Avr4
autofluorescence
+ Avr4
ARA6-RFP
+ Avr2
autofluorescence

Fig. 3.3. Cf-4 localizes to endosomes in a ligand-dependent manner and together with *Sl*SOBIR1. (A) Confocal micrographs show *N. benthamiana* leaf epidermal cells transiently expressing Cf-4-GFP without and with co-expression of ARA6-RFP and *Sl*SOBIR1-mCherry, treated with Avr4 or Avr2 (both at 100 µM), as indicated. The left panels show GFP fluorescence, middle left panels show autofluorescence and RFP/mCherry fluorescence, middle right panels depict the overlay images of the two fluorescence signals shown in the left and middle left panels, and the right panels show detail pictures of the dashed squares. Arrowheads point at mobile vesicles positive for Cf-4-GFP and ARA6-RFP and indicate co-localization of Cf-4-GFP with ARA6-RFP and *Sl*SOBIR1-mCherry at endosomes. Images were taken at three dpi and 90 min after elicitation; scale bars = 10 µm. (B) Confocal micrographs show *N. benthamiana* leaf epidermal cells transiently expressing Cf-4, C-terminally fused to the C-terminal half of YFP (YFPc) and *Sl*SOBIR1, C-terminally fused to the N-terminal half of YFP (YFPn, left panels), without or with co-expression of ARA6-RFP (middle left panels) and treated with Avr4 or Avr2 (both at 100 µM), as indicated. Co-localization between reconstituted YFP and RFP in the overlay images is depicted by the development of a yellow colour (middle, right panels). Dashed squares in these panels are shown as detail pictures (right panels). Arrowheads point at mobile vesicles in the upper right panel and indicate co-localization at endosomes in the middle right panel. Images were taken at three dpi and 90 min after elicitation; scale bars = 10 µm.

Because SOBIR1 is required for Cf-4-mediated HR and immunity (Liebrand et al., 2013), and I could show that it internalized from the PM in complex with Cf-4 upon Avr4 treatment, I hypothesized that it may be required for Cf-4 endocytosis. It has been shown that SOBIR1 is required for the tissue-level accumulation of Cf-4 (Liebrand et al., 2013), and indeed upon *TRV*-mediated silencing of the *N. benthamiana* homologs *NbSOBIR1* and *NbSOBIR1-like*, I observe a reduction in fluorescent signal of Cf-4-GFP, which can be restored upon complementation by affinity tagged *At*SOBIR1-Myc or the kinase dead variant *At*SOBIR1-KD-Myc (**fig. S8A,C**). Interestingly, only co-expression with *At*SOBIR1-Myc, and not *At*SOBIR1-KD-Myc, could restore Avr4-induced Cf-4-GFP internalization, indicating that this requires fully functional SOBIR1 (**fig. S8A,B**).

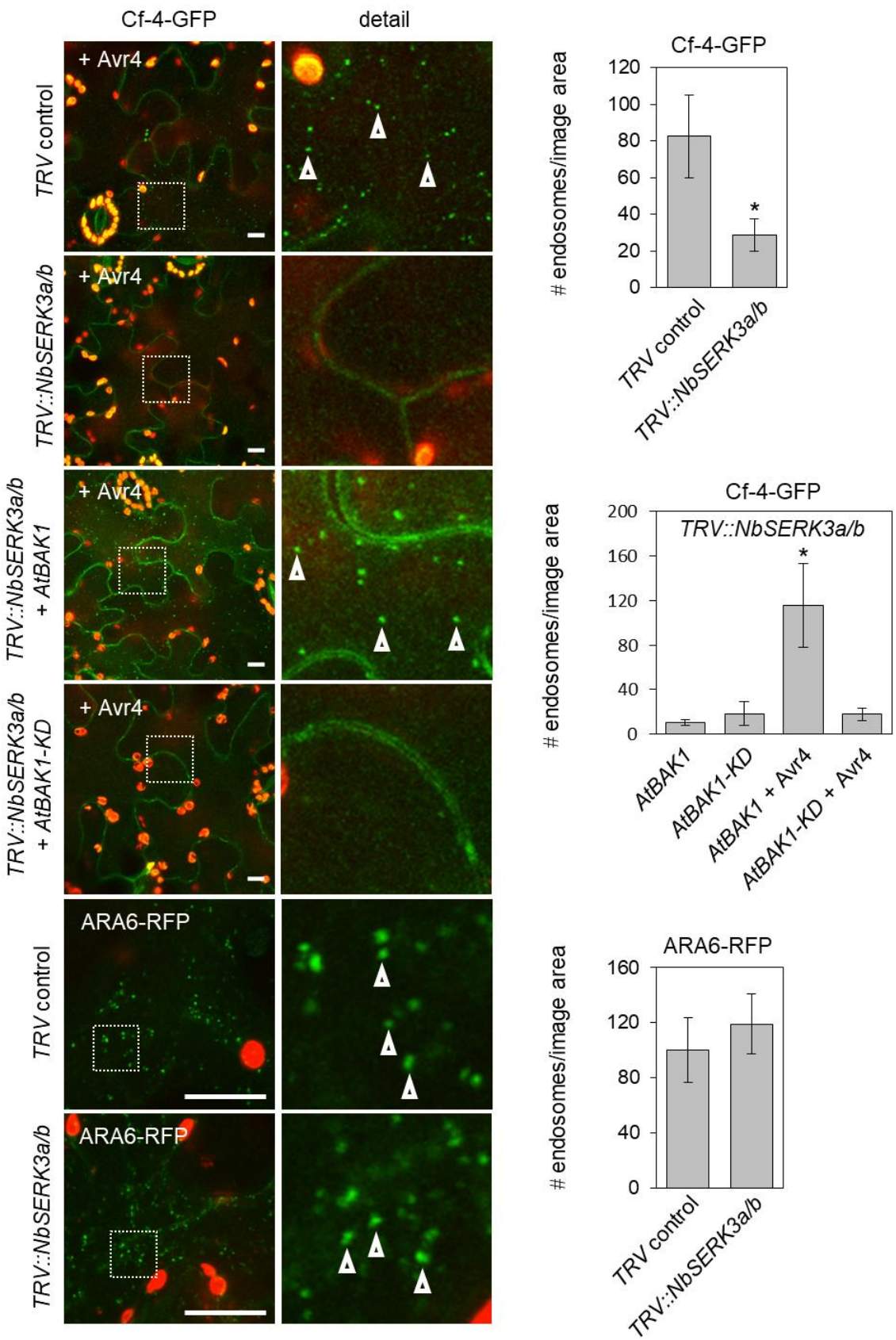
Cf-4-GFP
detail
+ Avr4
TRV control
TRV::NbSERK3a/b
TRV::NbSERK3a/b + AtBAK1
TRV::NbSERK3a/b + AtBAK1-KD
ARA6-RFP
endosomes/image area
Cf-4-GFP
120
100
80
60
40
20
0
*
TRV control
TRV::NbSERK3a/b
Cf-4-GFP
TRV::NbSERK3a/b
200
160
120
80
40
0
*
AtBAK1
AtBAK1-KD
AtBAK1 + Avr4
AtBAK1-KD + Avr4
ARA6-RFP
160
120
80
40
0
TRV control
TRV::NbSERK3a/b

Fig. 3.4. Cf-4 endocytosis requires BAK1/SERK3. Leaves of Cf-4-GFP-*N. benthamiana* stable and wild type *N. benthamiana* plants were TRV-silenced for *NbSERK3a/b* and *GUS* as a control for three weeks and subsequently used to transiently express *At*BAK1, *At*BAK1-KD, and ARA6/RabF1-RFP as indicated for three days. Confocal micrographs show Cf-4-GFP localisation upon treatment with Avr4 (100 µM, left panels) and ARA6/RabF1-RFP-labelled endosomes (left panels), and detail pictures from dashed squares (middle panels). Arrowheads point at Cf-4-GFP- and ARA6/RabF1-RFP-positive vesicles. Quantification of Cf-4-GFP- and ARA6/RabF1-RFP-positive vesicles was done with EndoQUANT (right panels, bars depict means ± 2 SE; n = 6; $p < 0.05$; statistical significant differences are indicated by asterisks). Note that much fewer Cf-4-GFP-positive vesicles are observed in *NbSERK3a/b*-silenced leaves compared to the *TRV*-silenced control. The amount of Cf-4-GFP-positive vesicles increased upon transient co-expression of *At*BAK1/SERK3 but not when its kinase-inactive variant *At*BAK1-KD was co-expressed. No difference in the amount of ARA6/RabF1-RFP-positive endosomes was observed when *NbSERK3a/b* was silenced. Images were taken 90 min after Avr4 elicitation; scale bars = 10 µm. See Fig. S.7 for transcript abundance of silenced genes and protein levels of Cf-4. The above microscopy experiments were performed in collaboration with Alexandre Evrard.

3.2 - CF RLPS RECRUIT SERK FAMILY RLKS UPON ACTIVATION

3.2.1 - Cf-4 recruits BAK1/SERK3 and SERK1 upon activation

Well-studied RLK-type PRRs such as FLS2 and EFR recruit BAK1/SERK3 upon ligand perception (Roux et al., 2011). Having established that both Cf-4 and FLS2 endocytosis share the requirement for BAK1/SERK3 in endocytosis, I addressed a possible role for BAK1/SERK3 in Cf-4-mediated immunity using biochemical interaction studies, performed in collaboration with Thomas Liebrand and Guozhi Bi (Laboratory of Phytopathology, Wageningen UR, The Netherlands). We performed transient co-expression of Cf-4-GFP, *Sl*SOBIR1-HA and *Sl*SERK3a-Myc in *N. benthamiana*, treated the leaves with Avr4, Avr2 or flg22, and purified either Cf-4-GFP or *Sl*SERK3a-Myc using immunoprecipitation. In all conditions, *Sl*SOBIR1-HA co-purified with Cf-4-GFP as revealed by western blot (**figs. 3.5, S9**), corresponding to their known constitutive interaction and the reconstitution of signal in BiFC experiments (**fig. 1;** Liebrand et al., 2013). In addition, upon pulldown of *Sl*SERK3a-Myc, *Sl*SOBIR1-HA co-purified under all conditions, which contrasts with the findings of Liebrand et al., 2013, who did not detect *Sl*SERK3a-GFP in *Sl*SOBIR1-Myc purifications. This may be explained by the use of biochemical methods with different sensitivities, but it is conceivable that *Sl*SOBIR1 and *Sl*SERK3a interact through another RLP.

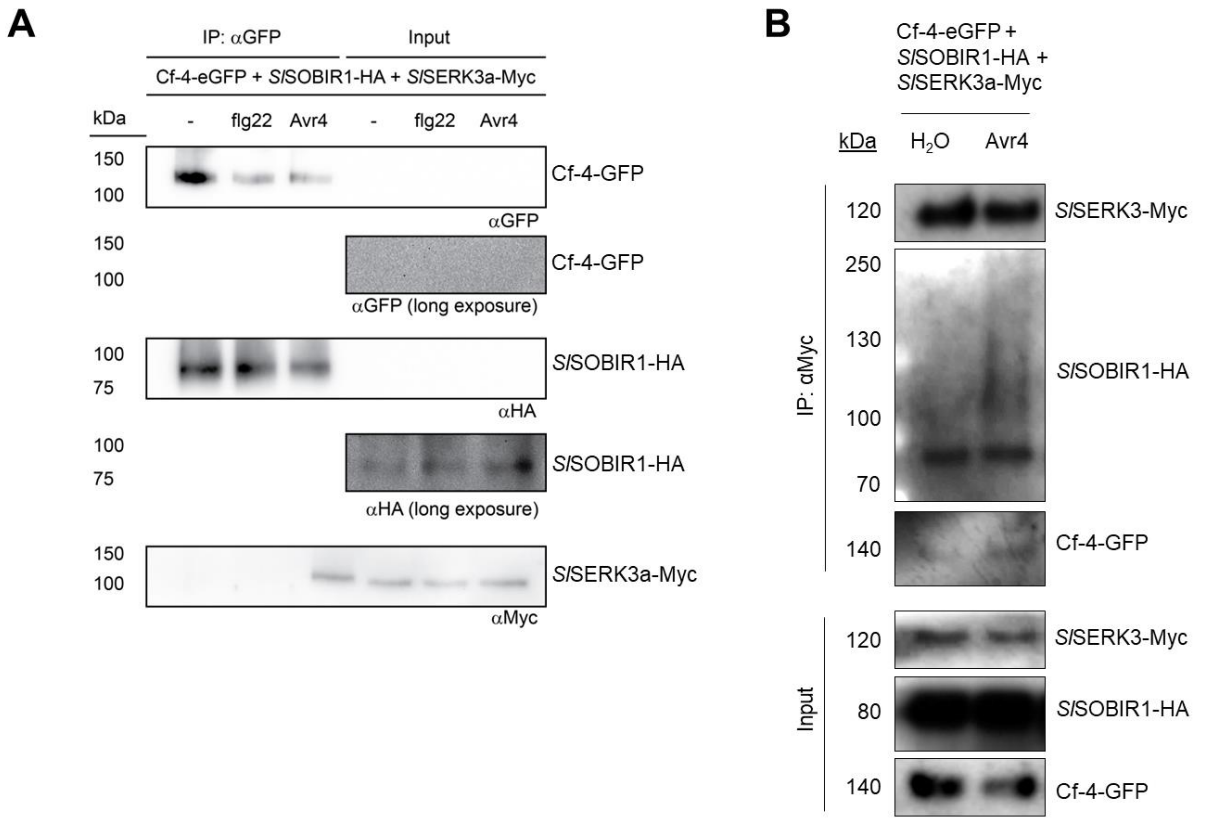

Fig. 3.5. *Sl*SERK3a interacts with Cf-4. (A) Co-immunoprecipitation from GFP-trap bead pull-downs on *N. benthamiana* co-expressing Cf-4-GFP, *Sl*SOBIR1-HA and *Sl*SERK3a-Myc. Leaf samples were taken at two dpi, after 60 min treatments without or with 10 µM flg22 or 100 µM Avr4, as indicated. Total proteins (input) and immunoprecipitated proteins (IP) were subjected to SDS/PAGE and blotted. Blots were incubated with αGFP, αHA or αMyc antibodies for the detection of immunoprecipitated Cf-4-GFP and co-purifying *Sl*SOBIR1-HA and *Sl*SERK3a-Myc, respectively. Note that differences in the amount of immunoprecipitated Cf-4-GFP in the mock treatment, as compared to Avr4 and flg22 treatments, were not observed across replicates (Fig. S.14). These GFP-trap immunoprecipitation experiments were performed by Thomas Liebrand (B) Co-immunoprecipitation from Myc-trap bead pull-downs on *N. benthamiana* co-expressing Cf-4-GFP, *Sl*SOBIR1-HA and *Sl*SERK3a-Myc. Leaf samples were taken at two dpi, after 15 min treatments without or with water (H_2O) or 100 µM Avr4, as indicated. Total proteins (input) and immunoprecipitated proteins (IP) were subjected to SDS/PAGE and blotted. Blots were incubated with αMyc, αHA or αGFP antibodies for the detection of immunoprecipitated *Sl*SERK3a-Myc and co-purifying *Sl*SOBIR1-HA and Cf-4-GFP, respectively, and proteins were detected using a method with increased sensitivity as compared to panel (A).

Interestingly, only upon Avr4 treatment, and not Avr2 or flg22 control treatments, did *Sl*SERK3a-Myc co-purify with Cf-4-GFP (**figs. 3.5A, S9**). Conversely, *Sl*SERK3a-Myc purifications were enriched in Cf-4-GFP in Avr4 treated samples compared to water treatment (**fig. 3.5B**). Taken together, these data point at ligand-induced heterodimerization as is observed for RLK-type PRRs (Monaghan and Zipfel, 2012). Interestingly, upon purification of *Sl*SERK3a-Myc from Avr4

treated samples, we observed a “smear” pattern migrating at higher molecular weights of co-purifying *Sl*SOBIR1-HA, providing evidence of Avr4-induced posttranslational modifications on the *Sl*SERK3a-interacting pool of *Sl*SOBIR1-HA.

3.2.2 - Cf-4 and Cf-9 both recruit SERK members upon activation

It has previously been shown that another SERK member, *Sl*SERK1, is genetically required for Cf-4 mediated resistance in tomato (Fradin et al., 2011). Therefore, we addressed whether Cf-4 similarly recruits SERK1 upon activation. Upon purification of Cf-4-GFP, we could reveal *Sl*SERK1-Myc already interacting under Avr2 control treated conditions, but observed a marked enhancement of co-purifying *Sl*SERK1-Myc in Avr4 treated leaves (**fig. S9**). While in this expression system *Sl*SERK1-Myc accumulated to higher levels than *Sl*SERK3-Myc, possibly explaining ectopic interactions with Cf-4-GFP, it is also possible that Cf-4 exists in a preformed complex with *Sl*SOBIR1 and *Sl*SERK1, which upon activation of Cf-4 becomes stabilized and recruits additional *Sl*SERK3a.

Cf-4 is highly homologous to Cf-9, which detects *C. fulvum* Avr9 (Thomas et al., 1997). To investigate whether SERK recruitment might be a more generalized mechanism by which RLPs initiate immune signaling, we purified Cf-9-GFP from leaves additionally co-expressing *Sl*SOBIR1-HA and either *Sl*SERK3a-Myc or *Sl*SERK1-Myc, under Avr9 treatment or Avr4 control treatments. As a result, we observed that similar to Cf-4, *Sl*SERK3a-Myc and *Sl*SERK1-Myc strongly co-purified with Cf-9-GFP only upon activation by Avr9 (**fig. S10**). Taken together, these data suggest that other SOBIR1-dependent RLPs may similarly recruit SERK family members to initiate signaling, as has recently been shown for ELICITIN RESPONSE (ELR) and RLP23 (Albert et al., 2015; Du et al., 2015).

3.3 - SERK MEMBERS MEDIATE AVR4-TRIGGERED IMMUNITY

3.3.1 - Cf-4 hypersensitive response requires SERK members

Upon activation by Avr4, Cf-4 triggers HR in *N. benthmiana* which could be suppressed upon silencing of *NbSOBIR1* and *NbSOBIR1-like* (**fig. 3.6A;** Liebrand et al., 2013). Because *Sl*SERK3a was recruited to Cf-4 upon activation by Avr4, and was required for Cf-4 endocytosis, I hypothesized that *Nb*SERK3a might also be involved in immune signaling of Cf-4. To address this, in collaboration with Thomas Liebrand and Ruby Bye, we silenced *NbSERK3a/b* using VIGS, and revealed that this significantly reduced Avr4-triggered HR in *N. benthamiana* stably expressing Cf-4, whereas Avr4 could consistenly induce HR in *TRV* control inoculated Cf-4 plants (**figs. 3.6A, S7**). The capacity for *NbSERK3a/b*-silenced plants to initiate HR was not generally affected, as this was still induced by the autoactive NLR RxD460V and pro-apoptotic factor BCL2-ASSOCIATED PROTEIN X (BAX; Lacomme and Santa Cruz, 1999; Bendahmane et al., 2002).

Because *TRV::NbSERK3a/b* inoculation also affected transcript abundance of *NbSERK1* as measured in qRT-PCR (**fig. S7**), it is conceivable that Avr4-triggered HR may require *NbSERK1*, which would be in line with the published finding that full Cf-4 mediated immunity to *C. fulvum* in tomato required *SlSERK1* (Fradin et al., 2011).

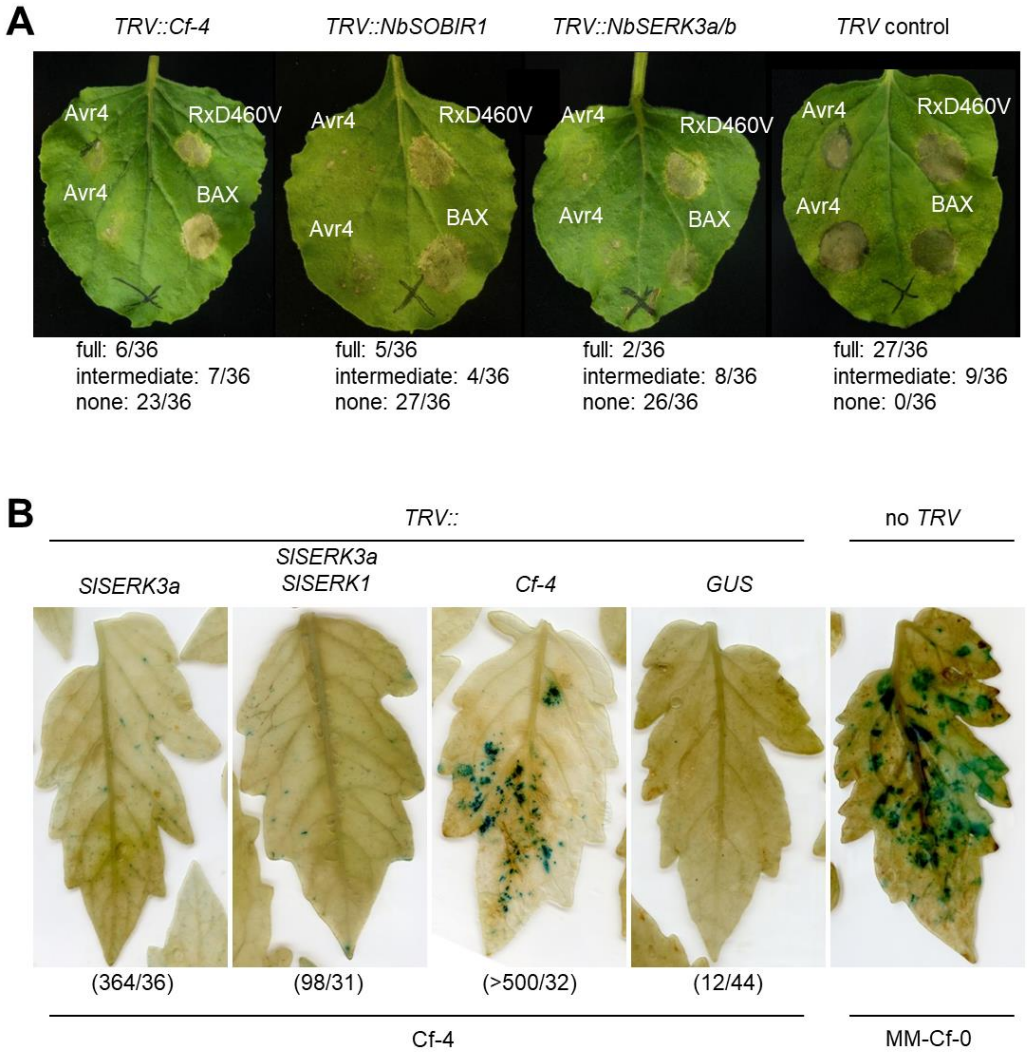

Fig. 3.6. *Sl*SERK3a is required for Avr4-triggered HR and immunity against *C. fulvum*. (A) Leaves of transgenic *N. benthamiana* plants stably expressing Cf-4-GFP that had been *TRV*-silenced for either *Cf-4*, *NbSOBIR1*, *NbSERK3a/b* or for *GUS* as control, and were subsequently *A. tumefaciens*-infiltrated with Avr4 (OD_{600} = 0.03), RxD460V (OD_{600} = 0.1) and BAX (OD_{600} = 0.5) as indicated. Images were taken three days after *A. tumefaciens* infiltration. HR is observed as brownish cell death. The numbers below the panels indicate the occurrence of full HR, intermediate or no symptoms out of 36 Avr4 *A. tumefaciens* infiltrations that were performed. (B) Leaves two weeks after inoculation with an Avr4-secreting, *GUS*-transgenic strain of *C. fulvum* of MM-Cf-0 tomato as a control, and Cf-4 tomato that had been inoculated with recombinant *TRV* constructs targeting *Cf-4*, *SlSERK3, SlSERK1* or *GUS* three weeks earlier. To visualize *C. fulvum* colonization, leaves were stained for GUS activity. The amount of successful colonization attempts (blue spots) versus the total amount of Cf-4 leaves that were sampled is indicated between parentheses. The above infection and HR assays were performed by Ruby Bye, Thomas Liebrand and Guozhi Bi.

3.3.2 - Cf-4-mediated resistance in tomato requires *Sl*SERK3

To investigate whether BAK1/SERK3 is required for Cf-4-mediated resistance in tomato, collaborating with with Thomas Liebrand and Ruby Bye, we silenced *SlSERK3* individually, or *SlSERK3a* together with *SlSERK1* using VIGS, and tested for colonization success of *C. fulvum* carrying Avr4 and the GUS reporter gene. In both cases, *C. fulvum* colonized leaves more strongly than in *TRV* control leaves, as evidenced by increased GUS staining and subsequent quantification (**fig. 3.6B**). Because silencing of Cf-4 itself even further increased *C. fulvum* colonization success (**fig. 3.6B**), it is possible that VIGS only partially knocks down the expression of *SlSERK3* and *SlSERK1* allowing for some Cf-4 activation, and/or that there is functional redundancy between thes two SERKs. These data together show that BAK1/SERK3 is a key positive regulator of full Cf-4-mediated immunity upon Avr4 perception.

DISCUSSION

3.4 - Cf-4 and SOBIR1 work with SERKs to initiate immunity and receptor endocytosis

The Cf signaling pathway is essential for the immune response of tomato to *C. fulvum* (Stergiopoulos and de Wit, 2009; Rivas and Thomas, 2005). A number of Cf signaling components were identified through genetic and proteomic approaches, but the mechanism by which Cf-4 initiates downstream signaling remained unclear (Liebrand et al., 2014). In the present study, I show that both SERK1 and SERK3 are recruited to the Cf-4 receptor in an Avr4-responsive manner, a mechanism that was additionally confirmed for Avr9-induced activation of Cf-9.

Consistently, I show that Cf- 4 requires these RLKs for its function in order to initiate HR and restrict fungal colonization as silencing of the respective genes in *N. benthamiana* and tomato suppresses Avr4-induced HR symptom formation and facilitates fungal penetration, respectively. My observations imply that Avr4 enhances the formation of a complex of Cf-4 and *Sl*SERK1/3 to induce Cf-4 signaling. Furthermore, I confirm that Cf-4 interacts with SOBIR1 at the plasma membrane and, could demonstrate ligand-induced SERK3-dependent late endocytic trafficking of the Cf-4 RLP together with *Sl*SOBIR1 as a novel pathway in Cf-mediated downstream events.

3.5 - Ternary receptor complexes form

The finding that Cf-4 and SOBIR1 are present in complex and recruit additional RLKs to form multimeric complexes upon activation is in agreement with existing data on RLP-SOBIR1 systems. *Solanum microdontum* (wild tomato) ELICITIN RESPONSE (ELR) is an RLP that detects the MAMP elicitin, and recruits SERK3 upon activation, while ELR maintains interaction

with SOBIR1 independent of activation status (Domazakis et al., 2018; Du et al., 2015). Furthermore, Arabidopsis RLP23, which activates upon binding of the MAMP Nep1-like protein (NLP)-derived peptide nlp20, interacts with SOBIR1 independent of activation status, and recruits BAK1/SERK3 upon activation (Albert et al., 2015). However, the above data, including from the present study, were obtained from tissue-level biochemical analyses, and cannot fully exclude that separate pair-wise interactions between RLP-SOBIR1 and RLP-SERK3 may exist. It would be interesting to more precisely address this question through RLP-purification and subsequent non-denaturing gel electrophoresis, or with *in vivo* fluorescence-based association assays.

3.6 - Different SERKs may do the job

In my experiments, Cf-4 associated with SERK1 before activation, and more strongly upon Avr4 treatment (**fig. S9**). In addition, SERK1 has been shown to be required for full Cf-4 immunity in tomato (Fradin et al., 2011). The recruitment and requirement of multiple SERK members has been shown in existing studies on RLPs dependent on SOBIR1. Arabidopsis RLP23 interacted with SOBIR1 and SERK4 before activation, and recruited increased amounts of SERK1, SERK2, SERK3 and SERK4 upon activation by nlp20 (Albert et al., 2015). Additionally, SERK members showed functional redundancy in mediating RLP23 associated outputs (Albert et al., 2015). On the other hand, Arabidopsis RESPONSIVENESS TO BOTRYTIS POLYGALACTURONASES 1 (RBPG1)/RLP42, which interacts with SOBIR1 and triggers HR upon detection of fungal endopolygalacturonase, did not recruit SERK3 and did not depend on SERK3 for HR (Zhang et al., 2014a).

The well-characterized RLK-type PRRs FLS2 and EFR also recruit multiple SERKs upon activation, or interact with SERK members at steady state. FLS2 interacted with Arabidopsis SERK1, SERK2, BAK1/SERK3 and BKK1/SERK4 upon expression in *N. benthamiana* before activation, and upon activation FLS2 most strongly recruited BAK1/SERK3, but also recruited additional SERK1 and SERK2 (Roux et al., 2011). Similarly, EFR recruited equal amounts SERK1, SERK2, BAK1/SERK3 and BKK1/SERK4 upon activation (Roux et al., 2011), but for most FLS2 and EFR outputs, BAK1/SERK3 is the major contributor (Schwessinger et al., 2011). As observed for RLPs, there are SERK3-independent outputs, as evidenced by the capacity for *bak1* mutants to trigger elevated SA-levels and PEN3 cell-surface focal accumulation upon activation of FLS2 by flg22 (Underwood and Somerville, 2013; Yamada et al., 2016).

These data taken together, for both RLP-SOBIR1 activation, as well as PRR-based cell-surface immune activation, the requirements for specific SERK members can vary. Since I could restore Avr4-induced Cf-4 endocytosis in *NbSERK3a/b* and partial *NbSERK1*-silenced plants through expression of the singular Arabidopsis BAK1/SERK3, I hypothesize that this member is the major

determinant for Cf-4 triggered outputs, but its ability to complement Cf-4 HR and full tomato immunity to *C. fulvum* remains to be demonstrated.

3.7 - Cf-4-SOBIR1 as a two-component PRR

The requirement of SERK members hints at clear similarities between the Cf-4/Cf-9 effector receptors and FLS2 MAMP receptor pathways, further evidenced by overlapping transcriptional reprogramming upon activating FLS2- and Cf-mediated immune responses (Navarro et al., 2004). This overlap potentially involves the regulation of downstream responses through similar components which, in addition to the SERK family members, include the receptor-like cytoplasmic kinases BOTRYTIS- INDUCED KINASE 1 (BIK1), and AVRPPHB SUSCEPTIBLE 1-LIKE 1 (PBL1) kinases downstream of FLS2, and the AVR9/CF-9 INDUCED KINASE 1 (ACIK1) regulating Cf-4 immunity, as well as the CAST AWAY kinase involved in SOBIR1/EVR signaling (Burr et al., 2011; Monaghan and Zipfel, 2012; Liebrand et al., 2014).

Given these similarities, it is conceivable that the constitutive association between the RLP Cf-4 and the RLK *Sl*SOBIR1 represents a PRR complex, in which the Cf-4 ectodomain mediates specific ligand recognition and the *Sl*SOBIR1 kinase domain is regarded as the signaling part. This is in contrast to PRRs exemplified by FLS2, in which both functions are present within the same molecule. Ligand-enhanced interaction of PRRs with SERK member RLKs is subsequently required to trigger receptor endocytosis and further downstream signaling by both RLP- and RLK-type PRRs (**fig. 3.7**).

3.8 - Shared mechanisms of receptor endocytosis

Receptor-mediated endocytosis is part of the eukaryotic immune response and in addition to FLS2 and Cf-4, for example, is also found for the EFR and PEPR1 RLKs (Husebye et al., 2006; Robatzek et al., 2006; Spallek et al., 2013; Mbengue et al., 2016; Ortiz-Morea et al., 2016). An important role of receptor-mediated endocytosis is to control the abundance of receptor (complexes) at the plasma membrane, a process that is well established in animals and involves lysosomal/vacuolar degradation (Lemmon and Schlessinger, 2010). Activated FLS2 traffics into the late endosomal pathway and is a cargo of multivesicular bodies localizing to the lumen of these late endosomes for delivery to the vacuole (Beck et al., 2012a; Spallek et al., 2013; Mbengue et al., 2016). This pathway could be responsible for the flg22-induced FLS2 degradation, because chemicals affecting endosomal trafficking inhibit the degradation of this receptor (Smith et al., 2014). Our colocalization data strongly suggest that activated Cf-4 is also targeted for vacuolar degradation through the late endosomal pathway, consistent with the observation that Cf-4-GFP protein levels are reduced upon Avr4 elicitation (**fig. S1**; Choi et al., 2013).

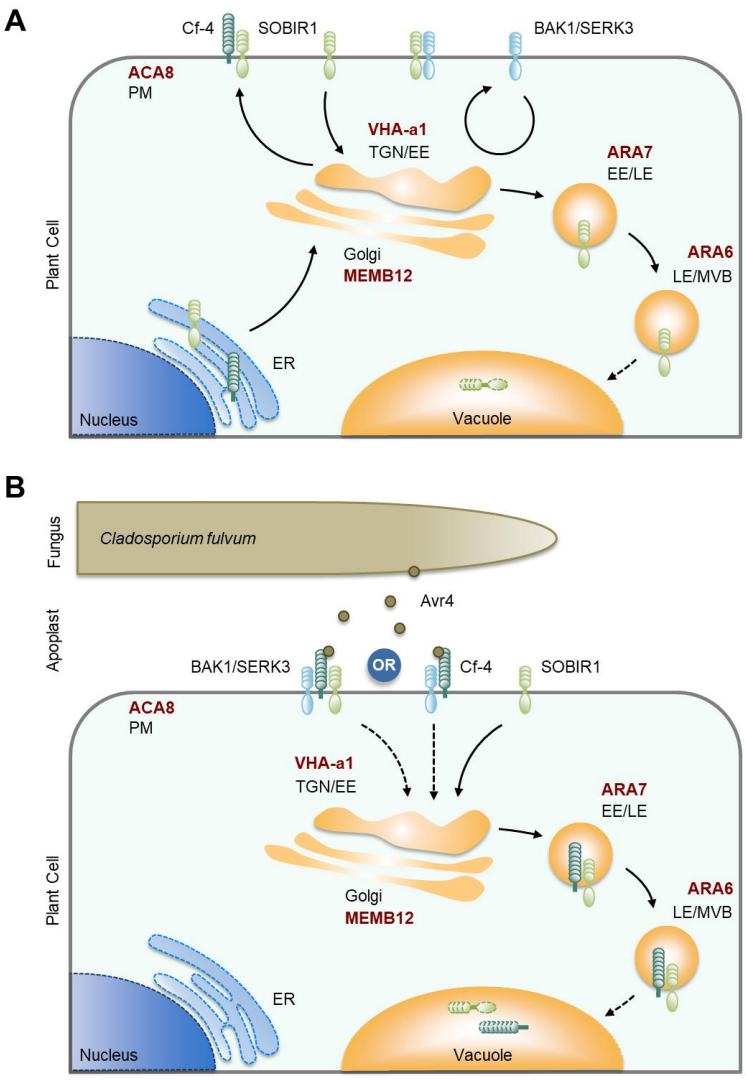

Fig. 3.7. Model of the Cf-4, SOBIR1 and SERK3 subcellular trafficking pathways. (A) Un-elicited: Following its folding and maturation in the endoplasmic reticulum (ER), Cf-4 is predominantly trafficked to the plasma membrane, where it constitutively interacts with SOBIR1, which itself is constitutively endocytosed. SOBIR1 can interact with BAK1/SERK3, a co-receptor known to recycle between the plasma membrane and the *trans*-Golgi network/early endosome. (B) Elicited: Upon colonization of Cf-4 tomato leaves, *C. fulvum* secretes Avr4 into the apoplast, which is recognized by Cf-4 and promotes interaction of Cf-4 with BAK1/SERK3. This complex is required for Cf-4-mediated immunity (not shown) and endocytosis into ARA7- and ARA6-positive compartments of the late endosomal pathway, destined for vacuolar degradation. Subcellular localization of markers (ACA8, MEMB12, VHA-a1, ARA6 and ARA7) used in this study is depicted in brown lettering. TGN, *trans*-Golgi network; EE, early endosome; LE, late endosome; MVB, multivesicular body.

Endosomal sorting for vacuolar degradation requires the transfer of ubiquitin to the plasma membrane cargo, and subsequent deubiquitination of the cargo at multivesicular bodies (Beck et al., 2012b). In line with this, the *Pto* DC3000 effector AvrPtoB ubiquitinates the kinase domain of FLS2, promoting its degradation (Göhre et al., 2008), and upon activation by flg22, ubiquitin-

ligases PLANT U-BOX 12 (PUB12) and PUB13 ubiquitinate FLS2, resulting in its degradation (Lu et al., 2011)**.** Ubiquitination processes have also been implicated in Cf downstream signaling pathways upon activation (Navarro et al., 2004). Is there any evidence for ubiquitination on RLP receptor complexes? The ubiquitin ligase CYS, MET, PRO, AND GLY PROTEIN CMPG1 is required for Cf-4 and Cf-9 HR (Gilroy et al., 2011). *Phytophthora* effector Avr3a targets CMPG1 and suppresses the immune response to elicitin, which is mediated by ELR, an RLP that interacts with SOBIR1 and recruits SERK3 (Domazakis et al., 2018; Du et al., 2015). However, based on localization and functional studies, CMPG1 is likely to function in the nucleus (Bos et al., 2010). Tobacco Avr9/Cf-9-Rapidly-Elicited 189 (ACRE189)/ Avr9/Cf-9–INDUCED F-BOX1 (ACIF1) and ACRE276/PUB17 are required for Cf-4 and Cf-9 mediated HR, but both most likely function in the nucleus (van den Burg et al., 2008; He et al., 2015; Yang et al., 2006). Finally, Suppressor of G2 Allele of SKP1 (SGT1) which is homologous to ubiquitin-ligase complex interacting proteins in yeast, is required for Cf-4 and Cf-9 HR, but also for intracellular NLR-mediated immunity, and most likely functions further downstream of both types of immune receptors (Peart et al., 2002).

Taken together, these data point at positive roles for ubiquitination in Cf-triggered outputs. Unlike the direct ubiquitination of the FLS2 cytosolic domain, the abovementioned Cf-associated ubiquitination proteins are not thought to function at the PM themselves, but predominantly in the nucleus or further downstream of initial Cf activation. That makes them unlikely to have a role in direct modification of the ubiquitination status of the RLP-SOBIR1 receptor complexes. However, I observe increased molecular weight “smear” patterns in SOBIR1 co-purifying with SERK3 upon activation of Cf-4 (**fig. 3.5**), suggesting posttranslational modifications of SOBIR1 in active complexes. In agreement with this, the de-ubiquitinating tobacco enzyme UBIQUITIN-SPECIFIC PROTEASE 12 (UBP12) modulates Cf-4 and Cf-9-mediated HR (Ewan et al., 2011), and the Arabidopsis homolog *At*UBP12 localizes to the nucleus and cytosol, which leaves the possibility that it mediates cytosolic ubiquitination processes such as those on cell-surface receptors (Cui et al., 2013).

3.9 - Cf-4 as a pattern recognition receptor

C. fulvum Avr4 is considered an effector, which makes Cf-4 a receptor functioning in effector-triggered immunity (ETI), in line with its historic classification as an R-protein (Thomas et al., 1997; Hammond-Kosack and Kanyuka, 2007). However, I could demonstrate that it shares similar requirements for signal initiation at the cell surface with RLK-type PRRs such as FLS2, which functions as MAMP detector and confers MAMP-triggered immunity. This points at early convergence of ETI and PTI. Besides my data that suggest both perception systems at the cell surface converge early on the shared module SERK3, other findings support the notion that Cf-4 can be considered a PRR.

Cf-4 not only recognizes the Avr4 protein secreted by *C. fulvum*, but is also activated by Avr4 orthologs produced by the banana pathogen *Mycosphaerella fijiensis* and the pine-infecting fungus *Dothistroma septosporum* (Stergiopoulos et al., 2010; de Wit et al., 2012). *Cf*Avr4, *Mf*Avr4 and *Ds*Avr4 bind to chitin and consequently protect the fungal cell wall against hydrolysis by secreted host chitinases (Van den Burg et al., 2003; van den Burg et al., 2006; van Esse et al., 2007; Stergiopoulos et al., 2010; Mesarich et al., 2016). It has been suggested that, reminiscent of MAMP recognition, the chitin-binding motif of Avr4 is the pattern that is recognized through interaction with the LRRs of Cf-4 (Thomma et al., 2011). However, natural allelic variants of *C. fulvum* Avr4 that avoid detection by Cf-4 were mutated in cysteine residues that affect protein folding and thus susceptibility to cleavage by apoplastic proteases (Van den Burg et al., 2003). While the resulting lower accumulation of Avr4 can thus limit activation of Cf-4, it is remarkable that detection avoidance by wild Avr4 alleles did not seem to occur through mutations in the chitin binding effector domain.

Recently, a conserved Avr4 proline residue necessary for Cf-4 HR elicitation was identified within all three abovementioned Avr4 homologs (P87 of *C. fulvum* Avr4), and is dispensable for chitin binding but hypothesized to provide protein stability in the apoplast (Van Den Burg et al., 2004; Mesarich et al., 2016). Conversely, on tomato pathogen *Pseudocercospora fuligena* Avr4, which also binds chitin, protects against chitinases, and triggers Cf-4 HR, the chitin binding pocket is not the pattern detected by Cf-4, as the mutations (N89A, D69A) that reduced chitin affinity still triggered Cf-4 HR (Kohler et al., 2016). Furthermore, *Pf*Avr4 mutations that did not alter chitin binding, but showed a reduced capacity to trigger Cf-4 HR (W88A, N89A, D96A), were rendered sensitive to proteolytic degradation in *N. benthmiana* apoplasts (Kohler et al., 2016).

Taken together, the above data support the hypothesis that Cf-4 detects a conserved fold on Avr4 orthologs across distantly related pathogens, which protects the effector from proteolytic cleavage. The detection capacity of Cf-4 for such a conserved pattern provides further reason to consider it a PRR. Similarly, the *N. benthamiana* SOBIR1-dependent RLP RESPONSE TO XEG1 (RXEG1) recognizes the apoplastic *Phytophthora sojae* virulence factor XEG1 independent of XEG1 mutations or allelic variations which disrupt its virulence function, and the tomato RLP Eix2 recognizes fungal ETHYLENE-INDUCING XYLANASE (EIX) despite mutations that abolish its enzymatic β-1-4-xylanase activity (Wang et al., 2018; Furman-Matarasso et al., 1999).

3.10 – RLP-SOBIR1 as a cell-surface sensor-helper platform

Cf RLPs are encoded by highly duplicated genes, generating allelic diversity thought to be driven by host-pathogen co-evolution, especially at the LRR sensor domain. The *Cf-4* gene itself is neighboured by several homologs originating from duplication events, leading to novel specialization such as detection capacity for variations of the same effector, such as Avr4E which

is detected by the Cf-4 homolog Hcr9-4E (Takken et al., 1999). Cf-9, also present on the same locus, shares near full identity with Cf-4 in the cytosolic domain, but is divergent in its LRR domains, suggesting diversifying selection to adapt to novel pathogen effectors such as Avr9 (Wulff et al., 2009). Similar clustering and duplication patterns are observed for Arabidopsis RLP genes (Mondragon-Palomino and Gaut, 2005). Yet, Arabidopsis encodes only one *SOBIR1*, and tomato encodes only *SOBIR1* and *SOBIR1-like*, and current knowledge suggests RLPs depend on SOBIR1 for stability and signaling capacity (Liebrand et al., 2013).

The current data on diverse RLP-type PRRs converging on SOBIR1 at the plasma membrane for signal transduction upon activation bring to mind the recently emerging “sensor-helper” model of intracellular NLRs. There, many sensor-NLRs confer recognition specificity to novel patterns, and converge upon a limited number of helper-NLRs for signal transduction and initiation of immunity (Wu et al., 2017, 2018). Thus, the RLP-SOBIR1 system may provide a similar, but cell-surface based sensor-helper platform, freeing up RLP-encoding genes to generate variation, but maintaining common downstream components, allowing for flexible evolutionary adaptation to changing invasion patterns in the apoplast.

CHAPTER 4

IMMUNE SIGNALING-INDUCED CHANGES IN THE LOCALIZATION OF ARA7/RABF2B AND ITS CO-PURIFYING PROTEOME

RESULTS

4.1 – THE LOCALIZATION PATTERN OF ARA7/RABF2B CHANGES UPON IMMUNE STIMULUS

4.1.1 - ARA7 focally accumulates at the cell periphery upon MAMP and pathogen stimulus

Rab GTPases have previously been shown to accumulate at pathogen interfaces. Late endosomal functioning Rab GTPases ARA7 and RABG3c accumulate around *Phytophthora infestans* haustoria (Bozkurt et al., 2015), and ARA7 and ARA6 both accumulate around haustoria of *Golovinomyces orontii* (Inada et al., 2016). Furthermore, ARA6-positive endosomes accumulate around attempted penetration sites of *Blumeria graminis* f.sp. *hordei* (Nielsen et al., 2012, 2017b)**.** Finally, RABE1d focal accumulations were observed at the cell surface upon bacterial infiltration (Speth et al., 2009). This prompted me to investigate whether ARA7 responds in a similar way when challenged with bacterial presence.

I challenged plants expressing YFP-ARA7 under the ubiquitin-10 promoter (Geldner et al., 2009) by injecting water, 10 µM flg22, or the compatible bacterial pathogen *Pseudomonas syringae* pv. *tomato* DC3000 (*Pto* DC3000) at an OD_{600} of 0.2 and I observed the infiltrated tissue using confocal microscopy at 6 h post-infiltration. Strikingly, both upon flg22 and *Pto* DC3000 infiltration, ARA7 vesicles strongly concentrated at the cell periphery in both mesophyll and epidermal cells (**fig. 4.1**). This response peaked between 6-7 h after both treatments, and subsided below observable levels at >8 hpi. The ARA7 concentration at the cell periphery was also observed in water treatments, but in a small minority of cells. The accumulations did not move throughout the cell but remained in one location, and showed a high motility of vesicles within the cluster. Multiple accumulations per cell were observed, but were always adjacent to the cell periphery. Accumulations were observed at positions that did not correspond to the presence of bacteria at the cell surface. This could be a result of the bacteria detaching from the cell surface, perhaps upon sample preparation which involves infusing the apoplast with water, or because of the unnaturally high bacterial titers infiltrated into the apoplast, excess free-floating MAMPs such as flagellin are detected by the host cells at other positions. Taken together, results suggest that ARA7 concentration at the cell surface is a previously unidentified part of the antibacterial immune response.

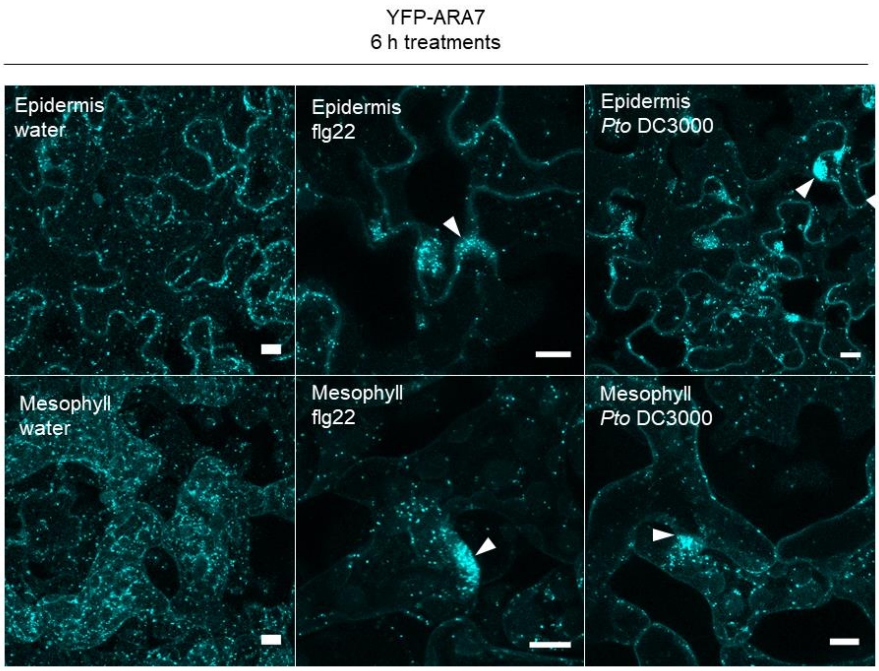

Figure 4.1. YFP-ARA7-positive compartments focally accumulate in response to flg22 and bacterial infection independent of host tissue types. Confocal micrographs show cross-sections of 4 weeks-old Arabidopsis epidermal (top panels) and mesophyll (bottom panels) leaf cells from transgenic YFP-ARA7 lines, represented as z-projections. Leaves were inoculated with *Pto* DC3000 bacteria (OD_{600} = 0.2) and flg22 (1 µM) as indicated and incubated for 6 hours before confocal microscopy; 63 × objective; scale bars = 10 µm. Blue colouring indicates YFP-ARA7-positive fluorescence signals. Arrowheads point at clusters of ARA7 vesicles. Images are representative of three experimental replicates.

4.1.2 - ARA7 focal accumulations occur under bacterial infection sites

It is known that *Pto* DC3000 attaches to the cell surface in order to secrete effectors into the host cytosol, I therefore tested whether ARA7 concentrations at the cell periphery correspond to the attachment site of *Pto* DC3000. In order to do this, I used an mCherry-expressing *Pto* DC3000-strain kindly provided by Sebastian Pfeilmeier (Jacob Malone laboratory, John Innes Centre, Norwich, UK). I infiltrated a suspension of these bacteria into YFP-ARA7-expressing plants as described above, and observed mesophyll tissue at 6-7 hpi using confocal microscopy. Strikingly, ARA7 focal accumulations frequently occurred at the cell periphery in locations where *Pto* DC3000-mCherry bacteria were also found (**fig. 4.2A**). On some occasions, two bacteria were found in a head-to-tail pairwise manner, as shown in **fig. 4.2A**. When observed at 3 hpi or earlier, no cell-surface localized immobile bacteria were observed. The observation of ARA7 focal accumulations occurring where bacteria were attached to the cell surface, suggests that these accumulations may play a role in defense specifically at this location.

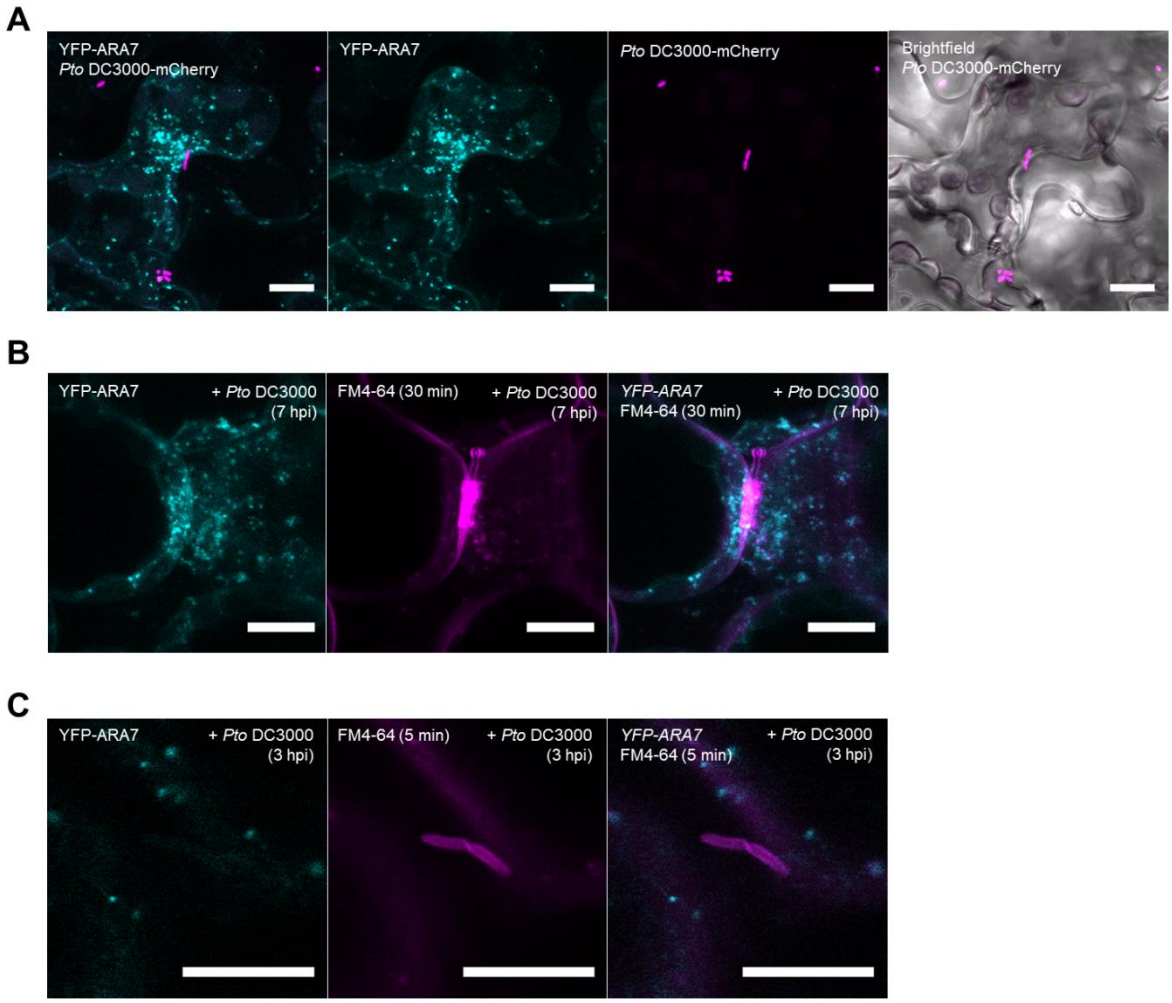

Figure 4.2. Focal accumulation of YFP-ARA7-positive compartments is targeted to bacterial infection sites. (A) Confocal micrographs (z-projections) show YFP-ARA7 and *Pto* DC3000-mCherry in 4 wk-old Arabidopsis mesophyll tissue, 6 hours after syringe infiltration of bacterial suspensions. Bacterial OD_{600} = 0.2 upon infiltration. Lower right panel shows bright field + *Pto* DC3000-mCherry. 63 × objective; scale bars = 10 µm. (B) Confocal micrographs (single focal plane) show YFP-ARA7 and FM4-64 (1 µM) at 7 hours after infiltration of Pto DC3000 bacteria without mCherry fluorophores at OD_{600} = 0.2, and at 30 minutes after infiltration of FM4-64. 63 × objective; scale bars = 10 µm. (C) Confocal micrographs (single focal plane) show YFP-ARA7 and FM4-64 (1 µM) at 3 hours after infiltration of Pto DC3000 bacteria without mCherry fluorophores at OD_{600} = 0.2, and at 5 minutes after infiltration of FM4-64. 63 × objective; scale bars = 10 µm.

In order to test whether the observed ARA7 concentrations at the cell periphery reflect a locally increased endocytic activity, I performed uptake experiments with the lipophilic endocytic tracer dye FM4-64. FM4-64 associates with the lipid bilayer at the PM, is internalized, and starts accumulating at late endosomes when measured ca. 30 minutes after application but not at earlier time points (Beck et al., 2012b). FM4-64 also associates with membranes of *Pto* DC3000

shortly after application, allowing for visualisation of bacterial cells (see **fig. 4.2C**). I applied FM4-64 to leaves that exhibited ARA7 focal accumulation as confirmed using confocal microscopy at 6-7 h after infiltration of *Pto* DC3000, and then evaluated the co-localization of YFP-ARA7 and FM4-64. Interestingly, only a small pool of YFP-ARA7-positive endosomes that were concentrated at infection sites were stained by FM4-64 (**fig. 4.2B**). Bacterial cells could be visualised by intense FM4-64 staining (**fig. 4.2B**). While it remains possible that local endocytic activity was upregulated before application of FM4-64, the observation that few endosomes in ARA7 concentrations were stained within 30 minutes of dye application would suggest that either existing endosomes are concentrating, or endosomes resulting from increased endocytic activity do not spread throughout the cell but remain concentrated.

4.1.3 - A panel of different bacteria and MAMPs trigger ARA7 focal accumulation

The pathogen-induced focal accumulation of RABE1d has been shown to increase upon infiltration of *Pto* DC3000 AvrRpt2, which secretes the effector AvrRpt2 that triggers ETI (Speth et al., 2009). Conversely, a role for *Pto* DC3000 effectors has been identified in suppressing the occurrence of PEN3 cell-surface focal accumulations (Xin et al., 2013). To test whether disabled or ETI-triggering *Pseudomonas* bacteria affected the ARA7 polarized immune response, I infiltrated YFP-ARA7-expressing leaves with (i) *Pto* DC3000 COR-, which is deficient in the secretion of Coronatine, an agent that induces stomatal opening and contributes to virulence in the mesophyll; (ii) *Pto* DC3000 HrcC-, which does not form a type-3-secretion system to inject effectors; (iii) *Pto* DC3000 AvrRpt2 which triggers ETI; and (iv) the non-adapted *Pseudomonas syringae* pv. *tabaci* (*P. s.* pv. *tabaci*). In addition, I infiltrated mCherry-expressing strains of *Pto* DC3000 and *Pto* DC3000 HrcC- to test whether the presence of the mCherry molecule affected the ability to elicit focal accumulations. For comparison, I also infiltrated the MAMPs flg22 (10 µM) and chitin (ca. 10 mg/mL).

I observed the tissue at 6-7 hpi using confocal microscopy, taking lower magnification pictures of the mesophyll to capture numerous cells per field of view to allow for subsequent quantifications. Interestingly, all tested stimuli, including a water control, triggered focal accumulations of ARA7 at 6-7 hpi to various extent (**fig. 4.3**). The response is observed at a lower magnification of 20 × as strong YFP-ARA7 fluorescent maxima at the cell periphery of adaxial mesophyll cells. These results show that bacterial stimulus can trigger ARA7 focal accumulation despite the bacteria lacking Coronatine or HrcC, and independent of the presence or absence of a constitutively expressed mCherry fluorophore. Furthermore, focal accumulations were also observed upon infiltration with Pto DC3000 AvrRpt2, suggesting that the response occurs despite the activation of ETI signaling. Finally, both flg22 and chitin treatments triggered ARA7 focal accumulation in the mesophyll (**fig. 4.3**).

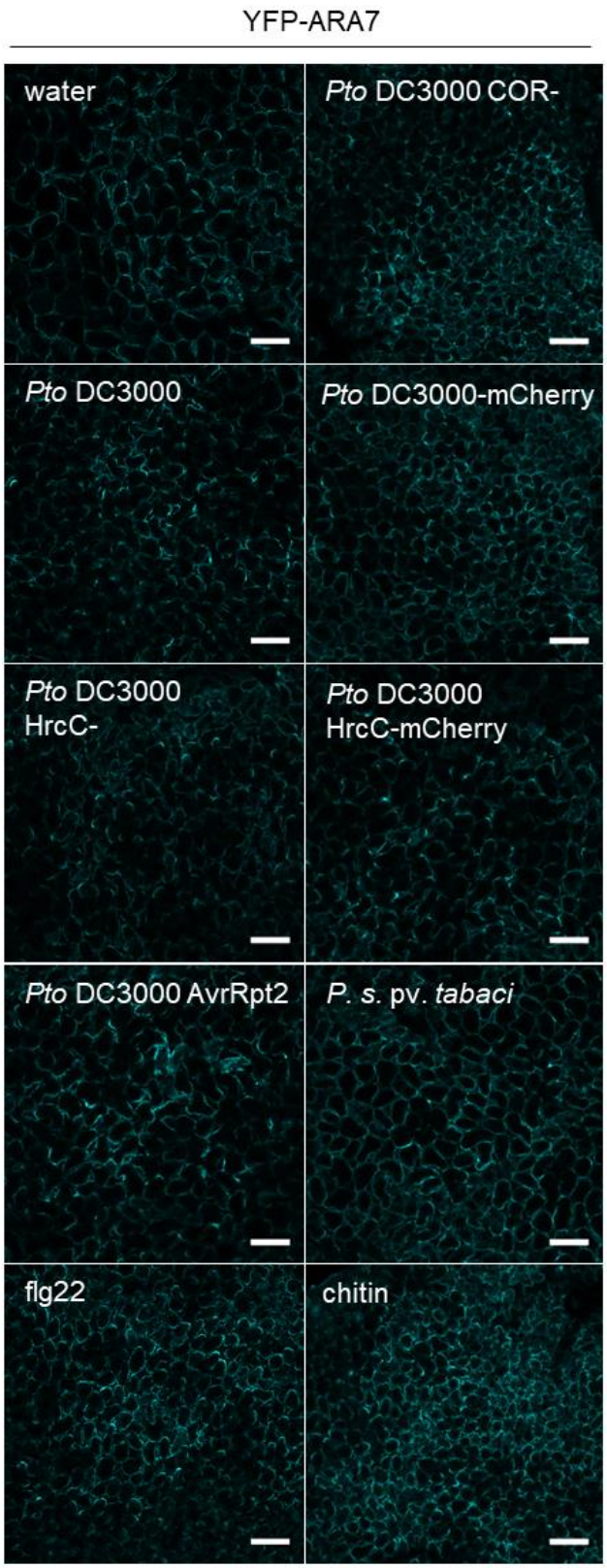

Figure 4.3. Focal accumulation of YFP-ARA7-positive compartments is conserved across different bacterial strains and MAMP stimuli. Representative confocal micrographs (single focal planes) of acquisition series of YFP-ARA7 in 4 wk-old Arabidopsis upper mesophyll tissue, 6-7 h after syringe infiltration of the indicated treatments. Upon application, bacterial OD_{600} = 0.2, flg22 = 1 µM and chitin = ca. 10 mg/mL. 63 × objective, scale bars = 100 µm.

Water treatments also induced ARA7 focal accumulation. Indeed, a “flooding response” has been described before, where re-injection of wildtype intracellular fluid extractions into the apoplast leads to MAPK activation, indicative of stress signaling (Romeis et al., 2001). PEN1/SYP121 and PEN3 accumulation at endosomes, thought to underlie their subsequent delivery at the cell surface, was also triggered to a minor extent under water treatments (Underwood et al., 2017). This raises the possibility that the clustering of endosomes, and resulting cargo accumulations to the cell surface, are part of a general stress response but can be targeted to pathogen positions. Because of this, I was interested in quantifying the response to see if any particular treatment induced accumulations at a level significantly above that of water treatment. To do this, I developed a short macro in the image analysis software FIJI (ImageJ) which is described in **fig. 4.4A**. Briefly, the software applies gaussian blur, intensity thresholding and area thresholding to separate bright, relatively large spots from the background. Finally, the number of resulting spots is extracted.

Analysing a series of images in this way revealed that flg22 treatment significantly and strongly induced focal accumulation (69 ± 16.10 foci / field of view (FOV); **fig. 4.4B,D**) in comparison to water (4.20 ± 2.22 foci / FOV). In a second replicate, flg22 also significantly induced focal accumulation compared to water (**fig. 4.4C,D**). *Pto* DC3000, which was tested in one experimental replicate, induced ARA7 focal accumulations significantly compared to water control. *Pto* DC3000-mCherry triggered significantly more ARA7 focal accumulations compared to water in only one experimental replicate (9.67 ± 3.28; **fig. 4.4C,D**). Similarly, *Pto* DC3000 HrcC- (6.14 ± 0.88 vs. 0 ± 0; **fig. 4.4C,D**) and *Pto* AvrRpt2 (29.00 ± 5.51 vs. 4.20 ± 2.22; **fig. 4.4B,D**) induced focal accumulations in only one experimental replicate. Interestingly, *P. syringae* pv. *tabaci* did not significantly trigger more ARA7 focal accumulations than water in both experimental replicates. *P. s.* pv. *tabaci* has been shown to elicit HR-like cell death in Arabidopsis Col-0, which is abolished in mutants lacking flagellin (Ishiga et al., 2005). In contrast, *Pto* DC3000-AvrRpt2 triggers NLR-mediated cell death, yet retained the capacity to elicit ARA7 concentrations beyond levels observed in water treatment. Knowing that *P. s.* pv. *tabaci* successfully colonizes Arabidopsis Col-0 in the absence of flagellin, and without eliciting cell death, it is conceivable that it secretes effectors that suppress trafficking responses in Col-0.

A

Workflow

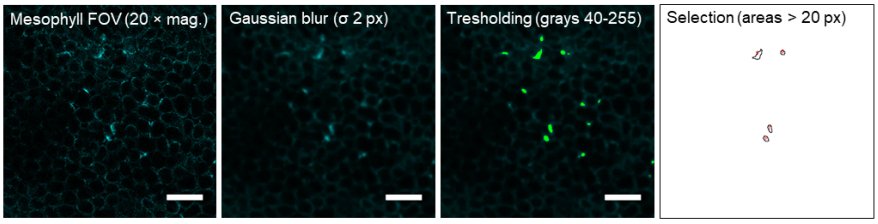

B

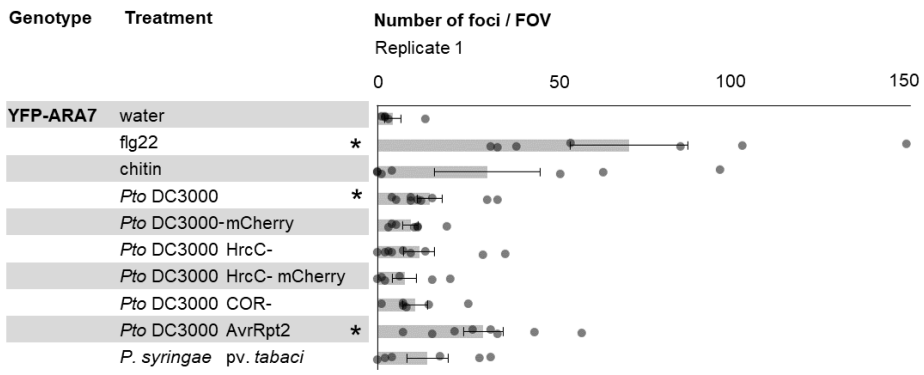

C

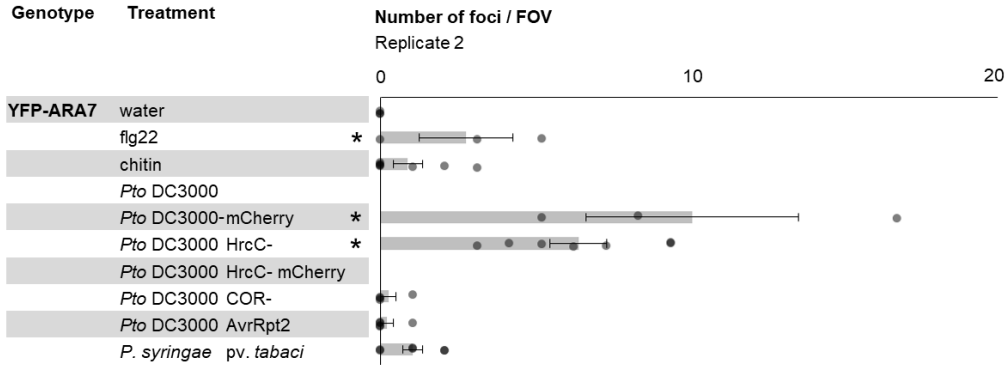

D

Genotype	Treatment	Number of foci / FOV Replicate 1 Mean	SE	*n*	Replicate 2 Mean	SE	*n*
YFP-ARA7	water	4.20	2.22	5	0.00	0.00	3
	flg22	* 69.00	16.10	7	* 2.67	1.45	3
	chitin	30.14	14.51	7	0.86	0.46	7
	Pto DC3000	* 14.22	3.46	9			
	Pto DC3000-mCherry	9.00	2.10	7	* 9.67	3.28	3
	Pto DC3000 HrcC-	11.33	4.15	9	* 6.14	0.88	7
	Pto DC3000 HrcC- mCherry	7.33	3.38	6			
	Pto DC3000 COR-	10.33	3.38	6	0.25	0.25	4
	Pto DC3000 AvrRpt2	* 29.00	5.51	8	0.20	0.20	5
	P. syringae pv. *tabaci*	13.67	5.58	6	1.00	0.31	7
YFP-ARA5	water	15.00	5.94	6	1.00	1.00	3
	Pto DC3000	15.67	3.51	9	4.67	0.88	3

Figure 4.4. Quantitative analysis reveals significant differences in focal accumulation of YFP-ARA7-positive compartments. (A) Workflow as encoded in a custom FIJI script, showing individual image modifications performed to obtain final number of focal accumulations per image as used in B-D. 20 × objective, scale bars = 100 µm. (B,C) Graphical representations of number of focal accumulations detected using the workflow in (A), showing individual measurements and mean (bars) ± SE (error bars) for indicated treatments corresponding to replicates shown in (D). (D) Overview listing the means ± SE of the number of YFP-ARA7 focal accumulations per field-of view, and *n* = number of images, for two replicates. Quantifications were performed in an automated way using confocal micrographs acquired as in Figure 2.3 at 6 hours after syringe infiltration of indicated treatments.

As is evident from visual inspection of the results (eg. **fig. 4.4A**), the FIJI macro does not pick up on all focal accumulations that would be identified by eye. There are focal accumulations of which the fluorescent signal locally contrast with the surrounding environment, but on a global level fall within the background. This is a limitation of using global filtering and thresholding to extract features. Furthermore, the macro was developed and optimized by using water treated and flg22-treated samples as the input, which might cause a bias toward being able to distinguish between those treatments, although the expectation is that the response looks the same independent of stimulus. Further optimization, employing local thresholding analysis, as well as using multiple stimuli to calibrate the script, would likely yield further improvements.

4.1.4 - ARA7 does not change in vesicle number upon immune stimulus (0-3 h)

In order to test whether increased trafficking requirements could be reflected by an upregulation in the number of ARA7 endosomes, I quantified them using high throughput confocal imaging of cotyledons under flagellin elicitation. Cotyledons of the *pUB::YFP-ARA7* genotype, alongside *pFLS2::FLS2-GFP* as a positive control, were submerged in liquid Murashige and Skoog medium (MS), or liquid MS + flg22 in a 96-wells optical plate.

Although no significant ARA7 focal accumulation was observed before ca. 6 h of flg22 or bacterial treatments, immune-related trafficking events are induced, such as the ligand-induced endocytosis of FLS2 which peaks between 1-1.5 h after addition of flg22 (Beck et al., 2012). In addition, cell-surface cargoes involved in defence such as PEN1 and PEN3 can be observed to accumulate at endomembrane compartments at 4 h after triggering immune signaling using flg22 (Underwood et al., 2017). I therefore examined the number of YFP-ARA7-positive endosomes. At 0.5, 1.5 and 2.5 h, measurements were started and performed across an acquisition window of 30 minutes, and the average numbers of detected endosomes for YFP-ARA7 and FLS2-GFP under control and flg22 treatments were calculated. Interestingly, no statistically significant differences in the number of YFP-ARA7 spots per field-of-view between control or flg22 treatments were detected in any time point (**fig. 4.5**). By contrast, the number of FLS2-GFP endosomes was significantly increased at 2 and 3 h after flg22 treatment compared to control treatment, with a maximum at 2 hpi, indicating that flg22 treatment could successfully induce

immune signaling (Beck et al., 2012b). The absence of statistically significant differences in the number of ARA7 vesicles upon flg22 treatment compared to control suggests that any differential requirements for endocytic traffic upon immune signaling are not met by a increase or decrease in the total number of vesicles within 3 hpi.

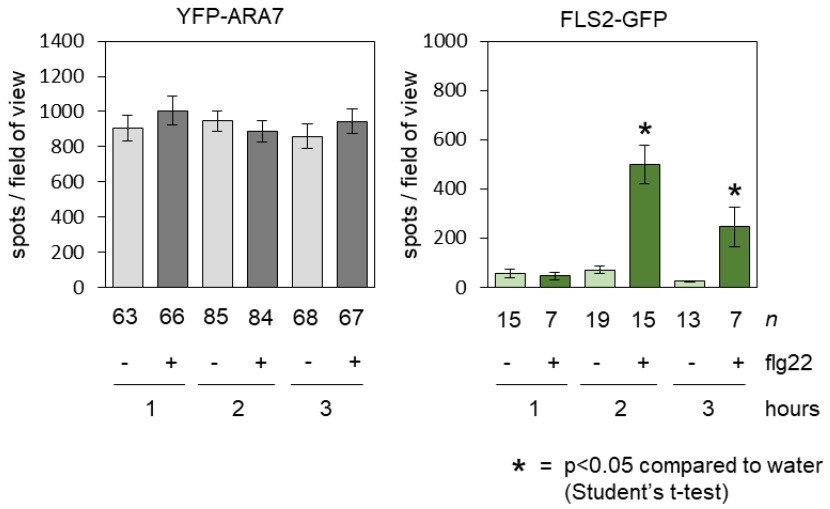

Figure 4.5. Quantitative analysis reveals no differences in the abundance patterns of YFP-ARA7-positive compartments. Graphs represent the number of detected YFP-ARA7- and FLS2-GFP-positive fluorescing spots (mean ± SE) per field-of-view from merged confocal micrograph epidermal cross-sections of 2 weeks-old Arabidopsis cotyledons. Transgenic *pUB::YFP-ARA7* or *pFLS2::FLS2-GFP* cotyledons were imaged using the Opera high-throughput confocal microscope at 1, 2 or 3 hours after water or 1.5 µM flg22 treatment. Asterisks indicate significant result compared to water treatments at p<0.05 (Student's t-test). *n* = number of images analyzed across 24 cotyledons (YFP-ARA7) or 6 cotyledons (FLS2-GFP). Graphs show data of one experiment, representative of three independent replications.

I used a constitutively expressing, Ubiquitin-10 promoter driven YFP-ARA7 line (Geldner et al., 2009), so any changes in endogenous ARA7 transcription, and resulting vesicle phenotypes, may be masked by this. However, ARA7 mRNAs did not evidently respond to flg22 treatment, as observed in GeneVestigator publicly available datasets (**fig. 4.8**). At later time points of 24 hpi with *Pto* DC3000, using endogenous promoter-driven RFP-ARA6 lines, Wang et al., 2014, could detect an increased number of LE/MVBs, which was corroborated by increased FM4-64 staining at endosomes. Rab GTPases can be highly regulated through modulation of their GTP hydrolysis activity and membrane association, by interacting regulatory proteins (Nielsen et al., 2008). It is currently unknown whether the ratio of membrane-associated to cytosolic ARA7 changes upon immune stimulus.

4.2 - THE ARA7 CO-PURIFYING PROTEOME CHANGES UPON IMMUNE STIMULUS

4.2.1 - Purifying ARA7 from seedlings under water and flagellin conditions

The polarized immune response of YFP-ARA7-positive vesicles suggests that ARA7 plays a role in the cell-surface delivery of defense components. To investigate this, I set out to identify ARA7-interacting proteins, and cargoes of ARA7 endosomes, with the goal to compare resting-state and immune stimulated conditions. For this, I used a method of immunoprecipitation and mass spectrometry from Arabidopsis seedlings that was previously developed in our laboratory and shown to identify endosomal enriched proteins in a trafficking pathway-specific manner (Heard et al., 2015). To allow for substantial transcriptional reprogramming upon flg22 treatment (Denoux et al., 2008; Jiménez-Góngora et al., 2015), and anticipating to immunoprecipitate ARA7 from tissue where endosomes are accumulating defence-related cargoes (Underwood et al., 2017) yet do not markedly change in localization (**fig. 4.5**), I selected a time point of 3 h flg22 treatment.

I grew Arabidopsis seedlings of the genotypes *pUB::YFP-ARA7* and *pUB::YFP* in liquid MS medium for 8 days, and subjected both to 3 h of water or 1.5 µM flg22 treatment, starting the timer after 1.5 minutes of vacuum application (**fig. 4.6A**). I included YFP as a control, as proteins may unspecifically bind to the affinity beads, the bead-bound nanobody, or the YFP domain used to purify ARA7. I then performed immunoprecipitation using YFP affinity beads, separated proteins using 1D gel electrophoresis, and subjected the resulting samples to mass spectrometry analysis performed by Jan Sklenar (Proteomics Support Team, The Sainsbury Laboratory, Norwich, UK; **fig. 4.6A**). The above experiment was performed a total of three times independently.

As a result, 882 proteins co-purified with YFP-ARA7 under water treatment, and 1101 proteins co-purified with YFP under water treatment (**fig. 4.6B**). In order to determine a specific YFP-ARA7 co-purifying proteome, I decided the total number of detected peptides for a given protein in the YFP-ARA7 purification should be more than 4x greater than the total number of peptides in the YFP purification. Using this criterion, 723 proteins in the YFP-ARA7 purification were deemed unspecific, and 159 proteins remained, which I define as the YFP-ARA7 co-purifying proteome (**table 4.1**).

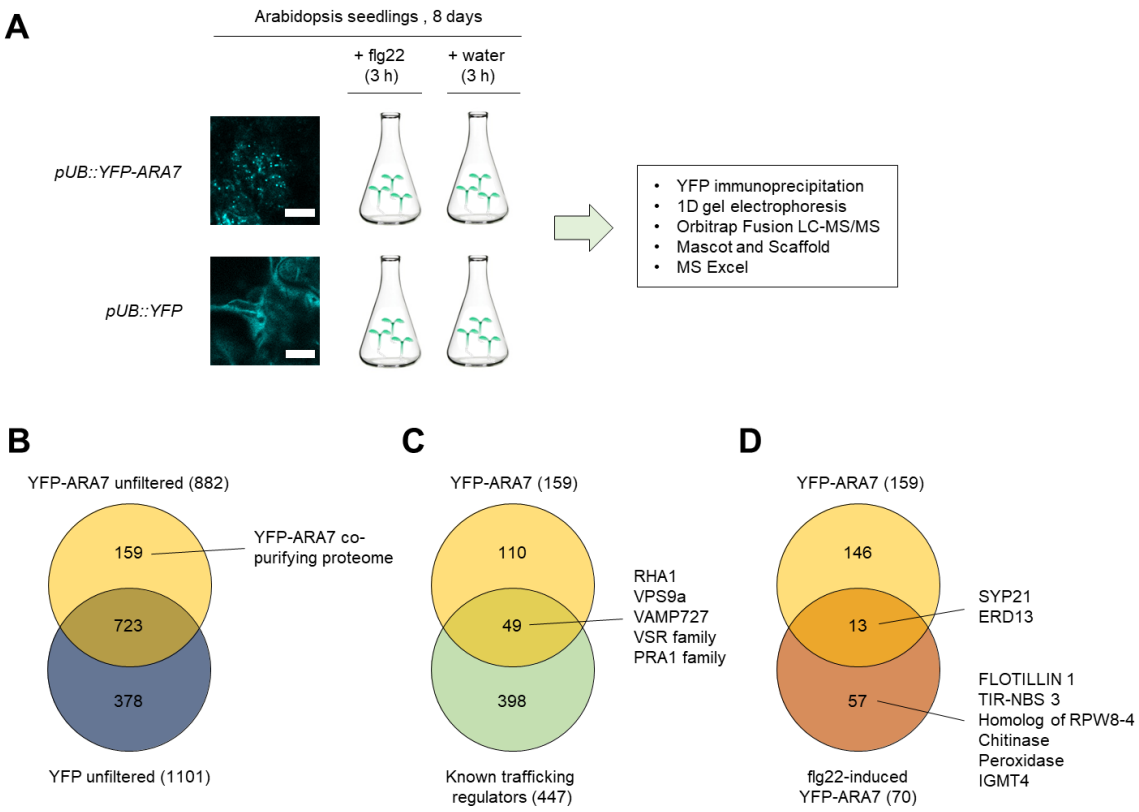

Figure 4.6. Identification of proteins associated with YFP-ARA7-positive compartments in a flg22-responsive manner. (A) Schematic overview shows experimental setup. Confocal micrographs show YFP fluorescent signal in z-projections of 8 days-old Arabidopsis seedlings expressing *pUB::YFP-ARA7* or *pUB::YFP*; scale bars = 10 µm. Seedlings were grown in liquid culture and treated with 1.5 µM flg22 and water for 3 hours before extraction (text box). (B) Venn-diagram shows groups of proteins co-purifying with the indicated bait proteins, as revealed by immunoprecipitation and mass spectrometry. Across three replicates, co-purifying proteins with YFP-ARA7-positive compartments were compared to YFP co-purifying proteins. The YFP-ARA7 co-purifying proteome was defined based on quality control criteria (present in >1 replicates, peptides = >5) and fold-change ratio of >4 in YFP-ARA7 compared to YFP. Details available in Table 4.1. (C) Venn-diagram shows YFP-ARA7 co-purifying proteins as compared with known trafficking regulators (source: Heard et al. 2015). Abundant trafficking regulators co-purifying with YFP-ARA7 listed. (D) Venn-diagram shows YFP-ARA7 co-purifying proteins without and with flg22 treatment, as compared with each other. Prominent proteins associating with YFP-ARA7-positive compartments in a flg22-responsive manner are shown in the call-out. Details available in table 4.3.

Table 4.1: ARA7 co-purifying proteome. Listed here is the ARA7 co-purifying proteome under water treated conditions. 8-day old seedlings of genotypes *pUB::YFP-ARA7* and *pUB::YFP* were treated with water or 1.5 µM flg22 for three hours, and subjected to immunoprecipitation using YFP affinity beads. Mass spectrometry was performed in collaboration with Jan Sklenar, Paul Derbyshire and Frank Menke (The Sainsbury Laboratory, Norwich, UK). To determine co-purifying proteomes, Scaffold software was used to retain proteins with a ProteinProphet score of 99% based on a minimum of 2 spectra with a PeptideProphet score of 95%. MS Excel was then used to retain proteins with at least 5 spectra across all three replicates in the YFP-ARA7 water-treated samples, with an occurence in more than 1 of these replicates, and an abundance increase of at least 4x compared to matching YFP controls. (*Columns 1-8*) Observed in # of replicates, and Spectra in combined replicates: Numbers and associated green cell-shading intensities indicate in how many experimental replicates the protein was detected, or how many spectra for that protein were identified in all three replicates combined, separated for water or flagellin treatment. (*Columns 9-10*) Enrichment factors: For each protein, the number of total spectra across three replicates of the green-labeled (rightmost) pulldown was divided by the number of total spectra in red-labeled (left-most) pulldown. Log10 values that correspond to these ratios are displayed in this table. Green or red bars are graphical representations of magnitude and direction of positive (green) or negative (red) values, centered at 0. (*Columns 11-12*) Locus ID and associated names. Source: TAIR10, accessed through www.genevestigator.org. The table is sorted for total spectral numbers in “YFP-ARA7 water”, in descending order.

Table 4.1: ARA7 co-purifying proteome

Observed in # of replicates				Spectra in combined replicates				Enrichment factor (log_{10})		Protein information	
YFP-ARA7		YFP		YFP-ARA7		YFP		YFP YFP-ARA7	Y7 water Y7 flg22		
water	flg22	water	flg22	water	flg22	water	flg22			Locus ID	Protein name
3	3	3	3	1160	1362	40	18	1.46E+00	6.97E-02	AT4G19640	ARA7
3	3	3	3	350	293	82	17	6.30E-01	-7.72E-02	AT3G09630	Ribosomal protein L4/L1 family, SUPPRESSOR OF ACAULIS 56
3	3	2	2	186	141	6	3	1.49E+00	-1.20E-01	AT2G14720	BP80-2;1, MTV4, VSR2;1, VSR4, vacuolar sorting receptor 4
3	3			147	132			8.17E+00	-4.67E-02	AT1G24560	PLANT-UNIQUE RAB5 EFFECTOR 2, PUF2
3	3			134	110			8.13E+00	-8.57E-02	AT3G19770	ATVPS9A, VPS9, VPS9A, Vacuolar sorting protein 9 (VPS9) domain
3	3			122	79			8.09E+00	-1.89E-01	AT3G52850	ATELP, ATELP1, ATVSR1, BP-80, BP80, BP80-1;1, BP80B, GFS1, VSR1, VSR1;1
3	3			112	91			8.05E+00	-9.02E-02	AT3G58460	ATRBL15, RBL15, RHOMBOID-like protein 15
3	3	3	3	89	94	21	14	6.27E-01	2.37E-02	AT2G33120	ATVAMP722, SAR1, VAMP722, synaptobrevin-related protein 1
3	3			75	48			7.88E+00	-1.94E-01	AT4G20110	BP80-3;1, VSR3;1, VSR7, VACUOLAR SORTING RECEPTOR 7
3	3	1		73	62	1		1.86E+00	-7.09E-02	AT2G47960	unknown protein, homology to TRAPP
3	3			71	66			7.85E+00	-3.17E-02	AT2G36360	Galactose oxidase/kelch repeat superfamily protein
3	3	1		70	65	1		1.85E+00	-3.22E-02	AT5G65950	unknown protein, homology to TRAPPI-components
3	3			65	42			7.81E+00	-1.90E-01	AT3G54300	ATVAMP727, VAMP727, VAMP727, vesicle-associated membrane protein 727
3	3			64	65			7.81E+00	6.73E-03	AT5G16280	Tetratricopeptide repeat (TPR)-like superfamily protein
3	3	3	3	60	56	8	8	8.75E-01	-3.00E-02	AT1G73110	P-loop containing nucleoside triphosphate hydrolases superfamily protein
3	3	1		57	51	4		1.15E+00	-4.83E-02	AT5G49720	ATGH9A1, DEC, GH9A1, IRX2, KOR, KOR1, RSW2, TSD1, glycosyl hydrolase 9A1
3	3	2	2	57	95	3	2	1.28E+00	2.22E-01	AT3G20720	unknown protein
3	3	1		55	41	2		1.44E+00	-1.28E-01	AT4G39820	Tetratricopeptide repeat (TPR)-like superfamily protein
3	3	3	2	52	39	11	5	6.75E-01	-1.25E-01	AT1G48900	Signal recognition particle, SRP54 subunit protein
3	3			50	37			7.70E+00	-1.31E-01	AT1G69340	appr-1-p processing enzyme family protein
3	3	1		48	53	1		1.68E+00	4.30E-02	AT4G30260	Integral membrane Yip1 family protein
3	3	2	1	48	36	5	1	9.82E-01	-1.25E-01	AT1G09330	ECHIDNA
3	3	3	3	46	45	9	5	7.09E-01	-9.55E-03	AT5G35160	Endomembrane protein 70 protein family
2	2	2		45	36	9		6.99E-01	-9.69E-02	AT1G02780	emb2386, Ribosomal protein L19e family protein
3	3	3	2	44	59	9	3	6.89E-01	1.27E-01	AT2G38360	PRA1.B4, prenylated RAB acceptor 1.B4
3	3	2	1	43	45	8	1	7.30E-01	1.97E-02	AT1G32050	SCAMP family protein
2	2			41	23			7.61E+00	-2.51E-01	AT1G77140	ATVPS45, VPS45, vacuolar protein sorting 45
3	3	2	2	41	51	6	5	8.35E-01	9.48E-02	AT4G12650	Endomembrane protein 70 protein family
3	3	1	1	40	63	1	1	1.60E+00	1.97E-01	AT3G11820	AT-SYR1, ATSYP121, ATSYR1, PEN1, SYP121, SYR1, syntaxin of plants 121
3	2	2	1	40	28	2	1	1.30E+00	-1.55E-01	AT4G19210	ATRLI2, RLI2, RNAse l inhibitor protein 2
3	3	2	1	40	42	7	2	7.57E-01	2.12E-02	AT1G62020	Coatomer, alpha subunit
2	3	2	2	37	49	3	4	1.09E+00	1.22E-01	AT3G56110	PRA1.B1, prenylated RAB acceptor 1.B1
3	3			36	36			7.56E+00	0.00E+00	AT4G36440	unknown protein
3	3		1	35	37		1	7.54E+00	2.41E-02	AT1G61250	SC3, SCAMP3, secretory carrier 3
3	3	1		34	26	1		1.53E+00	-1.17E-01	AT5G05170	ATCESA3, ATH-B, CESA3, CEV1, IXR1, Cellulose synthase family protein
2	2			34	12			7.53E+00	-4.52E-01	AT1G48090	calcium-dependent lipid-binding family protein
3	3			32	15			7.51E+00	-3.29E-01	AT1G30450	ATCCC1, CCC1, HAP5, cation-chloride co-transporter 1
3	3	2	1	32	38	6	1	7.27E-01	7.46E-02	AT3G28290	AT14A, Protein of unknown function (DUF677)
2	2			31	35			7.49E+00	5.27E-02	AT2G47240	CER8, LACS1, AMP-dependent synthetase and ligase family protein
3	3	1		30	38	1		1.48E+00	1.03E-01	AT5G22360	ATVAMP714, VAMP714, VAMP714, vesicle-associated membrane protein 714
3	3	3	3	30	38	7	9	6.32E-01	1.03E-01	AT1G11890	ATSEC22, SEC22, Synaptobrevin family protein
3	3	2	1	29	29	5	2	7.63E-01	0.00E+00	AT3G05000	TRS33, TRAPPI-component

3	3			29	29			7.46E+00	0.00E+00	AT1G08770	PRA1.E, prenylated RAB acceptor 1.E
3	3	2		27	25	5		7.32E-01	-3.34E-02	AT1G02130	ARA-5, ARA5, ATRAB1B, ATRABD2A, RA-5, RABD2A, RAS 5
3	3	1		27	51	2		1.13E+00	2.76E-01	AT2G36850	ATGSL08, ATGSL8, CHOR, GSL08, GSL8, glucan synthase-like 8
2	2			27	20			7.43E+00	-1.30E-01	AT2G26890	GRV2, KAM2, DNAJ heat shock N-terminal domain-containing protein
3	2	1		26	10	2		1.11E+00	-4.15E-01	AT5G13560	unknown protein
3	3	3	2	25	20	4	5	7.96E-01	-9.69E-02	AT5G42220	Ubiquitin-like superfamily protein
3	3	2		25	25	3		9.21E-01	0.00E+00	AT5G04830	Nuclear transport factor 2 (NTF2) family protein
2	2			24	26			7.38E+00	3.48E-02	AT1G59820	ALA3, aminophospholipid ATPase 3
3	2			24	6			7.38E+00	-6.02E-01	AT2G14740	ATVSR3, BP80-2;2, VSR2;2, VSR3, VSR3, vaculolar sorting receptor 3
2	2			23	37			7.36E+00	2.06E-01	AT3G05280	Integral membrane Yip1 family protein
3	3	1		23	21	3		8.85E-01	-3.95E-02	AT5G11040	AtTRS120, TRS120, TRS120
3	3			22	17			7.34E+00	-1.12E-01	AT5G58030	TRS31, TRAPPI-component
3	2	1		22	15	1		1.34E+00	-1.66E-01	AT1G28490	ATSYP61, OSM1, SYP61, syntaxin of plants 61
3	3			21	26			7.32E+00	9.28E-02	AT1G75850	VPS35B, VPS35 homolog B
3	3			20	20			7.30E+00	0.00E+00	AT2G40316	unknown protein
3	2	1	1	20	10	4	1	6.99E-01	-3.01E-01	AT3G10350	P-loop containing nucleoside triphosphate hydrolases superfamily protein
3	3			19	18			7.28E+00	-2.35E-02	AT5G17230	PSY, PHYTOENE SYNTHASE
3	3			19	30			7.28E+00	1.98E-01	AT2G22475	GEM, GRAM domain family protein
2	2			18	18			7.26E+00	0.00E+00	AT2G17790	VPS35A, ZIP3, VPS35 homolog A
3	2		1	18	18		1	7.26E+00	0.00E+00	AT5G20490	ATXIK, XI-17, XIK, Myosin family protein with Dil domain
3	3	1		18	10	1		1.26E+00	-2.55E-01	AT2G30880	Pleckstrin homology (PH) domain-containing protein
3	3	1	3	18	16	4	6	6.53E-01	-5.12E-02	AT1G54270	EIF4A-2, eif4a-2
3	3			17	28			7.23E+00	2.17E-01	AT3G07160	ATGSL10, CALS9, gsl10, GSL10, glucan synthase-like 10
3	3	1		17	25	1		1.23E+00	1.67E-01	AT2G28520	VHA-A1, vacuolar proton ATPase A1
3	3			17	19			7.23E+00	4.83E-02	AT1G26670	ATVTI12, VTI12, VTI1B, Vesicle transport v-SNARE family protein
2	2	2	3	17	15	3	3	7.53E-01	-5.44E-02	AT2G43130	ARA-4, ARA4, ATRAB11F, ATRABA5C, RABA5C
3	3			16	16			7.20E+00	0.00E+00	AT5G45130	ATRAB-F2A, ATRAB5A, ATRABF2A, RAB-F2A, RAB5A, RABF2A, RHA1
3	3	1		16	8	2		9.03E-01	-3.01E-01	AT4G32285	ENTH/ANTH/VHS superfamily protein
2	3			15	19			7.18E+00	1.03E-01	AT5G54440	AtTRS130, CLUB, CLUB
3	2	1		15	14	2		8.75E-01	-3.00E-02	AT4G32410	AtCESA1, CESA1, RSW1, cellulose synthase 1
3	2			15	5			7.18E+00	-4.77E-01	AT5G42090	Lung seven transmembrane receptor family protein
2	2	1		15	17	1		1.18E+00	5.44E-02	AT1G52780	Protein of unknown function (DUF2921)
3	2			15	9			7.18E+00	-2.22E-01	AT5G20350	TIP1, Ankyrin repeat family protein with DHHC zinc finger domain
3	3			15	6			7.18E+00	-3.98E-01	AT2G03820	nonsense-mediated mRNA decay NMD3 family protein
3	3			14	15			7.15E+00	3.00E-02	AT1G31130	unknown protein
3	3	1		14	13	1		1.15E+00	-3.22E-02	AT3G58170	ATBET11, ATBS14A, BET11, BS14A, BET1P/SFT1P-like protein 14A
2	2	2		14	14	2		8.45E-01	0.00E+00	AT1G58684	Ribosomal protein S5 family protein
3	2			13	18			7.11E+00	1.41E-01	AT3G17900	unknown protein
3	3			13	17			7.11E+00	1.17E-01	AT1G27930	Protein of unknown function (DUF579)
3	3			13	28			7.11E+00	3.33E-01	AT3G05500	Rubber elongation factor protein (REF)
2	2			13	5			7.11E+00	-4.15E-01	AT5G44240	ALA2, aminophospholipid ATPase 2
3	3	1		13	17	1		1.11E+00	1.17E-01	AT3G47810	ATVPS29, MAG1, VPS29, Calcineurin-like metallo-phosphoesterase superfamily protein
3	3	1		13	12	1		1.11E+00	-3.48E-02	AT3G60340	alpha/beta-Hydrolases superfamily protein
3	3	2		13	10	2		8.13E-01	-1.14E-01	AT4G35870	early-responsive to dehydration stress protein (ERD4)
3	3	2	1	13	13	3	2	6.37E-01	0.00E+00	AT1G50500	ATVPS53, HIT1, VPS53, Membrane trafficking VPS53 family protein
2	1	2	1	13	7	3	2	6.37E-01	-2.69E-01	AT3G54840	ARA-6, ARA6, ATRAB5C, ATRABF1, RABF1, Ras-related small GTP-binding family protein
2	2			12	19			7.08E+00	2.00E-01	AT4G03550	ATGSL05, ATGSL5, GSL05, GSL05, GSL5, PMR4, glucan synthase-like 5
3	3			12	22			7.08E+00	2.63E-01	AT4G16120	COBL7, SEB1, COBRA-like protein-7 precursor

3	3	1		12	24	2		7.78E-01	3.01E-01	AT5G06320	NHL3, NDR1/HIN1-like 3
2	3	2		12	18	2		7.78E-01	1.76E-01	AT4G23430	NAD(P)-binding Rossmann-fold superfamily protein
3	3			12	13			7.08E+00	3.48E-02	AT1G30900	BP80-3;3, VSR3;3, VSR6, VACUOLAR SORTING RECEPTOR 6
2	2			12	11			7.08E+00	-3.78E-02	AT5G58440	SNX2a, sorting nexin 2A
3	2			12	3			7.08E+00	-6.02E-01	AT1G71270	ATVPS52, POK, TTD8, Vps52 / Sac2 family
2	3		3	12	12		3	7.08E+00	0.00E+00	AT1G79720	Eukaryotic aspartyl protease family protein
2	3	1	1	12	12	1	1	1.08E+00	0.00E+00	AT1G01910	P-loop containing nucleoside triphosphate hydrolases superfamily protein
3	1	1		11	3	1		1.04E+00	-5.64E-01	AT4G31850	PGR3, proton gradient regulation 3
3	2	1	1	11	8	1	2	1.04E+00	-1.38E-01	AT5G18230	transcription regulator NOT2/NOT3/NOT5 family protein
2	2			10	8			7.00E+00	-9.69E-02	AT5G64740	CESA6, E112, IXR2, PRC1, cellulose synthase 6
2	2			10	5			7.00E+00	-3.01E-01	AT1G25570	Di-glucose binding protein with Leucine-rich repeat domain
2	3	1		10	7	1		1.00E+00	-1.55E-01	AT4G19490	ATVPS54, VPS54, VPS54
2	1	1		10	4	1		1.00E+00	-3.98E-01	AT3G02260	ASA1, BIG, CRM1, DOC1, LPR1, TIR3, UMB1, auxin transport protein (BIG)
3	3			10	18			7.00E+00	2.55E-01	AT1G26830	ATCUL3, ATCUL3A, CUL3, CUL3A, cullin 3
3	2			10	9			7.00E+00	-4.58E-02	AT4G36720	HVA22K, HVA22-like protein K
2	2			10	9			7.00E+00	-4.58E-02	AT5G26240	ATCLC-D, CLC-D, chloride channel D
2	2			10	7			7.00E+00	-1.55E-01	AT5G07110	PRA1.B6, prenylated RAB acceptor 1.B6
3	2	1		10	13	1		1.00E+00	1.14E-01	AT4G38540	FAD/NAD(P)-binding oxidoreductase family protein
3	3	1	1	10	8	1	1	1.00E+00	-9.69E-02	AT4G34490	ATCAP1, CAP 1, CAP1, cyclase associated protein 1
3	3	2	2	10	9	2	3	6.99E-01	-4.58E-02	AT1G79530	GAPCP-1, glyceraldehyde-3-phosphate dehydrogenase of plastid 1
2	2	1		9	9	1		9.54E-01	0.00E+00	AT5G59840	Ras-related small GTP-binding family protein
2	2			9	12			6.95E+00	1.25E-01	AT3G05710	ATSYP43, SYP43, syntaxin of plants 43
3	2			9	5			6.95E+00	-2.55E-01	AT1G01960	BIG3, EDA10, ARF-GEF
2	2			9	14			6.95E+00	1.92E-01	AT2G39805	Integral membrane Yip1 family protein
3	3			9	13			6.95E+00	1.60E-01	AT1G06470	Nucleotide/sugar transporter family protein
2	1			9	5			6.95E+00	-2.55E-01	AT1G80500	SNARE-like superfamily protein
2	2			9	5			6.95E+00	-2.55E-01	AT2G05170	ATVPS11, VPS11, vacuolar protein sorting 11
2	2	1		9	14	1		9.54E-01	1.92E-01	AT4G25740	RNA binding Plectin/S10 domain-containing protein
2	2	1		9	6	1		9.54E-01	-1.76E-01	AT5G67400	RHS19, root hair specific 19
3	3	1	1	9	16	2	2	6.53E-01	2.50E-01	AT5G61240	Leucine-rich repeat (LRR) family protein
2	1	1		9	2	2		6.53E-01	-6.53E-01	AT1G09020	ATSNF4, SNF4, homolog of yeast sucrose nonfermenting 4
3	2	2	1	9	14	2	3	6.53E-01	1.92E-01	AT3G15980	Coatomer, beta' subunit
2	1	2	1	9	2	2	1	6.53E-01	-6.53E-01	AT5G58060	ATGP1, ATYKT61, YKT61, SNARE-like superfamily protein
2	2			8	8			6.90E+00	0.00E+00	AT3G20650	mRNA capping enzyme family protein
3	3			8	7			6.90E+00	-5.80E-02	AT3G07950	rhomboid protein-related
2	2			8	5			6.90E+00	-2.04E-01	AT2G34300	S-adenosyl-L-methionine-dependent methyltransferases superfamily protein
3	1			8	5			6.90E+00	-2.04E-01	ATCG01090	NDHI, NADPH dehydrogenases
2	1			8	3			6.90E+00	-4.26E-01	AT3G12010	unknown protein
3	2			8	3			6.90E+00	-4.26E-01	AT5G57030	LUT2, Lycopene beta/epsilon cyclase protein
3	3		3	8	55		28	6.90E+00	8.37E-01	AT1G21110	O-methyltransferase family protein
3	3	1	2	8	15	1	3	9.03E-01	2.73E-01	AT1G64650	Major facilitator superfamily protein
3	3	1	2	8	5	1	2	9.03E-01	-2.04E-01	AT1G78870	UBC13A, UBC35, ubiquitin-conjugating enzyme 35
2	2			7	3			6.85E+00	-3.63E-01	AT2G41770	Protein of unknown function (DUF288)
2	3			7	12			6.85E+00	2.34E-01	AT1G08930	ERD6, Major facilitator superfamily protein
2	3			7	12			6.85E+00	2.34E-01	AT4G26550	Got1/Sft2-like vescicle transport protein family
3	2			7	9			6.85E+00	1.09E-01	AT5G53530	VPS26A, vacuolar protein sorting 26A
2	2			7	6			6.85E+00	-6.69E-02	AT2G39750	S-adenosyl-L-methionine-dependent methyltransferases superfamily protein
3	3			7	5			6.85E+00	-1.46E-01	AT1G80240	Protein of unknown function, DUF642

3	3		1	7	13		1	6.85E+00	2.69E-01	AT1G74020	SS2, strictosidine synthase 2
2	2	1		7	9	1		8.45E-01	1.09E-01	AT1G67330	Protein of unknown function (DUF579)
3	3	1		7	8	1		8.45E-01	5.80E-02	AT3G28720	unknown protein
3	3	1		7	6	1		8.45E-01	-6.69E-02	AT3G13720	PRA1.F3, PRA8, PRA1 (Prenylated rab acceptor) family protein
2	2	1		6	11	1		7.78E-01	2.63E-01	AT5G57350	AHA3, ATAHA3, HA3, H(+)-ATPase 3
3	2			6	3			6.78E+00	-3.01E-01	AT3G16785	PLD ZETA 1, PLDP1, PLDZ1, PLDZETA1, phospholipase D P1
2	3			6	11			6.78E+00	2.63E-01	AT1G25420	Regulator of Vps4 activity in the MVB pathway protein
2	3			6	10			6.78E+00	2.22E-01	AT1G80360	Pyridoxal phosphate (PLP)-dependent transferases superfamily protein
2	2			6	8			6.78E+00	1.25E-01	AT3G53520	ATUXS1, UXS1, UDP-glucuronic acid decarboxylase 1
3	2			6	7			6.78E+00	6.69E-02	AT1G79050	recA DNA recombination family protein
2	2			6	6			6.78E+00	0.00E+00	AT1G67430	Ribosomal protein L22p/L17e family protein
3	2			6	6			6.78E+00	0.00E+00	AT1G67560	PLAT/LH2 domain-containing lipoxygenase family protein
3	3			6	5			6.78E+00	-7.92E-02	AT1G68310	Protein of unknown function (DUF59)
2	2			6	5			6.78E+00	-7.92E-02	AT2G35610	XEG113, xyloglucanase 113
2	3			6	4			6.78E+00	-1.76E-01	AT1G02475	Polyketide cyclase/dehydrase and lipid transport superfamily protein
2	1			6	3			6.78E+00	-3.01E-01	AT2G04280	unknown protein
2	3		1	6	4		1	6.78E+00	-1.76E-01	AT4G24550	Clathrin adaptor complexes medium subunit family protein
2	3	1		6	6	1		7.78E-01	0.00E+00	AT2G40690	GLY1, SFD1, NAD-dependent glycerol-3-phosphate dehydrogenase family protein
2	1	1		6	4	1		7.78E-01	-1.76E-01	AT3G15060	AtRABA1g, RABA1g, RAB GTPase homolog A1G
3	3	1	1	6	7	1	1	7.78E-01	6.69E-02	AT5G45620	Proteasome component (PCI) domain protein
2	3	1	3	6	21	1	4	7.78E-01	5.44E-01	AT5G16830	ATPEP12, ATSYP21, PEP12, PEP12P, SYP21, syntaxin of plants 21

4.2.2 - The ARA7 co-purifying proteome contains expected TGN/EE and LE/MVB proteins

In order to gather further confidence that the so-defined YFP-ARA7 co-purifying proteome is specific to ARA7, I filtered the proteome to retain only endomembrane trafficking regulators, by using a comprehensive manually curated list of regulators from (Heard et al., 2015). 49 trafficking regulators were found in the dataset (**fig. 4.6C**), which are listed in **table 4.2.** Besides ARA7 itself, the most abundant proteins in this resulting list are TGN/EE and LE/MVB-associated proteins, which correspond to the endomembrane compartments to which ARA7 localizes.

Vacular Sorting Receptors

I found proteins of the vacuolar sorting receptor (VSR) group, with VSR1/ELP/BP80, VSR4/MTV4, and VSR7 at high abundance (**table 4.2**). VSRs are present in the endomembrane system along the endocytic route. They localize to the PM, clathrin-coated vesicles and TGN/EE, as well as LE/MVBs (Robinson and Neuhaus, 2016). VSR4 cycles between TGN/EE and PM (Saint-Jean et al., 2010). VSR1/ELP/BP80 is strongly TGN/EE and MVB localized (Li et al., 2002). After performing their vacuolar sorting function, which does not occur at the LE/MVB, VSRs are themselves recycled to their original location by the membrane-associated retromer complex (Künzl et al., 2016). The core retromer complex contains subunits VPS26, 29 and 35 (Zelazny et al., 2013), and is found in its entirety in my ARA7 purifications (**table 4.2**). This complex has previously been demonstrated to be present at the LE/MVB (Heucken and Ivanov, 2017).

Table 4.2: Trafficking regulators in the ARA7 co-purifying proteome. Listed here is the ARA7 co-purifying proteome under water treated conditions, copied from **Table 4.1**, and filtered to retain only endomembrane trafficking regulators as defined in Heard et al. 2015.

Table 4.2: Traffic regulators in the ARA7 co-purifying proteome

Observed in # of replicates				Spectra in combined replicates				Enrichment factor (log10)		Protein information	
YFP-ARA7		YFP		YFP-ARA7		YFP		YFP YFP-ARA7	Y7 water Y7 flg22		
water	flg22	water	flg22	water	flg22	water	flg22			Locus ID	Protein name
3	3	3	3	1160	1362	40	18	1.46E+00	6.97E-02	AT4G19640	ARA7
3	3	2	2	186	141	6	3	1.49E+00	-1.20E-01	AT2G14720	BP80-2;1, MTV4, VSR2;1, VSR4, vacuolar sorting receptor 4
3	3			134	110			8.13E+00	-8.57E-02	AT3G19770	ATVPS9A, VPS9, VPS9A, Vacuolar sorting protein 9 (VPS9) domain
3	3			122	79			8.09E+00	-1.89E-01	AT3G52850	ATELP, ATELP1, ATVSR1, BP-80, BP80, BP80-1;1, BP80B, GFS1, VSR1, VSR1;1
3	3	3	3	89	94	21	14	6.27E-01	2.37E-02	AT2G33120	ATVAMP722, SAR1, VAMP722, synaptobrevin-related protein 1
3	3			75	48			7.88E+00	-1.94E-01	AT4G20110	BP80-3;1, VSR3;1, VSR7, VACUOLAR SORTING RECEPTOR 7
3	3			65	42			7.81E+00	-1.90E-01	AT3G54300	ATVAMP727, VAMP727, VAMP727, vesicle-associated membrane protein 727
3	3			64	65			7.81E+00	6.73E-03	AT5G16280	Tetratricopeptide repeat (TPR)-like superfamily protein
3	3	1		48	53	1		1.68E+00	4.30E-02	AT4G30260	Integral membrane Yip1 family protein
3	3	3	2	44	59	9	3	6.89E-01	1.27E-01	AT2G38360	PRA1.B4, prenylated RAB acceptor 1.B4
3	3	2	1	43	45	8	1	7.30E-01	1.97E-02	AT1G32050	SCAMP family protein
3	3	1	1	40	63	1	1	1.60E+00	1.97E-01	AT3G11820	AT-SYR1, ATSYP121, ATSYR1, PEN1, SYP121, SYR1, syntaxin of plants 121
3	3	2	1	40	42	7	2	7.57E-01	2.12E-02	AT1G62020	Coatomer, alpha subunit
2	3	2	2	37	49	3	4	1.09E+00	1.22E-01	AT3G56110	PRA1.B1, prenylated RAB acceptor 1.B1
3	3		1	35	37		1	7.54E+00	2.41E-02	AT1G61250	SC3, SCAMP3, secretory carrier 3
3	3	1		30	38	1		1.48E+00	1.03E-01	AT5G22360	ATVAMP714, VAMP714, VAMP714, vesicle-associated membrane protein 714
3	3	3	3	30	38	7	9	6.32E-01	1.03E-01	AT1G11890	ATSEC22, SEC22, Synaptobrevin family protein
3	3	2	1	29	29	5	2	7.63E-01	0.00E+00	AT3G05000	TRS33, TRAPPI-component
3	3			29	29			7.46E+00	0.00E+00	AT1G08770	PRA1.E, prenylated RAB acceptor 1.E
3	3	2		27	25	5		7.32E-01	-3.34E-02	AT1G02130	ARA-5, ARA5, ATRAB1B, ATRABD2A, RA-5, RABD2A, RAS 5
3	2			24	6			7.38E+00	-6.02E-01	AT2G14740	ATVSR3, BP80-2;2, VSR2;2, VSR3, VSR3, vaculolar sorting receptor 3
2	2			23	37			7.36E+00	2.06E-01	AT3G05280	Integral membrane Yip1 family protein
3	3	1		23	21	3		8.85E-01	-3.95E-02	AT5G11040	AtTRS120, TRS120, TRS120
3	3			22	17			7.34E+00	-1.12E-01	AT5G58030	TRS31, TRAPPI-component
3	2	1		22	15	1		1.34E+00	-1.66E-01	AT1G28490	ATSYP61, OSM1, SYP61, syntaxin of plants 61
3	3			21	26			7.32E+00	9.28E-02	AT1G75850	VPS35B, VPS35 homolog B
2	2			18	18			7.26E+00	0.00E+00	AT2G17790	VPS35A, ZIP3, VPS35 homolog A
3	2		1	18	18		1	7.26E+00	0.00E+00	AT5G20490	ATXIK, XI-17, XIK, Myosin family protein with Dil domain
3	3			17	19			7.23E+00	4.83E-02	AT1G26670	ATVTI12, VTI12, VTI1B, Vesicle transport v-SNARE family protein
2	2	2	3	17	15	3	3	7.53E-01	-5.44E-02	AT2G43130	ARA-4, ARA4, ATRAB11F, ATRABA5C, RABA5C
3	3			16	16			7.20E+00	0.00E+00	AT5G45130	ATRAB-F2A, ATRAB5A, ATRABF2A, RAB-F2A, RAB5A, RABF2A, RHA1
3	3	1		16	8	2		9.03E-01	-3.01E-01	AT4G32285	ENTH/ANTH/VHS superfamily protein
2	3			15	19			7.18E+00	1.03E-01	AT5G54440	AtTRS130, CLUB, CLUB
3	3	1		14	13	1		1.15E+00	-3.22E-02	AT3G58170	ATBET11, ATBS14A, BET11, BS14A, BET1P/SFT1P-like protein 14A
3	3	1		13	17	1		1.11E+00	1.17E-01	AT3G47810	ATVPS29, MAG1, VPS29, Calcineurin-like metallo-phosphoesterase superfamily protein
3	3	2	1	13	13	3	2	6.37E-01	0.00E+00	AT1G50500	ATVPS53, HIT1, VPS53, Membrane trafficking VPS53 family protein
2	1	2	1	13	7	3	2	6.37E-01	-2.69E-01	AT3G54840	ARA-6, ARA6, ATRAB5C, ATRABF1, RABF1, Ras-related small GTP-binding family protein
3	3			12	13			7.08E+00	3.48E-02	AT1G30900	BP80-3;3, VSR3;3, VSR6, VACUOLAR SORTING RECEPTOR 6
2	2			12	11			7.08E+00	-3.78E-02	AT5G58440	SNX2a, sorting nexin 2A
3	2			12	3			7.08E+00	-6.02E-01	AT1G71270	ATVPS52, POK, TTD8, Vps52 / Sac2 family
2	3	1		10	7	1		1.00E+00	-1.55E-01	AT4G19490	ATVPS54, VPS54, VPS54
2	2			10	7			7.00E+00	-1.55E-01	AT5G07110	PRA1.B6, prenylated RAB acceptor 1.B6

2	2			9	12			6.95E+00	1.25E-01	AT3G05710	ATSYP43, SYP43, syntaxin of plants 43
3	2			9	5			6.95E+00	-2.55E-01	AT1G01960	BIG3, EDA10, ARF-GEF
2	2			9	14			6.95E+00	1.92E-01	AT2G39805	Integral membrane Yip1 family protein
2	2			9	5			6.95E+00	-2.55E-01	AT2G05170	ATVPS11, VPS11, vacuolar protein sorting 11
3	2	2	1	9	14	2	3	6.53E-01	1.92E-01	AT3G15980	Coatomer, beta' subunit
2	1	2	1	9	2	2	1	6.53E-01	-6.53E-01	AT5G58060	ATGP1, ATYKT61, YKT61, SNARE-like superfamily protein
3	2			7	9			6.85E+00	1.09E-01	AT5G53530	VPS26A, vacuolar protein sorting 26A
3	3	1		7	6	1		8.45E-01	-6.69E-02	AT3G13720	PRA1.F3, PRA8, PRA1 (Prenylated rab acceptor) family protein
2	1	1		6	4	1		7.78E-01	-1.76E-01	AT3G15060	AtRABA1g, RABA1g, RAB GTPase homolog A1G
2	3	1	3	6	21	1	4	7.78E-01	5.44E-01	AT5G16830	ATPEP12, ATSYP21, PEP12, PEP12P, SYP21, syntaxin of plants 21

SNAREs

Soluble N-ethylmaleimide-sensitive factor Attachment Protein Receptors (SNAREs) are endomembrane pathway-specific, predominantly transmembrane proteins with cytosolic coiled-coil domains that mediate membrane fusion (Uemura et al., 2004; Lipka et al., 2007). In ARA7 purifications, I identified PEN1/SYP121 (**table 4.2**), which is a PM and TGN/EE-localized SNARE that cycles between these compartments (Nielsen et al., 2012; Nielsen and Thordal-Christensen, 2012; Assaad et al., 2004). Furthermore, I identified the TGN/EE-localized SNAREs SYP43 (Uemura et al., 2012) and SYP61, which functions in complex with VTI12 (Drakakaki et al., 2012), which itself is also identified in my ARA7 purifications (**table 4.1**). Further identified VPS45 is a regulatory protein of this SNARE complex, which also localizes to the TGN/EE (Zouhar et al., 2009). Curiously, the known SYP61 interaction partner SYP41 was not found (Zouhar et al., 2009). SNAREs further along the endocytic route that were identified are VAMP722, which co-localizes to the TGN/EE marker VHA-a1 which is also found in my dataset (**tables 4.1, 4.2**, (Zhang et al., 2011a)), and finally VAMP727 which localizes to the LE/MVB (Ebine et al., 2008).

Rab-GTPase associated proteins

In addition to these membrane-associated proteins, Rab GTPase-associated proteins such as VPS9a and PRA1 family proteins were identified. Importantly, VPS9a is the only gunanine nucleotide exchange factor (GEF) that is known to interact with and facilitate GTP-binding of all three Arabidopsis Rab5 proteins including ARA7 (Goh et al., 2007). PRA1 family proteins interact with Rab GTPases and allow the Rab to bind to the membrane (Alvim Kamei et al., 2008; Gendre et al., 2014). Most abundantly, I found PRA1.B4 and PRA1.B1, which were identified in previous ARA7 purifications (Heard et al., 2015), upon which colocalization of PRA1.B1 with ARA7 in leaf tissue was further confirmed (Heard et al., 2015). Finally, PUF2, mediates competition for activation between ARA7 and ARA6 on the same endosome and localizes to the LE/MVB compartment (Ito et al., 2018).

Novel proteins

Some proteins were found that are not known to localize to TGN/EE or LE/MVB compartments. The most abundant protein in ARA7 purifications, besides ARA7 itself, is SUPPRESSOR OF ACAULIS 56 (SAC56), which is an L4/L1 family integral subunit of ribosomes. Furthermore, both SEC22 and coatomer proteins function at the interface between ER and Golgi, with a role for SEC22 in anterograde traffic, and for a heptameric complex of coatomer subunits in retrograde traffic (Chatre, 2005; Brandizzi and Barlowe, 2013). Finally, PRA1.B6 localizes to the Golgi (Jung et al., 2011). Mostly, the above ER/Golgi associated proteins were found with low abundance.

4.2.3 - The ARA7 co-purifying proteome changes upon 3-h flagellin treatment

Having established that I can obtain a specific ARA7 proteome, I applied the technique to flagellin-treated Arabidopsis seedlings. I treated seedlings with 1.5 µM flg22 for three h, allowing for PTI-induced transcriptional upregulation and the accumulation of potential immune-related cargoes in endosomes. Then, I defined an ARA7 co-purifying proteome in the same way as I did for the above-described water treated conditions, and filtered the list to retain only proteins of which the associated spectral counts were upregulated at least twice in the flg22-treated conditions compared to water control. The flg22-upregulated ARA7 co-purifying proteome contains 70 proteins, of which 13 were also found under water control treatment, and 57 that were not. (**fig. 4.6D, table 4.3**).

GO-analysis shows enrichment for inorganic acid chemistry-related terms

In order to obtain a global picture of the biological processes in which the flg22-induced ARA7 interactors are involved, I performed a GO-term analysis querying for terms in the "biological process" category (**table S2**). Interestingly, there is a strong overrepresentation of metabolic processes such as organic and carboxylic acid metabolism as well as drug/small molecule metabolism, indicating that the purified compartment is chemically active, or contributes to changed metabolic processes at its location. In correspondence with the GO-term enrichment for general organic acid metabolism, among the flg22-induced ARA7 interactors (**table 4.3**) I find Indole Glucosinolate *O*-Methyl Transferase 4 (IGMT4).

Table 4.3: ARA7 co-purifying proteins that are more abundant upon flagellin treatment. Listed here is the ARA7 co-purifying proteome under flagellin treated conditions. 8-day old seedlings of genotypes *pUB::YFP-ARA7* and *pUB::YFP* were treated with water or 1.5 µM flg22 for three hours, and subjected to immunoprecipitation using YFP affinity beads. Mass spectrometry was performed in collaboration with Jan Sklenar, Paul Derbyshire and Frank Menke (The Sainsbury Laboratory, Norwich, UK). To determine co-purifying proteomes, Scaffold software was used to retain proteins with a ProteinProphet score of 99% based on a minimum of 2 spectra with a PeptideProphet score of 95%. MS Excel was then used to retain proteins with at least 5 spectra across all three replicates in the YFP-ARA7 flg22-treated samples, with an occurence in more than 1 of these replicates, an abundance increase of at least 4x compared to matching YFP controls, and an abundance increase of at least 2x compared to matching water treated controls. (*Columns 1-8*) Observed in # of replicates, and Spectra in combined replicates: Numbers and associated green cell-shading intensities indicate in how many experimental replicates the protein was detected, or how many spectra for that protein were identified in all three replicates combined, separated for water or flagellin treatment. (*Columns 9-10*) Enrichment factors: For each protein, the number of total spectra across three replicates of the green-labeled (rightmost) pulldown was divided by the number of total spectra in red-labeled (left-most) pulldown. Log10 values that correspond to these ratios are displayed in this table. Green or red bars are graphical representations of magnitude and direction of positive (green) or negative (red) values, centered at 0. (Columns *11-12*) Locus ID and associated names. Source: TAIR10, accessed through www.genevestigator.org. The table is sorted for total spectral numbers in "YFP-ARA7 flg22", in descending order.

Table 4.3: ARA7 co-purifying proteins that are more abundant upon flagellin treatment

Observed in # of replicates				Spectra in combined replicates				Enrichment factor (log_{10})		Protein information	
YFP-ARA7		YFP		YFP-ARA7		YFP		YFP YFP-ARA7	Y7 water Y7 flg22	Locus ID	Protein name
water	flg22	water	flg22	water	flg22	water	flg22				
	3				36			0.00E+00	7.56E+00	AT5G25250	FLOTILLIN 1
3	3	2	3	15	36	45	8	-4.77E-01	3.80E-01	AT2G30870	ATGSTF10, ATGSTF4, ERD13, GSTF10, glutathione S-transferase PHI 10
3	3	2	2	15	32	61	4	-6.09E-01	3.29E-01	AT5G41670	6-phosphogluconate dehydrogenase family protein
1	3	3	2	11	30	46	4	-6.21E-01	4.36E-01	AT5G01410	ATPDX1, ATPDX1.3, PDX1, PDX1.3, RSR4, Aldolase-type TIM barrel family protein
3	3			13	28			7.11E+00	3.33E-01	AT3G05500	Rubber elongation factor protein (REF)
	3				26			0.00E+00	7.41E+00	AT1G66090	TN3, ATTN3, TIR-NBS3
2	3	3	3	4	24	4	5	0.00E+00	7.78E-01	AT1G21130	IGMT4, Indole Glucosinolate O-Methyl Transferase 4
	3	1	2		21	4	4	-6.60E+00	7.32E+00	AT5G06860	ATPGIP1, PGIP1, polygalacturonase inhibiting protein 1
2	3	1	3	6	21	1	4	7.78E-01	5.44E-01	AT5G16830	ATPEP12, ATSYP21, PEP12, PEP12P, SYP21, syntaxin of plants 21
2	2	2	1	7	19	27	2	-5.86E-01	4.34E-01	AT3G53460	CP29, chloroplast RNA-binding protein 29
2	2			4	18			6.60E+00	6.53E-01	AT5G03700	D-mannose binding lectin protein with Apple-like carbohydrate-binding domain
1	2	3	2	7	17	19	4	-4.34E-01	3.85E-01	AT2G47000	ABCB4, ATPGP4, MDR4, PGP4, ATP binding cassette subfamily B4
1	2			1	16			6.00E+00	1.20E+00	AT4G24160	Lipid homeostasis alpha-beta hydrolase
2	2	1		4	16	1		6.02E-01	6.02E-01	AT1G78240	OSU1, QUA2, TSD2, S-adenosyl-L-methionine-dependent methyltransferase
3	3	1		7	16	6		6.69E-02	3.59E-01	AT5G26710	Glutamyl/glutaminyl-tRNA synthetase, class Ic
3	3	2	2	7	15	3	2	3.68E-01	3.31E-01	AT5G10730	NAD(P)-binding Rossmann-fold superfamily protein
2	3	2	1	6	15	50	1	-9.21E-01	3.98E-01	AT2G42600	ATPPC2, PPC2, phosphoenolpyruvate carboxylase 2
1	3			3	14			6.48E+00	6.69E-01	AT5G16550	unknown protein
1	3	1	1	1	14	11	1	-1.04E+00	1.15E+00	AT3G16530	Legume lectin family protein
1	2	2		2	14	16		-9.03E-01	8.45E-01	AT4G10480	Nascent polypeptide-associated complex (NAC), alpha subunit family protein
3	3	2	2	6	13	9	2	-1.76E-01	3.36E-01	AT4G12790	P-loop containing nucleoside triphosphate hydrolases superfamily protein
2	2	2		6	13	3		3.01E-01	3.36E-01	AT2G20120	COV1, Protein of unknown function (DUF502)
2	3	1		5	13	6		-7.92E-02	4.15E-01	AT4G23850	LACS4, AMP-dependent synthetase and ligase family protein
1	3	2	1	3	13	17	1	-7.53E-01	6.37E-01	AT5G42790	ARS5, ATPSM30, PAF1, proteasome alpha subunit F1
	2	1			12	1		-6.00E+00	7.08E+00	AT4G23180	CRK10
2	3	2		5	12	12		-3.80E-01	3.80E-01	AT2G34590	Transketolase family protein
	3				11			0.00E+00	7.04E+00	AT1G14540	PER4, PEROXIDASE 4
1	3	1		2	11	1		3.01E-01	7.40E-01	AT2G04400	Aldolase-type TIM barrel family protein
1	2	1		1	10	1		0.00E+00	1.00E+00	AT1G51800	IOS1
1	2	1		3	10	6		-3.01E-01	5.23E-01	AT4G08850	LRR-RLK, MIK2
1	3			2	10			6.30E+00	6.99E-01	AT1G52200	PLAC8 family protein
1	2		1	3	10		2	6.48E+00	5.23E-01	AT3G09900	ATRAB8E, ATRABE1E, RABE1e, RAB GTPase homolog E1E
2	3	1		4	10	1		6.02E-01	3.98E-01	AT1G55190	PRA1.F2, PRA7, PRA1 (Prenylated rab acceptor) family protein
1	2	1		3	10	3		0.00E+00	5.23E-01	AT2G30200	catalytics;transferases;[acyl-carrier-protein] S-malonyltransferases;binding
1	2	2		3	10	8		-4.26E-01	5.23E-01	AT5G63570	GSA1, glutamate-1-semialdehyde-2,1-aminomutase
1	2	2	1	3	10	13	2	-6.37E-01	5.23E-01	AT2G16600	ROC3, rotamase CYP 3
1	2	1	1	4	9	2	2	3.01E-01	3.52E-01	AT4G18800	ATHSGBP, ATRAB11B, ATRABA1D, RABA1d, RAB GTPase homolog A1D
3	3	3	1	4	9	9	1	-3.52E-01	3.52E-01	AT5G56030	AtHsp90.2, ERD8, HSP81-2, HSP90.2, heat shock protein 81-2
2	2			3	9			6.48E+00	4.77E-01	AT2G20840	Secretory carrier membrane protein (SCAMP) family protein
1	2	1		4	9	1		6.02E-01	3.52E-01	AT5G44790	HMA7, RAN1, responsive-to-antagonist 1 / copper-transporting ATPase (RAN1)
1	2	1	1	1	9	2	2	-3.01E-01	9.54E-01	AT1G03220	Eukaryotic aspartyl protease family protein
	2				9			0.00E+00	6.95E+00	AT2G39400	alpha/beta-Hydrolases superfamily protein

	3		2		9		2	0.00E+00	6.95E+00	AT2G43620	Chitinase family protein
2	3	1		4	9	4		0.00E+00	3.52E-01	AT1G55020	ATLOX1, LOX1, lipoxygenase 1
	3	2			9	13		-7.11E+00	6.95E+00	AT2G37040	ATPAL1, PAL1, PHE ammonia lyase 1
1	2	3	1	1	9	21	2	-1.32E+00	9.54E-01	AT5G43940	ADH2, ATGSNOR1, GSNOR, HOT5, PAR2, zinc-binding dehydrogenase family protein
1	3			3	8			6.48E+00	4.26E-01	AT1G73030	CHMP1A, VPS46.2, SNF7 family protein
1	3	1		2	8	1		3.01E-01	6.02E-01	AT3G17810	PYD1, pyrimidine 1
1	2	1		2	8	2		0.00E+00	6.02E-01	AT2G29720	CTF2B, FAD/NAD(P)-binding oxidoreductase family protein
2	3	1		3	8	18		-7.78E-01	4.26E-01	AT1G09130	ATP-dependent caseinolytic (Clp) protease/crotonase family protein
	3				7			0.00E+00	6.85E+00	AT3G50480	HR4, homolog of RPW8 4
2	2			3	7			6.48E+00	3.68E-01	AT4G20410	GAMMA-SNAP, GSNAP, gamma-soluble NSF attachment protein
2	3	1		2	7	1		3.01E-01	5.44E-01	AT2G21600	ATRER1B, RER1B, endoplasmatic reticulum retrieval protein 1B
1	3	1		2	7	1		3.01E-01	5.44E-01	AT3G55430	O-Glycosyl hydrolases family 17 protein
1	2	1		3	7	3		0.00E+00	3.68E-01	AT3G10380	ATSEC8, SEC8, subunit of exocyst complex 8
	2	1			7	5		-6.70E+00	6.85E+00	AT4G13780	methionine--tRNA ligase, putative / methionyl-tRNA synthetase, putative / MetRS, putative
	2				6			0.00E+00	6.78E+00	AT2G19160	Core-2/I-branching beta-1,6-N-acetylglucosaminyltransferase family protein
	2		1		6		1	0.00E+00	6.78E+00	AT4G08770	Peroxidase superfamily protein
1	2	1		1	6	1		0.00E+00	7.78E-01	AT3G17410	Protein kinase superfamily protein
1	2			1	6			6.00E+00	7.78E-01	AT3G63250	ATHMT-2, HMT-2, HMT2, homocysteine methyltransferase 2
1	2			2	6			6.30E+00	4.77E-01	AT3G47550	RING/FYVE/PHD zinc finger superfamily protein
2	2			2	6			6.30E+00	4.77E-01	AT5G02890	HXXXD-type acyl-transferase family protein
	2	1			6	2		-6.30E+00	6.78E+00	AT5G16300	Vps51/Vps67 family (components of vesicular transport) protein
1	2	1		2	6	3		-1.76E-01	4.77E-01	AT4G24840	COG2
1	2	1		2	6	3		-1.76E-01	4.77E-01	AT5G17380	Thiamine pyrophosphate dependent pyruvate decarboxylase family protein
1	2	2		2	6	6		-4.77E-01	4.77E-01	AT4G20830	OGOX1, OLIGOGALACTURONIDE OXIDASE 1
1	2	2		2	6	6		-4.77E-01	4.77E-01	AT5G45280	Pectinacetylesterase family protein
	2	2			6	7		-6.85E+00	6.78E+00	AT5G16970	AER, AT-AER, alkenal reductase
2	3	1		2	6	16		-9.03E-01	4.77E-01	AT3G52150	RNA-binding (RRM/RBD/RNP motifs) family protein
	2	2			6	21		-7.32E+00	6.78E+00	AT1G29880	glycyl-tRNA synthetase / glycine--tRNA ligase

Indole-3-glucosinolate pathway enzymes

IGMT4 is highly similar to its three homologs and clustered genes IGMT1-3 (Pfalz et al., 2016), of which IGMT1 and IGMT2 have been characterized to function as final catalyzers in the indole-3-glucosinolate based antimicrobial secretion pathway which involves PEN2 and PEN3 (Birkenbihl et al., 2017). IGMT1 and IGMT2 convert indole-3-methylglucosinolates (I3M) into 4-methodxyindole-3-methylglucosinolate (4MOI3M), in preparation for conversion into toxic end products by the atypical myrosinase PEN2 (Pfalz et al., 2011; Birkenbihl et al., 2017; Xu et al., 2016; Lu et al., 2015). Based on sequence homology, IGMT4 is likely to also be able to catalyze the I3M – 4MOI3M reaction, but this has not been conclusively shown. End products of this pathway, predominantly toxic indole-3-ylmethylamine (I3A) and indole-3-carboxylic acid (ICA) accumulate in *Pto* DC3000-infected tissue (Stahl et al., 2016) and have been previously described to accumulate and function in defense against filamentous fungi (Lipka et al., 2005; Bednarek et al., 2010; Oa et al., 2010).

It must be noted that, PENETRATION 3/PLEIOTROPIC DRUG RESISTANCE 8 (PEN3/PDR8), while not picked up by my filtering criteria, has the following spectral counts: YFP-ARA7 + water: 222, + flg22: 409, YFP + water: 84, + flg22: 37. It highly specifically associated with YFP-ARA7 under flg22 treated conditions, but only enriched with a factor of ca. 1.8 compared to water treatment, which is below the minimum factor of 2 that is required to be considered flg22-responsive under my filtering criteria. The spectral increase of PEN3 under flg22 conditions is noteworthy in the context of IGMT4 and indole glucosinolate metabolism

PEN3 is a PM-localized transmembrane ATP-binding cassette transporter which is thought to transport antimicrobial compounds generated by PEN2 (Stein et al., 2006). It has been shown to focally accumulate at the cell surface under fungal attempted penetration sites, and upon bacterial and flagellin or chitin MAMP challenge (Underwood and Somerville, 2008, 2013; Underwood et al., 2017; Xin et al., 2013). Finding it specifically associating with ARA7 upon flg22-treatment is interesting, because in microscopic analysis, PEN3 has been shown to accumulate at endosomes when measured at 4 h after MAMP-stimulus, and is proposed to traffic through the endocytic pathway to focal accumulations at the cell-surface (Underwood and Somerville, 2013; Underwood et al., 2017). The above finding provides evidence for a role in ARA7 endosomes in this redirection process.

The clathrin-independent endocytic protein FLOTILLIN

FLOTILLIN 1 (FLOT1) belongs to the family of membrane-bound flotillin/reggie-like proteins, which in animals have been well characterized to associate with the cytosolic leaflet of lipid bilayers, and function in bending membranes such as invagination of the plasma membrane in clathrin-independent endocytic processes (Glebov et al., 2006; Frick et al., 2007; Langhorst et al.,

2007). Flotillins interact with receptors and can organise them into a signaling platform in distinct lipid microenvironments (Otto and Nichols, 2011). In plants, FLOT1 has been described to be PM microdomain-associated (Jarsch et al., 2014; Jarsch and Ott, 2011), present in addition on endosomes, and functioning in clathrin-independent endocytosis (Li et al., 2012a). Furthermore, in the context of bacterial symbiosis with legumes, cell-surface symbiosis-pattern recognizing receptor LYK3 co-localizes with FLOT4, which is thought to reflect the assembly of a signaling platform to initiate bacterial infection (Downie, 2014; Haney et al., 2011).

Arabidopsis FLOT1 was found to accumulate at late endosomes in an increased manner upon flagellin immune stimulus (Yu et al., 2017). In animals, flotillins are considered good membrane microdomain markers, present in lipid environments high in saturated sphingolipids and cholesterol (Langhorst et al., 2007). Finding FLOT1 in ARA7 purifications upon flagellin treatment points at the possibility for a change in lipid composition on TGN/EE or LE/MVB compartments during immunity. Interestingly, in mammals, flotillins that are present at endosomes are associated with MVB targeting to the plasma membrane (Meister and Tikkanen, 2014).

Receptors, oxidative stress, and the cell wall

Several receptor kinases (CRK10, IOS1, MIK2) were found to be upregulated in ARA7 purifications upon flg22 treatment. Cysteine-rich receptor-like kinase 10 (CRK10) belongs to the RLK subfamily of cysteine-rich receptor-like kinases (CRKs), which have a wide range of functionality in abiotic and biotic stresses, pathogen defense and cell death (Chen et al., 2003; Ederli et al., 2011). A subset of CRKs, including CRK10, are implicated in regulating the dynamics of MAMP-induced stomatal closure, an intermediate response that occurs at a time scale of several hours post elicitation, potentially through sensing of ROS as a secondary messenger (Bourdais et al., 2015; Kimura et al., 2017). Functionally distinct cell-surface receptors undergo ligand-induced endocytosis, and accumulate in LE/MVBs upon perception of extracellular patterns, a response generally observed to peak between 1-1.5 h after treatment (Ben Khaled et al., 2015; Mbengue et al., 2016; Ortiz-morea et al., 2016). Although not demonstrated for CRKs, finding CRK10 in ARA7 purifications at 3 h after perception of immune stimulus could point at secondary messenger-induced endocytosis, potentially through perception of extracellular reactive oxygen species. Finally, I find proteins that could function in the protection against oxidative stress, such as two peroxidases (PEROXIDASE 4 (PER4) and AT4G08770), and Glutathione Transferase 10 (GSTF10, (Sappl et al., 2009)).

IMPAIRED OOMYCETE SUSCEPTIBILITY 1 (IOS1) is a broad regulator of antifungal and antibacterial cell-surface perception, and interacts with and regulates complex formation of various other transmembrane receptors such as FLS2, EFR and CERK1 (Yeh et al., 2016). MALE DISCOVERER 1-INTERACTING RECEPTOR LIKE KINASE 2 (MIK2) is a cell-wall

integrity sensing RLK with various functions in response to abiotic and biotic stress, including antifungal defense (Van der Does et al., 2017). Finding these receptors at the endocytic pathway suggests that they are undergoing increased turnover in response to a stimulus. Since ligand-induced endocytosis of well-studied receptors peaks between 1-1.5 h (Ben Khaled et al., 2015), if IOS1 and MIK2 also undergo ligand-induced endocytosis, it could be in response to a secondary messenger in response to MAMP treatment. Considering the broad involvement of IOS1 in receptor complexes, and the involvement of MIK2 in cell wall integrity sensing, potentially these modules are engaged in response to cell wall modifications performed by the plant cell itself upon immune stimulus. This could be coupled to the modification of cell-wall polymers which are increasingly cross-linked in the presence of reactive oxygen species (Tenhaken, 2015).

Atypical immune receptors TN3 and HR4

Peptides of the two atypical intracellular immune receptors TIR-NBS3 (TN3) and Homolog of RPW8-4 (HR4) were found in ARA7 purifications, specifically upon flg22 treatment (**table 4.3**).

TN3 is a truncated member of the NOD-like receptor (NLR) type, which typically contain a coiled-coil (CC) or Toll-Interleukin Receptor (TIR) domain, a nucleotide binding site (NBS) and a leucine-rich repeat domain (LRR). TN3 lacks the typical LRR domain, and has been previously shown to be localized to the nucleo-cytosol, and to trigger a hypersensitive response when overexpressed in *N. benthamiana* (Nandety et al., 2013).

HR4 is a short transmembrane (TM) CC-domain-containing atypical resistance protein. In Arabidopsis ecotype Col-0, there are four homologs (HR1-4), named after the ortholog RPW8.2 which is found in ecotype Ms-0 (Xiao et al., 2001). RPW8.2 is the most extensively characterized orthologue, and has been shown to be carried on VAMP721/VAMP722-positive vesicles to the pathogen interface upon *G. orontii* infection, which requires a short targeting motif (Kim et al., 2014). On-site, RPW8.2 promotes encasement formation, accumulation of ROS and can trigger a hypersensitive response (Gao et al., 2009). Recently, it was shown that HR3, the closest RPW8.2 orthologue in Col-0, accumulates at the extrahaustorial interface upon infection with *Golovinomyces cichoracearum*, and the same work showed fluorescently tagged HR4 accumulating there when transiently expressed in *N. benthamiana* (Berkey et al., 2017).

Because of its high specificity to ARA7 upon flagellin treatment (**table 4.3**), and the well described direct roles for NLRs in plant immunity, I selected TN3 for further characterization. NLRs mediate the recognition and signal transduction at the earliest events in the intracellular detection of pathogen-effector mediated immunomodulatory effects, suggesting that these processes could also be occurring near to ARA7, or an ARA7-involving process. Previously, TN2 has been shown to interact biochemically with another trafficking regulator, the exocyst tethering complex subunit Exo70B1, and was shown to be required for previously unexplained constitutive defense

responses in the *exo70b1* mutant background (Zhao et al., 2015). In addition, RPW8-type proteins have been shown to be central regulators of NLR-mediated defense, and exhibited pathogen-targeting subcellular trafficking behavior, which was required for full immunity. Knowing that ARA7 vesicles accumulate under bacterial pathogens, and ARA7 seems to recruit HR4 upon MAMP-stimulus, I selected HR4 for further characterization.

4.3 – TIR-NBS 3 INTERACTS WITH ARA7 AND LOCALIZES TO THE NUCLEUS, CYTOSOL AND MOBILE PUNCTAE

4.3.1 - Confirming the identification of TN3 in flagellin-treated ARA7 purifications

I obtained the amino acid sequences of the two most abundant TN3 peptides detected across three replicates of YFP-ARA7 purifications upon flagellin treatment, and used Protein BLAST (NCBI web interface) to match the peptides against the known Arabidopsis protein database (TAIR10). As a result, the only protein with a 100% identity score to each peptide was TN3 (AT1G66090), with the exception of the peptide VMTIFYGVNPSDVRK, which also fully aligned with a predicted protein encoded by a transposable element (OAP18409.1; **fig. 4.7A**). Furthermore, I graphically mapped which peptides were found across all MS analyses on flg22-induced ARA7-purifications, together with their position in the TN3 amino acid sequence (**fig. 4.7B**). Thus, I could confirm that both TIR and NBS domains of the same protein were detected in all three replicates of the experiment (**fig. 4.7B**).

Next, based on data from the only publication characterizing TN3 to date (Nandety et al., 2013), I obtained a list of all TIR-NBS proteins. The authors defined and phylogenetically aligned 21 Arabidopsis TIR-NBS genes alongside 30 TIR-X proteins; lacking NBS and LRR domains, but including a variable C-terminal domain. I excerpted from their work the TN and TX genes most closely related to TN3, re-aligned them using Clustal Omega (EMBL web suite), and reproduced the encoded domain structure schematically (**fig. 4.7C**). The closest homolog of TN3 is the pseudogenized *TIR-X 4* (*TX4*, AT1G56470), encoding for parts of a TIR-only protein, and the closest homolog of *TN3* sharing the TIR-NBS domain organisation is *TIR-NBS13* (*TN13*, AT3G04210) with a genomic sequence identity of 50% and a protein sequence identity of 45%. In the phylogenetic alignment of close *TN3* homologs, I included more distantly related *TN1* (genomic identity = 46%, protein identity = 28%) as an outgroup (**fig. 4.7C**).

A

NCBI protein BLAST results (top-10)

Max score	Total score	Query cover	E value	Identity	Accession	Description	Comment
Peptide query VMTIFYGVNPSDVRK							
52.8	52.8	100%	3.00E-10	100%	OAP18409.1	hypothetical protein AXX17_AT1G59770	transposable element
52.8	52.8	100%	3.00E-10	100%	AAM67051.1	disease resistance protein, putative	TN3
52.8	52.8	100%	3.00E-10	100%	NP_176783.1	Disease resistance protein (TIR-NBS class)	TN3
50.3	66.2	100%	2.00E-09	93%	BAC43641.2	putative disease resistance protein	RLMB1
50.3	66.2	100%	2.00E-09	93%	NP_176572.1	Disease resistance protein (TIR-NBS-LRR class) family	RLM1B
50.3	66.2	100%	2.00E-09	93%	OAP12203.1	hypothetical protein AXX17_AT1G57340	pre-tRNA
50.3	66.2	100%	2.00E-09	93%	NP_1320566.1	Disease resistance protein (TIR-NBS-LRR class) family	unknown
50.3	66.2	100%	2.00E-09	93%	OAP12204.1	hypothetical protein AXX17_AT1G57340	pre-tRNA
48.6	48.6	100%	9.00E-09	93%	NP_176571.1	Disease resistance protein (TIR-NBS-LRR class) family	AT1G63870
47.7	47.7	100%	2.00E-08	87%	CAB10216.1	disease resistance N like protein	predicted TMV resistance
Peptide query LSLQEQLLSQVLNEKDIR							
59.6	59.6	100%	2.00E-12	100%	AAM67051.1	disease resistance protein, putative	TN3
59.6	59.6	100%	2.00E-12	100%	NP_176783.1	Disease resistance protein (TIR-NBS class)	TN3
48.1	48.1	100%	2.00E-08	89%	OAP18409.1	hypothetical protein AXX17_AT1G59770	transposable element
40.1	40.1	94%	2.00E-05	71%	AHN95331.1	DM2B	RPP1-like cluster
40.1	40.1	94%	2.00E-05	71%	AHN95342.1	DM2E	RPP1-like cluster
38.8	38.8	100%	5.00E-05	72%	OAO94433.1	hypothetical protein AXX17_AT5G57450	DNA repair
37.5	55.6	94%	1.00E-04	65%	ACJ64858.1	disease resistance protein RPP1-like protein R4	RPP1-like
36.7	53	88%	3.00E-04	69%	BAD94052.1	disease resistance - like protein	AT3G44400
36.7	53	88%	3.00E-04	69%	NP_190026.1	Disease resistance protein (TIR-NBS-LRR class) family	AT3G44400
36.7	53	88%	3.00E-04	69%	ADI80539.1	recognition of Peronospora parasitica 1	RPP1

B

C

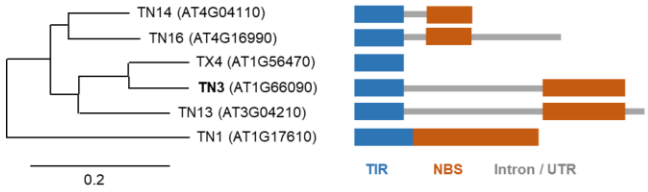

D

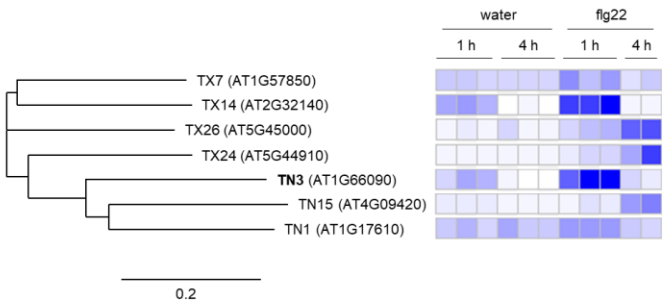

Figure 4.7. TN3 associates with YFP-ARA7-positive compartments in a flg22-responsive manner. (A) Overview shows top-10 search results using NCBI protein BLAST (Organism: *Arabidopsis thaliana*) of two most abundant TN3 peptides identified by mass spectrometry analysis of immunopurified YFP-ARA7-positive compartments upon flg22 treatment. (B) Schematic overview shows the primary TN3 amino acid sequence indicating annotated domains and individually labelled detected peptides identified by mass spectrometry analysis of immunopurified YFP-ARA7-positive compartments upon flg22 treatment. (C) A phylogenetic tree of TN3-related family members was generated using genomic sequences of *TN*/*TX* genes most closely related to *TN3* (source: Nandety et al. 2013, and graphical representation of domain organisations therein). Alignments and phylogenies were obtained using online available EMBL-EBI Clustal Omega and Simple Phylogeny bioinformatics tools. Legend = 0.2 substitutions / base pair. (D) Phylogenetic tree of flg22-responsive TN3-related family members was generated using genomic sequences of *TN*/*TX* genes (source: Nandety et al. 2013) exhibiting flg22-responsive expression as determined by AffyMetrix chip data, GeneVestigator dataset AT-00107 (F. Brunner and B. Schildknecht). GeneVestigator heatmap shows abundance of indicated transcripts upon flg22 treatments for 1 or 4 hours.

Finally, of all *TN* genes (Nandety et al., 2013), I obtained data on transcriptional changes upon flg22 treatment as available through GeneVestigator-linked affymetrix data, extracted those genes whose transcripts were upregulated upon flg22 treatment, and aligned them using Clustal Omega based on genomic sequences, including *TN1* which is not strongly flagellin-responsive as an outgroup (**fig. 4.7D**). Interestingly, of all tested transcripts, *TN3* responded strongest to flg22 treatment, peaking at 1 hpi, followed by *TX14* transcripts also peaking at 1 hpi, of which the protein was not detected in any of my ARA7 purifications. *TX26*, *TX24* and *TN15* responded moderately to flagellin, at a time point of 4 hpi.

In conclusion, I identified TN3 specifically in flg22-treated ARA7 purifications, found that it has a closest homolog in TN13 which shares its TIR-NBS domain organisation, and found that it is one of few strongly flg22-induced *TN/TX* transcripts.

4.3.2 - TN3 interacts with ARA7 in a flg22 independent manner

In order to confirm the TN3-ARA7 interaction with an independent method, I cloned the coding sequence from cDNA, and generated binary vectors encoding C-terminal GFP and RFP fluorescent protein fusions under the control of the Arabidopsis UBIQUITIN-10 promoter (pUB). I delivered *pUB::TN3-RFP* transiently into *pUB::YFP-ARA7* leaf protoplasts using PEG-mediated transfection, and included a vector encoding *p35S::FLS2-FLAG* to enhance the capacity for flagellin recognition. I then treated protoplasts with water or flagellin, and at 3 hpi I performed YFP-ARA7 immunoprecipitations using the same method as used to prepare mass spectrometry samples as described above. Interestingly, upon western blot analysis of purified samples, I could show that TN3-RFP co-purified with YFP-ARA7 upon both water and flg22 treatment (**fig. 4.8A**). This suggests that TN3 interacts with ARA7 independently of immune stimulus. Importantly, *TN3* transcription is known to be strongly upregulated at 1 hour after flg22-stimulus (**fig. 4.7D, fig. 4.8C**), so it is possible that in mass spectrometry analysis, natively expressed TN3 was not

detected in ARA7 purifications under water treatment because the gene was significanly less expressed compared to flg22-treated conditions.

Confocal microscopy analysis of a sample of the protoplast samples revealed that TN3-RFP localizes to the nucleus and the cytosol, whereas YFP-ARA7 localizes to the cytosol and mobile vesicles (**fig. 4.8B, upper panels**). This localization pattern did not change at three h post flg22 treatment (**fig. 2.8B, lower panels**). I conclude that here, TN3 is nucleocytosolic, consistent with data on *Agrobacterium*-mediated transiently overexpressed *35S::TN3-GFP* in *Nicotiana benthamiana* leaves (Nandety et al., 2013).

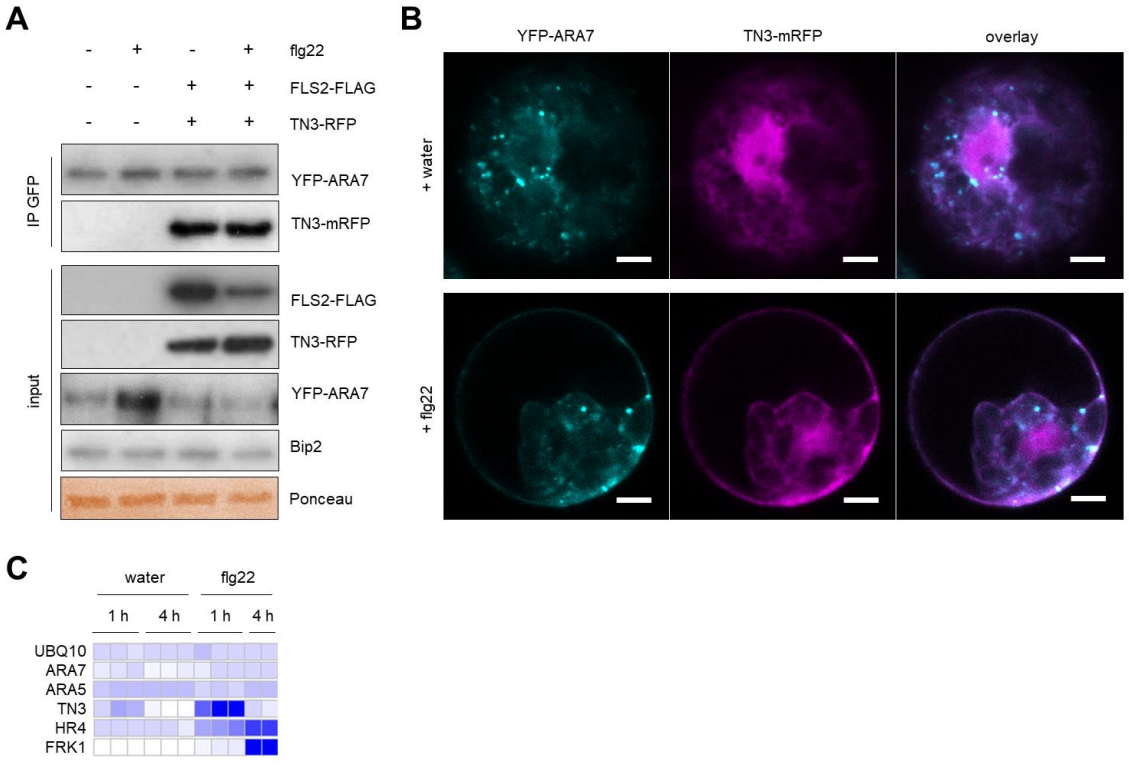

Figure 4.8. Constitutively expressed TN3-RFP associates with YFP-ARA7 independent of flg22 stimulation in Arabidopsis protoplasts. (A) Immunoblot of anti-GFP-immunoprecipitated YFP-ARA7 reveals association with TN3-RFP. Protoplasts from 4 weeks-old leaves were transiently transfected with p*UB::YFP-ARA7*, p*UB::TN3-mCherry* and p*UB::FLS2-FLAG*, incubated for 16 hours for co-expression, and then subjected to flg22 treatment for 3 hours. YFP- and FLAG-tagged proteins were revealed using anti-GFP-HRP and anti-FLAG-HRP conjugated antibodies, respectively. RFP-tagged TN3 and Bip2 were revealed using primary anti-RFP and anti-Bip2 antibodies, then secondary alkaline phosphatase-conjugated antibodies. Ponceau staining was performed on input membranes after antibody treatments for loading control. (B) Confocal micrographs of protoplasts as prepared in (A), showing YFP signal (left panels), RFP signal (middle panels) and overlay (right panels) in z-projections, at 3 hours after indicated treatments. 63 × objective, scale bars = 10 µm. (C) GeneVestigator heatmap shows relative abundance of indicated Arabidopsis transcripts upon flagellin treatment of 1 or 4 hours (AffyMetrix chip data, GeneVestigator dataset AT-00107, F. Brunner and B. Schildknecht)

The interaction of TN3 and ARA7 is now corroborated by two independent experimental methods, and microscopic analysis suggests TN3 and ARA7 co-localize in the cytosol, and TN3 is not enriched at vesicle structures. This could indicate that the interaction takes place in the cytosol preferentially, or involves only a small subpool of TN3. However, constitutively driven expression of TN3 may lead to ectopic localization of TN3 as compared to the endogenous situation, and it is unknown whether TN3 has an interaction preference for subpools of ARA7.

4.3.3 - TN3 interacts with ARA7 on ARA7 vesicles in bimolecular fluorescence complementation experiments

To further probe the interaction between TN3 and ARA7 with an independent method, and aiming to investigate whether TN3 interacts specifically with ARA7 or could also interact with secretory RABs (ARA5/RABD2a), homologous endocytic RABs (ARA6/RABF2a), or RABs further along the endocytic pathway (RABG3b), I employed bimolecular fluorescence complementation (BiFC; split-YFP). I generated binary vectors encoding TN3 C-terminal fusions with the YFP C- and N-termini (*p35S::TN3-YFPc*, *p35S::TN3-YFPn*), and performed *Agrobacterium*-mediated transient co-expressions with BiFC fusions of other RAB-GTPases in *N. benthamiana* leaves. Transient expression of individual RAB-GTPases tagged with YFPc/n in the absence of the complementary YFPn/c terminus does not result in fluorescent YFP signal (**fig. 4.9A, top and left peripheral panels**).

Co-expression of TN3-YFPc and YFPn-ARA7, or the reverse combination of TN3-YFPn and YFPc-ARA7 exhibited clear reconstitution of fluorescent signal was observed on punctae (**fig. 4.9A,B**). The fluorescent YFP signal co-localized with mCherry-ARA7-labeled endocytic vesicles, but not with mCherry-ARA5 labeled secretory vesicles (**fig. 4.9B**). No evident fluorescent signal was observed in the cytosol. Upon co-expression of TN3-YFPn and YFPc-ARA5, no significant reconstitution of fluorescent signal was observed (**fig. 4.9A**). YFPc-ARA5 could be successfully expressed in *N. benthamiana* leaves using this method, as evidenced by the reconstitution of signal in co-expression with YFPn-ARA7 (**fig. 4.9A**). ARA5 and ARA7 are expected to occur in proximity to one another, as both partially localize to the TGN/EE compartment.

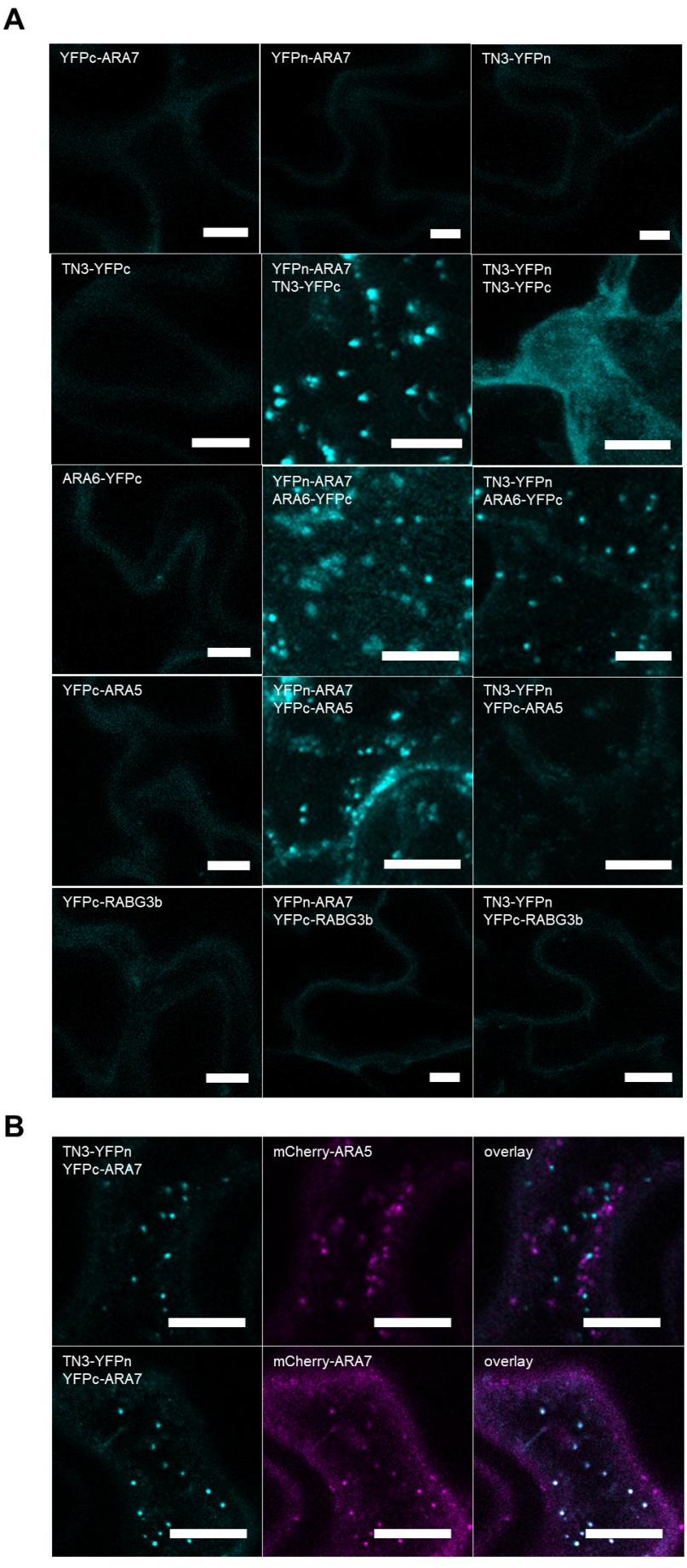
A
YFPc-ARA7
YFPn-ARA7
TN3-YFPn
TN3-YFPc
YFPn-ARA7
TN3-YFPc
TN3-YFPn
TN3-YFPc
ARA6-YFPc
YFPn-ARA7
ARA6-YFPc
TN3-YFPn
ARA6-YFPc
YFPc-ARA5
YFPn-ARA7
YFPc-ARA5
TN3-YFPn
YFPc-ARA5
YFPc-RABG3b
YFPn-ARA7
YFPc-RABG3b
TN3-YFPn
YFPc-RABG3b
B
TN3-YFPn
YFPc-ARA7
mCherry-ARA5
overlay
TN3-YFPn
YFPc-ARA7
mCherry-ARA7
overlay

Figure 4.9. Constitutively expressed TN3-RFP colocalizes and associates with YFP-ARA7-positive compartments in *N. benthamiana*. (A) Bimolecular flurorescence complementation (BiFC). Confocal micrographs showing signal of reconstituted YFP molecules in *Nicotiana benthamiana* adult leaves at 2 days after infiltration of *Agrobacterium tumefaciens* strain GV3101 carrying the indicated bimolecular fluorescence complementation constructs. Combinations of infiltrated constructs are indicated in panels. 63 × objective, scale bars = 10 µm. (B) As in (A), but bimolecular complementations were co-infiltrated with *A. tumefaciens* carrying indicated mCherry-tagged constructs. 63 × objective, scale bars = 10 µm.

Co-expression of TN3-YFPn with LE/MVB-localized RAB-GTPase ARA6-YFPc also reconstituted strong fluorescent signal on punctae, suggesting association of TN3 and ARA6 on endomembrane compartments (**fig. 4.9A**). Fluorescently tagged ARA6 and ARA7 were shown to substantially overlap on the same compartment in earlier studies (Ueda et al., 2004), and indeed upon co-expression of YFPn-ARA7 and ARA6-YFPc, fluorescent signal was observed on punctae, which are likely LE/MVB compartments. Due to the substantial co-localization of ARA6 and ARA7 on endosomes, it is possible that ARA7-associated TN3-YFPn is present on LE/MVBs, where as a consequence it is brought in close proximity to locally present ARA6-YFPc molecules, leading to reconstitution of YFP signal.

TN3-YFPn in combination with tonoplast-localized RAB7-GTPase YFPc-RABG3b did not result in a reconstituted signal (**fig. 4.9A**), together with the absence of fluorescent signal upon co-expression of TN3-YFPn and YFPc-ARA5, suggesting that TN3 specifically associates with RAB-GTPases at the LE/MVB, and not with secretory or vacuolar RAB-GTPases. Co-expression of YFPn-ARA7 and YFPc-RABG3b also did not lead to substantial recovery of fluorescent signal. This confirms specificity, since ARA7 induces its own dissociation and subsequent recruitment of RAB7 proteins to compartments through interaction with, and activation of, intermediate endosomal-localized regulators (Singh et al., 2014b; Cui et al., 2014b), and from localization studies, ARA7 is present at LE/MVBs but not tonoplast. Another RAB7 member RABG3f was shown to be present at the tonoplast but not LE/MVBs. Preliminary data suggests that RABG3b localizes to the tonoplast (**Kopischke et al., submitted**).

Co-expresion of TN3-YFPn and TN3-YFPc resulted in the reconstitution of flurorescent signal in the cytosol, and not the nucleus (**fig. 4.9A**), which is notably different from the nucleocytosolic localization of TN3-RFP as observed in transient expression in Arabidopsis protoplasts (**fig. 4.8A**). It is possible that the reconstituted molecule TN3-YFP-TN3 with a predicted molecular weight of 122 kDa exceeds the maximum size of passive diffusion through nuclear pores, or alternatively, the reconstituted dimer could fail to recruit the necessary interaction partners for active transport into the nucleus. It remains to be demonstrated whether TN3 molecules dimerize in the absence of forced dimerization using YFP fragments.

In conclusion, using BiFC I could show that TN3 exists in close proximity to the LE/MVB-localized RAB5-GTPases ARA7 and ARA6, but not with secretory ARA5 or late endocytic/tonoplastic RAB7 member RABG3b. It is interesting to find the irreversibly bound ARA7-TN3 dimer at ARA7-positive endosomes, because when separately tagged, TN3 did not enrich at vesicles but co-localized with ARA7 predominantly in the cytosol. TN3 in combination with ARA6 reconstituted YFP fluorescent signals, raising the hypothesis that TN3 may interact with other endosomal Rab GTPases in addition to ARA7.

4.3.4 - TN3 localizes to the nucleus, cytosol and mobile punctae in Arabidopsis leaves

Transient expression by particle delivery

Next, I was interested in probing the localization of TN3 in intact Arabidopsis leaves. In a previous study, novel mass-spectrometry-identified ARA7-interactors of the PRA1 family of RAB-regulator proteins have been confirmed to co-localize with ARA7 on endosomes upon transient expression using particle bombardment (Heard et al., 2015).

In order to achieve this, I generated constructs in the small pGEM-T vector backbone, using the Ubiquitin-promoter-driven fluorescently tagged TN3-RFP expression cassette that I generated for transient expression in Arabidopsis protoplasts and *N. benthamiana* leaves. I used gold-particle based tissue bombardment on separated Arabidopsis leaves to deliver the construct into the *pUB::YFP-ARA7* background, and analysed cells using confocal microscopy one day after particle delivery.

In successfully transformed cells, TN3-RFP exhibited a nucleocytosolic and punctate localization pattern, where YFP-ARA7 located to endosomes and the cytosol (**fig. 4.10A**). TN3 puncate were less numerous than ARA7 punctae (data not shown). The mobility of TN3 punctae becomes evident in confocal micrographs where the path of mobile punctae corresponds to the direction of confocal laser scanning acquisition, as shown in **fig. 4.10A, right panels**. Secondly, in time-course acquisitions of cells expressing TN3-RFP, the mobility of both YFP-ARA7 vesicles and TN3-RFP punctae can be observed as punctate signals observed at t = 0 s were not found in later acquisitions at t = 5 s or 10 s (**fig. 4.10B**). TN3-RFP punctate signals did not overlap with YFP-ARA7-positive vesicles, but TN3-RFP cytosolic signal overlapped with YFP-ARA7 cytosolic signal.

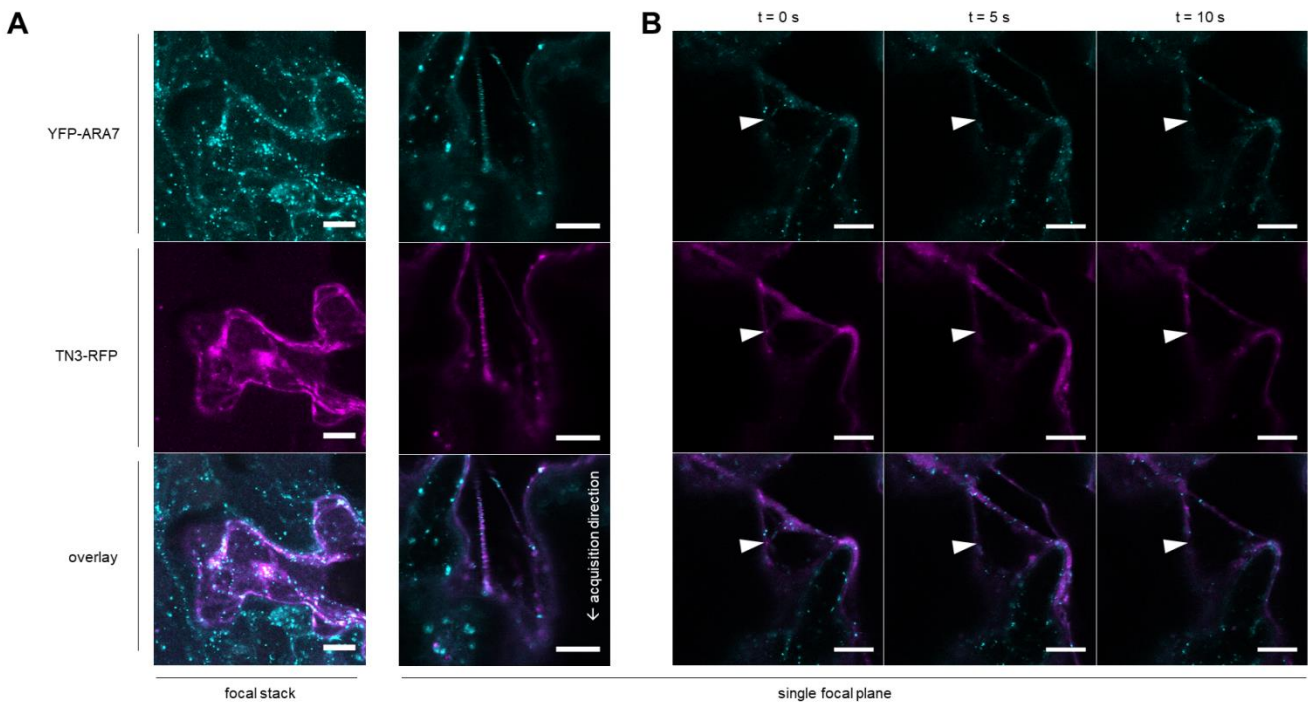

Figure 4.10 Constitutively expressed TN3-GFP localizes to vesicles, the cytosol and the nucleus in transiently expressing Arabidopsis leaf pavement cells. (A) Confocal micrographs of leaf epidermal cells of genotype *pUB::YFP-ARA7* at ca. 16 h after tissue-bombardment using gold particles coated with the binary vector carrying *pUB::TN3-mRFP*. Left panels: z-projection of co-expressing cell. Right panels: single focal acquisition of co-expressing cell. Label and arrow indicate laser scanning direction during image acquisition. (B) As in (A), but showing three time points of an acquisition time-series. Arrowheads in t = 0, 5, 10 s point at the location of an RFP-positive puncta at t = 0 s. 63 × objective, scale bars = 10 µm.

Stable transgenic expression

In order to investigate TN3 localization patterns in non-transiently expressing tissue, in collaboration with Matthew Smoker and Jodie Taylor (Tissue Culture & Transformation Support Team, The Sainsbury Laboratory, Norwich, UK) I generated Arabidopsis lines expressing *pUB::TN3-GFP* in a Col-0, *pUB::RFP-ARA7* (source: Karin Schumacher, Heidelberg, Germany) and *tn3* (SALK_018440.56.00) mutant background. *tn3* lines contain a T-DNA insertion in the *TN3* promoter, and homozygosity for the insertion was confirmed by genomic DNA extraction and PCR using insert- and gene-specific primers.

In all backgrounds, confocal microscopic analysis revealed that TN3-GFP was predominantly localized to the nucleus and cytosol (**fig. 4.11A, B**), matching patterns found in Arabidopsis and *N. benthamiana* transient systems, and in addition TN3-GFP signal showed a weakly labeled punctate pattern, which in some cases could reflect cytosolic strands oriented in the z-direction (**fig. 4.11B, lower panels**). These punctae did not overlap with RFP-ARA7 vesicles.

In conclusion, the nucleocytosolic and punctate localization patterns of TN3-GFP corresponded to the nucleocytosolic pattern in protoplasts, and the nucleocytosolic and punctate localization found upon transient expression in Arabidopsis using particle delivery. The identity of TN3 mobile punctae remains to be demonstrated, as well as any potential TN3 localization pattern changes upon MAMP-stimulus.

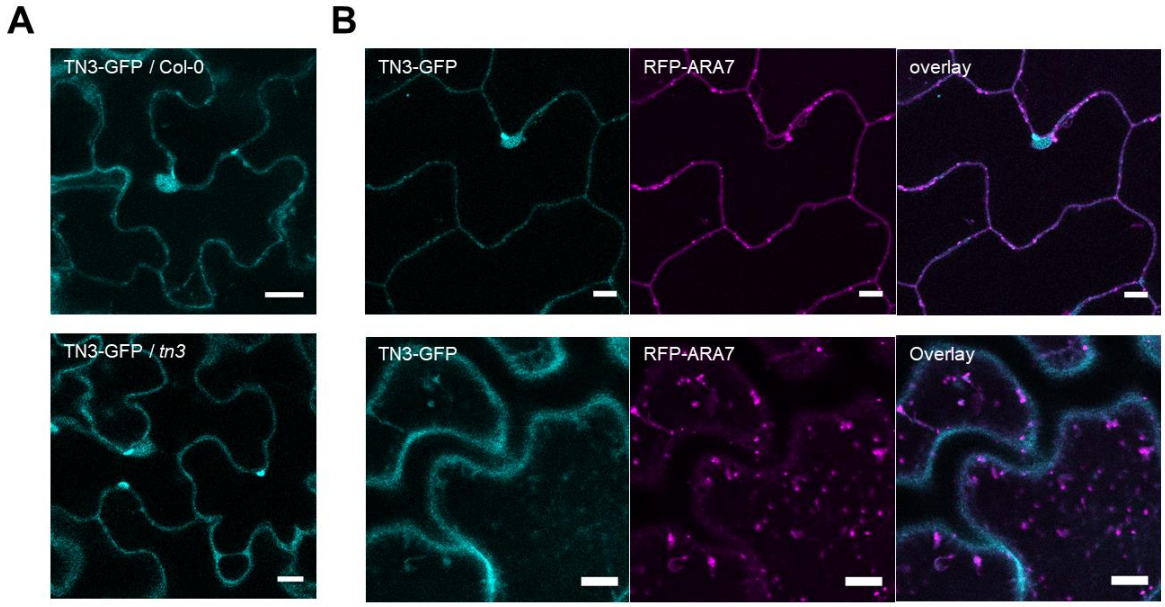

Figure 4.11. Constitutively expressed TN3-GFP localizes to vesicles, the cytosol and the nucleus in transgenic Arabidopsis plants. (A,B) Confocal micrographs showing GFP (A, B) and RFP (B) signals of 4 wk-old Arabidopsis leaf epidermis of indicated genotypes. *pUB::TN3-GFP* was introduced into (A) Col-0 or *tn3* and (B) *pUB::RFP-ARA7* using *Agrobacterium tumefaciens* and floral dipping. Microscopic analysis was performed T1 plants selected at 2 weeks using BASTA/PPT. 63 × objective, scale bars = 10 µm.

4.3.5 - The TN3 localization pattern does not change upon bacterial stimulus

It is possible that TN3 may show the same pathogen-induced focal accumulation pattern as ARA7 in the same time frame. To test this, I syringe-infiltrated *Pto* DC3000 wildtype, and *Pto* DC3000-mCherry fluorescently tagged bacteria into fully developed leaves of 4-week old *tn3* / *pUB::TN3-GFP* Arabidopsis plants, and analysed cells using confocal microscopy.

Between 6-7 h after infiltration of *Pto* DC3000, the time point at which ARA7 showed focal accumulations, I did not observe a change in the predominantly nucleocytosolic localization of TN3-GFP (**fig. 4.12A**). While cell-periphery-localized structures were observed, these are nuclei, as evidenced by the visible decrease in TN3-GFP-intensity in the nucleolus. To be able to visualise bacterial contact sites, I infiltrated Pto DC3000-mCherry bacteria. However, when observing multiple bacterial contact sites with immobilized Pto DC3000-mCherry bacteria, no obvious localization pattern changes, or accumulations, of TN3-GFP were observed (**fig. 4.12A, lower panels, B**). For nearly all bacterial contact sites that were analysed in earlier experiments, YFP-ARA7 concentration was observed at infection sites.

I conclude that TN3 does not focally accumulate like ARA7 upon bacterial infection, but shows no evident changes in its predominantly nucleocytosolic localization pattern. This raises further questions on the nature of the interaction between TN3 and ARA7, because the predominant localization of ARA7 at these time points is at clearly observable vesicle clusters. TN3 may be involved in guarding many host processes, including those that are ARA7 dependent.

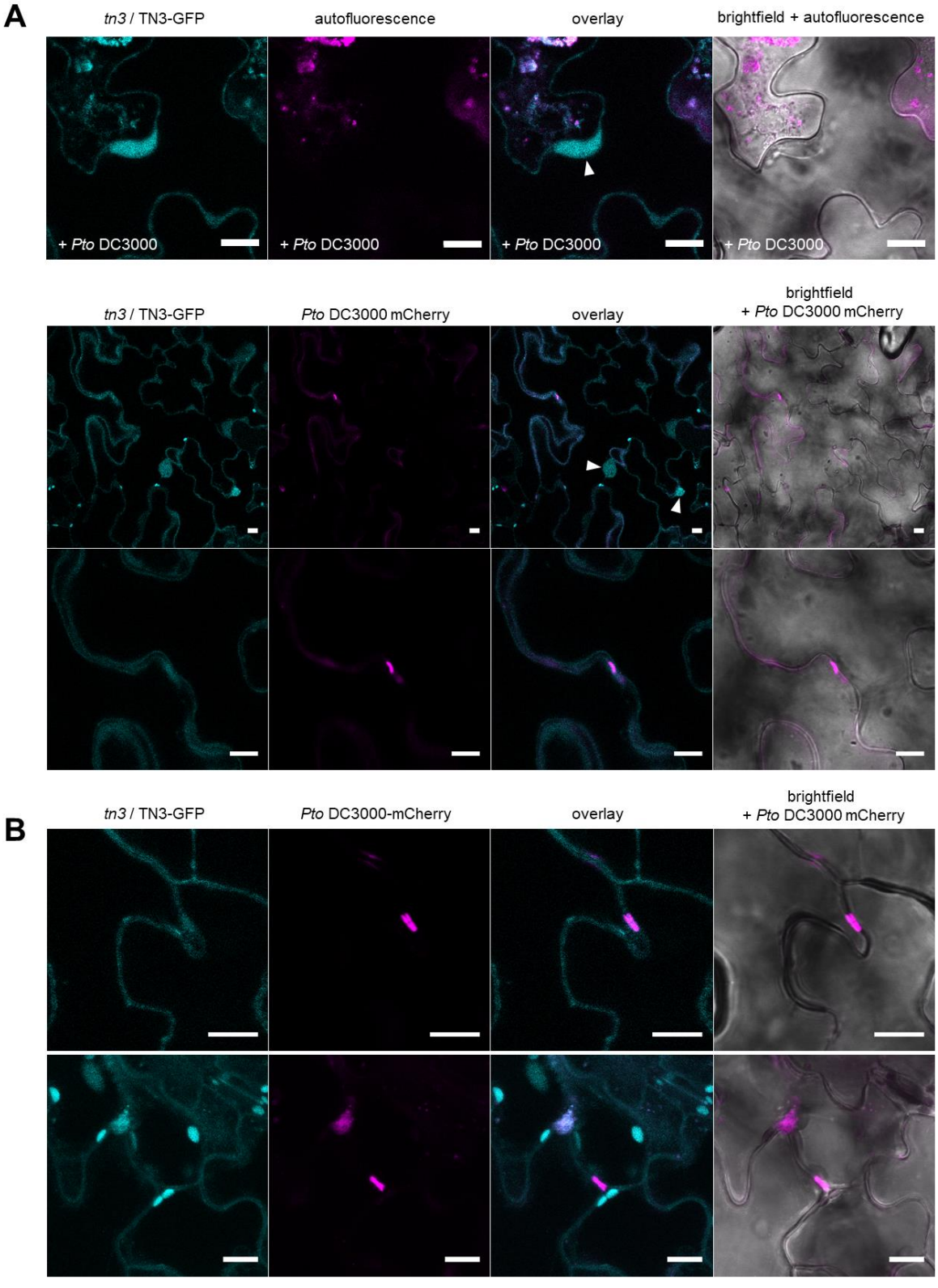
A
tn3 / TN3-GFP
autofluorescence
overlay
brightfield + autofluorescence
+ Pto DC3000
+ Pto DC3000
+ Pto DC3000
+ Pto DC3000
tn3 / TN3-GFP
Pto DC3000 mCherry
overlay
brightfield
+ Pto DC3000 mCherry
B
tn3 / TN3-GFP
Pto DC3000-mCherry
overlay
brightfield
+ Pto DC3000 mCherry

Figure 4.12. TN3-GFP does not show focal accumulation in response to bacterial infection. (A) Confocal micrographs showing GFP (A, B) and autofluorescence (A) or mCherry signals (A,B) in leaf epidermal cells of 4 wk-old T1 Arabidopsis plants expressing *pUB::TN3-GFP* in a *tn3* background, 6 hours after syringe infiltration with wildtype *Pto* DC3000 bacteria (A, top panels) or at 6 hours after syringe infiltration of *Pto* DC3000-mCherry (A, bottom panels; B, all panels). Arrowheads point at nuclei. 63 × objective, scale bars = 10 µm. (B) Additional observations of immobile *Pto* DC3000-mCherry bacteria at plant cell surfaces, as in (A) lower panels.

4.4 – HOMOLOG OF RPW8 4 LOCALIZES TO MITOCHONDRIA

4.4.1 - Confirming the identification of HR4 in flagellin-treated ARA7 purifications

As a second candidate that was identified in ARA7 purifications upon flg22 treatment only, I selected Homolog of RPW8 4 (HR4) for follow-up investigation. RPW8 homologs, and the well-studied orthologue in Ms-0 RPW8.2, have been shown to exhibit accumulation around pathogen interfaces of powdery mildews in *Arabidopsis* and *N. benthamiana* (Berkey et al., 2017; Wang et al., 2013; Kim et al., 2014), and confer broad-spectrum resistance to infectious powdery mildews (Xiao et al., 2001). It is possible that ARA7 could play a role in directing the localization of HR4, potentially contributing to its functioning in immunity.

I obtained amino acid sequences of the two peptides identified in mass spectrometry, and used Protein BLAST (NCBI web interface) to match the peptides against the known Arabidopsis protein database (TAIR10). Both peptides returned predominantly 100 % sequence identity to HR4, with the exception of peptide “TMESISPVRDR”, identified in two experimental replicates, which also matched against the transcription factor bHLH147, but with only 63% coverage of the HR4 peptide sequence (**fig. 4.13A**). Next, I graphically mapped the identified HR4 peptides to its amino acid sequence, with annotated transmembrane (TM) and coiled-coil (CC) domains. One detected peptide covers the N-terminus of HR4, with a 4-amino acid overlap into the N-terminal TM-domain (**fig. 4.13B**).

While the coiled-coil domain of HR4 was not detected in my experiments, two peptides were found in separate experimental replicates that match between the TM and CC domains (**fig. 4.13B**). In addition to using SCAFFOLD PeptideProphet and ProteinProphet confidence treshholds during mass-spectrometry data analysis in preparation for defining ARA7-co-purifying proteomes, I also intended to confirm that the peptides I found for HR4 were specific to HR4, and not to other HR family members. Indeed, the N-terminal peptide “MPIAELAVIK” matched with a highly HR4-specific inserted stretch of amino acids at the N-terminus, as can be observed when aligning HR1-4 and plotting the location of this peptide in the multiple sequence alignment (**fig. S14**). In addition, the second peptide “TMESISPVRDR” fully matched with a sequence that aligns with all HR homologs, but is specific to HR4 on amino acid level, and not to HR1,2 or 3 (**fig. S14**).

A

NCBI protein BLAST results (top-10)

Max score	Total score	Query cover	E value	Identity	Accession	Description	Comment
Peptide query MPIAELAVIK							
35.4	35.4	100%	2.00E-04	100%	BAF01383.1	hypothetical protein	HR4
35.4	35.4	100%	2.00E-04	100%	NP_566933.1	homolog of RPW8 4	HR4
35.4	35.4	100%	2.00E-04	100%	BAD94912.1	hypothetical protein	HR4
35.4	35.4	100%	2.00E-04	100%	ACJ05895.1	HR4	HR4
35.4	35.4	100%	2.00E-04	100%	ACJ05896.1	HR4	HR4
35.4	35.4	100%	2.00E-04	100%	NP_001325500.1	homolog of RPW8 4	HR4
35.4	35.4	100%	2.00E-04	100%	ACJ05897.1	HR4	HR4
32	32	100%	3.00E-03	90%	OAP05460.1	hypothetical protein AXX17_AT3G44680	Histone deacetylase 9
32	32	100%	3.00E-03	90%	OAP05459.1	hypothetical protein AXX17_AT3G44680	Histone deacetylase 9
23.5	35.6	100%	2.90E+00	75%	OAP06235.1	hypothetical protein AXX17_AT3G44740	tRNA synthase
Peptide query TMESISPVRDR							
39.2	39.2	100%	9.00E-06	100%	BAF01383.1	hypothetical protein	HR4
39.2	39.2	100%	9.00E-06	100%	NP_566933.1	homolog of RPW8 4	HR4
39.2	39.2	100%	9.00E-06	100%	BAD94912.1	hypothetical protein	HR4
39.2	39.2	100%	9.00E-06	100%	NP_001325500.1	homolog of RPW8 4	HR4
34.1	34.1	100%	6.00E-04	91%	ACJ05896.1	HR4	HR4
34.1	34.1	100%	6.00E-04	91%	ACJ05897.1	HR4	HR4
28.6	28.6	100%	5.40E-02	82%	ACJ05895.1	HR4	HR4
26.1	26.1	63%	4.40E-01	100%	NP_566567.1	sequence-specific DNA binding transcription factor	bHLH147
21.8	21.8	63%	1.50E+01	86%	NP_192706.5	conserved telomere maintenance component 1	AT4G09680
21.8	21.8	63%	1.50E+01	86%	NP_001329551.1	conserved telomere maintenance component 1	AT4G09680

B

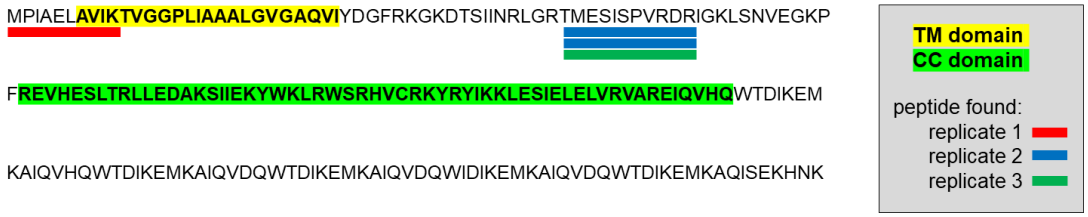

C

Figure 4.13. HR4 associates with YFP-ARA7-positive compartments in a flg22-responsive manner. (A) Overview shows top-10 search results using NCBI protein BLAST (Organism: *Arabidopsis thaliana*) of two most abundant HR4 peptides identified in mass spectrometry analysis of immunopurified YFP-ARA7 upon flg22 treatment. (B) Schematic overview shows the primary HR4 amino acid sequence indicating annotated domains and individually labelled detected peptides identified by mass spectrometry analysis of immunopurified YFP-ARA7 upon flg22 treatment. (C) Phylogenetic tree of all four Homologs of RPW8.2 (HR1-4) was generated using genomic sequences of all four HR genes (source: The Arabidopsis Information Resource (TAIR)-10). Alignments and phylogenies were obtained using online available EMBL-EBI Clustal Omega and Simple Phylogeny bioinformatics tools. Legend = 0.2 substitutions / base pair.

In a multiple sequence alignment based on genomic sequences of all four Col-0 Homolog of RPW8 genes using Clustal Omega (EMBL web suite), HR4 aligns most closely to HR3 (**fig. 4.13C**). In a recent study that further analysed the function of HR1, HR2, HR3 and HR4 from Col-0, HR3 was found to have the most pronounced effects on powdery mildew resistance (Berkey et al., 2017). In addition, HR3 has been previously suggested to be most similar to the ancestral gene that gave rise to RPW8.1 and RPW8.2 in Ms-0, as well as HR1-4 in Col-0 (Xiao et al., 2005). Interestingly, HR3 was found a the papilla under *Golovinomyces cichoracearum* attempted penetration sites in the leaf epidermis, in addition to subsequently formed encasements around the haustorial neck (Berkey et al., 2017). In addition, upon transient expression in *N. benthamiana,* HR4 was found to accumulate around *G. cichoracearum* encasements (Berkey et al., 2017). In my studies, finding HR4 interacting with ARA7 upon MAMP-stimulus is consistent with ARA7 accumulating around haustoria of *Golovinomyces orontii* and *Phytophthora infestans* (Bozkurt et al., 2015; Inada et al., 2016), and specifically at encasements in the interaction with *Blumeria graminis* f.sp. *hordei* (Nielsen et al., 2017b), but at this point it is unknown whether HR4 also accumulates at bacterial infection sites.

4.4.2 - HR4 localizes to the periphery of mitochondria

Next, I sought to reveal HR4 subcellular localization using fluorescent tagging and confocal microscopy. To probe for colocalization with ARA7, and potential other subcellular localizations, I generated binary expression vectors that encode *pUB::HR4-GFP* and *pUB::HR4-RFP*, which are ubiquitin-promoter driven C-terminally GFP and RFP-tagged versions of HR4, based on its coding sequence obtained through reverse-transcription from mRNA.

Upon transient *Agrobacterium*-mediated expression in *N. benthamiana* leaves, HR4-GFP localized to punctae that did not overlap with co-expressed mCherry-ARA7 under untreated conditions, or after syringe-infiltration of flg22 at 3 h, matching flg22 treatment time points at which HR4 was originally found in mass spectrometry of ARA7 purifications (**fig. 4.14A**). In order to probe the identity of these mobile HR4-GFP-positive punctae, I co-expressed HR4-GFP with published mitochondrial (**fig. 4.14B**) and peroxisomal (**fig. 4.14C**) RFP-tagged markers (Nelson et al., 2007) in *N. benthamiana*. HR4-GFP fully co-localized with the mitochondrial marker, and upon closer inspection, can be seen to localize more strongly to the periphery of these mitochondria (**fig. 4.14B**), pointing at a potential outer membrane association. HR4-GFP did not colocalize with the peroxisomal marker (**fig. 4.14C**). Syringe infiltration of flg22 into HR4-GFP and mitochondrial marker co-expressing *N. benthamiana* leaves did not change the co-localization pattern of HR4 with mitochondria (**fig. 4.14B, lower panels**).

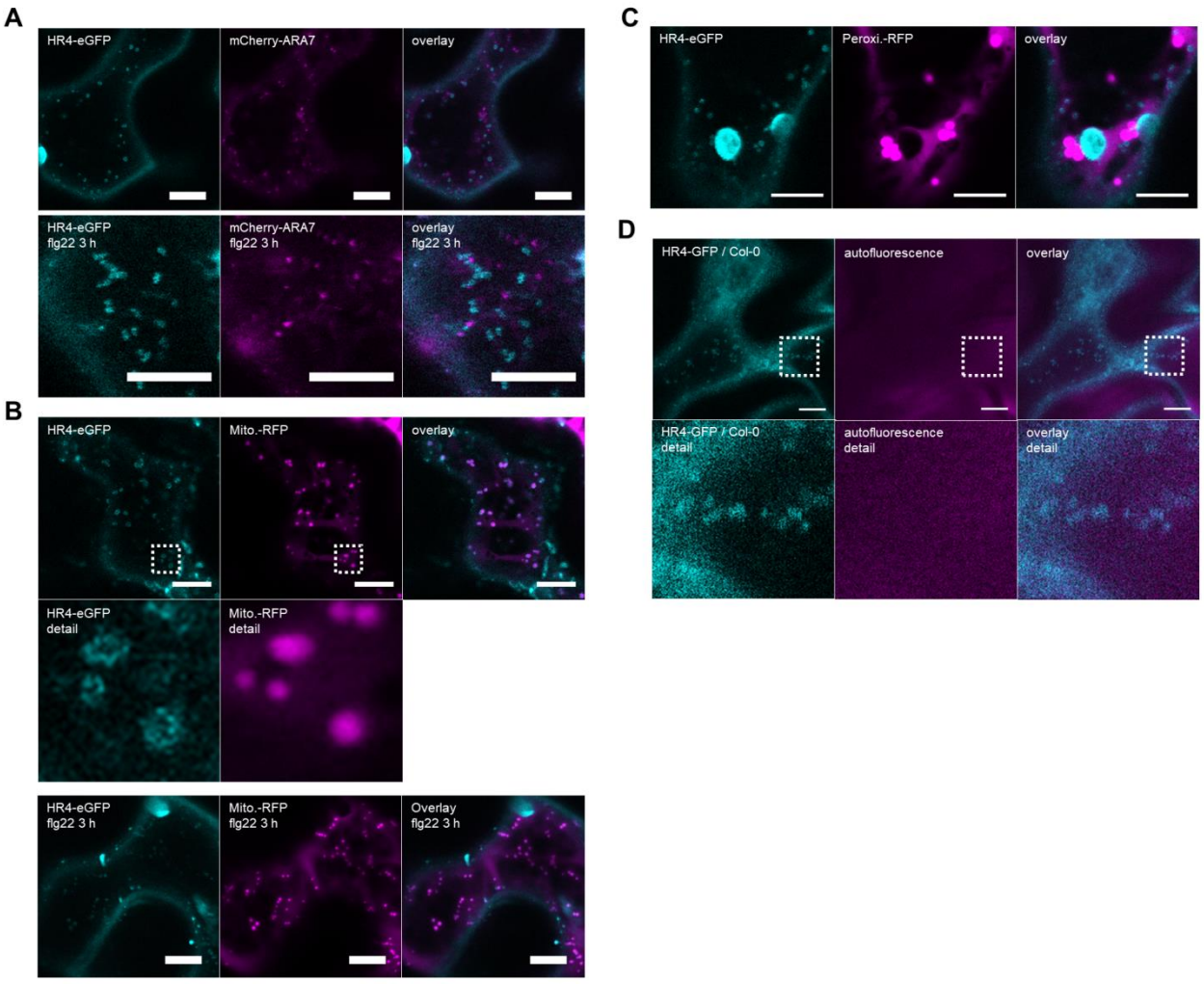

Figure 4.14. HR4-GFP does not colocalize with mCherry-ARA7-positive compartments. (A-C) Confocal micrographs showing GFP and RFP/mCherry channels in *Nicotiana benthamiana* adult leaves transiently co-expressing the indicated constructs through *Agrobacterium tumefaciens* mediated transformation at 2 dpi. Images were acquired without treatments, or after 3 hours flg22 (10 µM) treatments where indicated. (A) HR4-GFP In colocalization with ARA7, (B) in colocalization with Mito.-RFP mitochondrial marker (Nelson et al. 2007) Dotted boxes in (B) indicate region of interest shown in detail below. 63 × objective, scale bars = 10 µm. (D) Confocal micrographs of leaf epidermal cells of 4 wk-old T1 Arabidopsis plants expressing *pUB::HR4-GFP* in a Col-0 background. Dotted boxes in (B) indicate region of interest shown in detail below. 63 × objective, scale bars = 10 µm.

In collaboration with Matt Smoker and Jodie Taylor (Tissue Culture & Transformation Support Team, The Sainsbury Laboratory, Norwich, UK), I generated *Arabidopsis* plants transgenically expressing *pUB::HR4-GFP* in the Col-0 background, and upon confocal analysis could confirm that HR4-GFP localizes to mobile structures that are strongly reminiscent of mitochondria (**fig. 4.14D**). It remains to be conclusively demonstrated that these structures are indeed mitochondria.

In conclusion, the evidence I gathered using fluorescent tagging and confocal microscopy suggests that HR4 localizes to the periphery of mitochondria, and does not localize to ARA7-positive vesicles. Since mitochondria have been described to accumulate and immobilize under attempted penetration sites of powdery mildew (Fuchs et al., 2015a), it could be that the local high abundance of mitochondria, in concert with local accumulation of ARA7, may lead to their close proximity and potentially their association.

4.5 - TN3 AND HR4 ARE REQUIRED FOR PLANT IMMUNITY

4.5.1 *TN3* and *HR4* are not required for basal and flagellin-induced antibacterial immunity

Flagellin-induced resistance to *Pto* DC3000

TN3 and HR4 proteins have a role in immunity. I therefore tested the infection success of a panel of bacterial, fungal and oomycete pathogens on Arabidopsis T-DNA insertion mutants or SALK lines, generated by the Salk Institute for Biological Studies, affected in *TN3* (*tn3*, SALK_018440.56.00, insertion in promoter of AT1G66090) and *HR4* (*hr4,* SALK_208828, insertion in first intron of AT3G50480). The T-DNA insertion lines were confirmed for homozygous insertion using PCR with insert- and gene-specific primers on genomic DNA extractions.

The association of native TN3 and HR4 with ARA7 was dependent on flg22 stimulation. I therefore tested whether *tn3* and *hr4* are affected in their ability to induce resistance to syringe-infiltrated *Pto* DC3000 bacteria upon 1-day pre-treatment with flg22. I performed the experiment with water infiltration as a control, to also reveal potential basal resistance defects in either mutant. Upon measuring *in planta* bacterial proliferation after three days of incubation in water pre-treated plants, I observed no statistically significant differences between Col-0, *fls2, tn3*, or *hr4* (**fig. 4.15A**). The lack of difference in bacterial infection success between Col-0 and *fls2* in this type of assay has been described before (Nekrasov et al., 2009). Interestingly, flg22 treatment successfully induced bacterial resistance in Col-0, *tn3* and *hr4*, indicating that neither mutant is affected in mounting flg22-induced defenses. Mutant *fls2* plants did not show statistically significant differences in bacterial colonization between water or flg22-pretreatments (**fig. 4.15A, left panel**).

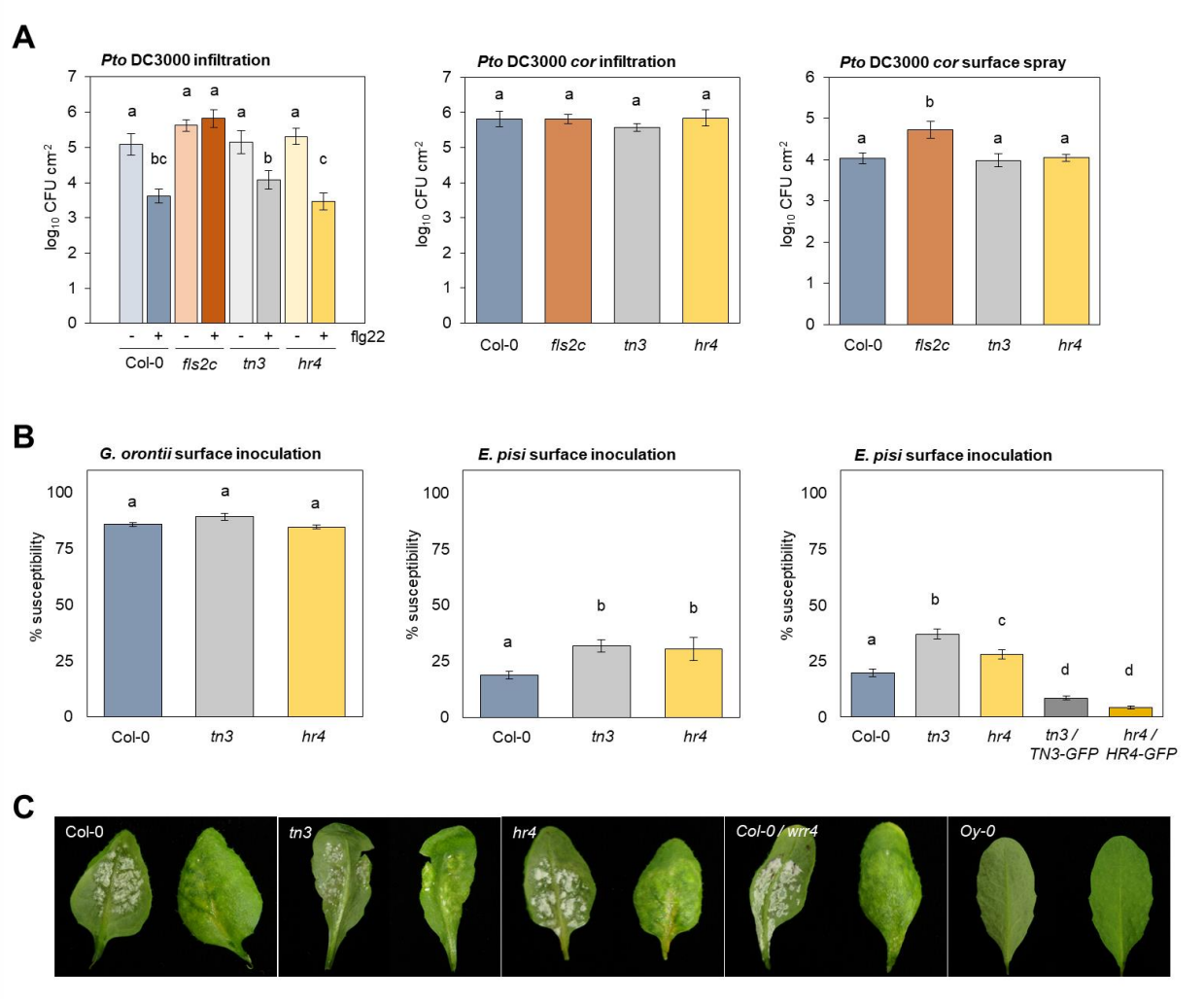

Figure 4.15. TN3 and HR4 are required for plant immunity. (A) Bar graphs represent growth of *Pto* DC3000 and *cor* bacteria as number of bacterial colony-forming units (CFU) per cm^2. 4 weeks-old Arabidopsis leaves of Col-0, *fls2*, *tn3* and *hr4* genotypes. Plants were infected with the indicated bacteria by syringe-infiltration without and with 1 µM flg22 induction 1 day prior bacterial infection, or spray inoculation, and harvested at 3 dpi. Experiments show results (bars = mean, error bars = SE, *n* = 8 plants per treatment) of one experiment, representative of a set of three replicates. (B) Bar graphs represent penetration success (% spores forming cell-penetrating structures) of *Golovinomyces orontii* or *Erisyphe pisi* after spore application on the surface of 6 weeks-old Arabidopsis leaves of the indicated genotypes. Coommassie staining and microscopic analysis to visualise fungal structures were performed at 48 hpi. Experiments show combined data of four independent experimental replicates. Between 400-600 total spores per treatment per experiment were examined. (A,B) Letters indicate significance grouping after one-way ANOVA analysis and post-hoc Tukey significance testing ($p < 0.05$). (C) Macroscopic images show symptoms of disease progression on abaxial and adaxial sides of 5 wk-old Arabidopsis leaves inoculated with *Albugo candida* Ex1 and imaged at 21 dpi. Images show symptoms representative of ca. 10 plants per treatment, experiment was performed once. Infection assays in (B) were performed in collaboration with Dr. Hannah Kuhn, laboratory of Prof. Ralph Panstruga, RWTH Aachen University, Aachen DE. Infection assays in (C) were performed in collaboration with Baptiste Castel MSc., laboratory of Prof. Jonathan Jones, The Sainsbury Laboratory, Norwich UK.

Resistance to *Pto* DC3000 *cor*

Work from our laboratory revealed that *ara7* mutants are more susceptible to *Pto* DC3000 *cor* bacteria (Bourdais et al., 2018, submitted). Because it is possible that TN3 and HR4 may function in the same pathway as ARA7 during immune responses, I tested the infection success of *Pto* DC3000 *cor* on *tn3* and *hr4*.

I chose to perform infections for both syringe-infiltrated bacteria and surface-spray inoculated bacteria. Upon syringe infiltration, I observe no statistical differences in bacterial proliferation of *Pto* DC3000 *cor* between Col-0, *fls2, tn3* and *hr4* (**fig. 4.15A, middle panel**). Spray-inoculation also did not reveal statistically significant differences when comparing Col-0 to *tn3* and *hr4*, but *Pto* DC3000 *cor* bacteria were more successful on *fls2c,* consistent with the inability to close stomata in response to flg22 (Spallek et al., 2013**;** Bourdais et al. 2018., submitted).

I conclude that *tn3* and *hr4* are not impaired in basal or flg22-induced resistance against *Pto* DC3000, or basal resistance against virulence-impaired *Pto* DC3000 *cor* bacteria. While *Pto* DC3000 is an adapted pathogen of Arabidopsis, potential more subtle resistance effects of TN3 or HR4 that might have been masked by the action of coronatine at both stomatal or post-stomatal defenses, are not revealed in this assay.

4.5.2 - TN3 and HR4 are required for immunity against nonadapted powdery mildew

Filamentous pathogens that project infection structures into plant cells elicit the delivery of host membranes, including from endocytic origin, to extrahaustorial membranes. LE/MVBs fuse with the EHM of *G. orontii* and deliver cell wall materials there (Micali et al., 2011), LE/MVB-associated RABG3c targets *P. infestans* haustoria (Bozkurt et al., 2015), and the presence of both secretory and endocytic vesicles around *Hyaloperonospora arabidopsidis* haustoria suggests the direction of a variety of vesicle trafficking pathways to infection structures (Lu et al., 2012). ARA7 itself accumulates at haustoria of powdery mildews, and is involved in resistance against *Bgh* (Nielsen et al., 2017b; Inada et al., 2016). Homologs of RPW8 were shown to function in antifungal resistance (Berkey et al., 2017), and NLRs in general can function in the detection of fungal effectors (Stotz et al., 2014; Selin et al., 2016). For these reasons, I was interested to test whether *tn3* and *hr4* may be affected in resistance against powdery mildew. These experiments were performed in collaboration by Hannah Kuhn (RWTH Aachen University, Aachen, Germany).

Upon application of spore suspensions to the leaf surface of Col-0, *tn3* and *hr4*, and subsequent quantification of the percentage of spores successfully forming secondary hyphae, we found that compared to Col-0, *tn3* and *hr4* were equally susceptible to the adapted powdery mildew *G. orontii* (**fig. 4.15B, left panel**). However, both *tn3* and *hr4* were more susceptible to the non-

adapted powdery mildew *Erisyphe pisi* (**fig. 4.15B, middle and right panels**). This prompted us to test whether the phenotype could be reversed upon constitutive expression of TN3 and HR4 in their respective mutant backgrounds. In addition to the *tn3* / *pUB::TN3-GFP* plants used in localization studies described elsewhere in this work, I generated *hr4* / *pUB::HR4-GFP* lines in collaboration with Matt Smoker and Jodie Taylor (Tissue Culture & Transformation Support Team, The Sainsbury Laboratory, Norwich, UK). Upon testing for *E. pisi* resistance, we found that both *tn3* / *pUB::TN3-GFP* and *hr4* / *pUB::HR4-GFP* complementation lines were significantly more resistant than Col-0 or their respective mutant backgrounds (**fig. 4.15B, right panels**). This indicates that the fluorescent fusion proteins TN3-GFP and HR4-GFP are functional.

4.5.3 - TN3 and HR4 are not required for resistance against the downy mildew *Albugo candida* Ex1

In collaboration with Baptiste Castel (Jonathan Jones group, The Sainsbury Laboratory, Norwich, UK), we tested for altered resistance of *tn3* and *hr4* to the adapted oomycete pathogen *Albugo candida* isolate Exeter1 (Prince et al., 2017). Upon inspection of disease symptoms 21 days after spray inoculation of spore suspensions, we found that Col-0, *tn3* and *hr4* generally exhibited similar levels of yellowing and *A. candida* sporulation, whereas susceptible genotype Col-0 / *wrr4* (Borhan et al., 2008) showed higher levels of sporulation, and resistant Arbidopsis ecotype Oy-0 (Baptiste Castel, PhD thesis) showed no signs of sporulation or yellowing (**fig. 4.15C**).

Taken together, these results point at a role for both TN3 and HR4 in defence against nonadapted powdery mildew. This result raises questions on the mechanisms by which both proteins achieve this, of subject to further study.

4.5.4 - Constitutive expresion of TN3-GFP and HR4-GFP does not provoke a cell death response in *Nicotiana* species.

TN3 has been previously described to trigger a hypersensitive response in *N. benthamiana* upon 35S-driven overexpression of untagged versions (Nandety et al., 2013), a response which was exacerbated by co-infiltration of a flg22 solution. To test for potential autoactivity of TN3-GFP, I used *Agrobacterium*-mediated transient expression in *N. tabacum* of *pUB::TN3-GFP* from the binary vector used for the generation of Arabidopsis transgenic lines. I performed the assay initially in *N. tabacum* due to its general predisposition to reveal NLR-mediated auto-HR in a more evident manner than *N. benthamiana* (Amey Redkar, Jonathan Jones lab, personal communication).

Upon transient expression of *TN3-GFP* in *N. tabacum*, and macroscopic observation at four days post infiltration, no cell death symptoms were observed (**fig. 4.16, top left panel**). In order to match the original finding of 35S::TN3-induced cell death (Nandety et al., 2013), I performed the same analysis in *N. benthamiana*, which also did not trigger cell death (**fig. 4.16, lower left**

panel). The construct can be successfully transiently expressed using *Agrobacterium*, as evident from further localization studies in *N. benthamiana* (**fig. 4.17A,B,C**).

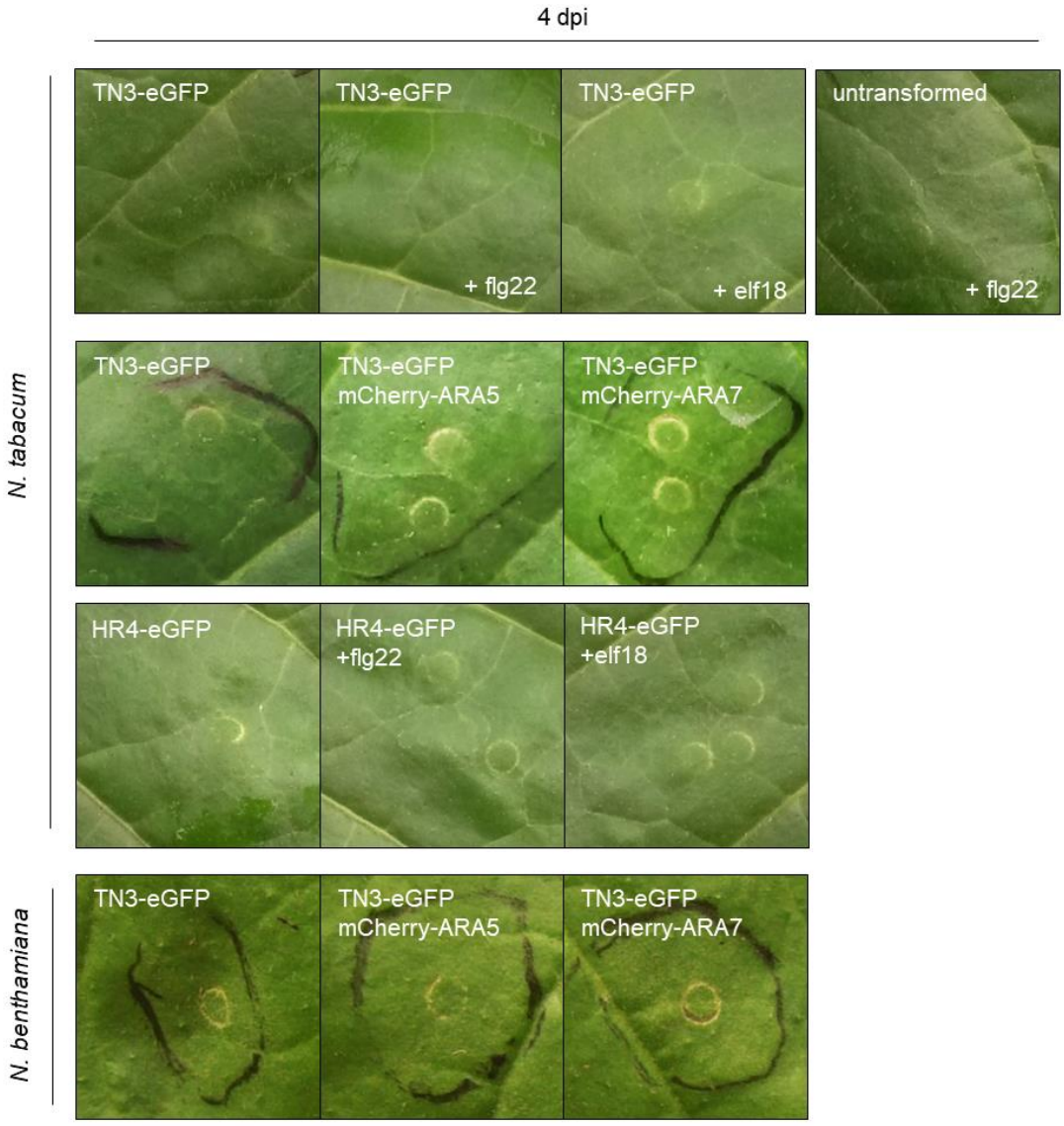

Figure 4.16. Constitutive expression of TN3-GFP and HR4-GFP does not provoke a cell death response in *Nicotiana* species. Representative macroscopic images show no obvious cell death symptoms upon constitutive expression of GFP-tagged TN3 and HR4 in *Nicotiana*. *Nicotiana tabacum* or *Nicotiana benthamiana* leaf regions were transiently transformed with *Agrobacterium tumefaciens* using the indicated combinations of constructs without and with infiltration of 10 µM flg22. Images were taken at 4 dpi.

Since flg22 treatment was shown to exacerbate the cell death response of *35S::TN3* (Nandety et al., 2013), I co-infiltrated *Agrobacterium tumefaciens* carrying *pUB::TN3-GFP* with a solution of flg22, and as a control I co-infiltrated the bacterial Elongation Factor-Tu (EF-Tu) immunogenic epitope elf18, which is not recognized by *Nicotiana* spp. which lack the cognate PRR EFR (Lacombe et al., 2010). However, in neither case, cell death symptoms were observed (**fig. 4.16, top and bottom panels**).

In parallel, I tested transient expression of *pUB::HR4-GFP*, which was functional in recovering mildew resistance defects of the *hr4* genotype, and reveal that in *N. tabacum,* no cell death symptoms were observed, in untreated and flg22 or elf18 co-treated leaves (**fig. 4.16, third row panels**). Flagellin can be perceived by *N. tabacum*, which endogenously expresses a homolog of FLS2 (Wei et al., 2012).

Based on the biochemical interaction studies of ARA7 and TN3, I hypothesized that TN3 may interact with, and potentially monitor the integrity of, ARA7 or a component of the ARA7 greater complex. Therefore, co-expression with *ARA7* may alter the capacity of TN3 to induce cell death upon constitutive expression. To tes tthis, I performed *Agrobacterium*-mediated co-expression of *pUB::TN3::GFP* with *pUB::mCherry-ARA7* and as a control included *pUB::mCherry-ARA5*. However, in neither *N. benthamiana* or *N. tabacum* this lead to an induction of cell death at 4 dpi (**fig. 4.16, middle and lower rows**).

The above results suggest that transient ubiquitin-promoter-driven expression of fluorescently tagged TN3 and HR4, which functioned in mildew resistance, does not trigger cell death responses in *Nicotiana* spp., independent of MAMP-signaling. It is possible that the fluorescent tag interferes with the induction of cell death by TN3-overexpression as was previously found for 35S::TN3 untagged overexpression in *N. benthamiana* (Nandety et al., 2013). In addition, potentially the accumulation levels of TN3 when driven by the weaker ubiquitin promoter are below the threshold needed to trigger cell death, which may not be the case upon 35S-driven overexpression. One experimental replicate testing untagged *pUB::TN3* expression in *N. tabacum* did not result in cell death.

4.5.5 - Constitutively expressed TN3-GFP exhibits localization patterns non-responsive to flg22 in *Nicotiana benthamiana*.

In order to verify whether ubiquitin-promoter-driven fluorescently tagged versions of TN3 and HR4 could be successfully expressed using *Agrobacterium*-mediated expression, I performed confocal microscopy localization studies in *N. benthamiana* leaves using *pUB::TN3-GFP*, *pUB::TN3-RFP* and *HR4-GFP,* and included co-expression of *pUB::mCherry-ARA7* and *pUB::mCherry-ARA5*. I found that TN3-GFP and TN3-RFP localized to the nucleus and cytosol (**fig. 4.17A**), largely matching the localization pattern found in Arabidopsis leaves.

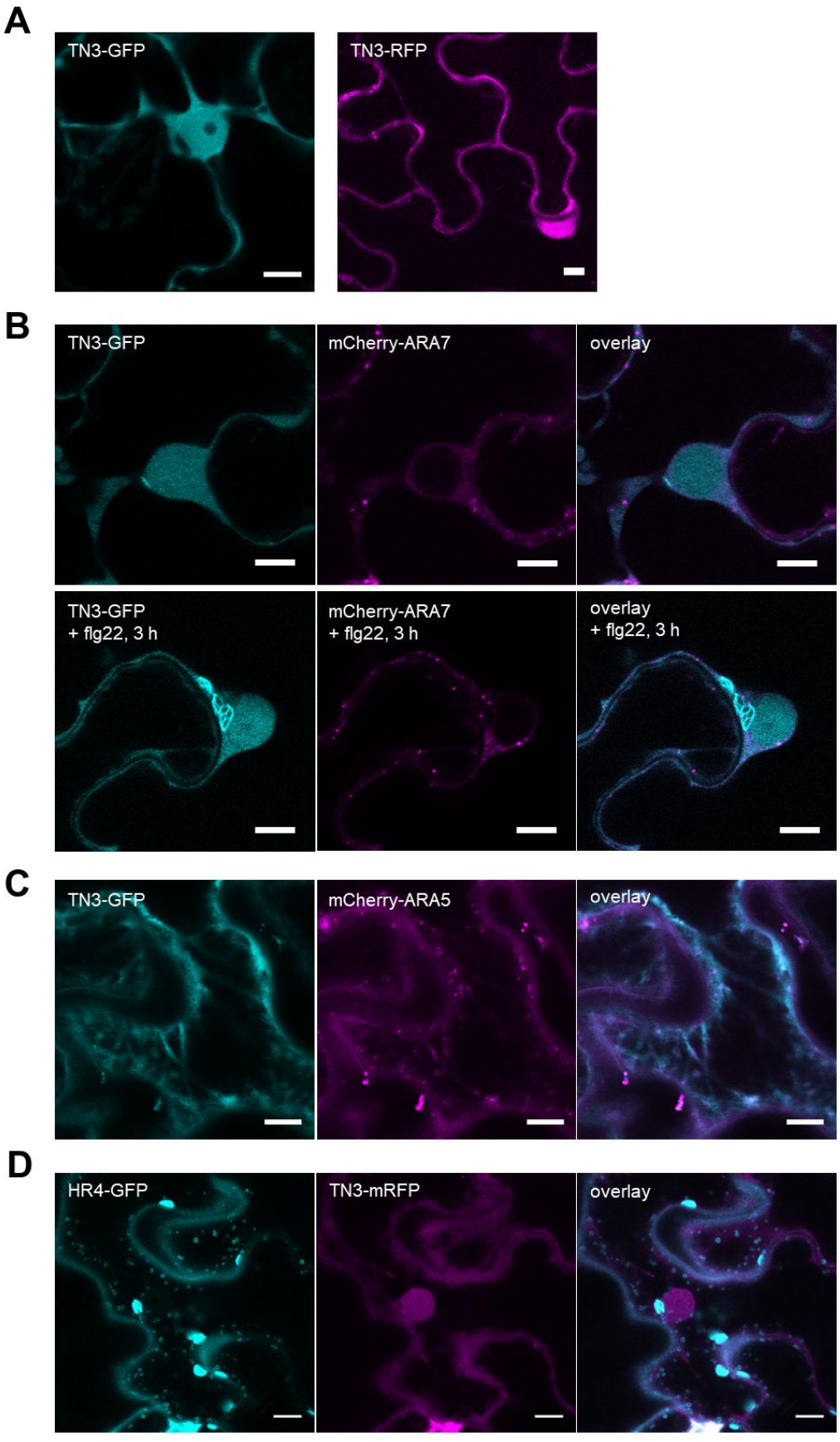
A
TN3-GFP
TN3-RFP
B
TN3-GFP
mCherry-ARA7
overlay
TN3-GFP
+ flg22, 3 h
mCherry-ARA7
+ flg22, 3 h
overlay
+ flg22, 3 h
C
TN3-GFP
mCherry-ARA5
overlay
D
HR4-GFP
TN3-mRFP
overlay

Figure 4.17. Constitutively expressed TN3-GFP exhibits localization patterns non-responsive to flg22 in *Nicotiana benthamiana.* (A-C) Confocal micrographs of *Nicotiana benthamiana* adult leaves transiently co-expressing the indicated constructs through *Agrobacterium tumefaciens* mediated transformation at 2 dpi. Images acquired after 3 hours flg22 (10 µM) treatments in lower panels of (B). (A) Expressing single TN3-GFP or TN3-RFP constructs, (B) co-expressing TN3-GFP and mCherry-ARA7, (C) co-expressing TN3-GFP and mCherry-ARA5, (D) co-expressing HR4-GFP and TN3-RFP. 63 × objective, scale bars = 10 µm.

Co-expression with fluorescently tagged ARA7 or ARA5 did not induce a localization change of TN3-GFP, and overlapping signals were only found in the cytosol (**fig. 4.17B**). This pattern did not change upon 3 h flg22 treatment (**fig. 4.17B**), timed to match the ligand treatments performed in Arabidopsis seedlings in preparation for immunoprecipitation/mass-spectrometry experiments. It is noteworthy that upon *TN3-GFP* co-expression with *mCherry-ARA5*, the fluorescent signals overlapped in the cytosol (**fig. 4.17C**), but in BiFC/split-YFP experiments (**fig. 4.9**), and immunoprecipitation/mass-spectrometry experiments described in chapter 3 of this thesis, ARA5 did not interact with TN3 upon untreated, water control or flagellin-induced conditions. This provides further evidence that cytosolic TN3 does not unspecifically associate with Rab GTPases due to possible ectopic localization. The localization pattern of TN3-GFP in *N. benthamiana* is predominantly the same as found for Arabidopsis, with the exception that in Arabidopsis, a minor amount of mobile TN3-GFP punctae were found.

Since both HR4 and TN3 interacted with ARA7 upon flg22 treatment as identified in mass spectrometry experiments, I tested whether co-expression of fluorescently tagged TN3 and HR4 could influence their localizaton (**fig. 4.17D**), which was not the case. HR4-GFP still localized to punctae likely to represent mitochondria, and TN3-RFP remained nucleocytosolic. In summary, co-expression of functional TN3-GFP and HR4-GFP with tested RAB-GTPases, or with each other, does not change the localization pattern of these proteins in *N. benthamiana*, independent of flg22 treatment.

DISCUSSION

4.6 - ARA7 exhibits dynamic localization patterns

I found that, between 6-7 hours after infiltration of *Pto* DC3000 or the bacterial MAMP flg22, ARA7-positive vesicles tend to cluster at the cell periphery. These clusters coincided with the position of bacteria attached to the cell surface (**fig. 4.1**). The focal accumulations of ARA7 also occurred to a lower extent in water treatments, but upon quantification using a FIJI macro, I could show that in some experimental replicates, they could be triggered significantly more by *Pto* DC3000 wildtype, or expressing mCherry, as well as by effector disarmed *Pto* DC3000 HrcC- and the ETI-triggering *Pto* DC3000 AvrRpt2 (**fig. 4.3-4**). Qualitatively, it was striking that whenever a cell-surface localized *Pto* DC3000-mCherry bacterium was observed, most often an ARA7 vesicle cluster was found beneath it. There were many occasions of ARA7 vesicle clusters that did not coincide with bacterial presence.

Notably, the response came up at ca. 6 hpi, and subsided quickly after ca. 7 hpi, with no obvious localization changes before. Why not cluster immediately? While it is possible that concentration of ARA7 at the cell periphery starts at earlier time points, I could not visualise this using confocal microscopy before ca. 6 hpi, but found numerous accumulations rapidly appearing subsequently. I hypothesize that at earlier time points, plants load endosomes with defense related cargoes, await the position of pathogen attack, and then mass-deliver endosomal contents in a focused manner, thus achieving high concentrations of defensive components delivered in the pathogen-defined location. This is corroborated by the existing finding that the cell-surface defense module PEN3 increased in abundance at endosomal compartments at 4 hours of flg22 treatment, whereas PEN3 cell-surface focal accumulations were measurable at >6 hpi (Underwood and Somerville, 2013).

It is known that default secretory Rab GTPases such as RabE1d cluster at the cell surface at these time points, upon bacterial presence (Speth et al., 2009). Therefore, it is possible that, coupled to an increased local secretory activity, endocytosis may need to be upregulated locally to maintain membrane integrity. Using the lipophilic tracer dye FM4-64, I could show that the majority of ARA7 vesicles present in clusters under bacteria are pre-existing, as the majority of them are not marked with FM4-64 at 30 minutes of staining (**fig. 4.2**), whereas at this time point the externally applied dye reaches LE/MVBs (Beck et al., 2012b). This indicates that most of the ARA7 vesicles in the observed clusters do not derive from locally increased endocytic activity. However, bacteria-induced changes along membrane trafficking pathways might alter the rate of FM4-64 uptake and distribution throughout the endomembrane network, which I did not test at earlier time points.

The phenomenon of pathogen-induced endosomal concentration at the cell surface has been well described in response to attempted fungal penetration, where endosomal Rab GTPases are thought to contribute to the formation of defensive structures, and the delivery of intraluminal vesicles by fusing with the plasma membrane, which then become extracellular vesicles (EVs, (Boevink, 2017)).

The endosomal ARA7 and vacuolar RABG3c accumulate around *Phytophthora infestans* haustoria (Bozkurt et al., 2015), and ARA7 and ARA6 both accumulate around *Golovinomyces orontii* haustoria (Inada et al., 2016). ARA6 endosomes also accumulate under attempted penetration sites of *Blumeria graminis* f.sp. *hordei* (Nielsen et al., 2012, 2017a; An et al., 2006). More recently, the LE/MVB localized ARA6 was further implicated in the delivery of endosomes upon infection with *Botrytis cinerea*. LE/MVBs fused with the PM at host-pathogen contact sites as evidenced from electron microscopy studies, and confocal analysis showed strong clustering of ARA6 vesicles at this location (Cai et al., 2018). Similar to my FM4-64 analyses, the authors use the endocytic tracer dye FM4-64 on *B. cinerea* infected tissue and show that upon 30 minutes staining, ARA6 vesicle clusters were not co-stained by FM4-64, providing evidence that they are existing, relocalizing vesicles (Cai et al., 2018). Interestingly, the authors identify Tetraspanin 8 (TET8) as a *bona fide* EV cargo, which I do not identify in any of my proteomic analysis of ARA7, suggesting a more specialized role for ARA6 in this process. While I have not demonstrated that bacterial-induced ARA7 concentration at the cell surface is coupled to their fusion to the PM, the previously known accumulation around pathogen interfaces of RabF GTPases and their incorporation to the EHM suggests that ARA7 can fuse and deliver contents at the plasma membrane during immune responses. I suggest that this response is at least partially conserved in response to host detection of bacteria at specific extracellular positions.

ARA7 has been implicated in the delivery of defence molecules to the plant-pathogen interface before. GTP-locked ARA7-QL, which cannot complete its activation cycle and normally forms enlarged ARA7-positive LE/MVBs (Jia et al., 2013), accumulated in the haustorial encasement in response to the non-adapted pathogen *Blumeria graminis* f.sp. *hordei* (*Bgh*, (Nielsen et al., 2017b)). Encasements are callose-rich structures that are formed secondary to the initial callose-rich cell-surface papillae (Nielsen et al., 2017b). Interestingly, the authors conclude that while ARA6 vesicles accumulate near *Bgh* infection structures (Nielsen et al., 2012), it is not ARA6, but activation of ARA7 through its interacting ARF-GEF VPS9a thus confers pre-invasive immunity to *Bgh.* Upon infection with the adapted fungal pathogen *G. orontii*, it has been shown that ARA7 does accumulate around the haustorium, but with the conspicuous absence of its activator VPS9a, leading to the hypothesis that the EHM of adapted pathogens adopts a modified endosomal identity, likely through the modulation of host processes by pathogen secreted

effectors (Inada et al., 2016). Possibly, the targeting of Rab regulatory proteins is guarded by NLRs such as the ARA7-interacting TN3 described in this thesis.

There are existing data that support that upon bacterial infection, endosomes fuse in an increased manner with the PM, thus releasing intraluminal vesicles which are then considered EVs (Rutter and Innes, 2017). *Pto* infection promoted the amount of EVs secreted by Arabidopsis, as revealed by quantifying membrane amounts in purifications of apoplastic fluid (Rutter and Innes, 2017). In fact, the EV proteome derived from those purifications was most similar to the published ARA7 proteome (Rutter and Innes, 2017; Heard et al., 2015). This supports a role for ARA7 LE/MVBs in secreting EVs in response to pathogens. Based on my data, I would suggest that this occurs in a targeted manner, thus I propose that EVs are secreted from LE/MVBs that fuse to bacterial infection sites. However, Rutter and Innes (2017) found Patellin1 to be a *bona fide* marker of EVs, which I do not find in my ARA7 purifications (**tables 4.1, 4.3**). In addition, they use PEN1 as an EV marker, which is found in my ARA7 purifications, but does not evidently respond in quantity upon immune stimulus (**table 4.1**)

While the above studies point at different roles for both ARA6 and ARA7 in the delivery of defence components to different pathogens, as of yet, it is not clear how they contribute to post-stomatal antibacterial immunity. It would therefore be interesting to test also ARA6 for clustering at the 6-7 hpi time point in response to bacterial infiltration, in combination with bacterial apoplastic infection assays in both *ara7* and *ara6*, to further probe their involvement.

4.7 - ARA7 purifications likely represent a Rab-associated complex

In order to reveal proteomic changes along the endocytic pathway upon immune stimulus at time points preceding the clustering of ARA7 under bacterial infection sites, I purified ARA7 from 3-hours water or flg22 treated seedlings, and performed mass spectrometry analysis (**tables 4.1-3, fig. 4.6**). I used a previously published method, where the authors could successfully categorise proteins in separate membrane trafficking pathways using purifications of a panel of membrane-associated baits (Heard et al., 2015). However, my purifications lead to substantially different co-purifying proteomes than were published, yet overlapping to some extent (**fig. S.5**). There are several underlying causes that could lead to this. Firstly, for ARA7, I used YFP affinity purification, whereas Heard et al. (2015) used RFP purifications. Secondly, a different model of mass spectrometer was used for my experiments. Finally, the way in which I define my YFP-ARA7 proteome, comparing it to YFP purifications and requiring a 4-fold spectral count increase, differs from the method used in Heard et al. (2015), who applied a statistical analysis method “SAINT” in order to separate the different endomembrane compartment proteomes based on confidence scores for each protein (Choi et al., 2011). I inspected the ARA7 co-purifying proteomes that resulted from my pulldown/mass-spec experiments and conclude that the majority of abundant

proteins correspond to the known subcellular localization and function of ARA7, making the co-purifying proteome suitable for discovering novel interactors of the ARA7 complex upon flg22 treatment, which was my goal.

It is uncertain whether complete endomembrane compartments are purified using the method I employ**.** Heard et al. (2015) point out that ca. 30% of cargoes identified in ARA7 purifications contain transmembrane domains, suggesting that at least part of the vesicle membrane was co-purified. However, my proteomes differed considerably (**fig. S.5**). When inspecting my ARA7 co-purifying proteome (**tables 4.1-2**), it is evident that the majority of co-purifying proteins are known to associate with membranes on the cytosolic side (SNAREs, coatomer, SCAMPs) or are Rab GTPase-associated (PRA1 members, PUF2, VPS9a). However, I do find cargoes of the pathway such as CESAs, glucan synthases and PEN3, but they all contain transmembrane domains. A minority of proteins, such as CER8 and ubiquitin-like proteins do not contain transmembrane domains. From these co-purifying proteins, I conclude that I purify the greater Rab GTPase-interacting complex at minimum, and from TM-domain containing proteins, I speculate that at least membrane fragments originating from TGN/EE-LE/MVB co-purified with ARA7. Taking all evidence together, this suggests that I purified membrane-associated ARA7, because the cytosolic phase interacts with a limited amount of proteins, mostly belonging to the Rab regulatory complex (Saito and Ueda, 2009b), and co-purifying proteins that I found such as SNAREs are membrane-integral and do not cycle between cytosolic and membrane-associated states.

A number of Golgi proteins passed my criteria of defining an ARA7 co-purifying proteome, as they were associated with YFP-ARA7 with a factor of more than four-fold compared to YFP controls. When comparing my ARA7 proteome to the published Golgi proteome obtained using the same affinity purification method (Heard et al., 2015), I observe that ca. 7% (11 out of 159) ARA7 proteins were found in the Golgi proteome. This is comparable to the amount of Golgi proteins that were found in the ARA7 proteome from the same publication, where ca. 10% (29 out of 280) of ARA7 proteins were also identified in Golgi. Yet, my ARA7 “Golgi contaminants” overlapped with the published ARA7 “Golgi contaminants” with only 4 out of 11 proteins. Overlap included VAMP722, PRA1.B1 and two Endomembrane Protein 70 members.

It is possible that the purification method is inaccurate to some extent, and purifies unspecific proteins or contaminants. However, they could also reflect constitutive biogenesis of the YFP-ARA7 fusion protein, the transcription of which is driven by the constitutively active Ubiquitin-10 promoter (Geldner et al., 2009). Co-localization analysis of Golgi-TGN/EE-localized ARA5 with ARA7 showed no punctate overlap (**chapter 5, figure 5.5**), so it is unlikely that a high abundance of YFP-ARA7 is present at the Golgi. However, fluorescent signal can only occur when the newly synthesized YFP chromophore is fully matured, so a subpool of “dark” YFP-ARA7 may be present at the Golgi. Alternatively, TGN/EE and Golgi may be linked to some extent, and difficult

to separate. Indeed, the TGN/EE partially originates from the Golgi (Ito et al., 2017), and there is a closely Golgi-Associated (GA) pool of TGN/EE, separate from Golgi-Independent (GI) TGN/EE (Uemura et al., 2014).

Strikingly, CONSERVED OLIGOMERIC GOLGI 2 (COG2, AT4G24840), a Golgi-functioning tethering factor, which was low abundant, but upregulated in ARA7 upon flg22 treatments in my purifications (**table 4.3**), was predicted to be the target of *H. arabidopsidis* HaRxL60, HaRxL73, HaRxLL518 and ATR13, as well as *G. orontii* effector candidate OEC25 (Mukhtar et al., 2011; Weßling et al., 2014). COG2 has been detected in a vacuolar proteomic study (Carter, 2004), pointing at its likely trafficking from the Golgi to vacuole, which could occur through ARA7 TGN/EE and LE/MVBs. With COG known to function in intra-Golgi trafficking processes, ARA7 is unlikely to be its biologically relevant localization, or the location at which effectors target it. However, it would be interesting to confirm this using bimolecular fluorescence complementation with predicted interacting effectors, pinpointing the location of their interaction in relation to ARA7.

In addition to some Golgi proteins, at higher abundances I find ER localized proteins such as ribosomal proteins, ribosomal-associated signal-particle proteins, and SEC22 which functions in ER-Golgi export (**table 4.1**). While ARA7 is a broad endocytic marker localizing to TGN/EE and LE/MVB, it has not been described to localize to the ER. Potentially, above-described biosynthesis of YFP-ARA7 could lead to some purification of ER proteins, but the high abundance of the ribosomal protein SUPPRESSOR OF ACAULIS 56 gives pause. An explanation may be found in the observations that LE/MVBs physically associate with ER, which facilitates endosomal streaming, and that ER-localized VAP27 proteins physically participate in early clathrin-mediated endocytosis as well as bridge the ER to TGN/EE, where ARA7 also localizes (Stefano et al., 2018, 2015). Seeing the critical role for the ER in physically guiding endocytic processes involving TGN/EE and LE/MVB, it would be interesting to see whether the described ER-localized modules responsible for this are also involved in guiding ARA7 vesicles to the pathogen interface. Indeed, ER itself was found to focally accumulated under fungal attempted penetration sites (Fuchs et al., 2015). While ribosomal proteins in my ARA7 purifications could simply reflect close physical association, it is also conceivable that proteins newly synthesized in response to pathogen detection hitch-hike on LE/MVBs en-route to the cell-surface or to the vacuole, thus bypassing extra translocation and posttranslational modification steps in the Golgi.

In animal systems, bacteria have been well described to employ effectors to target both endocytic and secretory Rab GTPases and their regulatory complexes, modulating host trafficking to their benefot (Brumell and Scidmore, 2007; Stein et al., 2012; Spanò and Galán, 2017). In plants, fungal effectors from *G. orontii* and *H. arabidopsidis* have been predicted to interact with PRA1 proteins, which are regulators of Rab GTPases, using large scale yeast-2-hybrid (Y2H) screens (Mukhtar et al., 2011; Weßling et al., 2014), but these interactions have not been subject to

further study. Interestingly, upon ARA7 purifications, I identified PRA1.F2 in water treated samples, which interacted with *G. orontii* effector candidate OEC65 in the abovementioned Y2H screen. Secondly, upon flg22 treatments, ARA7 purifications identified PRA1.F3, which was predicted to interact with *G. orontii* OEC65 and *H. arabidopsidis* HaRxL74. Neither interacted with the library of *Pto* DC3000 effectors in the same study (Mukhtar et al., 2011; Weßling et al., 2014). This points at a role for pathogen effectors in modulating Rab activity in plants.

While I could find Rab regulatory proteins such as PRA1 family proteins, and VPS9a, I also identify at least one Rab effector, as reflected by PLANT UNIQUE RAB EFFECTOR 2 (PUF2; Ito et al. 2018). However, other known ARA7 effectors such as SAND/MONENSIN SENSITIVITY 1 (SAND/MON1), CALCIUM CAFFEINE ZINC SENSITIVITY 1 (CCZ1) and ENDOSOMAL RAB EFFECTOR WITH PX-DOMAIN (EREX) proteins were not identified (Singh et al., 2014a; Sakurai et al., 2016). Of EREX, it is known to function in endosomal delivery to the protein storage vacuole in seed maturation, which is a process that does not occur in seedlings. The absence of SAND/MON1 and CCZ1 is puzzling, as they are involved in the conversion of Rab5, to which ARA7 belongs, into Rab7-identity of membrane compartments in default vacuolar targeted trafficking (Singh et al., 2014b). It could be that the pool of ARA7 interacting with these effectors at the last stages of vacuolar targeted LE/MVB traffic is small, preventing MON1/CCZ1 peptide counts to reach the detection threshold.

4.8 - The ARA7 proteome contains defence-related proteins

Major players in the production of indole-3-glucosonolate based antimicrobials are Indole Glucosinolate *O*-Methyl Transferase (IGMT) proteins, of which I identify IGMT4 upregulated in ARA7 upon flg22 treatment. The subcellular localization of IGMT proteins is as of yet unclear, but they function in an enzymatic pathway of which other components have known localizations (Pfalz et al., 2011; Xu et al., 2016). What could be the relevance for IGMT4 appearance on endosomes in this context? Before export into the apoplastic space, indole-3-glucosinolate-derived antimicrobial metabolites need to be catalyzed in sequence by CYTOCHROME P 81 (CYP81) family enzymes, IGMT enzymes, and finally myrosinases, among which PEN2, and the full functioning of enzymatic chain is also necessary for antibacterial resistance (Clay et al., 2009; Burow and Halkier, 2017; Birkenbihl et al., 2017). PEN2, which I did not identify, is known to localize to mitochondria, which immobilize under attempted penetration sites, and is there involved in the last step of antimicrobial production (Fuchs et al., 2015b). We also know that IGMT proteins produce metabolites which are substrates for PEN2, but it is unknown where IGMTs are localized (Birkenbihl et al., 2017). The conversion step before is mediated by CYP81 proteins (Fuchs et al., 2015b), which are ER resident, and of which I find no members in my purifications. Therefore, finding IGMT4 in ARA7 purifications upon flg22 only could point at a mechanism to bring these intermediate enzymes to the biologically relevant location at the

pathogen infection site. ER and LE/MVB can physically associate, and both ER and LE/MVB concentrate under pathogen infection sites (Fuchs et al., 2015b). Seeing as the final metabolites of this completed enzymatic pathway are toxic, it would make sense to keep the components separate until the end products are necessary. My proteomic studies don't answer where the metabolites themselves are located, but they are said to be exported by transmembrane transporters such as PEN3, which also make use of the redirected endocytic pathway to focally accumulate. Knowing that the full functionality of this enzymatic pathway is required for antibacterial immunity (Clay et al., 2009), I hypothesize that the ER also focally reorganises at the site of bacterial attack, but this remains to be demonstrated.

Finding PEN3 associating with ARA7 upon flg22 treated conditions is interesting, because it matches the endocytic accumulation of this protein at membrane compartments as previously observed at 4 h of flg22 treatment (Underwood et al., 2017), and provides more evidence for a role of the LE/MVB in focal accumulation of PEN3 upon immune stimulus. The observed timings of 6-7 hours flg22 treatment leading to ARA7 vesicle clustering in my experiments, matches existing observations that PEN3 cell-surface focal accumulations can be observed from ca. 6 hours onward (Underwood and Somerville, 2013). These data together support the notion that the time upon which I chose to analyze flg22-induced changes along endomembrane compartments is suitable for revealing the loading of endosomes with defence cargoes. In this context, it would be interesting to test for PEN3 focal accumulations in *ara7* and *ara6* mutants upon pathogen and MAMP stimulation.

It has been shown that upon leaf infiltration with *Pto* DC3000, PEN3 accumulations at the cell surface subside rapidly after ca. 7 hours, which is thought to be an effector-mediated process (Xin et al., 2013). If the endosomal clustering I observe underlies the targeting of PEN3 to the cell surface there, the effector-mediated removal of such focal accumulations is unlikely to be a result of interfering with the continuous endosomal delivery of PEN3, because I could not observe the ARA7 clustering response after ca. 7 hpi, even upon flg22-only treatments. This is also supported by published fluorescence recovery after photobleaching (FRAP) experiments on PEN3 (Underwood and Somerville, 2013). Rather, it is likely that effectors affect the stability of PEN3 in the plasma membrane.

The protein with the strongest increase in spectral counts in ARA7 purifications upon flg22 treatment compared to water treatment was FLOTILLIN 1 (FLOT1). FLOT1 is a membrane-associated protein, which associates with high-sterol and sphingolipid membrane regions also known as detergent-resistant membranes (DRMs). In plants, it functions in clathrin-independent endocytosis (Li et al., 2012b), and in both plants and animals is thought to participate in modulating the spatial organisation of cell-surface localized transmembrane receptors (Otto and Nichols, 2011; Haney et al., 2011; Downie, 2014).

In addition, in animals, flotillins have been shown to function on the endosome, where they localize to sphingolipid/sterol-rich membrane regions as well, and there participate in targeting endocytosed cargoes for recycling back to the PM (Langhorst et al., 2007; Meister and Tikkanen, 2014). ARA7 and FLOT1 partially overlapped on FM4-64 and VHA-a1 positive endosomes in an increased manner upon flg22 treatment at 1 hour of flg22 treatment (Yu et al., 2017). DRM enrichment has conversely revealed the co-purification of the well studied TGN/EE marker VHA-a1, thus providing further evidence that the TGN/EE contains such domains where FLOT1 is present - noting that VHA-a1 marked TGN/EE overlaped with ARA7 in microscopy studies and VHA-a1 is found in my ARA7 proteome (Borner et al., 2005; Dettmer et al., 2006). Finding FLOT1 in ARA7 purifications could signify a change in lipid composition along the endocytic pathway. Since pathogen infection induces the focal accumulation of known defence cargoes, which is thought to be mediated by redirection of LE/MVB-dependent traffic, and sterol/sphingolipid-associating FLOT1 in animals has been implicated in mediating the return of endocytosed cargoes to the PM, these findings together could point at a flg22-induced upregulation of PM-directed secretory capacity on the ARA7 pathway which is normally targeted to the vacuole.

High sterol/sphingolipid subdomains on TGN/EE, where FLOT1 could preferentially accumulate, have recently been show to overlap with the SYP61 -marked domain, which I also co-purified with ARA7, but independent of flg22 stimulus (Wattelet-Boyer et al., 2016). The authors demonstrate that the SYP61 domain is involved in default secretion and not recycling, whereas the low-sphingolipid/sterol domain marked by RABA2a, which I do not co-purify with ARA7, was shown to mediate PM-TGN/EE recycling and not default secretion. This would seem to conflict with the hypothesis that appearance of FLOT1 on ARA7 signifies a more recycling identity on this compartment, but is in line with a role for PM-targeting, as default secretory compartments also mediate PM delivery.

Other data suggest that LE/MVB-localized ARA6 is the endosomal Rab that mediates endosome-to-PM delivery at resting conditions, and in host-microbe associated processes (Ebine et al., 2011a; Cai et al., 2018). To further elucidate the potential endosomal-localized functions of FLOT1 in the context of immunity, and whether this underlies an increased secretory role for normally endocytic compartments, it would therefore be interesting to test for flg22-induced colocalization changes of FLOT1 with both ARA7 and ARA6 upon pathogen and MAMP stimulus, in combination with pathogen infection trials in published FLOT1 knockdown lines (Li et al., 2012b).

4.9 - The atypical NLRs TN3 and HR4 mediate plant immunity

Using mass spectrometry and biochemical methods, I could show that TN3 and ARA7 interact, yet in endogenous conditions, this is likely underpinned by induced transcription of *TN3* in

repsonse to flg22 (**fig. 4.7**). In bimolecular fluorescence complementation (BiFC) studies, I could show that TN3 and ARA7 reconstituted a fluorescent signal on ARA7 endosomes (**fig. 4.9**). Upon interaction in this type of experiment, the interaction partners are irreversibly linked by the fluorophore. This could mean that normally, TN3 interacts with ARA7 in a dynamic reversible way, or with only a subpool of ARA7, but this transient or partial interaction be fully captured by irreversible binding through BiFC, with ARA7 now "sequestering" TN3 molecules and accumulating them at endosomes. I hypothesize that I purify a greater Rab-associated complex at minimum, which probably includes the cytosolic and membrane bound pool. Perhaps TN3 has an interaction preference for cytosolic localized, GDP-bound inactive pools of ARA7, rather than all ARA7, or for membrane-associated GTP-bound ARA7, and as a result in BiFC would follow ARA7 throughout its activation cycle. Notably, TN3 also reconstituted a signal with the LE/MVB-localized ARA6, which could point at TN3 interacting with Rab5 GTPases in general, or with a common interactor of Rab5 GTPases, out of which their activator VPS9a or their shared endosomal localized effector PUF2 could be candidates. This would be interesting to further confirm using biochemical interaction studies, and could point at host NLR surveillance of Rab GTPase activity.

I tested Arabidopsis Col-0 T-DNA insertion lines *tn3* and *hr4* for their capacity to mount resistance against bacterial pathogens. Because of the flg22-induced appearance of these proteins in my purifications, I included a flg22-induced resistance test to *Pto* DC3000 bacteria. However, neither mutant line was affected in flg22-induced or basal resistance to *Pto* DC3000, nor in basal resistance to *Pto* DC3000 *cor* (**fig. 4.15**). By contrast, single mutants of other *TN* genes, such as *tn2* and *tn13*, have been shown to be affected in bacterial resistance (Zhao et al., 2015; Roth et al., 2017). The absence of resistance phenotypes in *tn3* and *hr4* in my bacterial infection assays could be explained by the fact that *Pto* DC3000 is well adapted to Arabidopsis, and *Pto* DC3000 *cor*, although lacking coronatine, can still secrete type-3 effectors. Alternatively, *Pto* DC3000 may not secrete the effectors that would trigger TN3 or RPW8-based resistance.

Upon challenge with filamentous pathogens, out of *G. orontii*, *Albugo candida* Ex1 and *E. pisi*, only the latter, non-adapted pathogen showed increased infection success on both *tn3* and *hr4* plants (**fig. 4.15**). Importantly, expression of *TN3-GFP* and *HR4-GFP* in their respective mutants could rescue resistance above wildtype levels, demonstrating that both are required for anti-fungal immunity and are functional as GFP-tagged fusion protein. Since ectopic expression of R-proteins can lead to constitutive activation of defences, the constitutive expression of both genes driven by the Ubiquitin-10 promoter could explain the heightened resistance to *E. pisi.* By contrast, 35S overexpression lines of HR4 mediate resistance against *G. cichoracearum* comparable to Col-0 wildtype plants (Berkey et al., 2017). However, *G. cichoracearum* is an

adapted pathogen on Arabidopsis. I conclude that both TN3 and HR4 function in non-host resistance to powdery mildew.

HR4 is a homolog of the relatively well-studied atypical immune receptor RPW8.2 and associates to ARA7 upon flg22 trigger. Surprisingly, HR4-GFP, which is functionally complementing the *hr4* mutant phenotype, localized to the periphery of mitochondria in *N. benthamiana* and similarly in Arabidopsis independent of flg22 stimulus (**fig. 4.14**). This is surprising, because I identified HR4 in ARA7 purifications, which does not localize to mitochondria. While the co-localization pattern of ARA7 and HR4 did not change upon 3 hours flg22 treatment in *N. benthamiana*, it remains possible that HR4 more closely associates with ARA7 in Arabidopsis upon immune stimulation, or has broader targeting specificity dependent on pathogen infection, perhaps directed by NLR association or activation. It is also possible that fluorescent tagging of HR4 alters its subcellular localization, but I could show that it does not affect its function in antifungal resistance (**fig. 4.15**). To my knowledge, I do not identify any other mitochondrial localized proteins in ARA7 purifications.

HR4 and its homologs HR1-3 in Col-0 have been shown to all accumulate around *G. orontii* haustoria (Berkey et al., 2017). Interestingly, HR2-YFP was found in ring structures surrounding chloroplasts, and in a different study, a subset of C-terminally truncated mutants of RPW8.2 localized to stromule-like membranes that surrounded and connected chloroplasts ((Berkey et al., 2017; Wang et al., 2013)). While RPW8 proteins are membrane targeted through their N-terminal TM domain (Wang et al., 2013), this points at a role for membrane specificity determination of the C-terminus, which is divergent between RPW8 homologs in Col-0 (**fig. S14**). Yet, upon alignment of HR1-4 amino acid sequences, I observe a N-terminal extension for HR4 which is not present in HR1-3 (**fig. S.4**), which could confer differential localization compared to other HR members (Berkey et al., 2017).

RPW8.2 is a homologue of HR4, and was shown to be carried on secretory VAMP721/VAMP722-positive vesicles to the pathogen interface, and in EM-studies was shown to localize to the EHM proper (Kim et al., 2014). While VAMP721 and ARA7 in fluorescent colocalization studies showed considerably different punctate localizations in stable transgenic Arabidopsis root cells (Zhang et al., 2011a), both VAMP721 and VAMP722 were present in the ARA7 proteome (**table 4.1-4.2**), which could reflect close association of ARA7 and VAMP721/722 at the TGN/EE, and which could lead to association of ARA7 with HR proteins that might be carried on these vesicles.

RPW8-type proteins are potent inducers of cell death, and are required for signal activation of entire NLR subfamilies (Collier et al., 2011; Bonardi et al., 2011). Although the mechanism by which RPW8-type proteins activates resistance remains poorly characterized, there is a potential lead. The so called RPW8-domain describes full-length RPW8 and its homologs, and is present

as an N-terminal domain in tobacco NRG1 and homologs (Peart et al., 2005) and Arabidopsis ADR1 (Collier et al., 2011). Expression of the RPW8 part of various ADR1/NRG1 variants resulted in cell death, and it is known that RPW8 is membrane targeted (Collier et al., 2011; Wang et al., 2007). Interestingly, RPW8 domains are homologous to HELL domains present on fungal NLRs (Daskalov et al., 2016). HELL domains and RPW8 domains both have membrane targeting functions in cell death processes (Daskalov et al., 2016). The authors point out that it is likely that the HELL domain itself achieves this through inducing membrane pore formation on location. The above data, in line with the observation that HR4 contributes to defence against a biotrophic fungus (**fig. 4.15**), which is commonly associated with hypersensitive cell death, it is conceivable that HR4 plays a membrane-localized role in activating NLR-mediated cell death.

TN3 interacted with ARA7, which was induced upon initiation of immune signaling in endogenous conditions, and we found that TN3 is required for full immunity against non-host powdery mildew. How could TN3 work? Limited information is available on the mechanism of TN3 signaling. Upon 35S overexpression in *N. benthamiana*, (Nandety et al., 2013) found that TN3 induced a hypersensitive response, which was exacerbated by flg22 co-infiltration, and which was dependent on the typical NLR signaling module EDS1. Additionally, 35S overexpression lines in Arabidopsis could only be retrieved in an *eds1* background (Nandety et al., 2013). In my hands, transient expression of *pUB::TN3-GFP* in *Nicotiana* spp. did not trigger any symptoms of HR (**fig. 4.16**), whereas *p35S::TN3* has been shown to trigger the strongest HR symptoms in *N. benthamiana* out of all tested *TN* genes (Nandety et al., 2013). My fluorescently tagged construct is functional in resistance, as evident from pathogen infection assays (**fig. 4.15**), and is expressed in *N. benthamiana* (**fig. 4.17**). It is conceivable that my Ubiquitin-10 promoter-driven *pUB::TN3-GFP* construct does not accumulate enough TN3 protein compared to the higher expressed *p35S::TN3*.

Other TN proteins have been reported to engage immune signaling through unconventional means. TN2 interacts with the trafficking regulators Exo70B1 and SNAP33, and triggers autoimmunity in an *exo70b1* background, implicating it in the guarding of Exocyst components, or an Exocyst-dependent process (Zhao et al., 2015). Interestingly, TN2 interacted also with CALCIUM-DEPENDENT PROTEIN KINASE 5 (CPK5), and CPK5 was required for the autoimmune response in *exo70b1* (Liu et al., 2017). CPK5 is a known component of early PTI signaling, and required for full resistance against *Pto* DC3000 (Dubiella et al., 2013). I did not identify any CPKs in ARA7 purifications upon flg22 (**table 4.3**).

TN proteins are thought to function in complex with full-length NLRs. A single amino-acid substitution near the TIR-domain of TN1/CHILLING SENSITIVE 1 (CHS1) lead to an autoimmune phenotype upon exposure of plants to low temperatures, which was dependent on the presence of the full-length TNL SUPPRESSOR OF CHL1-2 3 (SOC3), and on the typical NLR signaling

components EDS1 and PAD4 (Zbierzak et al., 2013; Zhang et al., 2017). The CHS1 autoactive variant also physically interacted with SOC3. The *SOC3* gene is genomically in close proximity to *CHS1*, and interestingly, also *TN2*, raising the possibilty that TN2 is also dependent on this full-length NLR. While TN3 does not cluster with these genes, or full-length NLRs in the Arabidopsis genome, from Y2H screens it has been predicted to interact with the full-length NLR RPP13-LIKE PROTEIN 1 (RPPL1), which would be a prime candidate for further study in the context of TN3-mediated immune signaling.

To my knowledge, the only NLR to be detected at endosomes is potato (*Solanum tuberosum*) R3a, which confers resistance to the late-blight causative agent *Phytophthora infestans*, carrying the effector Avr3a (Engelhardt et al., 2012). Avr3a interacts with dynamin, and interferes with dynamin-mediated endocytic processes (Chaparro-Garcia et al., 2015). Interestingly, *St*R3a localized to the cytosol in resting conditions, and only accumulated at endosomes upon co-expression of Avr3a (Engelhardt et al., 2012). In the case of TN3 however, I could not observe a change in its nucleocytosolic localization upon leaf infiltration with *Pto* DC3000 bacteria, which inject a range of type-3 effectors (**fig. 4.12**). From existing Y2H studies, TN3 is predicted to interact with the type-3 effector HopY1 (Nandety et al., 2013), which is present in *Pto* DC3000. It would be interesting to co-express fluorescent TN3 fusions together with HopY1 in the absence of virulent *Pto* DC3000, or together with an unbiased panel of type-3 effectors, and follow TN3 localization over time. Seeing as *tn3* mutants showed enhanced susceptibility upon infection with the nonadapted fungal pathogen *Erisyphe pisi* (**fig. 4.15**), we are further investigating TN3 localization upon infection with *E. pisi*.

Upon broader phylogenetic analysis of *TN* genes compared to plant protein databases, it was found that *TN3* aligns closely to the tobacco NLR *N* (Nandety et al., 2013). N requires the helper-NLR N-Requirement gene 1 (NRG1) to function in antiviral immunity (Peart et al., 2005). NRG1 encodes a CC-NLR, of which the CC domain is homologous to RPW8 proteins (Collier et al., 2011). Since I found both TN3 and the RPW8 homolog HR4 in the same ARA7 purification upon flg22 treatment, this could implicate TN3 and HR4 functioning together.

CHAPTER 5:

IMMUNE SIGNALING-INDUCED CHANGES IN THE LOCALIZATION OF THE SECRETORY RAB GTPASE ARA5/RABD2A AND ITS CO-PURIFYING PROTEOME IN COMPARISON TO THE ENDOCYTIC ARA7/RABF2B

RESULTS

5.1 – THE LOCALIZATION PATTERN OF ARA5/RABD2A CHANGES UPON IMMUNE STIMULUS

5.1.1 - ARA5 focally accumulates at the cell periphery upon pathogen stimulus

The default secretory pathway is involved in the targeting of defense components to pathogen contact sites at the cell periphery upon pathogen or MAMP-stimulus (Kwon et al., 2008; Assaad et al., 2004; Kalde et al., 2007), and regulators of this pathway such as the SNARE PEN1/SYP121 accumulate under pathogen attack sites and around pathogen invasion structures (Kwon et al., 2008; Nielsen and Thordal-Christensen, 2013). ARA5/RabF2b is a Rab GTPase that localizes to the Golgi and the TGN/EE (Pinheiro et al., 2009), and functions in default secretion. To examine whether regulators of the default secretory pathway were targeted to pathogen contact sites, I syringe-infiltrated leaves of 4-weeks old *pUB::YFP-ARA5* plants with a suspension of fluorescently labelled *Pto* DC3000-mCherry (described in **chapter 4** of this thesis), and observed the localization pattern of ARA5 using confocal microscopy.

No evident localization pattern changes in YFP-ARA5 occurred before 6 h of measurement, but between 6-7 h after bacterial inoculation, strong clustering of ARA5 vesicles was observed at the cell periphery, at locations where apoplastic *Pto* DC3000-mCherry were also observed **(fig. 5.1A**). These focal accumulations occurred in mesophyll cells **(fig. 5.1A,B**) and epidermal cells. 6-7 h water control treatments did not provoke ARA5 focal accumulations to a similar extent when compared to infection with wildtype *Pto* DC3000 **(fig. 5.1B**). Bacterial infection triggered focal accumulations that could also be observed at lower magnifications in the adaxial mesophyll of infiltrated leaves **(fig. 5.1B**).

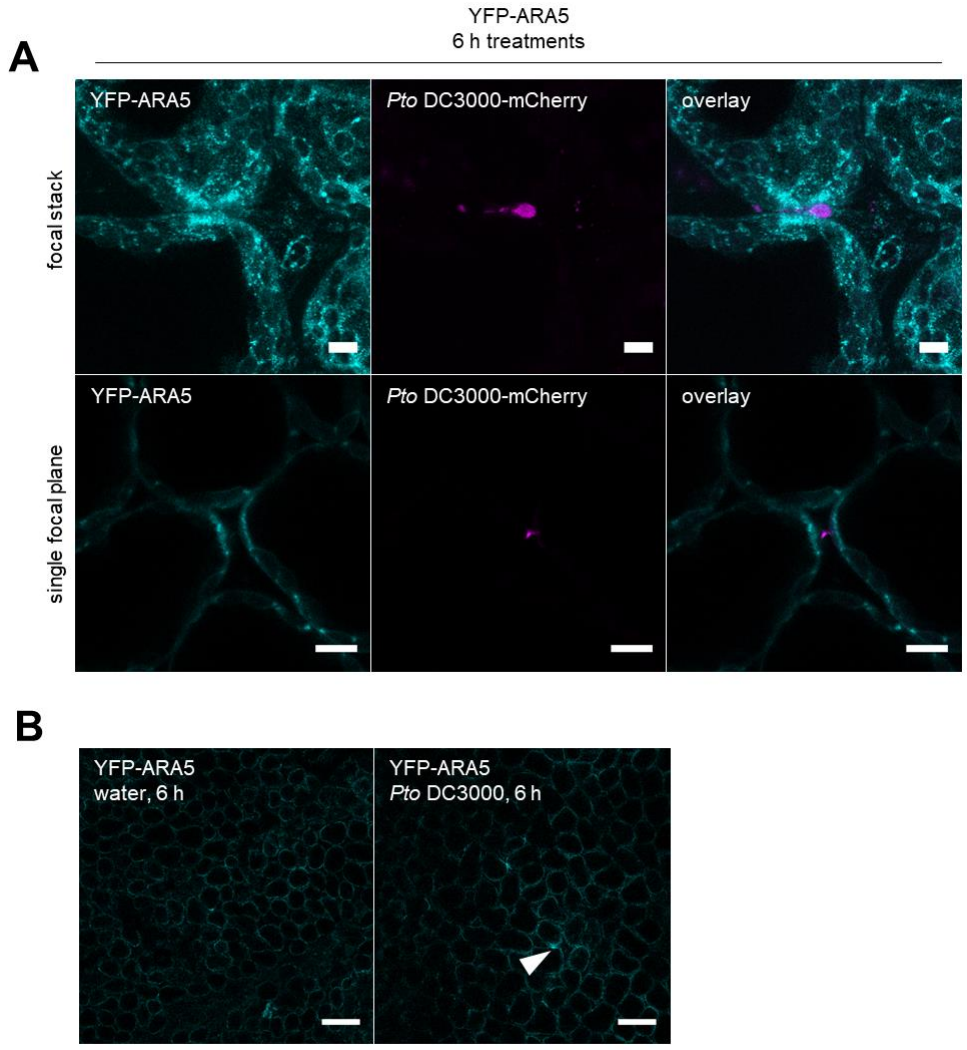

Figure 5.1. YFP-ARA5-positive compartments focally accumulate at bacterial infection sites. (A) Confocal micgrographs (z-projections) of YFP-ARA5 and *Pto* DC3000-mCherry in 4 wk-old Arabidopsis mesophyll tissue, 6 hours after syringe infiltration of bacterial suspensions. Bacterial OD_{600} = 0.2 upon infiltration. Top panels show maximum z-projection and bottom panels show single focal plane. Bacterial OD_{600} = 0.2 upon application. 63 × objective, scale bars = 10 µm. (B) Confocal micrographs of upper leaf mesophyll as in (A) but in the presence of Pto DC3000 and now using the 20 × objective, scale bars = 100 µm.

To quantify differences in the number of focal accumulations between water and bacterial treatment, I acquired images using the 20x magnification as used in figure **3.1B**, and applied the custom written FIJI macro that counts the number of fluorescent maxima per field of view, described in **chapter 4**. As a result, I could find no statistically significant differences between water and *Pto* DC3000 treatments, when applying a student's t-test **(fig. 5.2A,B**). However, bacteria on average showed a tendency to induce more ARA5 focal accumulations per field of view in both replicate 1 (15.67 ± 3.51 vs. 9.4 ± 1.98) and replicate 2 (4.67 ± 0.88 vs. 1.00 ± 1.00). Considering the qualitative observation that ARA5 focal accumulations were targeted to bacterial contact sites **(fig. 5.1**) and the trend for bacteria to induce more focal accumulations than water treatments **(fig. 5.2**), it is possible that secretory vesicles cluster in an enhanced manner at bacterial contact sites. The analysis could be improved by increasing the number of observations and experimental replications, and modifying the FIJI script to use local thresholding to improve accuracy of spot detection.

A

Genotype	Treatment	Number of foci / FOV					
		Replicate 1			Replicate 2		
		Mean	SE	*n*	Mean	SE	*n*
YFP-ARA5	water	9.4 ±	1.98	5	1.00 ±	1.00	3
	Pto DC3000	15.67 ±	3.51	9	4.67 ±	0.88	3

B

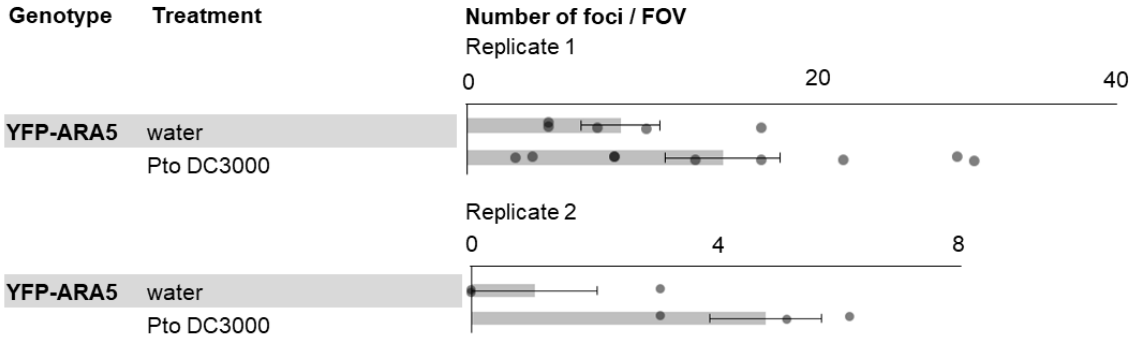

Figure 5.2. Quantitative analysis reveals no significant differences in focal accumulation of YFP-ARA5-positive compartments. (A) Overview listing mean ± SE and *n* = number of images for individual replicates, summarizing the number of YFP-ARA5 focal accumulations per field of view, for two replicates. Focal accumulations were quantified in an automated way using confocal micrographs acquired as in Figure 3.1B, at 6 hours after syringe infiltration of indicated treatments. (B) Graphical representations of data presented in (A). Dots show individual measurements and bars show mean ± SE (error bars) for indicated treatments corresponding to replicates shown in (B).

5.1.2 - ARA5 does not change in vesicle number upon immune stimulus (0-3 h)

Components of the secretory pathway are upregulated upon treatment with salicylic acid (SA), and are responsible for secretion of defense molecules such as PR1 (Wang et al., 2005; Kalde et al., 2007). Treatment with bacterial flg22 induces the accumulation of SA, and SA-mediated downstream responses (Tsuda et al., 2008). The upregulation of secretory pathway components could correlate with an increase in the number of secretory vesicles in the cell. To address this, I treated cotyledons of 2-week old *pUB::YFP-ARA5* seedlings with flg22 or water, and used high-throughput spinning disc confocal microscopy to obtain a large number of images over 3 h treatment, and quantified the number of vesicles per field of view using a custom-written script for the image analysis studio Acapella (PerkinElmer). I included water and flg22-treated cotyledons of genotype *pFLS2::FLS2-GFP* as a positive control. At 2 and 3 h after flg22 treatment, FLS2-GFP vesicle numbers were significantly upregulated compared to water treatment, consistent with previous observations (Beck et al., 2012b). By contrast, YFP-ARA5 vesicle numbers did not significantly change **(fig. 5.3**). While default secretory pathway components such as SYP121, SYP122 and SNAP33 are already activated within 10 minutes of flg22-treatment (Benschop et al., 2007; Pajonk et al., 2008). Constitutive expression of ARA5 results in a membrane-associated GTP-bound pool, and a cytosolic GDP-bound pool; in my analysis the upregulation of the secretory pathway is not reflected by an increased pool of membrane-associated ARA5-marked default secretory vesicles within 3 h of flg22-treatment.

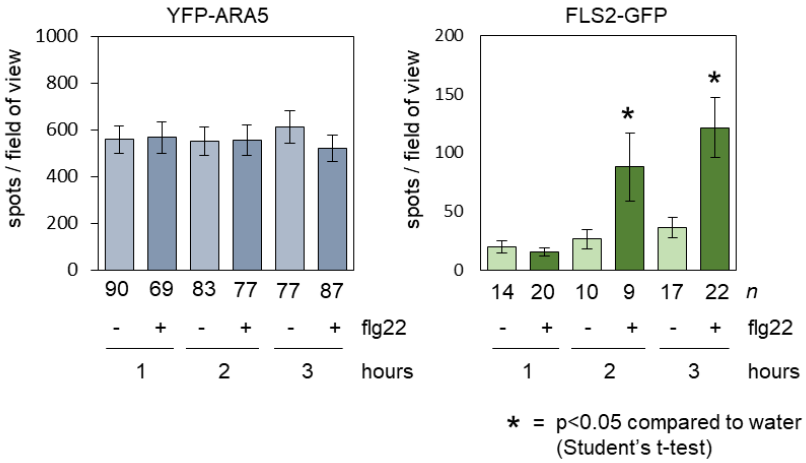

Figure 5.3. Quantitative analysis reveals no differences in the abundance patterns of YFP-ARA5-positive compartments. Graphical representation of number of detected spots (mean ± SE) per field-of-view in 2-wk old Arabidopsis cotyledon upper epidermal tissue expressing *pUB::YFP-ARA5* or *pFLS2::FLS2-GFP* and imaged using the Opera high-throughput confocal microscope at 1, 2 or 3 hours after water or 1.5 µM flagellin treatment. Asterisks indicate significant result compared to water

treatments at $p<0.05$ (Student's t-test). *n* = number of images analyzed across 24 cotyledons (YFP-ARA5) or 6 cotyledons (FLS2-GFP). Graphs show data of one experiment, representative of three independent replications.

5.2 - THE ARA5 CO-PURIFYING PROTEOME CHANGES UPON IMMUNE STIMULUS

5.2.1 - Purifying ARA5 from seedlings under water and flg22 conditions

Because I showed that ARA5 vesicles can cluster under bacterial contact sites, I was interested in revealing changes in the cargoes of these vesicles, which could be delivered to the location of pathogen attack. To investigate this, I applied the same technique as I used for analysis of ARA7 cargoes described in **chapter 4**. Briefly, I cultivated 8-day old Arabidopsis seedlings of genotype *pUB::YFP-ARA5* in liquid MS, alongside *pUB::YFP* as a negative control. I then treated the seedlings of both genotypes by applying the bacterial MAMP flg22 to the growth medium to a final concentration of 1.5 µM, and subsequently applied a vacuum to infiltrate the seedlings. I used water treatment as a negative control. Since SA induced the upregulation of defence-related secretory pathway genes, and SA is produced within hours of flg22 treatment (Tsuda et al., 2008), after 3 h of flg22 treament, I used immunoprecipitation as described before (Heard et al., 2015)**; Chapter 4 in this thesis)**, and subjected the samples to SDS-PAGE and mass spectrometry in collaboration with Jan Sklenar, Frank Menke and Paul Derbyshire (Proteomics Support Team, The Sainsbury Laboratory, Norwich UK).

After filtering the resulting proteomics data using Scaffold, I revealed 228 proteins in the YFP-ARA5 co-purifying proteome and 1101 proteins in the YFP co-purifying proteome **(fig. 5.4A**). In the same way as performed in Chapter 4 of this thesis, to select proteins that interacted specifically with ARA5, and not with affinity beads or the YFP fluorescent tags, for each protein I compared the spectral counts (number of peptides detected) across all three replications of YFP-ARA5 purifications and YFP purifications. I required the combined number of peptides in YFP-ARA5 purifications to be greater than 4x those in YFP purifications, and obtained a set of 77 proteins that I named the ARA5 co-purifying proteome **(fig. 5.4A, table 5.1**).

Table 5.1: ARA5 co-purifying proteome. Listed here is the ARA5 co-purifying proteome under water treated conditions. 8-day old seedlings of genotypes *pUB::YFP-ARA5* and *pUB::YFP* were treated with water or 1.5 µM flg22 for three hours, and subjected to immunoprecipitation using YFP affinity beads. Mass spectrometry was performed in collaboration with Jan Sklenar, Paul Derbyshire and Frank Menke (The Sainsbury Laboratory, Norwich, UK). To determine co-purifying proteomes, Scaffold software was used to retain proteins with a ProteinProphet score of 99% based on a minimum of 2 spectra with a PeptideProphet score of 95%. MS Excel was then used to retain proteins with at least 5 spectra across all three replicates in the YFP-ARA5 water-treated samples, with an occurence in more than 1 of these replicates, and an abundance increase of at least 4x compared to matching YFP controls. (*Columns 1-8*) Observed in # of replicates, and Spectra in combined replicates: Numbers and associated green cell-shading intensities indicate in how many experimental replicates the protein was detected, or how many spectra for that protein were identified in all three replicates combined, separated for water or flagellin treatment. (*Columns 9-10*) Enrichment factors: For each protein, the number of total spectra across three replicates of the green-labeled (rightmost) pulldown was divided by the number of total spectra in red-labeled (left-most) pulldown. Log10 values that correspond to these ratios are displayed in this table. Green or red bars are graphical representations of magnitude and direction of positive (green) or negative (red) values, centered at 0. (*Columns 11-12*) Locus ID and associated names. Source: TAIR10, accessed through www.genevestigator.org. The table is sorted for total spectral numbers in “YFP-ARA5 water”, in descending order.

Table 5.1: ARA5 co-purifying proteome

Observed in # of replicates				Spectra in combined replicates				Enrichment factor (log_{10})		Protein information	
YFP-ARA5		YFP		YFP-ARA5		YFP		YFP YFP-ARA5	Y5 water Y5 flg22		
water	flg22	water	flg22	water	flg22	water	flg22			Locus ID	Protein name
3	3	2		636	664	5		2.10E+00	1.87E-02	AT1G02130	ARA-5, ARA5, ATRAB1B, ATRABD2A, RA-5, RABD2A, RAS 5
3	3	3	3	519	594	84	37	7.91E-01	5.86E-02	AT1G59870	PEN3
3	3			181	125			8.26E+00	-1.61E-01	AT5G16280	Tetratricopeptide repeat (TPR)-like superfamily protein
3	3	1		147	104	1		2.17E+00	-1.50E-01	AT5G65950	unknown protein, homology to TRAPPI-components
3	3	1		144	114	1		2.16E+00	-1.01E-01	AT2G47960	unknown protein, homology to TRAPP
3	3			126	131			8.10E+00	1.69E-02	AT3G07160	ATGSL10, CALS9, gsl10, GSL10, glucan synthase-like 10
3	3	3	3	119	105	10	5	1.08E+00	-5.44E-02	AT2G29550	TUB7, tubulin beta-7 chain
3	3			67	49			7.83E+00	-1.36E-01	AT4G03550	PMR4
3	3	1		66	46	2		1.52E+00	-1.57E-01	AT4G39820	Tetratricopeptide repeat (TPR)-like superfamily protein
3	3	1		61	74	2		1.48E+00	8.39E-02	AT2G36850	ATGSL08, ATGSL8, CHOR, GSL08, GSL8, glucan synthase-like 8
3	3	3	2	61	45	9	3	8.31E-01	-1.32E-01	AT5G28540	BIP1, heat shock protein 70 (Hsp 70) family protein
3	3			55	40			7.74E+00	-1.38E-01	AT1G30450	ATCCC1, CCC1, HAP5, cation-chloride co-transporter 1
3	3	1	1	51	77	1	1	1.71E+00	1.79E-01	AT3G11820	AT-SYR1, ATSYP121, ATSYR1, PEN1, SYP121, SYR1, syntaxin of plants 121
3	3			49	35			7.69E+00	-1.46E-01	AT1G77140	ATVPS45, VPS45, vacuolar protein sorting 45
3	3	2	2	47	37	6	3	8.94E-01	-1.04E-01	AT2G14720	BP80-2;1, MTV4, VSR2;1, VSR4, vacuolar sorting receptor 4
3	3		1	46	39		1	7.66E+00	-7.17E-02	AT1G61250	SC3, SCAMP3, secretory carrier 3
3	3			45	33			7.65E+00	-1.35E-01	AT2G34420	LHB1B2, LHCB1.5, photosystem II light harvesting complex gene B1B2
3	3			40	64			7.60E+00	2.04E-01	AT1G65350	UBQ13, ubiquitin 13
3	3			37	23			7.57E+00	-2.06E-01	AT1G59820	ALA3, aminophospholipid ATPase 3
3	3			36	33			7.56E+00	-3.78E-02	AT3G17900	unknown protein
3	3			35	29			7.54E+00	-8.17E-02	AT5G54440	AtTRS130, CLUB, CLUB
3	3	1		35	28	1		1.54E+00	-9.69E-02	AT2G28520	VHA-A1, vacuolar proton ATPase A1
3	2			34	12			7.53E+00	-4.52E-01	AT2G34510	Protein of unknown function, DUF642
3	3	1	1	34	36	2	2	1.23E+00	2.48E-02	AT4G18800	ATHSGBP, ATRAB11B, ATRABA1D, RABA1d, RAB GTPase homolog A1D
3	3	2	2	32	17	6	5	7.27E-01	-2.75E-01	AT4G12650	Endomembrane protein 70 protein family
3	2	1		31	14	4		8.89E-01	-3.45E-01	AT5G49720	ATGH9A1, DEC, GH9A1, IRX2, KOR, KOR1, RSW2, TSD1, glycosyl hydrolase 9A1
3	2			29	9			7.46E+00	-5.08E-01	AT5G17230	PSY, PHYTOENE SYNTHASE
3	3			28	11			7.45E+00	-4.06E-01	AT3G52850	ATELP, ATELP1, ATVSR1, BP-80, BP80, BP80-1;1, BP80B, GFS1, VSR1, VSR1;1
3	3	1		28	17	2		1.15E+00	-2.17E-01	AT4G32410	AtCESA1, CESA1, RSW1, cellulose synthase 1
3	3			27	23			7.43E+00	-6.96E-02	AT3G58460	ATRBL15, RBL15, RHOMBOID-like protein 15
3	3			27	16			7.43E+00	-2.27E-01	AT3G05280	Integral membrane Yip1 family protein
3	3			26	11			7.41E+00	-3.74E-01	AT5G64740	CESA6, E112, IXR2, PRC1, cellulose synthase 6
3	3	1		26	16	1		1.41E+00	-2.11E-01	AT5G05170	ATCESA3, ATH-B, CESA3, CEV1, IXR1, Cellulose synthase family protein
3	3	1		26	13	1		1.41E+00	-3.01E-01	AT5G59840	Ras-related small GTP-binding family protein
3	3			25	17			7.40E+00	-1.67E-01	AT1G25570	Di-glucose binding protein with Leucine-rich repeat domain
3	3			22	11			7.34E+00	-3.01E-01	AT5G58030	TRS31, TRAPPI-component
3	2	1		22	11	2		1.04E+00	-3.01E-01	AT1G17840	ABCG11, ATWBC11, COF1, DSO, WBC11, white-brown complex homolog protein 11
3	3			19	21			7.28E+00	4.35E-02	AT4G31490	Coatomer, beta subunit
3	3			18	24			7.26E+00	1.25E-01	AT1G53440	Leucine-rich repeat transmembrane protein kinase
3	3			18	15			7.26E+00	-7.92E-02	AT3G15380	Plasma-membrane choline transporter family protein
3	3	1		17	15	3		7.53E-01	-5.44E-02	AT5G11040	AtTRS120, TRS120, TRS120
3	3			16	13			7.20E+00	-9.02E-02	AT3G05710	ATSYP43, SYP43, syntaxin of plants 43

3	3	1		16	15	1		1.20E+00	-2.80E-02	AT1G28490	ATSYP61, OSM1, SYP61, syntaxin of plants 61
3	3			15	15			7.18E+00	0.00E+00	AT4G36440	unknown protein
3	2			14	11			7.15E+00	-1.05E-01	AT4G16120	COBL7, SEB1, COBRA-like protein-7 precursor
3	2			13	5			7.11E+00	-4.15E-01	AT1G24560	PLANT-UNIQUE RAB5 EFFECTOR 2, PUF2
3	3			13	9			7.11E+00	-1.60E-01	AT1G26670	ATVTI12, VTI12, VTI1B, Vesicle transport v-SNARE family protein
3	3	1		13	22	2		8.13E-01	2.28E-01	AT5G06320	NHL3, NDR1/HIN1-like 3
3	2	1		12	11	1		1.08E+00	-3.78E-02	AT4G30260	Integral membrane Yip1 family protein
3	2	1		12	9	1		1.08E+00	-1.25E-01	AT1G56190	Phosphoglycerate kinase family protein
3	3	2	1	12	13	2	1	7.78E-01	3.48E-02	AT1G02080	transcription regulators
3	3			11	9			7.04E+00	-8.72E-02	AT4G20110	BP80-3;1, VSR3;1, VSR7, VACUOLAR SORTING RECEPTOR 7
3	3			11	9			7.04E+00	-8.72E-02	AT1G54320	LEM3 (ligand-effect modulator 3) family protein / CDC50 family protein
3	1			11	2			7.04E+00	-7.40E-01	AT5G09870	CESA5, cellulose synthase 5
3	3	1		11	24	1		1.04E+00	3.39E-01	AT4G23180	CRK10
3	2	1		11	4	1		1.04E+00	-4.39E-01	AT1G51500	ABCG12, ATWBC12, CER5, D3, WBC12, ABC-2 type transporter family protein
3	3	1		10	13	2		6.99E-01	1.14E-01	AT3G28710	ATPase, V0/A0 complex, subunit C/D
2	3	1		10	7	2		6.99E-01	-1.55E-01	AT1G53840	ATPME1, PME1, pectin methylesterase 1
2	3			9	15			6.95E+00	2.22E-01	AT5G54830	DOMON domain-containing protein
3	2			9	6			6.95E+00	-1.76E-01	AT3G05200	ATL6, RING/U-box superfamily protein
3	2			9	6			6.95E+00	-1.76E-01	AT1G29980	Protein of unknown function, DUF642
2	3			9	5			6.95E+00	-2.55E-01	AT1G28340	AtRLP4, RLP4, receptor like protein 4
3	3			9	4			6.95E+00	-3.52E-01	AT3G14790	ATRHM3, RHM3, rhamnose biosynthesis 3
3	3	1		9	9	1		9.54E-01	0.00E+00	AT5G57350	AHA3, ATAHA3, HA3, H(+)-ATPase 3
3	2			8	9			6.90E+00	5.12E-02	AT1G51630	O-fucosyltransferase family protein
3	3			8	10			6.90E+00	9.69E-02	AT5G04870	ATCPK1, CPK1, calcium dependent protein kinase 1
3	3			8	22			6.90E+00	4.39E-01	AT5G03700	D-mannose binding lectin protein with Apple-like carbohydrate-binding domain
2	3			8	7			6.90E+00	-5.80E-02	AT5G60670	Ribosomal protein L11 family protein
3	3			8	5			6.90E+00	-2.04E-01	AT5G61060	ATHDA5, HDA05, HDA5, histone deacetylase 5
3	1			8	2			6.90E+00	-6.02E-01	AT1G13900	Purple acid phosphatases superfamily protein
3	3			7	5			6.85E+00	-1.46E-01	AT1G01960	BIG3, EDA10, ARF-GEF
3	3			6	5			6.78E+00	-7.92E-02	AT2G14740	ATVSR3, BP80-2;2, VSR2;2, VSR3, VSR3, vaculolar sorting receptor 3
3	2			6	3			6.78E+00	-3.01E-01	AT1G27930	Protein of unknown function (DUF579)
3	3			6	11			6.78E+00	2.63E-01	AT2G45010	PLAC8 family protein
2	2			6	3			6.78E+00	-3.01E-01	AT2G20840	Secretory carrier membrane protein (SCAMP) family protein
2	1			6	4			6.78E+00	-1.76E-01	AT5G58420	Ribosomal protein S4 (RPS4A) family protein
3	3	1		6	6	1		7.78E-01	0.00E+00	AT5G22360	ATVAMP714, VAMP714, VAMP714, vesicle-associated membrane protein 714

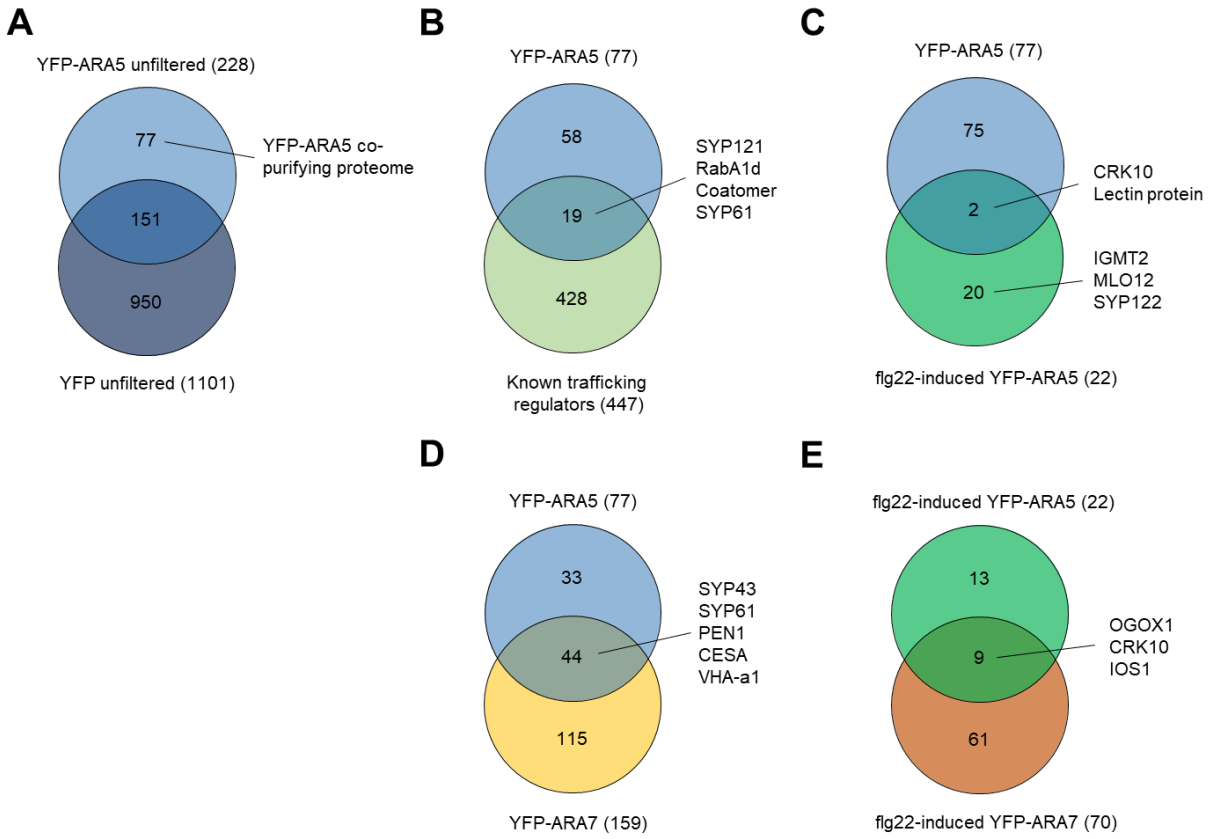

Figure 5.4. Identification of proteins associated with YFP-ARA5 in a flg22-responsive manner. (A) Venn-diagram shows proteins co-purifying with YFP-ARA5 from Arabidopsis seedlings, compared to proteins co-purifying with a YFP control, as revealed by immunoprecipitation and mass spectrometry. The YFP-ARA5 co-purifying proteome was defined based on quality control criteria (present in >1 replicates, peptides = >5) and fold-change ratio of >4 in YFP-ARA5 compared to YFP control. Details available in Table 5.1. (B) Venn-diagram showing YFP-ARA5 co-purifying proteins as revealed by immunoprecipitation and mass spectrometry, overlaid with known trafficking regulators (source: Heard et al. 2015). Call-out indicates prominent trafficking regulators found in YFP-ARA5. (C) Venn-diagram showing YFP-ARA5 co-purifying proteins as above, comparing before and after 3 hours of flagellin treatment. Call-outs indicate proteins present in both groups (top) or in the flagellin-treated group (bottom). Details available in Table 5.3. (D) Venn-diagram showing YFP-ARA5 co-purifying proteins as above, overlaid with YFP-ARA7 co-purifying proteins, both in the absence of flg22 treatment. Call-out indicates proteins present in both groups. Details available in table 5.4. (E) Venn-diagram showing YFP-ARA5 co-purifying proteins after 3 hours flagellin treatment, overlaid with YFP-ARA7 co-purifying proteins after 3 hours flagellin treatment. Call-out indicates proteins present in both groups. Details available in table 5.5.

5.2.2 - The ARA5 proteome contains known secretory pathway-associated proteins

In order to further verify the quality of the so-defined ARA5 co-purifying proteome, I compared the proteome to a comprehensive manually curated list of known Arabidopsis trafficking regulators (**Heard 2015**) and listed the results in **table 5.2**. 19 out of 77 proteins classified as trafficking regulators in this way (**fig. 5.4B, table 5.2**). Upon inspection, I observed that a majority of trafficking regulators found interacting with ARA5 were also identified in the water-treated ARA7 co-purifying proteome as defined in **chapter 4**. However, several regulators were unique to ARA5 and, based on existing knowledge, corresponded to the known Golgi and TGN/EE localization of ARA5.

Signature proteins identified in purifications of ARA5 specifically

RABA1d is a member of the Arabidopsis RAB11/RABA group, which consist of predominantly TGN/EE-to-PM secretory functioning RAB GTPases (Asaoka et al., 2013). RabA1 members were found to localize at TGN/EE, partially overlapping with TGN/EE-markers SYP43 and VHA-a1 (Asaoka et al., 2013). RABA members have different roles contributing to the cell wall composition, with single mutants affecting pectin, cellulose and hemicellulose (Lunn et al., 2013). In immunity, RABA1b, which is a close homolog of RABA1d, governs the secretion of newly synthesized cell-surface receptor FLS2 (Choi et al., 2013). More distant homologs of RABA1, such as RABA6a, are thought to have a function in endocytic traffic at the TGN/EE (Choi et al., 2013). Finding RABA1d in the ARA5 proteome corresponds to the partial TGN/EE localization of ARA5.

Tubulin 7 (TUB7), is protein found at high abundance interacting specifically with ARA5, and the only cytoskeletal component found in my ARA5 and ARA7 purifications. Golgi bodies attach to microtubules, and their motility along the cytoskeleton regulates the dynamics of the delivery and removal of cell-surface cargoes such as cellulose synthase complexes (CESA, (Crowell et al., 2009).

Coatomer (subunit AT4G31490) localizes to the Golgi, where multimeric complexes regulate retrograde traffic (Brandizzi and Barlowe, 2013). The ARA5 partial Golgi-localization leads me to expect Golgi-components in the purification. While this subunit was specific to ARA5, other coatomer subunits were identified in ARA7 purifications (c**hapter 4, tables 4.2, 4.3;** AT1G62020, AT3G15980).

Table 5.2: Trafficking regulators in the ARA5 co-purifying proteome. Listed here is the ARA5 co-purifying proteome under water treated conditions, copied from Table 5.1, and filtered to retain only endomembrane trafficking regulators as defined in Heard et al. 2015.

Table 5.2: Traffic regulators in the ARA5 co-purifying proteome

Observed in # of replicates				Spectra in combined replicates				Enrichment factor (log_{10})		Protein information	
YFP-ARA5		YFP		YFP-ARA5		YFP		YFP YFP-ARA5	Y5 water Y5 flg22	Locus ID	Protein name
water	flg22	water	flg22	water	flg22	water	flg22				
3	3	2		636	664	5		2.10E+00	1.87E-02	AT1G02130	ARA-5, ARA5, ATRAB1B, ATRABD2A, RA-5, RABD2A, RAS 5
3	3			181	125			8.26E+00	-1.61E-01	AT5G16280	Tetratricopeptide repeat (TPR)-like superfamily protein
3	3	3	3	119	105	10	5	1.08E+00	-5.44E-02	AT2G29550	TUB7, tubulin beta-7 chain
3	3	1	1	51	77	1	1	1.71E+00	1.79E-01	AT3G11820	AT-SYR1, ATSYP121, ATSYR1, PEN1, SYP121, SYR1, syntaxin of plants 121
3	3	2	2	47	37	6	3	8.94E-01	-1.04E-01	AT2G14720	BP80-2;1, MTV4, VSR2;1, VSR4, vacuolar sorting receptor 4
3	3		1	46	39		1	7.66E+00	-7.17E-02	AT1G61250	SC3, SCAMP3, secretory carrier 3
3	3			35	29			7.54E+00	-8.17E-02	AT5G54440	AtTRS130, CLUB, CLUB
3	3	1	1	34	36	2	2	1.23E+00	2.48E-02	AT4G18800	ATHSGBP, ATRAB11B, ATRABA1D, RABA1d, RAB GTPase homolog A1D
3	3			28	11			7.45E+00	-4.06E-01	AT3G52850	ATELP, ATELP1, ATVSR1, BP-80, BP80, BP80-1;1, BP80B, GFS1, VSR1, VSR1;1
3	3			27	16			7.43E+00	-2.27E-01	AT3G05280	Integral membrane Yip1 family protein
3	3			22	11			7.34E+00	-3.01E-01	AT5G58030	TRS31, TRAPPI-component
3	3			19	21			7.28E+00	4.35E-02	AT4G31490	Coatomer, beta subunit
3	3	1		17	15	3		7.53E-01	-5.44E-02	AT5G11040	AtTRS120, TRS120, TRS120
3	3			16	13			7.20E+00	-9.02E-02	AT3G05710	ATSYP43, SYP43, syntaxin of plants 43
3	3	1		16	15	1		1.20E+00	-2.80E-02	AT1G28490	ATSYP61, OSM1, SYP61, syntaxin of plants 61
3	3			13	9			7.11E+00	-1.60E-01	AT1G26670	ATVTI12, VTI12, VTI1B, Vesicle transport v-SNARE family protein
3	2	1		12	11	1		1.08E+00	-3.78E-02	AT4G30260	Integral membrane Yip1 family protein
3	3			11	9			7.04E+00	-8.72E-02	AT4G20110	BP80-3;1, VSR3;1, VSR7, VACUOLAR SORTING RECEPTOR 7
3	3			7	5			6.85E+00	-1.46E-01	AT1G01960	BIG3, EDA10, ARF-GEF
3	3			6	5			6.78E+00	-7.92E-02	AT2G14740	ATVSR3, BP80-2;2, VSR2;2, VSR3, VSR3, vaculolar sorting receptor 3
3	3	1		6	6	1		7.78E-01	0.00E+00	AT5G22360	ATVAMP714, VAMP714, VAMP714, vesicle-associated membrane protein 714

The protein with the highest abundance in non-elicited ARA5 purifications is PEN3. Briefly, PEN3 is a PM-localized transporter, thought to function in the export of antimicrobial compounds produced by PEN2 which is localized on mitochondria (Stein et al., 2006; Fuchs et al., 2015b). In **chapter 4**, I discussed the tendency for PEN3 to accumulate higher in ARA7 purifications under flg22 treatment when compared to water treatment (**chapter 4**), but in ARA5 purifications, PEN3 accumulates to similar levels as in flg22-elicited conditions (519 vs. 594 spectra, **table 5.1**). PEN3 shuttles between the PM-TGN/EE, but is also consitutively secreted. Both the secretory pathway as well as the endocytic pathway were shown to contribute to PEN3-accumulations in chemically-induced Golgi-TGN/EE aggregates (Mao et al., 2016). In un-elicited states, PEN3 furthermore localized to the PM, but also to mobile punctae adjacent to SYP32-marked Golgi (Underwood and Somerville, 2013; Mao et al., 2016). In flg22-elicited conditions, PEN3 accumulated at endosomal compartments (Underwood et al., 2017), but this is not reflected in a marked increase of spectra co-purifying with ARA5.

Novel proteins identified in ARA5 purifications

Unexpectedly abundant in ARA5 purifications, BiP1/Heat Shock Protein70 (HSP70) is a major ER-localized and functioning protein (Srivastava et al., 2013). This could reflect a contamination, or an interaction partner of ARA5 during its constitutive biosynthesis. However, since dominant negative studies showed that ARA5 functioned in the early secretory trafficking step between ER and Golgi, it could also reflect a previously unknown functional interactor in the ARA5 complex at early secretory steps.

5.2.3 - Proteins that are abundant in ARA5 purifications which also occur in ARA7

The following proteins identified in ARA5 purifications (**table 5.1**) were found for ARA7 as well (**tables 4.1, 5.4**). Here, I describe these proteins in the context of the secretory pathway localization and functionality of ARA5. In this section, I selected abundant proteins as found in ARA5 purifications, and in further sections where I describe the common proteome of ARA5 and ARA7, I prioritize proteins that are of most similar abundance in both.

Trafficking regulators

PEN1/SYP121 has been shown to be PM-localized, and recycle between the PM and TGN/EE compartment (Nielsen and Thordal-Christensen, 2012; Collins et al., 2003; Uemura et al., 2004). PEN1 engages the default secretory complex consisting of other SNAREs VAMP721, VAMP722 and SNAP33 in order to confer immunity against powdery mildew (Kwon et al., 2008). However, besides PEN1, members of this complex were not identified in my ARA5 purifications. PEN1 functions in the formation of the callose-rich extracellular papilla that is formed at sites of penetration attempts by filamentous pathogens, and contributes to the timely formation of these

structures (Collins et al., 2003; Assaad et al., 2004). Separate from its functioning in regulating membrane traffic, PEN1/SYP121 interacts with the potassium channel KC1 and positively affects its inward potassium permeability, thus regulating guard cell dynamics in stomatal opening (Grefen et al., 2010; Honsbein et al., 2009; Eisenach et al., 2012).

Two tetratricopeptide-repeat (TPR)-containing proteins (AT5G16280, AT4G39820) were identified with relatively high abundance in ARA5 purifications. While these proteins have yet to be characterized, a different TPR-containing protein HYPERSENSITIVE TO LATRUNCILIN B1 (HLB1) has recently been shown to localize to the TGN/EE, and regulates both secretory and endocytic traffic passing through this compartment (Sparks et al., 2016). Interestingly, HLB1 was found to interact and colocalize with and actin filaments, raising the TPR proteins I identified as interacting with ARA5 as possible candidates linking ARA5 compartments to the cytoskeleton.

Secretory Carrier Membrane Protein 3 (SC3) is part of a bigger family of Secretory Carrier Membrane Proteins (SCAMPs). In eukaryotes, SCAMPs are transmembrane proteins regulating post-Golgi traffic, and are associated with endocytic uptake and recycling to the PM, and localize to PM and endomembrane compartments (Fernández-Chacón and Südhof, 2000). While SC3 in Arabidopsis is uncharacterized, in rice, *Os*SCAMP1 localized to the PM and early endocytic compartments (Lam et al., 2007). Functionally, based on RNAi studies of SCAMPs in poplar (*Populus tremula*), they are implicated in the control of secondary cell-wall precursors and proteins involved in their trafficking (Obudulu et al., 2018).

VAMP714 is a member of the VAMP71 subgroup of Arabidopsis SNAREs, of which members are predominantly tonoplast-localized (Uemura et al., 2004). VAMP714 localizes to the tonoplast in localization and proteomic analysis studies, but it was also found on Golgi membranes (Uemura et al., 2004; Szponarski et al., 2004). The precise function of VAMP714 has yet to be determined, but its localization suggests a putative role in Golgi-vacuole trafficking (Leshem et al., 2006).

Finally, Vacuolar Sorting Receptor 4/Modified Transport to the Vacuole 4 (VSR4/MTV4) is involved in vacuolar delivery of vacuolar storage proteins (Zouhar et al., 2009), predominantly localized to the PM but also to SYP61-positive TGN/EE punctae (Nishimura et al., 2016). It must be noted that the SYP61 proteome contained ARA5 (Drakakaki et al., 2012), and my ARA5 proteome contained SYP61 (**tables 5.1, 5.2**).

Non-trafficking regulators

Glucan Synthase-Like (GSL) 8 and 10 are callose synthases that function in normal plant growth, with knockdown or knockout of the genes causing severe plant defects already at seedling stages (Töller et al., 2008; Chen et al., 2009). Additionally, GSL10 has been shown to function in male

gametogenesis, regulating asymmetric cell division at the microspore stage (Huang et al., 2009). Importantly, PMR4/GSL5 was found in ARA5 and ARA7 purifications.

PMR4 is a callose synthase involved in callose production in response to wounding and pathogen detection (Dong et al., 2005; Jacobs et al., 2003; Ellinger et al., 2013). PMR4 contributes to the formation of the callose-rich papilla upon pathogen attack, and accumulates in encasements surrounding *Golovinomyces orontii* haustoria (Meyer et al., 2009). PMR4 is also required for flg22-induced callose deposition (Clay et al., 2009). While bacterial infection, or treatment with the bacterial MAMP flagellin, trigger a significant extracellular accumulation of callose, the number of detected PMR4-associated spectra did not markedly increase or decrease in ARA5 or ARA7 purifications at 3 h after flagellin treatment.

Cation-Chloride Cotransporter 1 (CCC1) is member of a group of co-transporters that are thought to mediate the transmembrane exchange of potassium and sodium with chloride (Henderson et al., 2015). CCCs have been consistently found in earlier proteomic studies of the TGN/EE (Drakakaki et al., 2012; Groen et al., 2014), and localized to the Golgi and TGN/EE (Henderson et al., 2015), corresponding to the known localization of ARA5.

5.2.4 - The ARA5 co-purifying proteome changes upon 3-h flg22 treatment

Upon flg22 treatment for 3 h, the ARA5 co-purifying proteome changes **(fig. 5.4C**). 20 proteins absent from water treated samples were found to interact with ARA5 (**table 5.3**). Of two proteins (CRK10 and a lectin protein) identified under water treated conditions, associated spectra increased more than 2-fold in flg22 treated conditions.

Phosphorus metabolism and multi-organism-processes are overrepresented in the ARA5 co-purifying proteome upon flg22-stimulus

To obtain an impression of the global pattern of functional changes in the ARA5 co-purifying proteome, I performed an overrepresentation analysis of GO-terms listing biological functions (**table S4**) using the PANTHER Classification System (pantherdb.org). Most notably, processes including terms such as “phosphorylation” and “phosphorus metabolic process” are overrepresented. Looking at the details of the ARA5 co-purifying proteome under flg22 conditions (**table 5.3**), the list is enriched in protein kinases, receptor kinases and LRR-RLKs. Since these proteins can phosphorylate interaction partners, an overrepresentation of GO-processes including phosphorus can be explained. Finally, terms such as “defense to other organism” and “multi-organism process” appear, which makes sense in the context of studying proteomic changes upon application of a bacterial MAMP.

Proteins co-purifying with ARA5 upon flg22 stimulus that are not found in ARA7

Notable changes in the ARA5 co-purifying proteome upon 3 h flagellin treatment include INDOLE-GLUCOSINOLATE O-METHYLTRANSFERASE 2 (IGMT2) and MILDEW RESISTANCE LOCUS 12 (MLO12). IGMT2 is an enzyme that plays a catalytic role in the final steps of indole-glucosinolate derived antimicrobial production (Pfalz et al., 2011). It has been shown to convert indole-3-methylglucosinolate (I3M) into 4-methoxyindole-3-methylglucosinolate (4MOI3M), which in turn is converted by the mitochondrial-localized atypical myrosinase PEN2 (Fuchs et al., 2015b) into derivaties with broad antimicrobial activity (Stahl et al., 2016; Lipka et al., 2005; Oa et al., 2010). Interestingly, out of both ARA5 and ARA7 purifications, IGMT2 was only identified in flg22-treated ARA5 samples. In comparison, I identified the less well-characterized homolog IGMT4 specifically in the ARA7 proteome as strongly positively responsive to flg22 treatment (**table 4.3**). Previously, indole glucosinolate-related antimicrobial metabolism was shown to be required for flg22-induced callose deposition (Clay et al., 2009), which in turn is dependent on the glucan synthase PMR4 that was detected in ARA5 before flg22 elicitation (**table 5.1**).

Table 5.3: ARA5 co-purifying proteins that are more abundant upon flagellin treatment. Listed here is the ARA5 co-purifying proteome under flagellin treated conditions. 8-day old seedlings of genotypes *pUB::YFP-ARA5* and *pUB::YFP* were treated with water or 1.5 µM flg22 for three hours, and subjected to immunoprecipitation using YFP affinity beads. Mass spectrometry was performed in collaboration with Jan Sklenar, Paul Derbyshire and Frank Menke (The Sainsbury Laboratory, Norwich, UK). To determine co-purifying proteomes, Scaffold software was used to retain proteins with a ProteinProphet score of 99% based on a minimum of 2 spectra with a PeptideProphet score of 95%. MS Excel was then used to retain proteins with at least 5 spectra across all three replicates in the YFP-ARA5 flg22-treated samples, with an occurence in more than 1 of these replicates, an abundance increase of at least 4x compared to matching YFP controls, and an abundance increase of at least 2x compared to matching water treated controls. (*Columns 1-8*) Observed in # of replicates, and Spectra in combined replicates: Numbers and associated green cell-shading intensities indicate in how many experimental replicates the protein was detected, or how many spectra for that protein were identified in all three replicates combined, separated for water or flagellin treatment. (*Columns 9-10*) Enrichment factors: For each protein, the number of total spectra across three replicates of the green-labeled (rightmost) pulldown was divided by the number of total spectra in red-labeled (left-most) pulldown. Log10 values that correspond to these ratios are displayed in this table. Green or red bars are graphical representations of magnitude and direction of positive (green) or negative (red) values, centered at 0. (*Columns 11-12*) Locus ID and associated names. Source: TAIR10, accessed through www.genevestigator.org. The table is sorted for total spectral numbers in “YFP-ARA5 flg22”, in descending order.

Table 5.3: ARA5 co-purifying proteins that are more abundant upon flagellin treatment

Observed in # of replicates				Spectra in combined replicates				Enrichment factor (log_{10})		Protein information	
YFP-ARA5		YFP		YFP-ARA5		YFP		YFP YFP-ARA5	Y5 water Y5 flg22	Locus ID	Protein name
water	flg22	water	flg22	water	flg22	water	flg22				
	3				33			0.00E+00	7.52E+00	AT1G21120	IGMT2
3	3	1		11	24	1		1.04E+00	3.39E-01	AT4G23180	CRK10
3	3			8	22			6.90E+00	4.39E-01	AT5G03700	D-mannose binding lectin protein with Apple-like carbohydrate-binding domain
	3				22			0.00E+00	7.34E+00	AT1G14540	PER4, PEROXIDASE 4
2	3			2	20			6.30E+00	1.00E+00	AT5G04930	ALA1, aminophospholipid ATPase 1
2	3	1	1	2	16	2	2	0.00E+00	9.03E-01	AT1G03220	Eukaryotic aspartyl protease family protein
3	3	1		5	14	5		0.00E+00	4.47E-01	AT5G49760	Leucine-rich repeat protein kinase family protein
2	3			3	13			6.48E+00	6.37E-01	AT1G06840	Leucine-rich repeat protein kinase family protein
2	3	1		3	13	1		4.77E-01	6.37E-01	AT1G51800	IOS1
3	3			5	11			6.70E+00	3.42E-01	AT3G62370	heme binding protein
1	3	1		1	10	6		-7.78E-01	1.00E+00	AT4G08850	LRR-RLK, MIK2
2	3			3	9			6.48E+00	4.77E-01	AT1G52200	PLAC8 family protein
1	3			1	9			6.00E+00	9.54E-01	AT2G01180	ATLPP1, ATPAP1, LPP1, PAP1, phosphatidic acid phosphatase 1
	2				9			0.00E+00	6.95E+00	AT1G30700	FAD-binding Berberine family protein
2	3			3	8			6.48E+00	4.26E-01	AT1G09970	LRR XI-23, RLK7, Leucine-rich receptor-like protein kinase family protein
2	2			3	7			6.48E+00	3.68E-01	AT1G19110	inter-alpha-trypsin inhibitor heavy chain-related
1	2	3		2	7	25		-1.10E+00	5.44E-01	AT2G32730	26S proteasome regulatory complex, non-ATPase subcomplex, Rpn2/Psmd1 subunit
	3				7			0.00E+00	6.85E+00	AT2G39200	MLO12
	2				7			0.00E+00	6.85E+00	AT3G52400	ATSYP122, SYP122, syntaxin of plants 122
1	3	1		2	6	1		3.01E-01	4.77E-01	AT3G17410	Protein kinase superfamily protein
1	2	2		2	6	18		-9.54E-01	4.77E-01	AT3G14840	Leucine-rich repeat transmembrane protein kinase
	2	2			6	6		-6.78E+00	6.78E+00	AT4G20830	OGOX1, OLIGOGALACTURONIDE OXIDASE 1

Mildew Resistance Locus O 12 (MLO12) is a member of the MLO family of susceptibility factors, of which Arabidopsis MLO2 has been best characterized (Consonni et al., 2006; Panstruga, 2005; Kusch and Panstruga, 2017). They contain 7 transmembrane domains, and Arabidopsis MLO2 has been shown to be PM-localized (Bhat et al., 2005). In barley (*Hordeum vulgare*), where MLO was originally identified as a susceptibility locus to powdery mildew infection (*Blumeria graminis* f.sp. *hordei, Bgh*, (Büschges et al., 1997), MLO accumulates at the PM and enriched under pathogen penetration sites (Bhat et al., 2005). In my proteomic analysis, I identify MLO12 as positively responsive to flg22, which combined with data on ARA5 vesicles focally accumulating under bacterial attack sites **(fig. 5.1**) could indicate MLO12 also focally accumulates upon pathogen challenge.

Loss of MLO genes increases resistance to powdery mildews, but little is known about functions in antibacterial resistance. Loss of function mutations in pepper (*Capsicum annuum*) *MLO2*, of which the product localizes to the PM, enhanced resistance to bacterial pathogens, while introduction of *CaMLO2* into Arabidopsis enhanced its susceptibility to *Pto* DC3000 (Kim and Hwang, 2012). *Mlo2*-based resistance requires trafficking processes involving PEN1/SYP121, and the production of glucosinolate-derived antimicrobials in the PEN2/PEN3 pathway, of which components were also found in my proteomic studies (Assaad et al., 2004; Consonni et al., 2006; Dittgen et al., 2006; Bednarek et al., 2009). Little is known about the localization and function of MLO12, but enhanced mildew resistance in *mlo2/6/12* triple mutants did not have the trafficking and antimicrobial requirements as described for *mlo2* (Kuhn et al., 2017).

Aminophospholipid ATPase 1 (ALA1) is a lipid flippase. Flippases are generally involved in translocating lipids between leaflets of the lipid bilayer, thus achieving lipid asymmetry. For previously characterized lipid flippases, this process can contribute to the budding of vesicles by overcoming energetically unfavorable intermediate stages in membrane bending (Pomorski and Menon, 2006). ALA1 was found to be PM-localized, and together with ALA2 has a function in RNAi-based antiviral immunity, where it works in the same pathway as RNA-dependent DNA-polymerases (López-Marqués et al., 2012; Zhu et al., 2017). The precise functions of ALA1 are unclear, but its known PM-localization suggests it does not function at the TGN/EE. It could be that upon immune stimulus, ALA1 traffics to the cell surface to support membrane trafficking events there.

From GO-analysis showing a strong overrepresentation of terms involving phosphorus metabolism, and from inspection of the proteomic results, it becomes evident that proteins upregulated in ARA5 purifications upon flg22 treatment contain a number of receptor kinases (**table 5.3, table S4**). In fact, four LRR-RLKs were found in ARA5 upon flg22 treatment, which were not found in ARA7 purifications (AT5G49760, AT1G06840, AT3G14840 and LRR XI-23). Engagement of default secretion to support the MAMP-induced delivery of defence compounds to

the cell surface has been described before, with roles for PEN1/SYP121 in callose deposition and SYP132 in antimicrobial PR-1 secretion (Assaad et al., 2004; Kalde et al., 2007).

5.3 - THE ARA7 AND ARA5 CO-PURYFING PROTEOMES SHOW DIFFERENTIAL OVERLAP IN RESTING AND IMMUNE ACTIVATED CONDITIONS

5.3.1 - The shared ARA7 and ARA5 co-purifying proteome contains TGN/EE, cell wall, and membrane trafficking-associated proteins

In order to gain insight into the shared proteins interacting with both the secretory ARA5 and the endocytic ARA7, I combined both water-treated co-puryfing proteomes, and filtered the list to only retain proteins present in both purifications (**table 5.4, figure 3.4D**). Upon inspection, the list reveals the presence of typical TGN/EE markers such as VHA-a1, SYP43, SYP61 and VTI12, which is in accordance with the partial localization of both ARA7 and ARA5 to the TGN/EE (Gendre et al., 2014). Furthermore, when analyzing the shared proteome for overrepresentation of GO-terms in the classification of "biological function" (**table S5**), two themes appear, which broadly consist of (A) cell wall metabolism: callose and cellulose metabolism, primary cell wall formation, polysaccharide localization and biosynthesis, cell shape and cytokinesis; and (B) membrane trafficking: secretion, vacuolar targeting, vesicle tethering, docking and fusion, vesicle organisation and exocytosis. The appearance of these themes is in line with the expectation when considering the purifications were performed from rapidly developing 8-day old seedlings, with immunoprecipitation baits that both partially localize to the TGN/EE sorting hub. When studying the list of specific proteins present in both proteomes, prominent interactors with implications in both trafficking and immunity occur.

Table 5.4: ARA7 and ARA5 common co-purifying proteome. Listed here is the common ARA7- and ARA5 co-purifying proteome under water treated conditions. Proteomes were defined as described in legends of Tables 1 and 3 (water-treated YFP-ARA7 and YFP-ARA5 purifications), and associated values were listed in this table. (*Columns 1-8*) Observed in # of replicates, and Spectra in combined replicates: Numbers and associated green cell-shading intensities indicate in how many experimental replicates the protein was detected, or how many spectra for that protein were identified in all three replicates combined, separated for water or flagellin treatment. (*Column 9*) Enrichment factors: For each protein, the number of total spectra across three replicates of the green-labeled (rightmost) pulldown was divided by the number of total spectra in red-labeled (left-most) pulldown. Log10 values that correspond to these ratios are displayed in this table. Green or red bars are graphical representations of magnitude and direction of positive (green) or negative (red) values, centered at 0. (*Columns 10-11*) Locus ID and associated names. Source: TAIR10, accessed through www.genevestigator.org. The table is sorted for absolute differences in protein spectral counts between YFP-ARA5 and YFP-ARA7 in ascending order.

Table 5.4: ARA7 and ARA5 shared proteome

Observed in # of replicates				Spectra in combined replicates				Enrichment factor (log_{10})	Protein information	
YFP-ARA7		YFP-ARA5		YFP-ARA7		YFP-ARA5		ARA7 ARA5		
water	flg22	water	flg22	water	flg22	water	flg22		Locus ID	Protein name
3	3	3	3	22	17	22	11	0.00E+00	AT5G58030	TRS31, TRAPPI-component
3	3	3	3	12	24	13	22	3.48E-02	AT5G06320	NHL3, NDR1/HIN1-like 3, transmembrane protein
3	2	3	3	9	5	7	5	-1.09E-01	AT1G01960	BIG3, EDA10, ARF-GEF
3	3	3	2	12	22	14	11	6.69E-02	AT4G16120	COBL7, SEB1, COBRA-like protein-7 precursor
2	2	3	3	6	11	9	9	1.76E-01	AT5G57350	AHA3, ATAHA3, HA3, H(+)-ATPase 3
3	3	3	3	17	19	13	9	-1.17E-01	AT1G26670	ATVTI12, VTI12, VTI1B, Vesicle transport v-SNARE family protein
2	2	3	3	23	37	27	16	6.96E-02	AT3G05280	Integral membrane Yip1 family protein
3	3	3	3	23	21	17	15	-1.31E-01	AT5G11040	AtTRS120, TRS120, TRS120
3	2	3	3	22	15	16	15	-1.38E-01	AT1G28490	ATSYP61, OSM1, SYP61, syntaxin of plants 61
2	2	3	3	9	12	16	13	2.50E-01	AT3G05710	ATSYP43, SYP43, syntaxin of plants 43
3	3	3	2	13	17	6	3	-3.36E-01	AT1G27930	Protein of unknown function (DUF579)
3	3	3	3	34	26	26	16	-1.17E-01	AT5G05170	ATCESA3, ATH-B, CESA3, CEV1, IXR1, Cellulose synthase family protein
2	2	3	3	41	23	49	35	7.74E-02	AT1G77140	ATVPS45, VPS45, vacuolar protein sorting 45
3	3	3	3	41	51	32	17	-1.08E-01	AT4G12650	Endomembrane protein 70 protein family
3	3	3	2	19	18	29	9	1.84E-01	AT5G17230	PSY, PHYTOENE SYNTHASE
3	3	3	3	35	37	46	39	1.19E-01	AT1G61250	SC3, SCAMP3, secretory carrier 3
3	3	3	3	55	41	66	46	7.92E-02	AT4G39820	Tetratricopeptide repeat (TPR)-like superfamily protein
3	3	3	3	40	63	51	77	1.06E-01	AT3G11820	AT-SYR1, ATSYP121, ATSYR1, PEN1, SYP121, SYR1, syntaxin of plants 121
3	2	3	3	15	14	28	17	2.71E-01	AT4G32410	AtCESA1, CESA1, RSW1, cellulose synthase 1
2	2	3	3	24	26	37	23	1.88E-01	AT1G59820	ALA3, aminophospholipid ATPase 3
2	2	3	3	10	5	25	17	3.98E-01	AT1G25570	Di-glucose binding protein with Leucine-rich repeat domain
2	2	3	3	10	8	26	11	4.15E-01	AT5G64740	CESA6, E112, IXR2, PRC1, cellulose synthase 6
2	2	3	3	9	9	26	13	4.61E-01	AT5G59840	Ras-related small GTP-binding family protein
3	3	3	3	17	25	35	28	3.14E-01	AT2G28520	VHA-A1, vacuolar proton ATPase A1
3	2	3	3	24	6	6	5	-6.02E-01	AT2G14740	ATVSR3, BP80-2;2, VSR2;2, VSR3, VSR3, vaculolar sorting receptor 3
2	3	3	3	15	19	35	29	3.68E-01	AT5G54440	AtTRS130, CLUB, CLUB
3	3	3	3	36	36	15	15	-3.80E-01	AT4G36440	unknown protein, G-protein coupled receptor
3	2	3	3	13	18	36	33	4.42E-01	AT3G17900	unknown protein, heat-inducible transcription repressor
3	3	3	3	32	15	55	40	2.35E-01	AT1G30450	ATCCC1, CCC1, HAP5, cation-chloride co-transporter 1
3	3	3	3	30	38	6	6	-6.99E-01	AT5G22360	ATVAMP714, VAMP714, VAMP714, vesicle-associated membrane protein 714
3	3	3	2	57	51	31	14	-2.65E-01	AT5G49720	ATGH9A1, DEC, GH9A1, IRX2, KOR, KOR1, RSW2, TSD1, glycosyl hydrolase 9A1
3	3	3	3	27	51	61	74	3.54E-01	AT2G36850	ATGSL08, ATGSL8, CHOR, GSL08, GSL8, glucan synthase-like 8
3	3	3	2	48	53	12	11	-6.02E-01	AT4G30260	Integral membrane Yip1 family protein
2	2	3	3	12	19	67	49	7.47E-01	AT4G03550	ATGSL05, ATGSL5, GSL05, GSL05, GSL5, PMR4, glucan synthase-like 5
3	3	3	3	75	48	11	9	-8.34E-01	AT4G20110	BP80-3;1, VSR3;1, VSR7, VACUOLAR SORTING RECEPTOR 7
3	3	3	3	73	62	144	114	2.95E-01	AT2G47960	unknown protein, homology to TRAPP
3	3	3	3	70	65	147	104	3.22E-01	AT5G65950	unknown protein, homology to TRAPP
3	3	3	3	112	91	27	23	-6.18E-01	AT3G58460	ATRBL15, RBL15, RHOMBOID-like protein 15
3	3	3	3	122	79	28	11	-6.39E-01	AT3G52850	ATELP, ATELP1, ATVSR1, BP-80, BP80, BP80-1;1, BP80B, GFS1, VSR1, VSR1;1
3	3	3	3	17	28	126	131	8.70E-01	AT3G07160	ATGSL10, CALS9, gsl10, GSL10, glucan synthase-like 10
3	3	3	3	64	65	181	125	4.51E-01	AT5G16280	Tetratricopeptide repeat (TPR)-like superfamily protein
3	3	3	2	147	132	13	5	-1.05E+00	AT1G24560	PLANT-UNIQUE RAB5 EFFECTOR 2, PUF2
3	3	3	3	186	141	47	37	-5.97E-01	AT2G14720	BP80-2;1, MTV4, VSR2;1, VSR4, vacuolar sorting receptor 4
3	3	3	3	27	25	636	664	1.37E+00	AT1G02130	ARA-5, ARA5, ATRAB1B, ATRABD2A, RA-5, RABD2A, RAS 5

5.3.2 - Trafficking regulators identified in the shared ARA7 and ARA5 co-purifying proteome

The protein which occurred in both purifications with the most equal number of detected peptides was Trafficking Protein Particle Complex subunit 31 (TRS31). TRS31 belongs to the Trafficking Protein Particle complex I (TRAPP-I), which is a multimeric complex of tethering factors that in yeast mediates vesicle fusion events in the ER-Golgi step of the secretory pathway, and is thought to fulfil the same role in Arabidopsis (Vukašinović and Žárský, 2016; Cai et al., 2007). TRS120 and TRS13/CLUB, both TRAPP-II components, were also found in both proteomes. TRAPP-II functions in concert with the Exocyst tethering complex in secretion (Vukašinović and Žárský, 2016). TRAPP-II was shown to be functionally linked to RABA-class secretory Rab GTPases, where it is thought to act as the Guanine Exchange Factor, or activator, of these Rabs (Qi and Zheng, 2011). Notably, TRAPP-II did not show interaction or functional relationships with RABD-class RAB GTPases, to which ARA5/RABD2a belongs, with regard to the role for TRAPP-II in polar secretion of cell-surface localized PIN2 (Qi and Zheng, 2011; Pinheiro et al., 2009).

Previous proteomic studies that looked at TGN/EE marked by SYP61 and VHA-a1, which occur in my ARA7-ARA5 shared proteome, have identified both TRAPPI and TRAPPII subunits (Drakakaki et al., 2012; Groen et al., 2014). In yeast, TRAPPI works with coatomer COPII as a tethering factor in ER-to-Golgi delivery (Cai et al., 2007). While separate coatomer (COPI, COPII) subunits were identified in both ARA7 and ARA5, none of them were identified in my ARA7/ARA5 shared proteome.

Brefeldin-A-Inhibited Guanine nucleotide-exchange protein 3 (BIG3) is an Adenosine diphosphate Ribosylation Factor-Guanine Exchange Factor (ARF-GEF), or an activator of ARF proteins which recruit coat proteins to budding vesicles (Donaldson and Jackson, 2000). The family of BIG proteins in Arabidopsis consist of five members, which localize to the TGN/EE (Tanaka et al., 2009; Richter et al., 2014). Unlike the name suggests, BIG3 is Brefeldin-A (BFA)-insensitive and does not accumulate in the Golgi-TGN/EE clusters formed upon BFA treatment (Tanaka et al., 2009). BIG1-4, including BIG3, mediate default secretion, and not PM-TGN/EE-recycling, as tested using the recycling marker PIN1 (Richter et al., 2014). While BIG3 does not have a described role in immunity, the TGN/EE-localized BIG5/HopM1-interactor 7(MIN7) is required for full PTI and ETI to the bacterial pathogen *Pto* DC3000, and is targeted by the *Pto* DC3000 type-3 secreted effector HopM1 for proteolytic degradation (Nomura et al., 2011; Lozano-Durán et al., 2014).

Finding Aminophospholipid ATPase 3 (ALA3) in both ARA5 and ARA7 is interesting, as it is an established, Golgi-localized lipid flippase (Poulsen et al., 2008). ALA3 has been genetically shown to function in trichome development (Zhang and Oppenheimer, 2009), and in functional and localizatino studies shown to operate at the TGN/EE in mediating the TGN/EE-exit of the cell-

surface defense module PEN3, which then focally accumulates at pathogen attack sites (Underwood et al., 2017). While ALA3 has not been conclusively shown to localize to the TGN/EE before, identifying ALA3 in both Golgi-TGN/EE-localizing ARA5 and TGN/EE-LE/MVB-localizing ARA7 in my purifications supports a population of ALA3 existing at the TGN/EE. PEN3 normally recycles between the TGN/EE and PM under unelicited conditions, potentially implicating ARA5-marked TGN/EE in the endocytic recycling of PM cargoes. While ALA3 has an important role in facilitating the flg22-induced dynamic trafficking of PEN3 (Underwood et al., 2017), its peptide numbers associated with ARA7 and ARA5 pulldowns in my studies did not dramatically change upon flg22-treatment (**table 5.4**).

5.3.3 - Cell wall metabolism and biotic stress related proteins in the shared ARA7 and ARA5 co-purifyng proteome

COBRA-like protein 7 (CBL7) belongs to the larger group of cell-surface localized COBRA proteins, which are involved in cellulose biosynthesis, and which bind to cellulose (Sorek et al., 2014). CBL7 contains a cellulose-binding domain (Roudier, 2002), and COBRA proteins are thought to function as “polysaccharide chaperones”, facilitating the synthesis of cellulose (Sorek et al., 2014). The founding member of the family, COBRA itself, is GPI-anchored and necessary for cell expansion (Schindelman et al., 2001). In tomato (*Solanum lycopersicum*), knockdown of *SlCOBRA-like* leads to cell wall integrity problems and degradation in the tomato fruit, and overexpression resulted in thicker cell walls (Cao et al., 2012).

CELLULOSE SYNTHASE 1 (CESA1), CESA3 and CESA6, all present in both resting ARA7 and ARA5 co-purifying proteomes, comprise the full primary cell wall synthesis complex that is highly active at the seedling stage (Endler and Persson, 2011). Cellulose synthase complexes are delivered through canonical secretion to the PM, where they then deposit extracellular cellulose fibrils, guided by the orientation of cortical microtubules, and are removed from the PM through clathrin-mediated endocytosis (Paredez et al., 2006; Bringmann et al., 2012; Bashline et al., 2013). CESA secretion is Golgi-dependent, and regulated by the dynamics of individual Golgi stacks tracking microtubules (Crowell et al., 2009) – of which Tubulin 7 was found in my ARA5 purifications (**table 5.1**). In fact, CESA3 colocalized in fluorescent studies with Golgi and TGN/EE markers (Crowell et al., 2009), corresponding to my proteomic findings. CESA1,3 and 6 were also shown to be cargoes of the early clathrin-mediated endocytosis multimeric adaptor TPLATE complex (Sánchez-Rodríguez et al., 2018), although no clathrin or TPLATE complex components were identified in any of my purifications.

The protein that was second-to-most equally abundant in both ARA7 and ARA5 purifications is NON RACE-SPECIFIC DISEASE RESISTANCE 1(NDR1)/HAIRPIN INDUCED GENE 1(HIN1)-LIKE PROTEIN 3 (NHL3). NHL3 is predominantly PM-localized, and overexpression conferred

immunity to *Pto* DC3000 (Varet et al., 2003). The abundance of its mRNA was shown to increase upon bacterial infection, but only when ETI was activated by effector detection (Varet et al., 2003). In my proteomic studies, NHL3 is moderately positively responsive in detected peptides associating with both ARA7 and ARA5, but does not increase with a fold-ratio of greater than 2 to be considered flagellin responsive. While the role of NHL3 in immunity is not clarified, the PM-localized homolog NDR1 shows similarity to integrins, which in mammals are involved in cell-adhesion, and NDR1 is responsible for carrying out a subset of downstream responses of the NLRs RPS2 and RPS5 (Century et al., 1997). NDR1 has a role in cell membrane-cell wall adhesion, and interacts with RIN4, a PM-localized defense regulator, which is guarded by the NLRs RPS2 and RPM1 (Mackey et al., 2002; Axtell and Staskawicz, 2003). This raises the question of whether NHL3 could fulfil a similar cell-wall adhesive role.

5.3.3 - The shared ARA7 and ARA5 co-purifying proteome changes upon 3-h flg22 stimulus

In order to gain insight into cargoes that were upregulated in both the secretory and endocytic pathway upon immunity, I combined the ARA7 and ARA5 co-purifying proteomes under 3 h flg22-elicitation, and filtered the list to retain only proteins of which the number of peptides were upregulated with a factor of 2 or greater in both purifications (**table 5.5**). Out of 22 responding proteins in ARA5, and 70 in ARA7, 9 were shared between both baits (**figure 3.4E, table 5.5**). In line with ARA7 upon flg22 treatment, also the shared flg22-treated ARA7/ARA5 proteome conspicuously presents cell-wall integrity and oxidative stress themes, and contains receptor kinases.

Table 5.5: Proteins interacting with ARA7 and ARA5 that are more abundant upon flagellin treatment. Listed here are co-purifying proteins that are both upregulated upon flagellin treatment in ARA7- and ARA5 immunopurifications. Proteomes were defined as described in legends of Tables 2 and 4 (flg22-treated YFP-ARA7 and YFP-ARA5 purifications), and associated values were listed in this table. (*Columns 1-8*) Observed in # of replicates, and Spectra in combined replicates: Numbers and associated green cell-shading intensities indicate in how many experimental replicates the protein was detected, or how many spectra for that protein were identified in all three replicates combined, separated for water or flagellin treatment. (*Column 9*) Enrichment factors: For each protein, the number of total spectra across three replicates of the green-labeled (rightmost) pulldown was divided by the number of total spectra in red-labeled (left-most) pulldown. Log10 values that correspond to these ratios are displayed in this table. Green or red bars are graphical representations of magnitude and direction of positive (green) or negative (red) values, centered at 0. (*Columns 10-11*) Locus ID and associated names. Source: TAIR10, accessed through www.genevestigator.org. The table is sorted for absolute differences in protein spectral counts between YFP-ARA5 and YFP-ARA7 in ascending order.

Table 5.5: Proteins interacting with ARA7 and ARA5 that are more abundant upon flagellin treatment

Observed in # of replicates				Spectra in combined replicates				Enrichment factor (log_{10})	Protein information	
YFP-ARA7		YFP-ARA5		YFP-ARA7		YFP-ARA5		ARA7 flg22 ARA5 flg22		
water	flg22	water	flg22	water	flg22	water	flg22		Locus ID	Protein name
1	2	1	3	3	10	1	10	0.00E+00	AT4G08850	LRR-RLK, MIK2
1	2	1	3	1	6	2	6	0.00E+00	AT3G17410	Protein kinase superfamily protein
1	2		2	2	6		6	0.00E+00	AT4G20830	OGOX1, OLIGOGALACTURONIDE OXIDASE 1
1	3	2	3	2	10	3	9	-4.58E-02	AT1G52200	PLAC8 family protein
1	2	2	3	1	10	3	13	1.14E-01	AT1G51800	LRR RLK, IOS1
2	2	3	3	4	18	8	22	8.72E-02	AT5G03700	D-mannose binding lectin protein with Apple-like carbohydrate-binding domain
1	2	2	3	1	9	2	16	2.50E-01	AT1G03220	Eukaryotic aspartyl protease family protein
	3		3		11		22	3.01E-01	AT1G14540	PER4, PEROXIDASE 4
	2	3	3		12	11	24	3.01E-01	AT4G23180	CRK10

Some proteins, especially the receptor kinases MIK2 and IOS1, identified in this flg22-responsive shared proteome are already discussed in the endocytic context of ARA7 in **chapter 4**. Finding cell-surface receptors upregulated in the endocytic pathway upon immune stimulus suggests they are internalized through endocytosis in an increased manner. Coupled to this, it is interesting to find IOS1 which works together with a range of other cell-surface receptors, also upregulated in the secretory pathway, while several RLKs upregulated in secretory ARA5 (**table 5.3**) were not found upregulated in endocytic ARA7 (**table 4.3**). Potentially, IOS1 traffics together with its interacting receptor kinases, a concept which is reminiscent of the ligand-induced co-internalization of the receptor-like protein (RLP) Cf-4 and its interacting RLK (Postma et al., 2016).

OLIGALACTURONIDE OXIDASE 1 (OGOX1) is a flavin adenine dinucleotide (FAD)-binding berberine protein family of oxidoreductases that operates in cell wall metabolism (Daniel et al., 2015). Specifically, OGOX proteins are thought to control the spurious activation of DAMP-signaling activated by oligogalacturonides (OGs), which are pectin fragments that normally originate from plant cell wall damage (Benedetti et al., 2018). Indeed, OGOX1 has a high affinity for OGs, and oxidizes them through local production of H_2O_2 (Benedetti et al., 2018). Interestingly, the FAD-binding berberine proteins to which OGOX1 belongs are largely apoplastic, but OGOX1 contains a predicted GPI-anchoring site and can be released from membranes using phospholipase treatment (Elortza et al., 2006). OGOX1 contributes to the resistance to the necrotrophic pathogen *Botrytis cinerea* (Benedetti et al., 2018). The increase in spectral counts for OGOX1 in flg22-treated ARA7 and ARA5 purifications suggests this protein undergoes increased turnover at the cell surface, perhaps in preparation for the buffering of DAMP signaling normally triggered by pathogen-induced cell wall damage.

AT1G52200, a Placenta-specific-gene 8 (PLAC8) family protein, is a cysteine-rich, predicted transmembrane domain-containing protein with a yet uncharacterized function (Song et al., 2011). Homologous PLAC8 proteins in Arabidopsis have been better studied, with PLANT CADMIUM RESISTANCE 1 (PCR1) and PCR2 conferring tolerance to heavy metals such as zinc and cadmium, likely through multimeric complexes that produce a heavy metal transporting effect (Song et al., 2010, 2011). While not much is known about the role of heavy metals in plant immunity, they can be toxic themselves, or rate-limiting enzymatic co-factors. In the interaction between bacterial pathogens and their hosts, it has been shown that iron scavenging is an important strategy: Arabidopsis IRT-mediated iron uptake was involved in immune-signaling triggered by the presence of the bacterial siderophore deferroxiamine (Aznar et al., 2014). Bacteria require siderophores to compete with the host for iron, which is necessary for virulence, and bacterial overexpression of infection-upregulated *Pto* DC3000 iron metabolism-related genes

conferred enhanced virulence (Aznar et al., 2014; Nobori et al., 2018). Potentially, the cysteine-rich PLAC8 protein fulfils a metal-competing role in the apoplast.

Finally, the predicted protein kinase AT3G17410, upregulated in both ARA5 and ARA7 upon flg22, has been identified in Y2H studies as an interactor of the *Pseudomonas* type-3 effector AvrB (Weßling et al., 2014; Mukhtar et al., 2011). AvrB has been shown to trigger necrosis dependent on the host NLR RPM1, which localizes to the PM, and AT3G17410 has previously been identified in a proteomic analysis of the PM (El Kasmi et al., 2017; Marmagne et al., 2007). While AvrB triggers RPM1-dependent necrosis through modification of the host guardee RIN4 (Mackey et al., 2002), protein kinases have been shown to be required for these modifications (Liu et al., 2011; Xu et al., 2017)**.** AT3G17410 could be an additional player in this complex, increasing in turnover at the PM upon engagement of PTI signaling.

5.4 - ARA7 AND ARA5 LOCALIZE TO DISTINCT VESICLE POPULATIONS IN RESTING AND IMMUNE ACTIVATED CONDITIONS

5.4.1 - ARA7 and ARA5 do not co-localize at resting state

ARA7 and ARA5 function in endocytic and secretory processes respectively, but both partially localize to the TGN/EE (Pinheiro et al., 2009; Scheuring et al., 2011), and in my proteomic analysis of ARA7 and ARA5 purifications, showed partial overlap in their co-purifying proteomes (**table 5.4**). While Rab GTPases generally function and localize in distinct populations of vesicles, they can also overlap, as evidenced by the co-localization of ARA7 and ARA6/RABF2a on LE/MVBs (Ueda et al., 2004). In order to address whether ARA7 and ARA5 might also partially localize to the same compartment, I co-expressed fluorescently tagged versions under control of the Arabidopsis Ubiquitin-10 promoter in a transient manner in *N. benthamiana*. In addition, I crossed published Arabidopsis lines stably expressing fluorescently tagged versions of ARA7 and ARA5 also driven by the Ubiquitin-10 promoter (Geldner et al., 2009; Dettmer et al., 2006), and analyzed leaf epidermal cells of both systems using confocal microscopy **(fig. 5.5**). As a result, at resting state, YFP-ARA5 and mCherry-ARA7 localized to distinct populations of vesicles **(fig. 5.5A,B top panels**), corresponding to their known localization when expressed individually (Geldner et al., 2009; Dettmer et al., 2006). Since a subset of vesicles marked by both fluorescent proteins consists of TGN/EE, I conclude that they mark different subpopulations, or alternatively, different subdomains of TGN/EE.

5.4.2 - ARA7 and ARA5 do not co-localize upon 3 h flg22-treated conditions

Having established earlier that both ARA7 and ARA5 did not change in total vesicle numbers upon immune stimulus within 3 h flg22 treatment, in both purifications co-purifying proteins responsive to flg22 did show overlap (**table 5.5**). Therefore, I was interested in testing whether

this could be partially explained by a change in ARA7/ARA5 co-localization. In order to test this, I treated both *N. benthamiana* and Arabidopsis co-expressing fluorescently marked ARA7 and ARA5 with flg22, and observed leaf epidermal cells at 3 hpi to match timings used in vesicle quantification as well as proteomic analysis. In both systems, the co-localization pattern of ARA7 and ARA5 did not markedly change, as both still localized to distinct vesicle populations **(fig. 5.5A,B bottom panels**). While TGN/EE that is not marked by either ARA7 or ARA5 may exist, the above data taken together provide evidence that proteins co-purifying with both Rab GTPases are present at physically separate endocytic and secretory trafficking pathways at the same time.

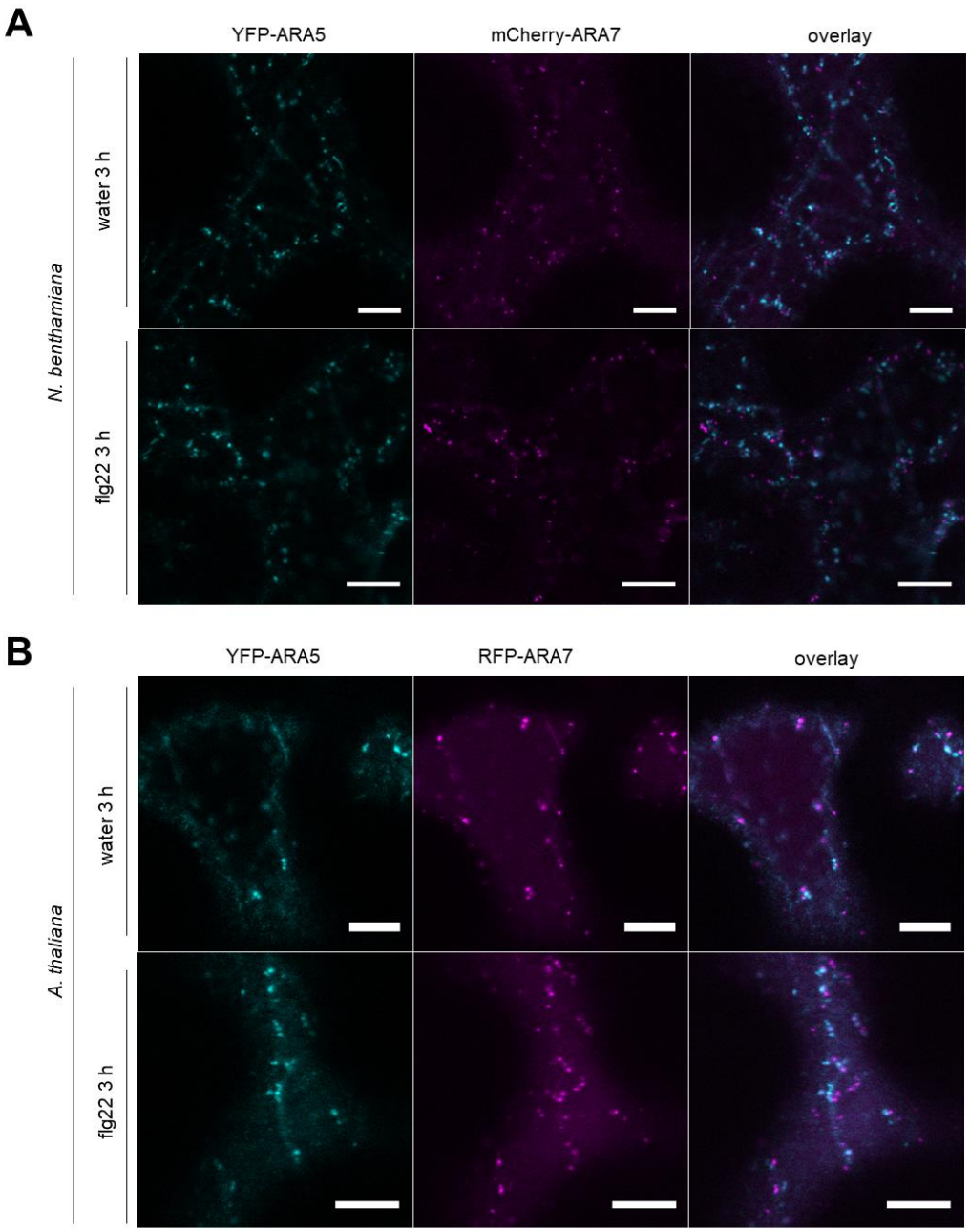

Figure 5.5. YFP-ARA5 and YFP-ARA7 are present at distinct compartments in *Nicotiana benthamiana* and Arabidopsis. (A) Confocal micrographs of *Nicotiana benthamiana* adult leaves transiently co-expressing YFP-ARA5 and mCherry-ARA7 through *Agrobacterium tumefaciens* mediated transformation at 2 dpi and at 3 hours after syringe-infiltration of water or flg22 (10 µM). (B) Confocal micrographs of leaf epidermal cells of 4 wk-old F1 Arabidopsis plants co-expressing *pUB::YFP-ARA5 and pUB::mCherry-ARA7*, 3 hours after syringe-infiltration of water or flg22 (10 µM). (A,B) 63 × objective and scale bars = 10 µm.

DISCUSSION

5.5 - ARA5 vesicles concentrate at the cell surface

ARA5 vesicles were observed to concentrate under bacterial contact sites after ca. 6 h of infiltration with *Pto* DC3000 (**figs. 5.1-2**), although upon quantification, no significant differences in number of ARA5 concentrations were observed between water treatment and *Pto* DC3000 infiltrations, which both triggered the response. It could be that *Pto* DC3000 partially suppresses the response, so it would be interesting to test flg22-only treatments too. In **chapter 4**, I could show that water also triggers ARA7 clustering to some extent, but for both ARA7 and ARA5, clusters were observed at bacterial infection sites. Concentration of ARA5-marked secretory pathway compartments that could be Golgi and/or TGN/EE, is in line with existing data that describe the secretory Rab GTPase RABE1d to focally accumulate upon bacterial challenge. Furthermore, expression of a constitutive active version fo RABE1d increased resistance against *Pto* DC3000 (Speth et al., 2009). While it has not been shown that RabE1d clusters are positioned under bacterial infection sites, secretory Rab GTPases can be themselves involved in defining spatially distinct locations at the cell surface, as evidenced by RABA5c, which located at the geometric cell edges and functioned in cell wall homeostasis there (Kirchhelle et al., 2016). The factors defining the precise locations of clustering of secretory Rab GTPases are unknown, but it is conceivable that in both pathogen and developmental context, the spatial cues could be conferred by physical stimuli.

The number of ARA5 vesicles did not change up to 3 hours after flg22 treatment in my high throughput confocal experiments. ARA5 vesicle clustering also was not observed before ca. 6 hpi upon bacterial infection. These findings together indicate that at up to 3 h of immune stimulus, while proteomic cargoes do change, the ARA5 vesicles do not respond by changing their dynamics. Genes functioning in the secretory pathway were upregulated upon application of SA to support PR1-secretion (Wang et al., 2005), and flg22-treatment has been shown to induce SA accumulation already at early time points (Tateda et al., 2015). However, the described gene upregulation response was measured at 1 dpi, instead of earlier time points at which I observed ARA5. This corresponds to the absence of the SA-induced secretory cargo PR1 in my ARA5 purifications, which might be identified upon purification at 1 dpi (Wang et al., 2005). Based on my data, I cannot exclude that at earlier time points, ARA5 compartment motility and/or turnover rates are altered, which may underlie an early increased secretory activity.

5.6 - The ARA5-specific proteome contains defence-related proteins and changes upon flg22 stimulus

In order to reveal proteomic changes along the default secretory pathway upon immune stimulus, I purified YFP-ARA5 from flg22-treated cells at 3 hrs, and performed mass spectrometry analysis. In addition, to gain insight in commonalities and differences between the endocytic and secretory pathways under these conditions, I compared the ARA5 resting and immune stimulated co-purifying proteomes to those of ARA7.

Proteins that exclusively fell within the ARA5 co-purifying proteome corresponded to its known localization and function, such as the secretory TGN/EE-localized Rab GTPase RABA1d (Asaoka et al., 2013), Tubulin, which guides Golgi dynamic localization (Crowell et al., 2009) and Coatomer, which functions in intra-Golgi trafficking. While a small pool of YFP-ARA5 may localize to the Golgi during its constitutive biosynthesis as driven by the Ubiquitin-10 promoter, the majority of ARA5 is likely to localize to its site of functioning on *trans*-Golgi and TGN/EE (Pinheiro et al., 2009; Geldner et al., 2009).

A highly abundant protein identified in ARA5, at similar abundance under water and flg22-treated conditions, is PEN3, which is known to predominantly localize to the PM (Underwood and Somerville, 2013). Its non-responsiveness to flg22 treatment is consistent with published data that *de novo* synthesis does not contribute to PEN3 focal accumulations at the cell surface (Underwood and Somerville, 2013), which together with my data suggests that ARA5 compartments and ARA5 TGN/EE does not contribute to this response. Conversely, in ARA7 purifications, PEN3 passed my criteria for co-purifying only upon flg22 treatment, in line with LE/MVBs underlying the focal accumulation response.

At steady state, PEN3 was found to traffic in a polar way. In roots, PEN3 localized to the outer lateral membrane, and was found to traffic through VHA-a1/SYP61/VTI12-positive typical TGN/EE compartments to do this (Mao et al., 2016) – all TGN/EE markers which were found in both my ARA5 and ARA7 purifications. Both secretory and endocytic traffic contributed to PEN3 localization at the TGN/EE (Mao et al., 2016), but in water treated conditions, I identified PEN3 only in ARA5, implicating ARA5-positive TGN/EE, rather than ARA7, in the steady state polar trafficking of PEN3. Its absence in ARA7 under my criteria suggests that its route to the cell surface at resting state does not depend on redirected LE/MVBs as it does under pathogen stimulated conditions.

Specifically upon flg22 treatment, and only in ARA5 purifications, MLO12 was identified (**table 5.3, fig. 5.4**). Little is known about the function of MLO12 in immunity, but together with MLO2 and MLO6 it belongs to the clade which is co-orthologous with barley Mlo, in which broad spectrum *mlo*-based resistance was originally identified (Panstruga, 2005). Out of this clade,

mlo2-based resistance is best studied. MLO2 localized to the PM, and polarly accumulates under pathogen attack sites (Panstruga, 2005; Consonni et al., 2006; Kusch and Panstruga, 2017; Bhat et al., 2005)**.** While MLO12 subcellular localization has not been studied, the MLO homolog NORTIA was found to localize to the Golgi in ovules, functioning in pollen tube reception – a process that does not occur in the seedlings from which I purified ARA5.

Mlo2 mutants require components of indolic acid metabolism (PEN2, PEN3), and membrane trafficking (PEN1/SYP121) for full resistance against powdery mildew (Kuhn et al., 2017). *Mlo2, mlo6 and mlo12* cooperatively contribute to mildew resistance, with *mlo2* resistance evident in single mutants, but *mlo6* and *mlo12* effects only visible as additive effects when in double mutants with *mlo2* or in the *mlo2/6/12* triple mutant (Consonni et al., 2006). Interestingly, *mlo2/6/12* triple mutants did not have the same requirements for indole glucosinolate metabolism or subcellular trafficking as compared to *mlo2* single mutants (Kuhn et al., 2017). This could mean that the function of MLO12 does not involve these components.In line with this, I do not find flg22-induced upregulation of PEN2, PEN3 or PEN1/SYP121 in ARA5 purifications, but IGMT2, a major player in the indole glucosinolate defense pathway is strongly upregulated.

While the above data describe the role of MLOs in immunity against fungal pathogens, MLOs may have different roles in modulating antibacterial immunity. Evidence for MLOs contributing to susceptibility comes from effector studies, as *Pseudomonas* HopZ2 targets MLO2 and requires it for full virulence (Lewis et al., 2012). In addition, loss-of-function mutations in pepper *CaMLO2* enhanced resistance to bacterial pathogens, and *CaMLO2* expression in Arabidopsis conferred enhanced susceptibility to *Pto* DC3000 (Kim and Hwang, 2012). On the other hand, *mlo2/6/12* triple mutants, which were more resistant to powdery mildew, were more susceptible to the non-adapted bacterial pathogen *P. syringae* pv. *maculicola* (Kusch and Panstruga, 2017), and *mlo2* and *mlo2/6/12* were not differentially affected in their resistance to *P. syringae* pv. *maculicola,* while the triple mutant was more susceptible to powdery mildew (Gruner et al., 2018). Taken together, MLOs can have ambiguous effects on antibacterial immunity, and it is yet unclear if MLO12 plays a role therein.This provides evidence that flg22-induced changes in the ARA5 co-puryfing proteome may be nonspecific to the type of MAMP used, but represent a more general status change independent of trigger. This could be consistent with the finding that mutants in flg22-upregulated ARA7-interacting proteins are susceptible to powdery mildew, and not bacterial pathogens.

MLOs have been implicated in modulating ROS signaling (Cui et al., 2018). I identified CRK10, PER4, and OGOX1 in ARA5 purifications upregulated upon flg22 treatment, all of which are implicated in processes involving ROS. CRK10 has a potential role in extracellular ROS perception (Bourdais et al., 2015), and MLO2 was recently found to be a negative regulator of extracellular ROS sensing, with all MLO proteins hypothesized to exert a similar role (Cui et al.,

2018). Their co-occurrence in my flg22-treated ARA5 purifications could point at a functional relationship, although the regulatory MLO2 role in ROS perception was shown to be partially uncoupled from its elevated resistance against mildew (Cui et al., 2018).

Barley MLO contains a calmodulin-binding domain, and its interaction with calmodulin is necessary for its function in downregulating immunity (Kim et al., 2002). MLO12 also contains a predicted calmodulin-binding domain (UniProt, accessed July 2018). Interestingly, PEN3, present in the ARA5-associated proteome at high abundance both under water and flg22 treated conditions, has been shown to interact with calmodulin, which, like PEN3 itself, is required for non-host resistance (Campe et al., 2016). PEN3 focally accumulates in response to bacteria and flg22, and is also required for full *mlo*-based resistance (Consonni et al., 2006; Underwood and Somerville, 2013; Xin et al., 2013). I find that both ARA7 and ARA5 cluster at the cell surface, which could mean that they both target the same location and delivering cargoes that otherwise would not co-accumulate. With MLOs functioning as susceptibility factors, and my data showing that PEN3 and MLO12 may be co-delivered at the cell surface, it is conceivable that MLO12 may downregulate calmodulin-involving processes on co-accumulating cell-surface defense components such as PEN3.

Taken together, while a function for MLO12 in antibacterial resistance has not been described, my proteomic results show that MLO12 co-purified with secretory ARA5 upon treatment with with a bacterial MAMP, and provide potential leads to further investigation of the modulation of immunity by MLOs in general.

5.7 - The shared ARA7 and ARA5 proteome contains TGN/EE proteins

Upon comparison of the resting state co-purifying proteomes of ARA7 and ARA5, their contents suggest that I purified TGN/EE-associated pools of both. Common TGN/EE markers such as SYP61, SYP43 and VHA-a1 are found (**table 5.4**), in addition to cargoes previously identified in TGN/EE-proteomic studies, such as SCAMP3, CESA1 and CCC1 (Groen et al., 2014; Drakakaki et al., 2012). In ARA7 purifications, ARA5 was identified, although at low abundance, which could explain why a majority of ARA5 interacting proteins were also captured by ARA7 purifications (**fig. 5.4D**). While upon microscopic analysis I did not find punctate overlap of ARA7 and ARA5 in Arabidopsis or *N. benthamiana* (**fig. 5.5**), upon co-expression in BiFC (split-YFP) experiments in *N. benthamiana*, ARA7 and ARA5 together reconstituted a punctate signal (**fig. 4.9**), indicating that they exist in close proximity, likely on separate domains of TGN/EE.

In ARA7 purifications I also identified ARA6, which reconstituted a BiFC signal with ARA7, and which has been described to largely localize to a subpopulation of ARA7 endosomes (Ueda et al., 2001). Because of their large overlap in published microscopic studies, I expected a high abundance of ARA6 in ARA7 purifications. However, it was recently shown that these two Rab5

GTPases compete for activation by VPS9a through their common effector PUF2 (Ito et al., 2018), and since Rab GTPase activation status governs their capacity for membrane association, this could indicate that they do not preferably exist in the same protein complex in a stable manner, thus leading to low levels of co-purification of ARA6 with ARA7.Additionally, seeing as the purification method used likely yields greater Rab complexes and not intact membrane compartments, it could be that despite their localization to the same membrane vesicles, ARA7 and ARA6 do not interact with each other.

Based on co-localization analyses from various publications, broadly two populations of TGN/EE can be distinguished, either marked by RabA1b, RabA2a and VAMP721 with known secretory functionality, or marked by SYP61, SYP43 and VHA-a1, with roles in both secretion and also endocytosis (Gendre et al., 2015). In the shared ARA5 and ARA7 co-purfying proteome, I did not capture RabA1b, RabA2a and VAMP721, but consistently identified SYP61, SYP43 and VHA-a1, independent of flg22 treatment (**table 5.4**). Since ARA5 and ARA7 did not overlap on punctae in confocal microscopy (**fig. 5.5**), I conclude that they can further divide this population of TGN/EE into subpopulations with secretory and endocytic functions respectively.

The shared ARA5 and ARA7 co-purifying proteome was rich in cell wall metabolism proteins, with cargoes such as CESA1, 3 and 6, comprising the full primary cell wall cellulose synthesis complex, glucan synthases including PMR4, CBL7 which facilitates cellulose biosynthesis, and NHL3, which is implicated in PM-cell wall adhesion. The callose synthase PMR4 has a positive role in defense against some pathogens, such as *Bgh* (Ellinger et al., 2013), but *pmr4* mutants show constitutively elevated SA levels, defense gene expression coupled with increased resistance to pathogens such as *G. cichoracearum*, providing challenges to studies that probe the role of PMR4-dependent callose deposition in immunity (Nishimura et al., 2003; Jacobs et al., 2003). PMR4 itself localizes predominantly to the PM, with increased vesicle localization and focal accumulation under the site of attempted penetration by powdery mildew at ca. 6 h after spore application (Ellinger et al., 2013).

While the PMR4 focal accumulation response has not been tested under flg22 treatment, this stimulus triggers cell-surface localized callose depositions fully dependent on PMR4 (Luna et al., 2011). Contrary to PEN3 found in ARA7 purifications upon flg22 treatment, PMR4 did not markedly change in abundance in my ARA7 or ARA5 purifications. Therefore, the defence-associated focal accumulation of PMR4 is unlikely to be underpinned by redirected endosomal traffic. A role for the secretory pathway is more likely, as PMR4 co-purified with ARA5 at higher abundance than with ARA7 (**table 5.4**). Here, PMR4 could be delivered from the secretory pathway, and undergo turnover and degradation through endocytosis. In line with PMR4 dependency on default secretory processes, overexpression of the secretory RabA4c has been

shown to enhance callose deposition and resistance to adapted *G. cichoracearum*, both dependent on PMR4 (Ellinger et al., 2014b).

5.8 - Upon flg22 treatment, the shared ARA7 and ARA5 proteome enriches with proteins functioning at the cell surface

Upon 3 h flg22 treatment, a small group of 9 proteins was upregulated in abundance in both ARA5 and ARA7 purifications. Due to the common TGN/EE localization of ARA5 and ARA7, proteins identified in both purifications are also likely to localize to this compartment, but do not necessarily function there. Shared interactors can function at other locations, as especially evidenced by the identification of resting state cargoes which have PM localizations and functions such as NHL3, CBL7, PEN1 and CESAs. Knowing that ARA5 and ARA7 maintain separate localization upon flg22 treatment, and that the majority of flg22-upregulated shared proteins have a cell surface localization (**table 5.5**), I interpret their upregulation in both purifications as a sign of an increased turnover at the cell surface, and discuss them in that context.

Three cell-surface receptor-like kinases (MIK2, CRK10, IOS1) were identified. While IOS1 has been shown to be a common interactor of many immune receptors (Yeh et al., 2016), MIK2 is a cell wall integrity sensor (Van der Does et al., 2017) and CRKs have been functionally implicated in ROS-perception upon host-microbe interactions, either directly or through spatial organization of ROS-perception modules (Bourdais et al., 2015; Kimura et al., 2017). The increased turnover of these receptors 3 h after flg22 treatment could point at ligand-induced endocytosis to achieve receptor degradation, as is observed for FLS2 (Beck et al., 2012b), coupled to upregulated secretion to replenish the PM-localized signaling capable pool. While these receptors have not been previously shown to undergo this process, cell surface receptors are capable of undergoing ligand-induced endocytosis upon perception of endogenous signals, such as BRI1 upon brassinolide steroid hormones in growth, (Martins et al., 2015), ERECTA-LIKE 2 upon epf peptides in stomatal development (Ho et al., 2016) and PEPR1 upon pep1 peptides as DAMP signals (Ortiz-Morea et al., 2016). ROS themselves can function as extracellular second messengers, and can induce antibacterial resistance (Sharma et al., 1996; Sewelam et al., 2016). For the cysteine-rich GPI-anchored enzyme OGOX1, which neutralizes oligogalacturonide DAMPs in the apoplast, increased turnover could be necessary to maintain an enzymatically active pool of receptors. For all the above membrane-associated candidates, it would be interesting to use fluorescence microscopy to study the subcellular dynamics at the 3 h flg22 treated time point, upon chemical disturbance of the cell wall, or external application of ROS, to confirm their ligand-induced endocytosis.

The above data taken together, I hypothesize that upon perception of flg22 stimulus, the plant is anticipating defense-related ROS-signaling processes and cell wall modifications. Why anticipate

cell wall damage in the interaction with bacterial pathogens? *Pto* DC3000 inserts type-3-secretion needles, but is not known to grossly modify the cell wall. However, infection with some bacteria, such as the opportunistic pathogen *Pseudomonas aeruginosa*, causes cavities in the cell wall at bacterial positions as seen in electron microscopy studies (Plotnikova et al., 2000). Coincidentally, while all flagellin perception in Col-0 is initiated by the singular flagellin receptor FLS2, the elicitor peptide flg22 corresponds to the immunogenic epitope on flagellin of *P. aeruginosa* (Felix et al., 1999). I hypothesize that the upregulation of cell wall integrity and ROS-sensing capacity upon flg22 elicitation is a generalized response, that prepares for a range of potential modifications by incoming pathogens, or function in sensing endogenous, potentially ROS-mediated cell wall modifications and ensure integrity is maintained even upon “false alarms” in the absence of continued infection.

Some LRR-RLKs upregulated in ARA5 upon flg22 were not identified in ARA7. While their ligands are yet unknown, this could provide evidence for increasing detection capacity at the cell surface in response to pathogen stimulus. It has been described that treatment with SA potentiates cells for the detection of flagellin and chitin, which is mediated through cell-surface receptors FLS2 and CERK1 (Tateda et al., 2015). There, increased potentiation is thought to be achieved through increased secretion of cell-surface receptors mediated through interaction with the ER-localized protein ACCELERATED CELL DEATH 6 (ACD6, (Zhang et al., 2014b). SA treatment increased the PM-resident pool of FLS2 in an ACD6-dependent manner, but when measured at 24 and 48 hpi, which does not match the timing of my flagellin treatments (Zhang et al., 2014b). However, treatment with flg22 has been shown to induce endogenous SA-signaling, detectable as early as 3 hours (Tsuda et al., 2008).

Determining the cognate ligands for the uncharacterized secreted, but not internalized receptors would be interesting, as they could be on the lookout for various anticipated MAMPs or DAMPs that associate with infection in a non-pathogen specific manner, making these receptors interesting in the context of engineering broad-spectrum resistance. Finally, to gain further insight in the specificity of upregulated proteins in my ARA5 and ARA7 purifications to various types of pathogens, it would be interesting to perform the same purifications upon treatment with a panel of additional MAMPs, such as chitin, lipopolysaccharides or elicitins.

5.9 - Expanding on the method

While the majority of co-purfying proteins in ARA5 and ARA7 purifications were not considered to be upregulated in response flg22 treatment (**figs. 4.6, 5.4**), they could still fulfil important functions in immunity. To address this, it would be relevant to perform my purifications under inhibition of dephosphorylation, and subject samples to phosphoproteomic analysis using mass spectrometry. This could reveal activity status changes on proteins such as receptor kinases

along the trafficking pathways, thus providing an extra layer of information that is not revealed by looking at abundance changes only.

Finally, my current data reveal proteomic changes between 3 h water and flg22 treatment, but it is possible that various suites of secretory and endocytic cargoes change in abundance at different time points after immune stimulus, perhaps relating in function to earlier occurring responses such as MAMP-induced endocytosis, apoplastic alkalinization and ROS burst, or later responses such as callose deposition, stomatal closure and systemic acquired resistance (Khaled et al., 2015). In combination with more precise methods of peptide quantitation, correlating protein abundance changes in secretory and endocytic pathways at different time points after immune stimulus may reveal novel functional relationships between groups of proteins that have not been implicated to work together before (Thul et al., 2017).

CHAPTER 6

GENERAL DISCUSSION

In the first stage of my PhD project, I set myself the following goals:

- Reveal the subcellular localization of Cf-4
- Reveal the subcellular localization of constitutively interacting Cf-4-SOBIR1 complexes
- Probe for ligand-induced subcellular localization dynamics of Cf-4 upon activation by Avr4
- Investigate the requirements for SERK members in Cf-dependent receptor outputs and immunity

Using microscopic analysis, I could successfully show that the tomato RLP-type PRR Cf-4 is localized to the plasma membrane, which confirms its long standing expected localization, in line with its function in detecting apoplastic Avr4 secreted by *C. fulvum* upon infection (Joosten et al., 1994; van den Burg et al., 2006). I could also show that it interacts there with its constitutive interaction partner SOBIR1, an RLK that is required for Cf-4 function (Liebrand et al., 2013). Upon activation, Cf-4 and SOBIR1 co-internalize, in a SOBIR1-kinase-activity dependent manner. This supports the notion of Cf-4-SOBIR1 functioning as a two-component PRR (Liebrand et al., 2014; Gust and Felix, 2014), as this response is shared by the well-characterized one-component RLK-type PRRs FLS2 (Robatzek et al., 2006; Khaled et al., 2015). These observations expand our view and reveal that the mechanism that underlies PRR turnover at the PM is generalisable to diverse classes of receptors.

I confirmed that Cf-4-SOBIR1 recruits the same early activation module BAK1/SERK3 and depend on it for outputs, which shows that RLP-SOBIR1-type PRR and RLK-type PRR activation converge at early steps. In the time since this discovery, several other RLP-SOBIR1 systems have been shown to engage with SERK members upon activation, further supporting the notion that this is a broadly generalisable PRR activation mechanism (Albert et al., 2015; Domazakis et al., 2018; Du et al., 2015; Wang et al., 2018).

My finding that Cf-4-SOBIR1 activation upon detection of the race-specific Avr4 effector shares components with detectors of broadly conserved MAMPs. This, combined with mounting evidence that Cf-4 detects conserved patterns on Avr4 orthologues from distantly related fungi independent of their ability to exert their main chitin binding effector function (Kohler et al., 2016; Mesarich et al., 2016), supports the increasingly blurring classic distinction between effector-triggered immunity and MAMP-triggered immunity (Thomma et al., 2011; Cook et al., 2015).

My data in combination with related recent discoveries on RLP activation broaden our understanding of cell-surface PRR dependent immune activation, but leaves the question: which SERKs specify which outputs? I could show that multiple SERKs were recruited to Cf-SOBIR1 complexes, and it has previously

been shown that one SERK can engage with RLKs that function in both defense and development (Chinchilla et al., 2009). Does the same apply to RLPs?

SOBIR1 affects developmental pathways too. Specifically, it downregulates the outputs of the RLK-type HAESA (HAE) and HAESA-LIKE 2 (HSL2), which form a cell-surface based developmental peptide receptor platform (Leslie et al., 2010a; Gubert and Liljegren, 2014). It is thought that SOBIR1 engages with HAE/HSL2 to target them for degradation, which in the light of my findings, could be through the endocytic vacuolar-targeted pathway. Indeed, subcellular trafficking components seem to be required for SOBIR1 effects on HAE/HSL2 (Liljegren et al., 2009).

Some RLPs in development seem to avoid SOBIR1 altogether, but engage with other scaffolding RLKs, such as the RLP CLAVATA 2 which depends on the RLK CORYNE for accumulation at the PM and signaling (Somssich et al., 2016). Interestingly, they too engage with poised PM-localized RLKs, as evidenced by their interaction with the RLK CLAVATA 1 (Muller et al., 2008; Bleckmann et al., 2010). No evidence for the involvement of SERK members in this system is reported, pointing at potential limits for the generalisability of the role of SOBIR1 and SERK in RLP-mediated signaling.

In the second stage of my PhD, I wanted to further clarify the role of Rab GTPases in immunity, and set myself the following goals:

- Investigate localization changes of ARA7 and ARA5 upon bacterial infection
- Reveal changes in ARA7 and ARA5-associated proteins after flg22-stimulus
- Identify flg22-responsive ARA7-interacting proteins which are defence-related
- Further characterize a subset of flg22-responsive ARA7 interacting defence-related proteins for roles in immunity

I revealed that especially the endocytic Rab GTPase ARA7 has the tendency to intensely concentrate under bacterial contact sites upon infection, which is shared by the secretory Rab GTPase ARA5 to a lower extent. This matches known endosomal responses in well-established fungal and oomyecete pathosystems (Inada et al., 2016; Nielsen et al., 2012; Cai et al., 2018), and expands the concept of LE/MVB spatial reorganisation to antibacterial immunity. Indeed, bacterial infection has been shown to upregulate extracellular vesicle secretion, a process which is thought to be underpinned by LE/MVB-dependent secretion (Wang et al., 2014, 2015; Rutter and Innes, 2017b).

I mapped proteomic changes along endocytic and secretory processes by performing mass spectrometry on purifications of ARA7 and ARA5 after the activation of the immune response to bacterial flagellin, and reveal that I most likely purified the greater complex associating with these Rab GTPases. Associating in an increased manner with ARA5 upon flagellin elicitation, I find several uncharacterized RLKs that may potentiate the cell surface with detection capacity for yet unknown ligands that may not be bacteria-specific. Additionally, I find a member of the MLO family, which are negative regulators of immunity

(Kusch and Panstruga, 2017). Based on its co-upregulation on ARA5 complexes with proteins that work in processes which have previously been suggested to be the client of MLO activity, I provide avenues for further study of MLO-based susceptibility (Kim et al., 2002; Campe et al., 2016; Cui et al., 2018).

Comparative proteomics in combination with co-localization studies between ARA7 and ARA5, provided evidence for these Rab GTPases further dividing a main TGN/EE sorting hub into secretory and endocytic domains respectively (Gendre et al., 2015; Wattelet-Boyer et al., 2016). In response to immune stimulus, shared proteins were upregulated, which points at increased secretion and endocytosis, and thus cell-surface turnover. These include proteins associated with ROS-metabolism and signaling, as well as cell-wall integrity sensing. These are known processes associated with host-activated modifications to the extracellular space upon MAMP perception.

Specifically associating with the endocytic Rab GTPase ARA7 upon immune stimulus, I find atypical resistance proteins TN3 and HR4, which I could show function in resistance to nonadapted powdery mildew, further supporting a generalized defense programme to be upregulated in the ARA7 complex. In parallel to TN3, I found the upregulation of a PRA1 Rab GTPase regulatory protein, which is a predicted target of both fungal and oomycete effectors (Weßling et al., 2014), together pointing at potential host guarding of the regulation of RabF-dependent processes. Further research should elucidate whether TN3 is the NLR responsible for monitoring endocytic traffic, and potentially unconventional endosomal secretion in plant immunity.

SUPPLEMENTAL MATERIALS

FIGURES

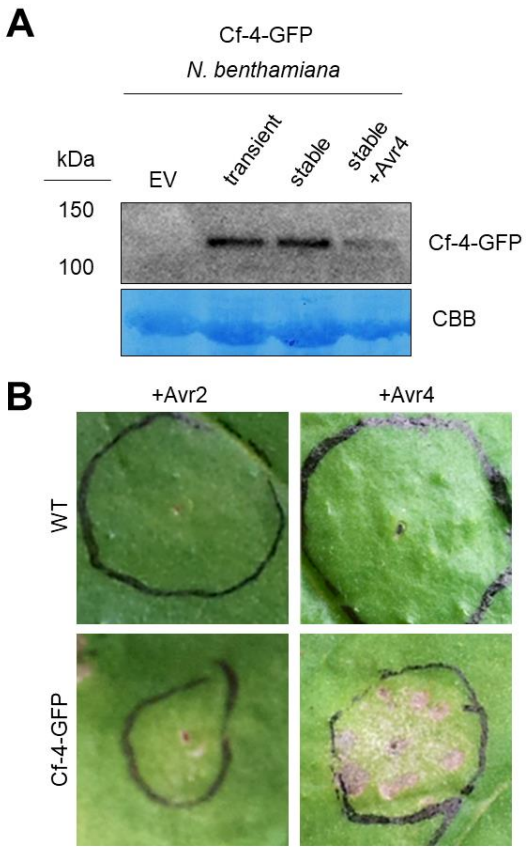

Fig. S.1. GFP-tagged Cf-4 migrates with the predicted molecular weight and is functional. (A) Western blot analysis of Cf-4-GFP transiently and stably expressed in *N. benthamiana*, without and with Avr4 (100 µM) treatment, as indicated. For transient expression, leaf samples were harvested at three days post infiltration (dpi) and Avr4 elicitation was done for 90 min. Blots were incubated with anti-GFP antibodies for the detection of Cf-4-GFP. CBB, Coomassie Brilliant Blue staining. (B) Images of N. benthamiana wild type (WT) leaves (top panel) and leaves transiently expressing Cf-4-GFP (bottom panel), treated with either Avr2 or Avr4 (300 µM), as indicated. Images were taken at five dpi and at four days after treatment with the Avrs.

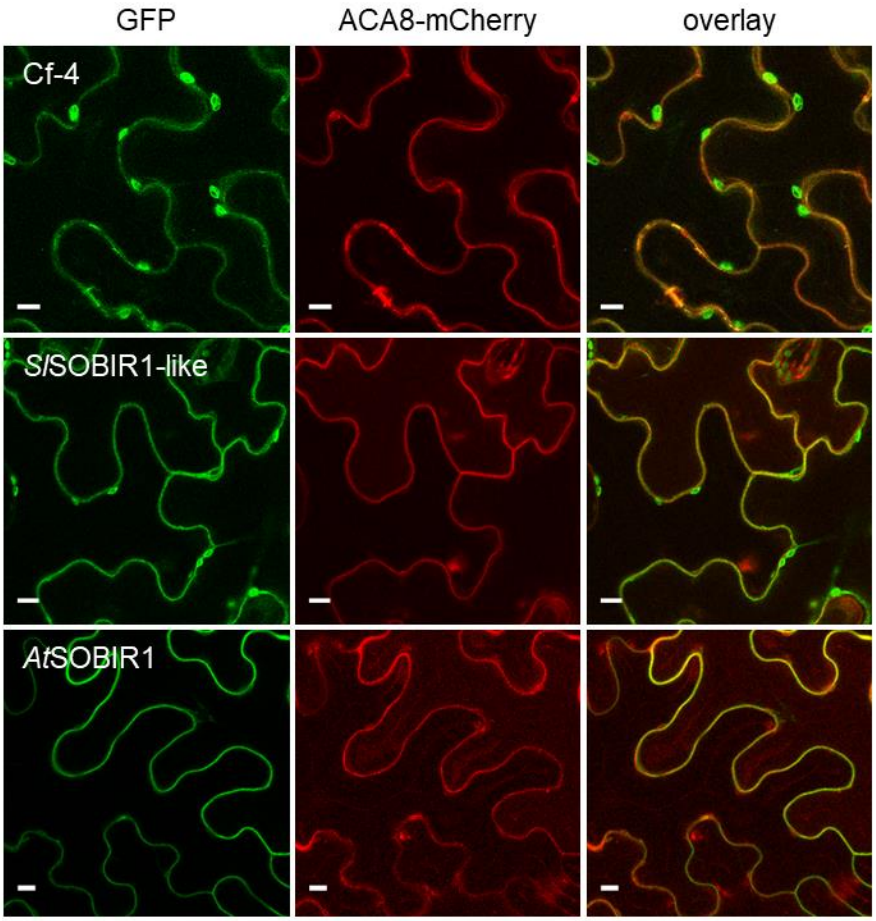

Fig. S.2. Subcellular localization of Cf-4, *Sl*SOBIR1-like and *At*SOBIR1. Confocal micrographs show *N. benthamiana* leaf epidermal cells stably expressing Cf-4-GFP and transiently expressing *Sl*SOBIR1-like-GFP and *At*SOBIR1-GFP as indicated (left panels), and co-expressing plasma membrane-localized ACA8-mCherry (middle panels). Overlay images indicate co-localization of the proteins fused to GFP and mCherry, as a yellow colour is produced (right panels). Images were taken at three dpi; scale bars = 10 µm.

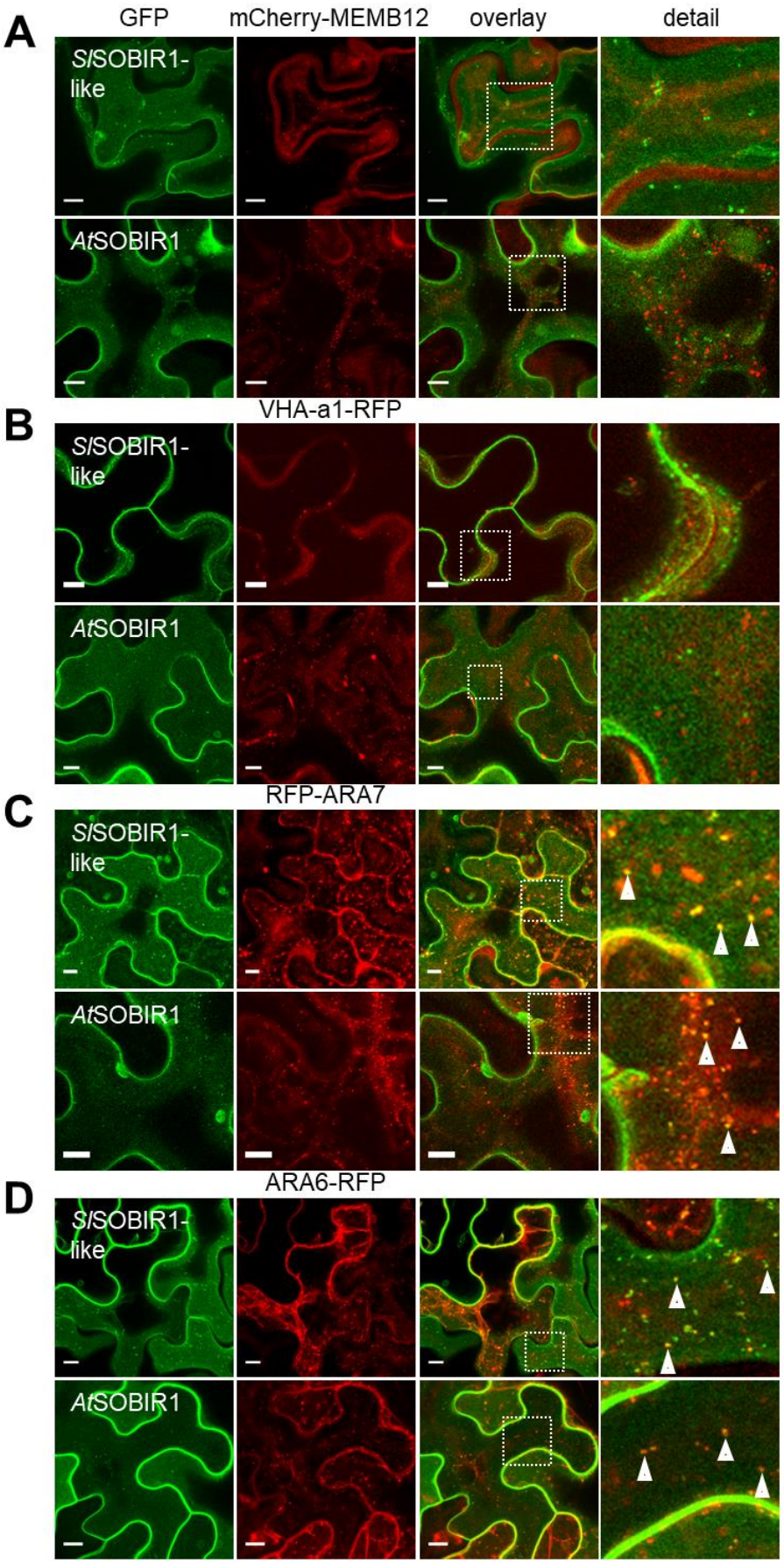
A
GFP
mCherry-MEMB12
overlay
detail
SlSOBIR1-like
AtSOBIR1
B
VHA-a1-RFP
SlSOBIR1-like
AtSOBIR1
C
RFP-ARA7
SlSOBIR1-like
AtSOBIR1
D
ARA6-RFP
SlSOBIR1-like
AtSOBIR1

Fig. S.3. *Sl*SOBIR1-like-GFP and *At*SOBIR1-GFP co-localize with endosomal markers. Confocal micrographs show *N. benthamiana* leaf epidermal cells transiently expressing *Sl*SOBIR1-like-GFP or *At*SOBIR1-GFP (left panels), and co-expressed mCherry/RFP-tagged organelle markers (middle, left panels). Overlay images indicate co-localization through generation of a yellow colour (middle, right panels). Dashed boxes indicated in the middle right panels are depicted as detail pictures on the right (right panels). Arrowheads point at co-localizing endosomes. Images were taken at three dpi; scale bars = 10 µm. (A) Co-expression of *Sl*SOBIR1-like-GFP/*At*SOBIR1-GFP with Golgi marker MEMB12-mCherry. (B) Co-expression of *Sl*SOBIR1-like-GFP/*At*SOBIR1-GFP with trans-Golgi network marker VHA-a1-RFP. (C) Co-expression of *Sl*SOBIR1-like-GFP/*At*SOBIR1-GFP with endosome marker RFP-ARA7/RabF2b. (D) Co-expression of *Sl*SOBIR1-like-GFP/*At*SOBIR1-GFP with late endosome marker ARA6/RabF1-RFP.

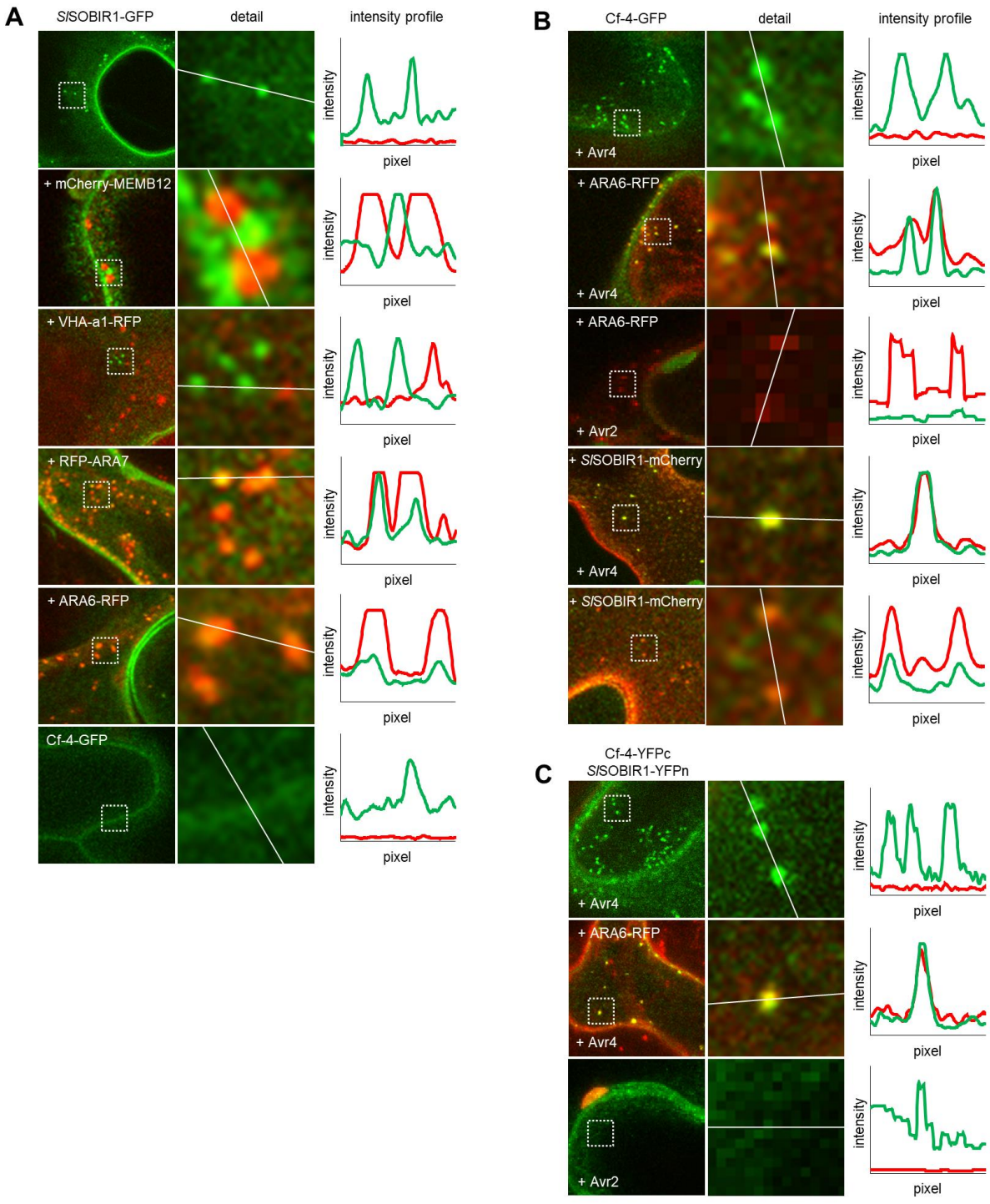

Fig. S.4. Line intensity profiles of Cf-4, *Sl*SOBIR1 and membrane markers. Confocal micrographs show transient co-expression of Cf-4-GFP, *Sl*SOBIR1-GFP or Cf-4-YFPc/*Sl*SOBIR1-YFPn with indicated membrane markers and effector treatments. Left column of panels correspond to confocal micrographs displayed in (A) Fig. 3.1, (B) Fig. 3.2A, (C) Fig. 3.2b. Dashed squares in these panels are shown as detailed pictures (magnified in middle column of panels). White lines in detailed pictures indicate the regions of interest (ROIs) that correspond to intensity profiles in the last panels. Intensity profiles indicate grey-value of pixels across the ROI in the green and red channels on a scale of 1-300.

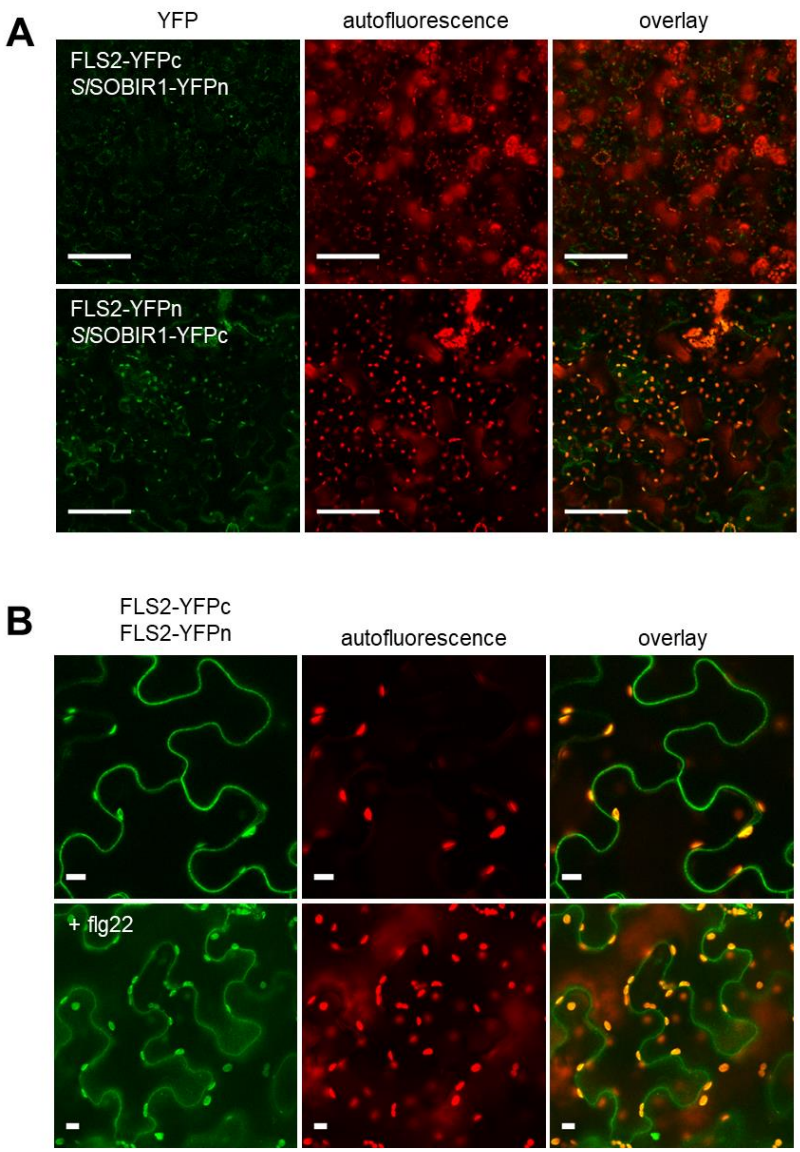

Fig. S.5. *Sl*SOBIR1 does not interact with FLS2 in BiFC experiments. (A) Confocal micrographs show *N. benthamiana* leaf epidermal cells transiently co-expressing FLS2 and *Sl*SOBIR1 C-terminally fused to the C- or N-terminal halves of YFP (YFPc and YFPn, respectively), as indicated. Left panels show absence or presence of YFP fluorescence, the middle panels show autofluorescence, and the right panels show the overlay of the fluorescence signals. Images were taken at two dpi, scale bars = 100 µm. (B) Confocal micrographs of *N. benthamiana* leaf epidermal cells transiently co-expressing FLS2-YFPc and FLS2-YFPn, either without or with flg22 treatment (10 µM) for 90 min, as indicated. Left panels show absence or presence of YFP fluorescence, the middle panels show autofluorescence, and the right panels show the overlay of the fluorescence signals. Images were taken at two dpi, scale bars = 10 µm.

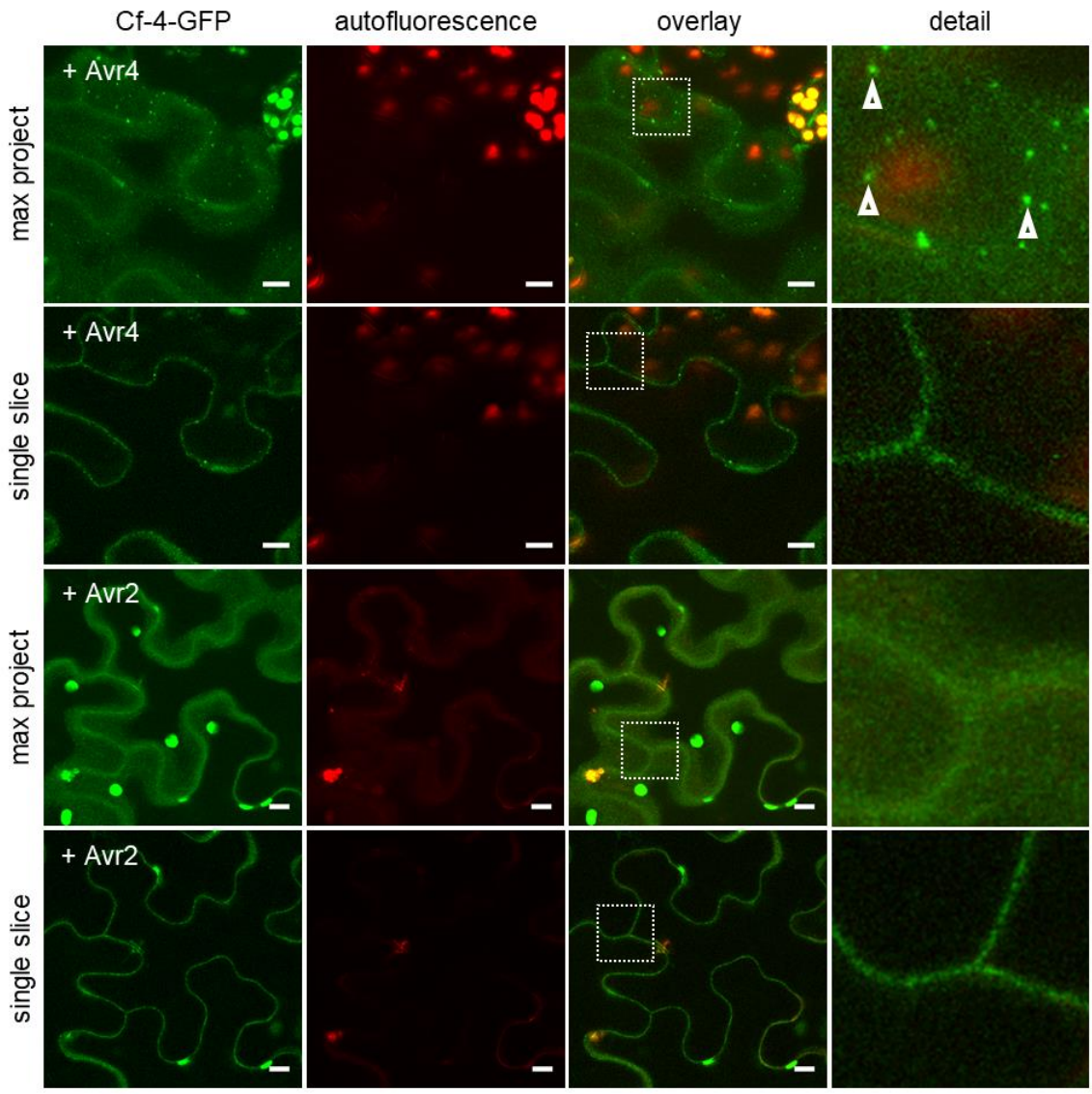

Fig. S.6. Cf-4-GFP undergoes Avr4-triggered endocytosis in stable transgenic plants. Confocal micrographs of Cf-4-GFP-transgenic *N. benthamiana* plants show leaf epidermal cells expressing Cf-4-GFP, either treated with Avr4 or Avr2 (both at 100 µM), as indicated. Left panels show GFP fluorescence, middle left panels show autofluorescence, and middle right panels show the overlay of the fluorescence signals shown in the left and middle left panels. Micrographs in rows 1 and 3 display maximum projected z-stacks to reveal vesicles, and rows 2 and 4 display their selected single focal plane outtakes to capture plasma membrane signal. Arrowheads in the detail pictures (right panels) point at mobile vesicles (top right panel). Images were taken at 90 minutes after elicitation; scale bars = 10 µm.

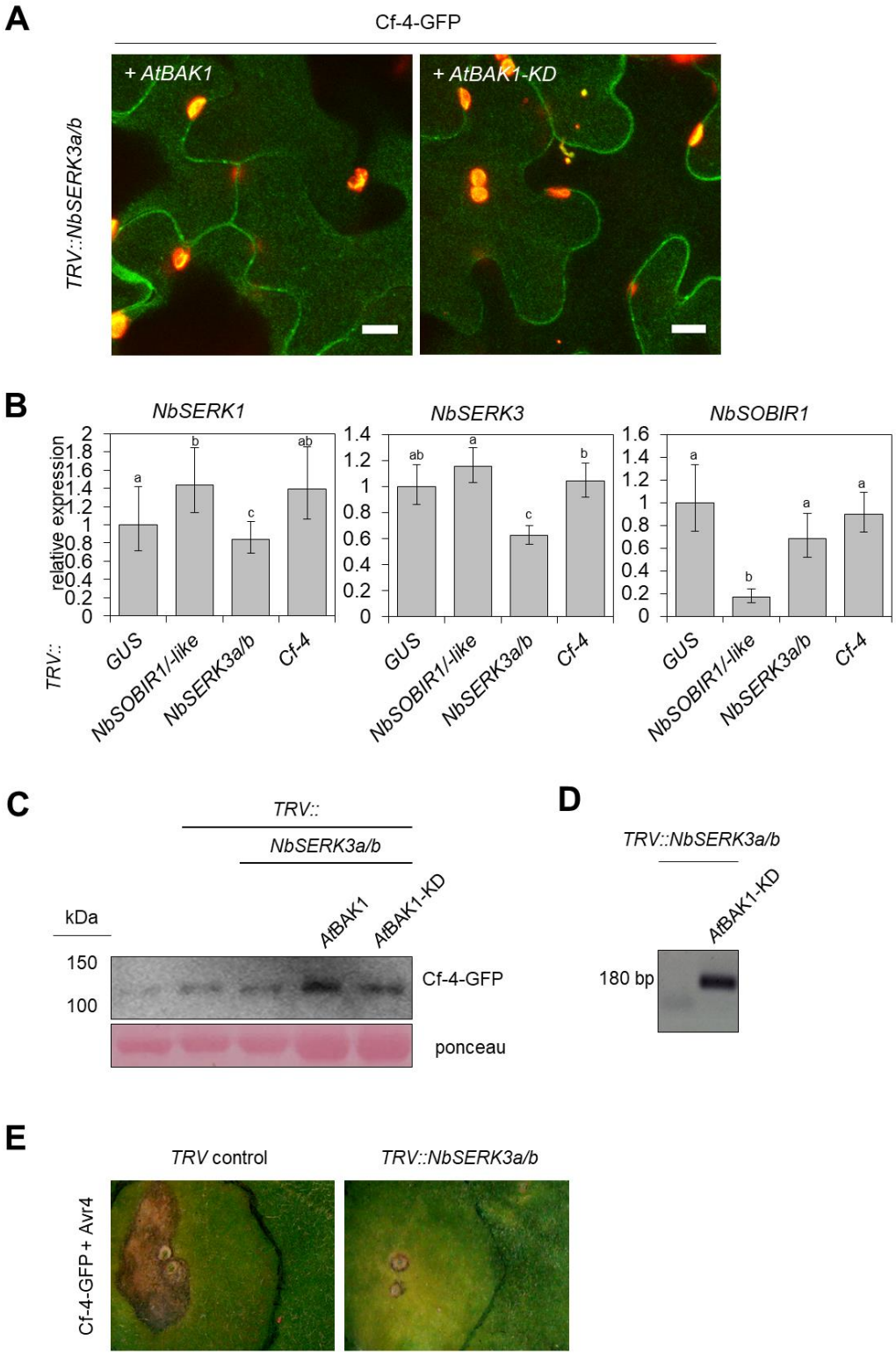
A
Cf-4-GFP
+ AtBAK1
+ AtBAK1-KD
TRV::NbSERK3a/b
B
NbSERK1
NbSERK3
NbSOBIR1
relative expression
TRV::
GUS
NbSOBIR1/-like
NbSERK3a/b
Cf-4
C
TRV::
NbSERK3a/b
kDa
AtBAK1
AtBAK1-KD
150
100
Cf-4-GFP
ponceau
D
TRV::NbSERK3a/b
AtBAK1-KD
180 bp
E
TRV control
TRV::NbSERK3a/b
Cf-4-GFP + Avr4

Fig. S.7. *Sl*SERK3 is required for Avr4-induced HR. (A) Leaves of *Cf-4-GFP-N. benthamiana* stable plants were *TRV*-silenced for *NbSERK3a/b* for three weeks and subsequently used to transiently express AtBAK1 and AtBAK1-KD, without treatment of Avr4. Images are representative of vesicle quantification data presented in Fig. 3.4. (B) qRT-PCR analysis showing *NbSERK1*, *NbSERK3a/b* and *NbSOBIR1* expression in *N. benthamiana* inoculated with the indicated *TRV* VIGS constructs. Expression of query genes was normalized to endogenous *NbActin* expression levels. Data presented have been combined from twelve (*NbSOBIR1* expression) or 24 (*NbSERK1* and *NbSERK3* expression) individual qRT-PCRs, based on three independent biological replicates, for each gene of which the expression was studied. Statistical differences (α=0.05) between groups were calculated by a one-way ANOVA and different groupings are indicated. Error bars represent the standard deviation. These qRT-PCR experiments were performed by Ruby Bye (C) Immunoblots from total protein extracts of *Cf-4-GFP*-transgenic *N. benthamiana* plants that were *TRV*-silenced for *NbSERK3a/b* and subsequently transiently transformed with *AtBAK1* and *AtBAK1-KD*. Cf-4-GFP was revealed with αGFP. Ponceau staining is shown for equal loading. (D) RT-PCR on cDNA obtained from total RNA extracts of *Cf-4-GFP*-transgenic *N. benthamiana* plants that were TRV-silenced for *NbSERK3a/b* and subsequently transiently transformed with *AtBAK1* and *AtBAK1-KD*. (E) Images show *N. benthamiana* leaves from *TRV::NbSERK3a/b*-inoculated plants and *TRV*-inoculated controls, transiently expressing *Cf-4-GFP* and treated with Avr4 protein (300 µM). *Cf-4-GFP* was agro-infiltrated at 3 weeks post inoculation with the recombinant *TRV* constructs and one day later the Avr4 protein was infiltrated. Images were taken at six days after Avr4 infiltration. HR is observed as brownish cell death.

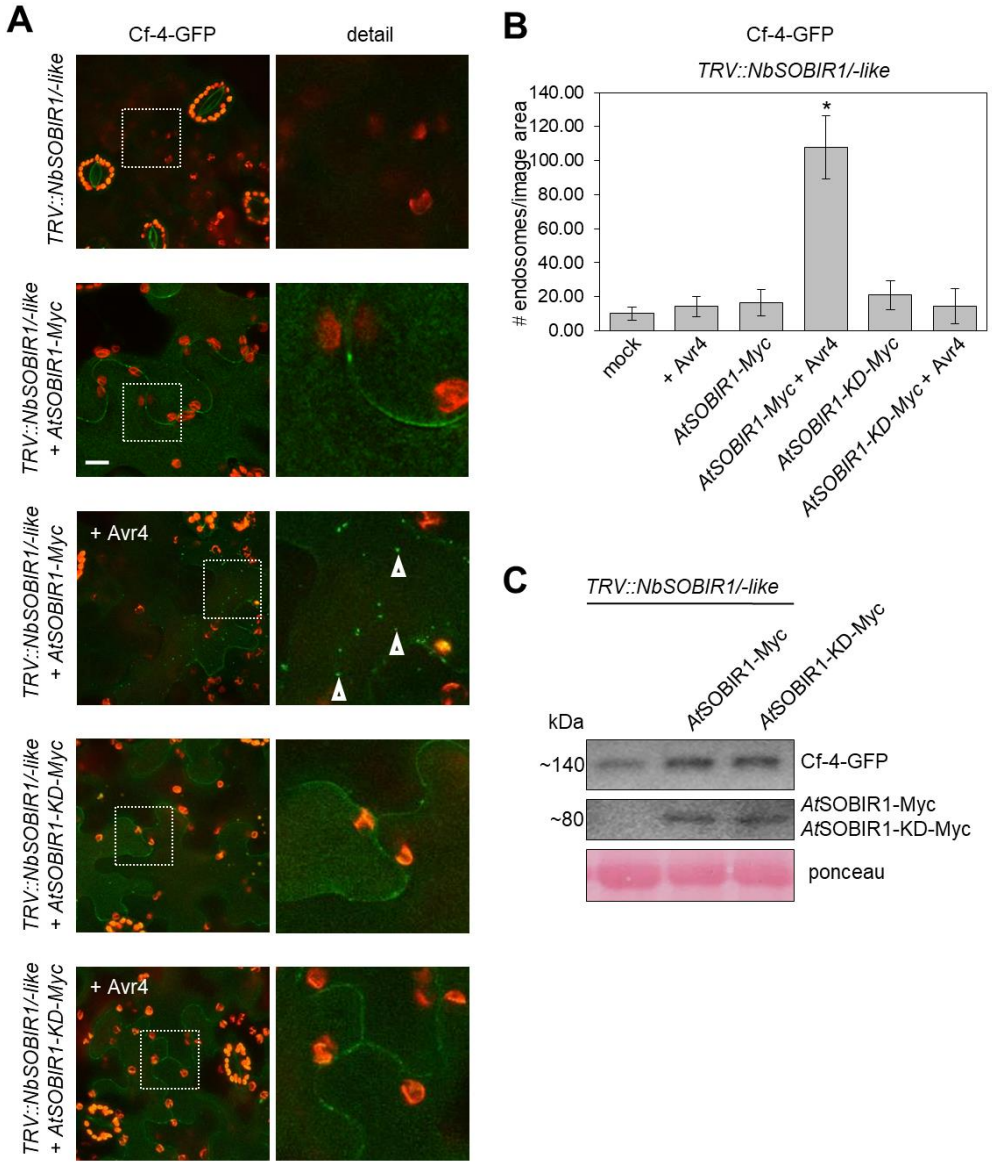

Fig. S.8. Cf-4 endocytosis requires SOBIR1 kinase activity. Leaves of *Cf-4-GFP* transgenic *N. benthamiana* plants that had been *TRV*-silenced for *NbSOBIR1/-like* were used for transient expression of *AtSOBIR1-Myc* and its kinase-inactive variant *AtSOBIR1-KD-Myc*. (A) Confocal micrographs show Cf-4-GFP localisation upon treatment with Avr4 (100µM, left panels) and detail pictures from dashed squares (middle panels). Arrowheads point at Cf-4-GFP-positive vesicles. Images were taken at three weeks after inoculation with *TRV*, at three dpi for transient expression, and at 90 min after elicitation; scale bars = 10 µm. (B) Quantification of Cf-4-GFP-positive vesicles was done with EndoQuant (bars depict means ± 2 SE; n = 6; $p < 0.05$; statistical significant differences are indicated by asterisks). Transient co-expression of *AtBAK1*, but not its kinase-inactive variant *AtBAK1-KD*, increased Cf-4-GFP-positive vesicles in *NbSOBIR1/-like*-silenced leaves. (C) Immunoblots from extracted total proteins of *Cf-4-GFP-transgenic N. benthamiana* plants that were *TRV*-silenced for *NbSOBIR1/-like* and subsequently transiently transformed with *AtSOBIR1-Myc* or *AtSOBIR1-KD-Myc*. Cf-4-GFP, AtSOBIR1-Myc and AtSOBIR1-KD-Myc were revealed with αGFP and αMyc antibodies as indicated. Ponceau staining is shown for equal loading.

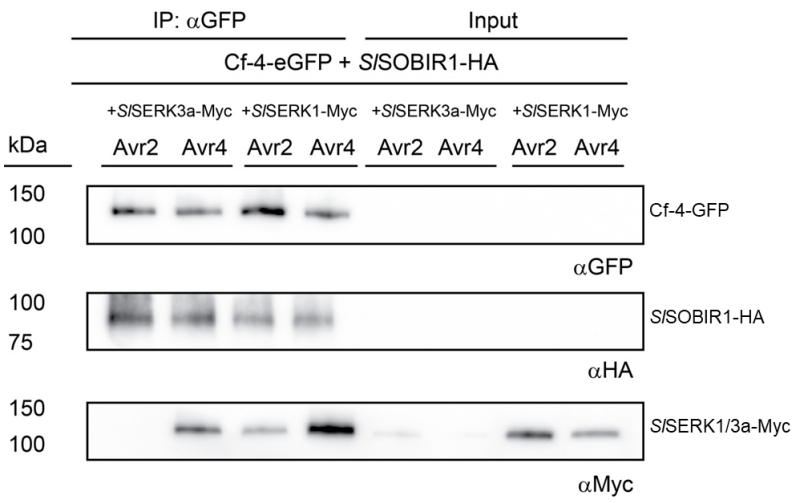

Fig. S.9. Both *Sl*SERK1 and *Sl*SERK3a interact with Cf-4. Co-immunoprecipitation from GFP-trap bead pull-downs on *N. benthamiana* co-expressing *Cf-4-GFP* and *SlSOBIR1-HA*, and either *SlSERK3a-Myc* or *SlSERK1-Myc*. Leaf samples were taken at two dpi, after 60 min treatment with Avr2 or Avr4 (100 µM), as indicated. Total proteins (Input) and immunoprecipitated proteins (IP) were subjected to SDS/PAGE and blotted. Blots were incubated with αGFP, αHA or αMyc antibodies for the detection of immunoprecipitated Cf-4-GFP and co-purifying *Sl*SOBIR1-HA and *Sl*SERK3a-Myc or *Sl*SERK1-Myc, respectively. These immunoprecipitations and western blot experiments were performed by Thomas Liebrand and Guozhi Bi.

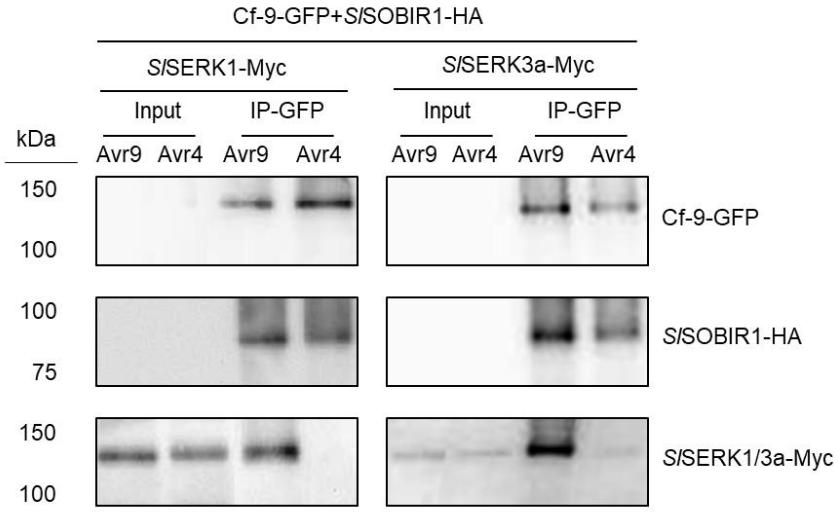

Fig. S.10. Avr9 induces interaction of Cf-9 with both *Sl*SERK1 and *Sl*SERK3a. Co-immunoprecipitation from GFP-trap bead pull-downs on *N. benthamiana* co-expressing Cf-9-GFP and *SlSOBIR1-HA*, and either *SlSERK1-Myc* or *SlSERK3a-Myc*. Leaf samples were taken at two dpi, after 60 min treatment with Avr9 or Avr4 (100 µM), as indicated. Total proteins (input) and immunoprecipitated proteins (IP) were subjected to SDS/PAGE and blotted. Blots were incubated with αGFP, αHA or αMyc antibodies for the detection of immunoprecipitated Cf-9-GFP and co-purifying *Sl*SOBIR1-HA and *Sl*SERK1-Myc or *Sl*SERK3a-Myc, respectively. These immunoprecipitations and western blot experiments were performed by Thomas Liebrand and Guozhi Bi.

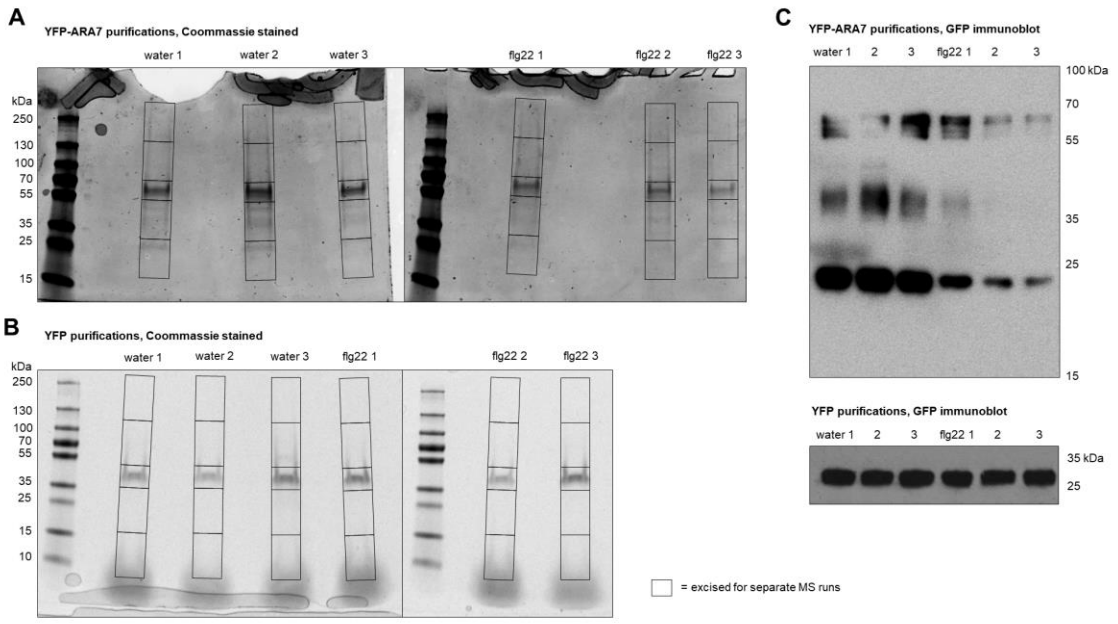

Fig. S.11. Immunoprecipitation and gel-staining of YFP-ARA7 and YFP in preparation for mass spectrometry. (A,B) Coommassie-stained gel pictures show individual replicates of anti-GFP immunoprecipitations from *pUB::YFP-ARA7* or *pUB::YFP* seedlings after running in SDS-PAGE on 4-20% agarose gradient gels. Boxes indicate incisions made to obtain separate gel samples for mass spectrometry analysis. Numbers (left) indicate molecular weight of individual ladder bands (Page Ruler Plus). (C) Immunoblot shows samples used in (A,B), probed with anti-YFP with anti-GFP-HRP conjugated antibodies. Numbers (right) indicate molecular weight of ladder bands (not shown).

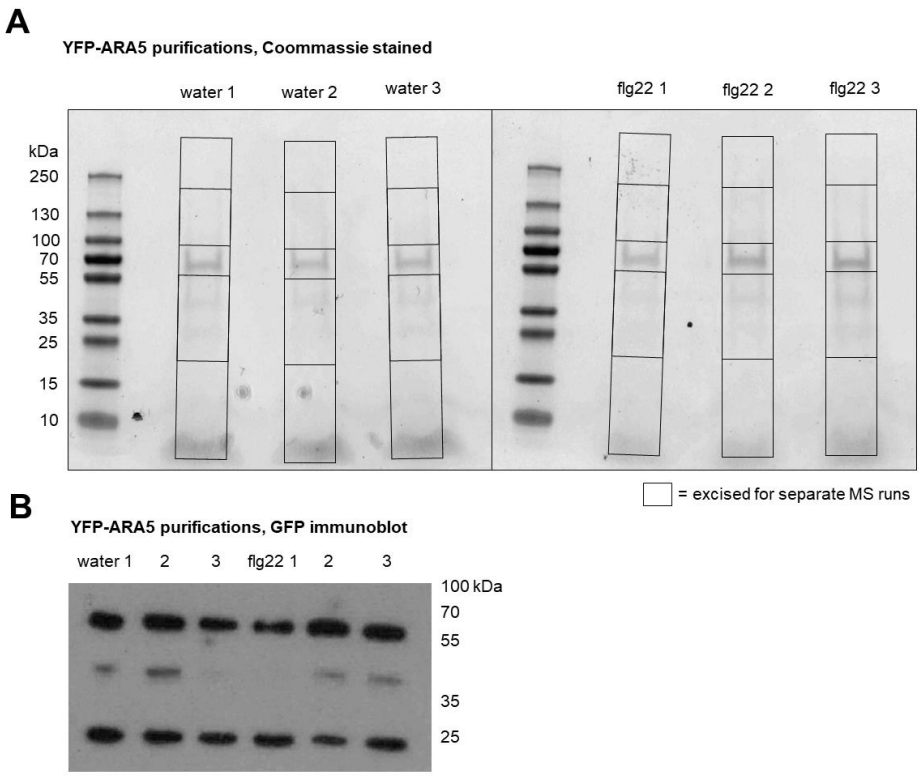

Fig. S.12. Immunoprecipitation and gel-staining of YFP-ARA5 in preparation for mass spectrometry. (A) Coommassie-stained gel pictures of individual replicates of GFP-antibody immunoprecipitations from *pUB::YFP-ARA7* seedlings after running in SDS-PAGE on 4-20% agarose gradient gels. Boxes indicate incisions made to obtain separate gel samples for mass spectrometry analysis. Numbers (left) indicate molecular weight of individual ladder bands (Page Ruler Plus). (B) Western blot image of samples used in (A), probing for YFP with a GFP-HRP conjugated antibody. Numbers (right) indicate molecular weight of ladder bands (not shown).

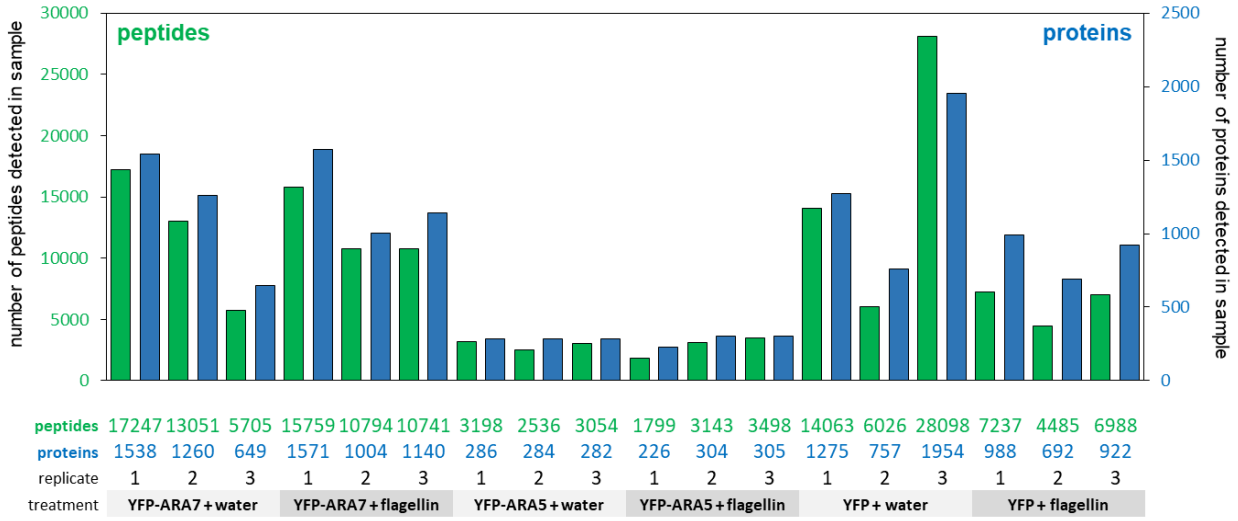

Figure S.13. Number of peptides and proteins detected by MS/MS in individual immunoprecipitations. Green bars indicate the number of peptides with a Scaffold PeptideProphet score of >95% identified in individual replicates of YFP-immunoprecipitations (values correspond to left axis). Blue bars indicate number of proteins detected with a Scaffold ProteinProphet score of >99% (values correspond to right axis). Immunoprecipitations were done from Arabidopsis seedlings expressing pUB-driven *YFP-ARA7*, *YFP-ARA5*, and *YFP* upon 3-hour water or 3-hour 1.5 µM flagellin infiltrations by vacuum, and analysis using mass-spectrometry. Spectra were obtained using an Orbitrap Fusion machine (Thermo) and matched to the MASCOT Arabidopsis protein database. SCAFFOLD was used to filter for 95% confidence spectra and proteins were detected when 2 unique spectra were found.

```
HR4       MPIAELAVIKTVGGPLIAAALGVGAQVIYDGFRKGKDTS-----IINRLGRTMESISPVR
HR1       MPLVE---------LLTSAALGLSLQLLHDAIIRAKERSLITRCILDRLDATLHKITPFV
HR2       MPLTE---------IIAGAALGLALQILHEAIQRAKDRSLTTSCILDRLDSTILRITPLM
HR3       MPVSE---------IMAGAALGLALQVLHDAIKKAKDRSLTTRCILDRLDATIFRITPLV
          **: *          : .****:. *:::::: :.*: *     *::**. *:  *:*.

HR4       DRIGKLSNVEGKPFREVHESLTRLLEDAKSIIEKYWKLRWSRHVCRKYRYIKKLESIELE
HR1       IKIDTLTEEVDEPFRKVIEELKRLLEKAIRLVDAYAELKL-RNLLRKYRYKRRIKELDSS
HR2       AKVEKLNKESDESLRKVFEDLKHLLEKAVVLVEAYAELKR-RNLLGKYRYKRRIKELEGS
HR3       TQVDKLSEEVEDSPRKVIEDLKHLLEKAVSLVEAYAELRR-RNLLKKFRYKRRIKELEAS
           :: .*.:   .  *:* *.*.:***.*  ::: * :*:  *::  *:** ::::.:: .

HR4       LVR-VAREIQVHQWTDIKEMKAIQVHQWTDIKEMKAIQVDQWTDIKEMKAIQVDQWIDIK
HR1       LRWMIDVDVQVNQWLDIKKLMGKMSEMNTKLDDITRQPMDIIEATGRSS-----------
HR2       LKWMVDVDVKVNQWADIKDLMAKMSEMNTKLEKIMGQPIDCIISEDNT-------NMDIV
HR3       LRWMVDVDVQVNQWVDIKELMAKMSEMNTKLDEITRQPTDCICFKSNHSTSQ-SSSQNIV
          *   :  :::*:** ***.: .   .  *.:..:     *      .

HR4       EMKAIQVDQWTDIKEMKAQISEKHNK-------------------------
HR1       ---------------E----EDGCTKPTIDIHFRWKNQT--KEHEIRFIFK
HR2       ERVD-------PSLEAKAGCSNSDSKPKIDIHLRWSKQS--KDHGIRFVLN
HR3       EETD-------RSLEEIVECSSDGSKPKIDIHIHWSSRKRNKDREIRFVLK
                           ..  .*
```

Figure. S.14. Clustal Omega multiple sequence alignment of all four "Homolog of RPW8" proteins in *Arabidopsis thaliana* ecotype Col-0. Protein sequences were retrieved from TAIR10 (Arabidopsis.org) and aligned using Clustal Omega Multiple Sequence Alignment (EMBL-EBI). Bold letters indicate peptides identified in MS/MS after YFP-ARA7 purifications upon flg22 treatment (**Fig. 4.13**). "*****" indicates 100% amino acid identity across homologs. "**:**" indicates conservation of amino acid with similar properties. "**.**" indicates conservation of amino acids with weakly similar properties.

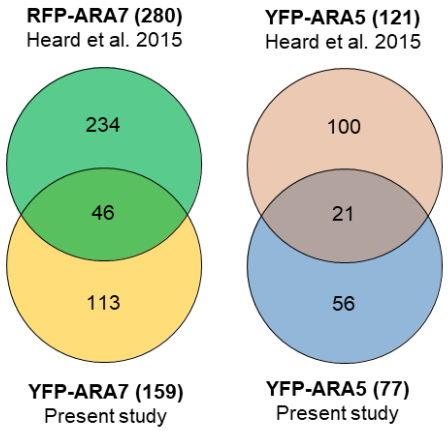

Figure. S.15 Venn diagram showing overlap in number of proteins between published endocytic/secretory associated proteomes from Heard et al. 2015. Protein lists were obtained from Heard et al. 2015, and the present study tables 4.1 (YFP-ARA7) and 5.1 (YFP-ARA5). Overlap between the datasets in number of proteins was calculated in MS Excel, and plotted in Venn-diagrams, and number of proteins in each group are displayed.

TABLES

Table S1: GO-term enrichment in the ARA7 co-purifying proteome. Listed here are the Gene Ontology (GO) terms (GO-database of 04-04-2018, “cellular component” group) associated with proteins in the ARA7 co-purifying proteome as defined in Table 4.1. To capture over- or underrepresentation of a GO-term in the dataset, an enrichment factor is listed, comparing the term‘s occurrence in the ARA7 co-purifying proteome to its occurrence in the TAIR10 reference genome. For this, the PANTHER classification system (version 20171205) and Fisher’s exact test ($p < 0.05$) were used. Finally, the number of proteins in the ARA7 co-purifying proteome associated with the GO classification is listed. Dots indicate GO terms that correspond to the known localization and function of ARA7. Bars indicate relative values.

Table S1: GO-term enrichment in the ARA7 co-purifying proteome		
Fold enrichment	**Number of proteins**	**Associated GO term (cellular component)**
>100	2	• TRAPPIII protein complex
>100	2	TRAPPII protein complex
98.22	4	TRAPP complex
95.49	5	retromer complex
85.94	3	GARP complex
57.3	5	Golgi transport complex
49.11	2	• multivesicular body membrane
45.84	4	• multivesicular body
45.84	4	• early endosome membrane
42.97	3	1,3-beta-D-glucan synthase complex
42.97	2	• trans-Golgi network membrane
40.93	15	• late endosome membrane
39.67	3	• endocytic vesicle
33.86	13	tethering complex
33.21	17	• late endosome
32.23	6	clathrin-coated vesicle membrane
32.23	3	• trans-Golgi network transport vesicle
31.25	6	• early endosome
31.25	2	COPI vesicle coat
28.44	46	• trans-Golgi network
27.79	27	• endosomal part
26.86	10	SNARE complex
26.36	25	• endosome membrane
24.66	35	• cytoplasmic vesicle part
24.56	2	COPI-coated vesicle membrane
23.11	57	• endosome
22.92	12	• cytoplasmic vesicle membrane
22.67	12	• vesicle membrane
22.42	9	coated vesicle membrane
20.22	6	• transport vesicle
19.93	8	clathrin-coated vesicle
19.07	65	cytoplasmic vesicle
18.97	65	• intracellular vesicle
18.09	4	• transport vesicle membrane
17.3	65	• vesicle
16.45	58	Golgi apparatus part
15.92	54	Golgi subcompartment
15.5	11	coated vesicle
14.16	7	Golgi-associated vesicle
12.73	4	Golgi-associated vesicle membrane
11.46	3	• vesicle coat
11.16	79	Golgi apparatus
10.93	25	Golgi membrane
6.89	52	bounding membrane of organelle

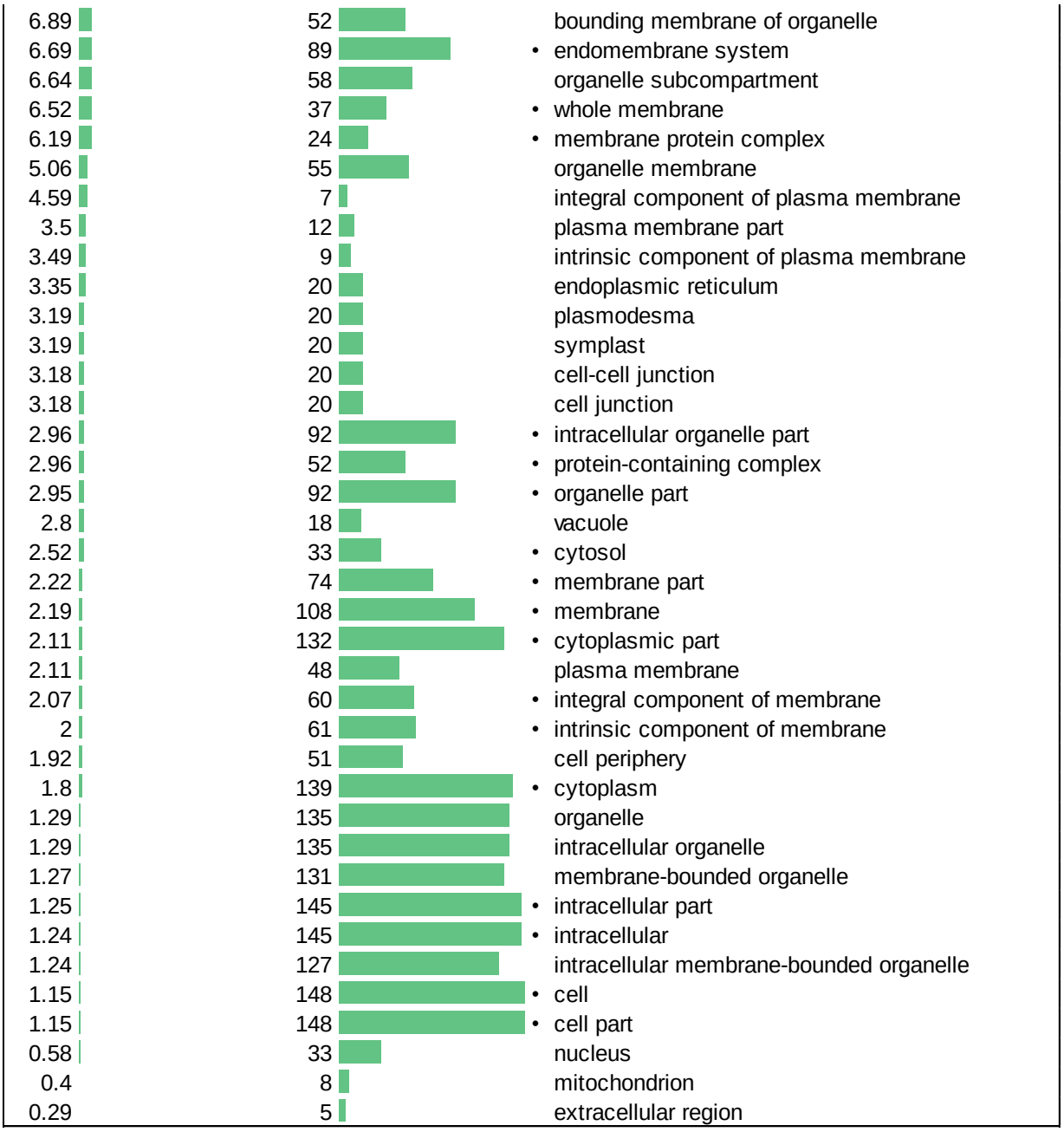
6.89 52 bounding membrane of organelle
6.69 89 • endomembrane system
6.64 58 organelle subcompartment
6.52 37 • whole membrane
6.19 24 • membrane protein complex
5.06 55 organelle membrane
4.59 7 integral component of plasma membrane
3.5 12 plasma membrane part
3.49 9 intrinsic component of plasma membrane
3.35 20 endoplasmic reticulum
3.19 20 plasmodesma
3.19 20 symplast
3.18 20 cell-cell junction
3.18 20 cell junction
2.96 92 • intracellular organelle part
2.96 52 • protein-containing complex
2.95 92 • organelle part
2.8 18 vacuole
2.52 33 • cytosol
2.22 74 • membrane part
2.19 108 • membrane
2.11 132 • cytoplasmic part
2.11 48 plasma membrane
2.07 60 • integral component of membrane
2 61 • intrinsic component of membrane
1.92 51 cell periphery
1.8 139 • cytoplasm
1.29 135 organelle
1.29 135 intracellular organelle
1.27 131 membrane-bounded organelle
1.25 145 • intracellular part
1.24 145 • intracellular
1.24 127 intracellular membrane-bounded organelle
1.15 148 • cell
1.15 148 • cell part
0.58 33 nucleus
0.4 8 mitochondrion
0.29 5 extracellular region

Table S2: GO-term enrichment in the ARA7 co-purifying proteome upon flagellin treatment. Listed here are the Gene Ontology (GO) terms (GO-database of 04-04-2018, "biological function" group) associated with proteins in the ARA7 co-purifying proteome as defined in Table 4.3. To capture over- or underrepresentation of a GO-term in the dataset, an enrichment factor is listed, comparing the term's occurrence in the ARA7 co-purifying proteome to its occurrence in the TAIR10 reference genome. For this, the PANTHER classification system (version 20171205) and Fisher's exact test ($p < 0.05$) were used. Finally, the number of proteins in the ARA7 co-purifying proteome associated with the GO classification is listed. Dots indicate GO terms that correspond to the known localization and function of ARA7. Bars indicate relative values.

Table S2: GO-term enrichment in ARA7 co-purifying proteins upregulated by flagellin treatment		
Fold enrichment	**Number of proteins**	**Associated GO term (biological process)**
12.09	5	Golgi vesicle transport
7.72	10	vesicle-mediated transport
7.19	8	cellular amino acid metabolic process
6.39	8	monocarboxylic acid metabolic process
6.15	16	carboxylic acid metabolic process
5.93	9	carboxylic acid biosynthetic process
5.93	9	organic acid biosynthetic process
5.76	17	oxoacid metabolic process
5.74	17	organic acid metabolic process
5.56	11	small molecule biosynthetic process
4.84	9	drug metabolic process
4.02	18	small molecule metabolic process
3.84	11	macromolecule localization
2.52	20	response to chemical
1.97	33	response to stimulus

Table S3: GO-term enrichment in the ARA5 co-purifying proteome. Listed here are the Gene Ontology (GO) terms (GO-database of 04-04-2018, "cellular component" group) associated with proteins in the ARA5 co-purifying proteome as defined in Table 5.1. To capture over- or underrepresentation of a GO-term in the dataset, an enrichment factor is listed, comparing the term's occurrence in the ARA5 co-purifying proteome to its occurrence in the TAIR10 reference genome. For this, the PANTHER classification system (version 20171205) and Fisher's exact test ($p < 0.05$) were used. Finally, the number of proteins in the ARA5 co-purifying proteome associated with the GO classification is listed. Dots indicate GO terms that correspond to the known localization and function of ARA5. Bars indicate relative values.

Table S3: GO-term enrichment in the ARA5 co-purifying proteome		
Fold enrichment	**Number of proteins**	**Associated GO term (cellular component)**
>100	2	• TRAPPIII protein complex
>100	2	• TRAPPII protein complex
>100	4	• trans-Golgi network membrane
>100	3	TRAPP complex
94.02	4	• Golgi transport complex
88.15	3	1,3-beta-D-glucan synthase complex
78.35	2	vacuolar proton-transporting V-type ATPase complex
54.24	2	proton-transporting V-type ATPase, V0 domain
47.01	2	• early endosome membrane
44.07	4	• clathrin-coated vesicle membrane
44.07	2	• trans-Golgi network transport vesicle
42.74	4	• early endosome
40.59	32	• trans-Golgi network
39.18	7	late endosome membrane
37.4	7	tethering complex
37.11	4	• transport vesicle membrane
34.57	5	• transport vesicle
33.58	2	proton-transporting V-type ATPase complex
31.34	8	• cytoplasmic vesicle membrane
31	8	• vesicle membrane
30.66	6	• coated vesicle membrane
28.05	7	late endosome
27.55	5	SNARE complex
25.78	31	• endosome
25.55	5	• clathrin-coated vesicle
22.11	38	• Golgi apparatus part
21.17	35	• Golgi subcompartment
21.11	10	• endosomal part
20.46	34	• cytoplasmic vesicle
20.35	34	• intracellular vesicle
20.23	14	• cytoplasmic vesicle part
20.23	7	• coated vesicle
19.59	3	• Golgi-associated vesicle membrane
18.56	34	• vesicle
17.31	8	• endosome membrane
16.59	4	• Golgi-associated vesicle
14.2	49	• Golgi apparatus
13.46	15	• Golgi membrane
8.46	36	• organelle subcompartment
8.25	4	plant-type vacuole
7.71	50	• endomembrane system
7.34	27	• bounding membrane of organelle
7.23	20	whole membrane
6.73	5	integral component of plasma membrane

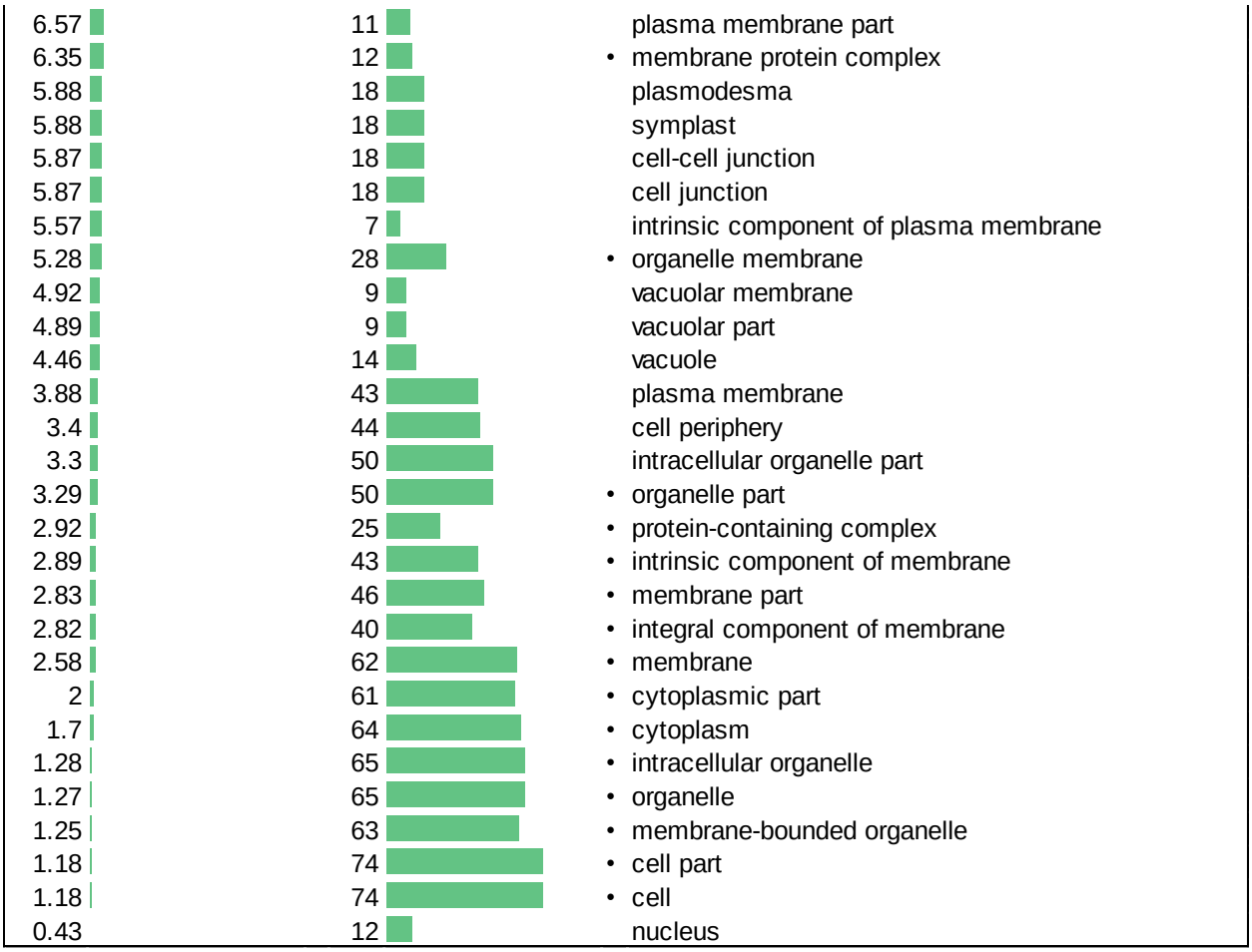
6.57 11 plasma membrane part
6.35 12 • membrane protein complex
5.88 18 plasmodesma
5.88 18 symplast
5.87 18 cell-cell junction
5.87 18 cell junction
5.57 7 intrinsic component of plasma membrane
5.28 28 • organelle membrane
4.92 9 vacuolar membrane
4.89 9 vacuolar part
4.46 14 vacuole
3.88 43 plasma membrane
3.4 44 cell periphery
3.3 50 intracellular organelle part
3.29 50 • organelle part
2.92 25 • protein-containing complex
2.89 43 • intrinsic component of membrane
2.83 46 • membrane part
2.82 40 • integral component of membrane
2.58 62 • membrane
2 61 • cytoplasmic part
1.7 64 • cytoplasm
1.28 65 • intracellular organelle
1.27 65 • organelle
1.25 63 • membrane-bounded organelle
1.18 74 • cell part
1.18 74 • cell
0.43 12 nucleus

Table S4: GO-term enrichment in the ARA5 co-purifying proteome upon flagellin treatment. Listed here are the Gene Ontology (GO) terms (GO-database of 04-04-2018, "biological function" group) associated with proteins in the ARA5 co-purifying proteome as defined in Table 5.3. To capture over- or underrepresentation of a GO-term in the dataset, an enrichment factor is listed, comparing the term's occurrence in the ARA7 co-purifying proteome to its occurrence in the TAIR10 reference genome. For this, the PANTHER classification system (version 20171205) and Fisher's exact test ($p < 0.05$) were used. Finally, the number of proteins in the ARA7 co-purifying proteome associated with the GO classification is listed. Dots indicate GO terms that correspond to the known localization and function of ARA7. Bars indicate relative values.

Table S4: GO-term enrichment in ARA5 co-purifying proteins upregulated by flagellin treatment

Fold enrichment	Number of proteins	Associated GO term (biological process)
20.56	5	protein autophosphorylation
10.05	8	protein phosphorylation
8.31	6	defense response to other organism
7.53	8	phosphorylation
6.04	9	phosphate-containing compound metabolic process
5.82	8	multi-organism process
5.81	9	phosphorus metabolic process
3.86	11	response to stress

Table S5: GO-term enrichment in the shared ARA7 and ARA5 co-puryfing proteome. Listed here are the Gene Ontology (GO) terms (GO-database of 04-04-2018, "biological function" group) associated with proteins in the shared ARA7 and ARA5 co-purifying proteome as defined in Table 5.4. To capture over- or underrepresentation of a GO-term in the dataset, an enrichment factor is listed, comparing the term's occurrence in the shared ARA7 and ARA5 co-purifying proteome to its occurrence in the TAIR10 reference genome. For this, the PANTHER classification system (version 20171205) and Fisher's exact test ($p < 0.05$) were used. Finally, the number of proteins in the shared ARA7 and ARA5 co-purifying proteome associated with the GO classification is listed. Bars indicate relative values.

Table S4: GO-term enrichment in the shared ARA7 and ARA5 co-purifying proteome		
Fold enrichment	**Number of proteins**	**Associated GO term (biological process)**
> 100	3	(1->3)-beta-D-glucan biosynthetic process
> 100	3	(1->3)-beta-D-glucan metabolic process
> 100	5	Golgi to vacuole transport
89.29	5	post-Golgi vesicle-mediated transport
83.34	2	cell plate assembly
78.13	5	protein targeting to vacuole
78.13	6	protein localization to vacuole
75.44	7	beta-glucan biosynthetic process
72.12	3	plant-type primary cell wall biogenesis
66.49	5	establishment of protein localization to vacuole
64.66	3	regulation of cell shape
62.5	3	protein secretion
62.5	3	peptide secretion
58.97	5	vesicle fusion
54.83	5	organelle membrane fusion
54.35	4	cellulose biosynthetic process
52.09	3	polysaccharide localization
50.88	7	beta-glucan metabolic process
44.65	5	vesicle docking
44.02	5	organelle localization by membrane tethering
44.02	5	membrane docking
42.81	5	membrane fusion
42.62	6	vacuolar transport
39.07	7	glucan biosynthetic process
38.66	6	vesicle organization
36.77	11	Golgi vesicle transport
34.34	5	organelle fusion
34.25	4	exocytosis
33.79	4	cellulose metabolic process
33.25	5	mitotic cytokinesis
32.22	5	cytoskeleton-dependent cytokinesis
32.22	5	cytokinesis
31.89	5	secretion by cell
29.94	8	cellular polysaccharide biosynthetic process
29.21	5	secretion
25.38	8	polysaccharide biosynthetic process
24.04	4	ER to Golgi vesicle-mediated transport
23.59	8	cellular carbohydrate biosynthetic process
23.15	3	monovalent inorganic cation homeostasis
21.51	17	vesicle-mediated transport
21.14	7	cellular glucan metabolic process
20.97	5	plant-type cell wall biogenesis
20.83	3	regulation of cell morphogenesis
20.35	7	glucan metabolic process

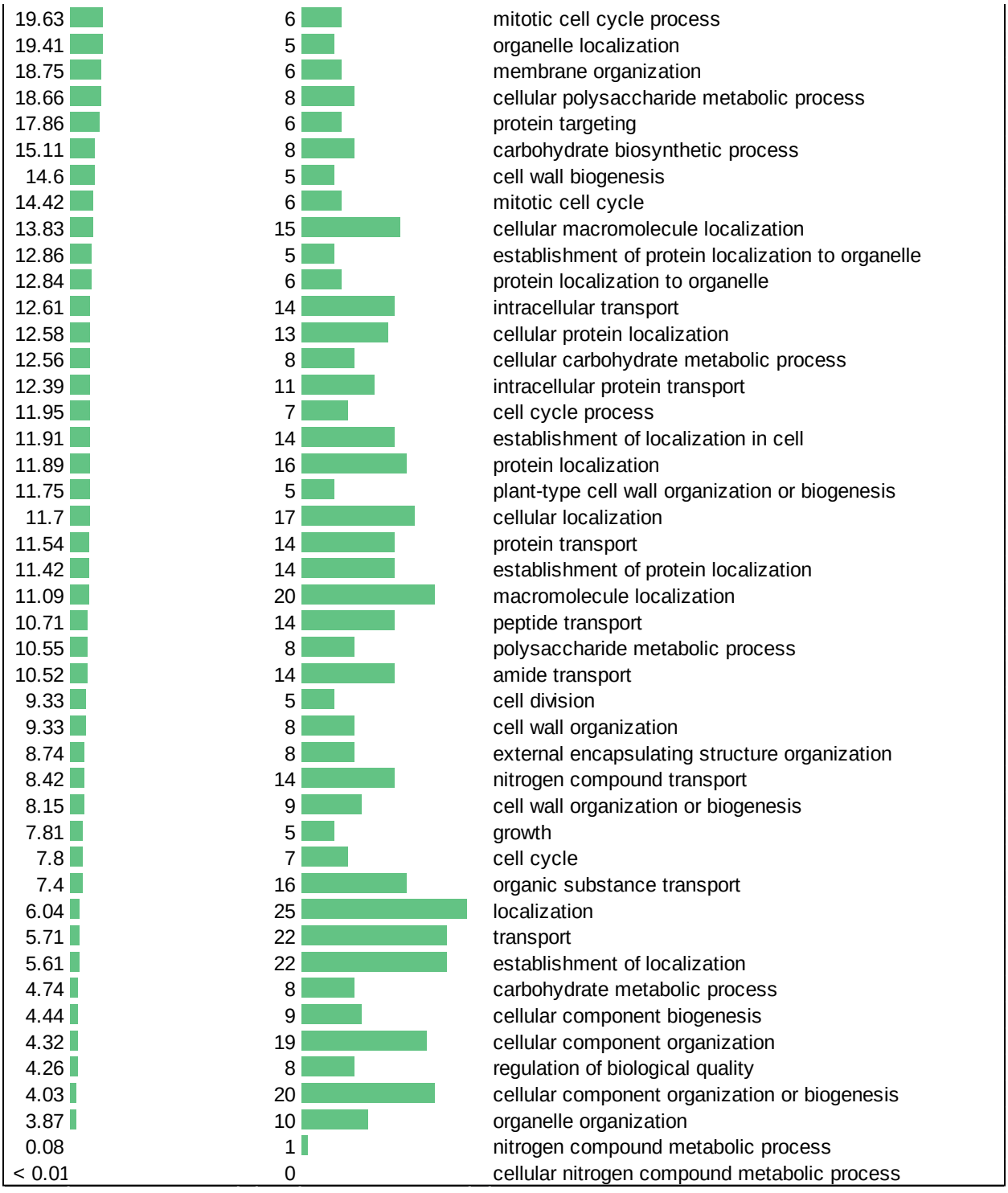

19.63	6	mitotic cell cycle process
19.41	5	organelle localization
18.75	6	membrane organization
18.66	8	cellular polysaccharide metabolic process
17.86	6	protein targeting
15.11	8	carbohydrate biosynthetic process
14.6	5	cell wall biogenesis
14.42	6	mitotic cell cycle
13.83	15	cellular macromolecule localization
12.86	5	establishment of protein localization to organelle
12.84	6	protein localization to organelle
12.61	14	intracellular transport
12.58	13	cellular protein localization
12.56	8	cellular carbohydrate metabolic process
12.39	11	intracellular protein transport
11.95	7	cell cycle process
11.91	14	establishment of localization in cell
11.89	16	protein localization
11.75	5	plant-type cell wall organization or biogenesis
11.7	17	cellular localization
11.54	14	protein transport
11.42	14	establishment of protein localization
11.09	20	macromolecule localization
10.71	14	peptide transport
10.55	8	polysaccharide metabolic process
10.52	14	amide transport
9.33	5	cell division
9.33	8	cell wall organization
8.74	8	external encapsulating structure organization
8.42	14	nitrogen compound transport
8.15	9	cell wall organization or biogenesis
7.81	5	growth
7.8	7	cell cycle
7.4	16	organic substance transport
6.04	25	localization
5.71	22	transport
5.61	22	establishment of localization
4.74	8	carbohydrate metabolic process
4.44	9	cellular component biogenesis
4.32	19	cellular component organization
4.26	8	regulation of biological quality
4.03	20	cellular component organization or biogenesis
3.87	10	organelle organization
0.08	1	nitrogen compound metabolic process
< 0.01	0	cellular nitrogen compound metabolic process

REFERENCES

Albert, I., Böhm, H., Albert, M., Feiler, C.E., Imkampe, J., Wallmeroth, N., Brancato, C., Raaymakers, T.M., Oome, S., Zhang, H., Krol, E., Grefen, C., Gust, A.A., Chai, J., Hedrich, R., Van Den Ackerveken, G., and Nürnberger, T. (2015). An RLP23-SOBIR1-BAK1 complex mediates NLP-triggered immunity. Nat. Plants **1**: 1–30.

Alvim Kamei, C.L., Boruc, J., Vandepoele, K., Van den Daele, H., Maes, S., Russinova, E., Inze, D., and De Veylder, L. (2008). The *PRA1* Gene Family in Arabidopsis. Plant Physiol. **147**: 1735–1749.

An, Q., Hückelhoven, R., Kogel, K.H., and van Bel, A.J.E. (2006). Multivesicular bodies participate in a cell wall-associated defence response in barley leaves attacked by the pathogenic powdery mildew fungus. Cell. Microbiol. **8**: 1009–1019.

Asaoka, R., Uemura, T., Ito, J., Fujimoto, M., Ito, E., Ueda, T., and Nakano, A. (2013). Arabidopsis RABA1 GTPases are involved in transport between the *trans*-Golgi network and the plasma membrane, and are required for salinity stress tolerance. Plant J. **73**: 240–249.

Assaad, F.F., Qiu, J., Youngs, H., Ehrhardt, D., Zimmerli, L., Kalde, M., Wanner, G., Peck, S.C., Edwards, H., Ramonell, K., Somerville, C.R., and Thordal-christensen, H. (2004). The PEN1 syntaxin defines a novel cellular compartment assembly of papillae. Am. Soc. Cell Biol. **15**: 5118–5129.

Austin, A.T. and Ballaré, C.L. (2014). Plant interactions with other organisms: molecules, ecology and evolution. New Phytol. **204**: 257-260.

Axtell, M.J. and Staskawicz, B.J. (2003). Initiation of RPS2-specified disease resistance in Arabidopsis is coupled to the AvrRpt2-directed elimination of RIN4. Cell **112**: 369–377.

Aznar, A., Chen, N.W.G., Rigault, M., Riache, N., Joseph, D., Desmaele, D., Mouille, G., Boutet, S., Soubigou-Taconnat, L., Renou, J.-P., Thomine, S., Expert, D., and Dellagi, A. (2014). Scavenging iron: a novel mechanism of plant immunity activation by microbial siderophores. Plant Physiol. **164**: 2167–2183.

Bar, M. and Avni, A. (2009a). EHD2 inhibits ligand-induced endocytosis and signaling of the leucine-rich repeat receptor-like protein *Le*Eix2. Plant J. **59**: 600–611.

Bar, M. and Avni, A. (2009b). EHD2 inhibits signaling of leucine rich repeat receptor-like proteins. Plant Signal. Behav. **4**: 682–684.

Bashline, L., Li, S., Anderson, C.T., Lei, L., and Gu, Y. (2013). The endocytosis of cellulose synthase in Arabidopsis is dependent on µ2, a clathrin-mediated endocytosis adaptin. Plant Physiol. **163**: 150–160.

Beck, M., Heard, W., Mbengue, M., and Robatzek, S. (2012a). The INs and OUTs of pattern recognition receptors at the cell surface. Curr. Opin. Plant Biol. **15**: 367–374.

Beck, M., Zhou, J., Faulkner, C., MacLean, D., and Robatzek, S. (2012b). Spatio-temporal cellular dynamics of the Arabidopsis flagellin receptor reveal activation status-dependent endosomal sorting. Plant Cell **24**: 4205–4219.

Bednarek, P., Kwon, C., and Schulze-Lefert, P. (2010). Not a peripheral issue: Secretion in plant-microbe interactions. Curr. Opin. Plant Biol. **13**: 378–387.

Bednarek, P., Piślewska-Bednarek, M., Svatoš, A., Schneider, B., Doubský, J., Mansurova, M., Humphry, M., Consonni, C., Panstruga, R., Sanchez-Vallet, A., Molina, A., and Schulze-Lefert, P. (2009). A glucosinolate metabolism pathway in living plant cells mediates broad-spectrum

antifungal defense. Science **323**: 101–106.

Bendahmane, A., Farnham, G., Moffett, P., and Baulcombe, D.C. (2002). Constitutive gain-of-function mutants in a nucleotide binding site-leucine rich repeat protein encoded at the *Rx* locus of potato. Plant J. **32**: 195–204.

Benedetti, M., Verrascina, I., Pontiggia, D., Locci, F., Mattei, B., De Lorenzo, G., and Cervone, F. (2018). Four Arabidopsis berberine bridge enzyme-like proteins are specific oxidases that inactivate the elicitor-active oligogalacturonides. Plant J. **94**: 260-273.

Benschop, J.J., Mohammed, S., O'Flaherty, M., Heck, A.J.R., Slijper, M., and Menke, F.L.H. (2007). quantitative phosphoproteomics of early elicitor signaling in Arabidopsis. Mol. Cell. Proteomics **6**: 1198–1214.

Bent, A. (2006). *Arabidopsis thaliana* floral dip transformation method. Methods Mol. Biol. **343**: 87–103.

Berkey, R., Zhang, Y., Ma, X., King, H., Zhang, Q., Wang, W., and Xiao, S. (2017). Homologues of the RPW8 resistance protein are localized to the extrahaustorial membrane that is likely synthesized de novo. Plant Physiol. **173**: 600–613.

Bhat, R.A., Miklis, M., Schmelzer, E., Schulze-Lefert, P., and Panstruga, R. (2005). Recruitment and interaction dynamics of plant penetration resistance components in a plasma membrane microdomain. Proc. Natl. Acad. Sci. **102**: 3135–3140.

Birkenbihl, R.P., Kracher, B., and Somssich, I.E. (2017). Induced genome-wide binding of three Arabidopsis WRKY transcription factors during early MAMP-triggered immunity. Plant Cell **29**: 20–38.

Bleckmann, A., Weidtkamp-Peters, S., Seidel, C.A.M., and Simon, R. (2010). Stem cell signaling in Arabidopsis requires CRN to localize CLV2 to the plasma membrane. Plant Physiol. **152**: 166-76.

Boch, J., Joardar, V., Gao, L., Robertson, T.L., Lim, M., and Kunkel, B.N. (2002). Identification of *Pseudomonas syringae* pv. *tomato* genes induced during infection of *Arabidopsis thaliana*. Mol. Microbiol. **44**: 73-88.

Boevink, P.C. (2017). Exchanging missives and missiles: the roles of extracellular vesicles in plant–pathogen interactions. J. Exp. Bot. **68**: 5411–5414.

Boller, T. and Felix, G. (2009). A renaissance of elicitors: perception of microbe-associated molecular patterns and danger signals by pattern-recognition receptors. Annu. Rev. Plant Biol. **60**: 379-406.

Bonardi, V., Tang, S., Stallmann, A., Roberts, M., Cherkis, K., and Dangl, J.L. (2011). Expanded functions for a family of plant intracellular immune receptors beyond specific recognition of pathogen effectors. Proc. Natl. Acad. Sci. **108**: 16463–16468.

Bonifacino, J.S. and Glick, B.S. (2004). The mechanisms of vesicle budding and fusion. Cell **116**: 153–166.

Borhan, M.H., Gunn, N., Cooper, A., Gulden, S., Tör, M., Rimmer, S.R., and Holub, E.B. (2008). *WRR4* Encodes a TIR-NB-LRR protein that confers broad-spectrum white rust resistance in *Arabidopsis thaliana* to four physiological races of *Albugo candida*. **21**: 757–768.

Borner, G.H.H., Sherrier, D.J., Weimar, T., Michaelson, L. V, Hawkins, N.D., Macaskill, A., Napier, J.A., Beale, M.H., Lilley, K.S., and Dupree, P. (2005). Analysis of detergent-resistant membranes in Arabidopsis. Evidence for plasma membrane lipid rafts. Plant Physiol. **137**: 104–116.

Bos, J.I.B., Armstrong, M.R., Gilroy, E.M., Boevink, P.C., Hein, I., Taylor, R.M., Zhendong, T., Engelhardt, S., Vetukuri, R.R., Harrower, B., Dixelius, C., Bryan, G., Sadanandom, A.,

Whisson, S.C., Kamoun, S., and Birch, P.R.J. (2010). *Phytophthora infestans* effector AVR3a is essential for virulence and manipulates plant immunity by stabilizing host E3 ligase CMPG1. Proc. Natl. Acad. Sci. **107**: 9909–9914.

Bourdais, G., Burdiak, P., Gauthier, A., Nitsch, L., Salojärvi, J., Rayapuram, C., Idänheimo, N., Hunter, K., Kimura, S., Merilo, E., Vaattovaara, A., Oracz, K., Kaufholdt, D., Pallon, A., Anggoro, D.T., Glów, D., Lowe, J., Zhou, J., Mohammadi, O., Puukko, T., Albert, A., Lang, H., Ernst, D., Kollist, H., Brosché, M., Durner, J., Borst, JW., Collinge, D.B. Karpiński, S. Lyngkjær, M.F. Robatzek, S. Wrzaczek, M. Kangasjärvi, J., CRK Consortium. (2015). Large-scale phenomics identifies primary and fine-tuning roles for CRKs in responses related to oxidative stress. PLoS Genet. **11**: e1005373

Boutrot, F. and Zipfel, C. (2017). Function, discovery, and exploitation of plant pattern recognition receptors for broad-spectrum disease resistance. Annu. Rev. Phytopathol. **55**: 257–286.

Bozkurt, T.O., Belhaj, K., Dagdas, Y.F., Chaparro-Garcia, A., Wu, C.H., Cano, L.M., and Kamoun, S. (2015). Rerouting of plant late endocytic trafficking toward a pathogen interface. Traffic **16**: 204–226.

Bozkurt, T.O., Schornack, S., Win, J., Shindo, T., Ilyas, M., Oliva, R., Cano, L.M., Jones, A.M.E., Huitema, E., van der Hoorn, R.A.L., and Kamoun, S. (2011). *Phytophthora infestans* effector AVRblb2 prevents secretion of a plant immune protease at the haustorial interface. Proc. Natl. Acad. Sci. **108**: 20832–20837.

Brading, P.A., Hammond-Kosack, K.E., Parr, A., and Jones, J.D.G. (2000). Salicylic acid is not required for Cf-2- and Cf-9-dependent resistance of tomato to *Cladosporium fulvum*. Plant J. **23**: 305-18.

Brandizzi, F. and Barlowe, C. (2013). Organization of the ER-Golgi interface for membrane traffic control. Nat. Rev. Mol. Cell Biol. **14**: 382–392.

Bringmann, M., Landrein, B., Schudoma, C., Hamant, O., Hauser, M.T., and Persson, S. (2012). Cracking the elusive alignment hypothesis: The microtubule-cellulose synthase nexus unraveled. Trends Plant Sci. **17**: 666–674.

Brumell, J.H. and Scidmore, M.A. (2007). Manipulation of Rab GTPase function by intracellular bacterial pathogens. Microbiol. Mol. Biol. Rev. **71**: 636–652.

Buono, R.A., Leier, A., Paez-Valencia, J., Pennington, J., Goodman, K., Miller, N., Ahlquist, P., Marquez-Lago, T.T., and Otegui, M.S. (2017). ESCRT-mediated vesicle concatenation in plant endosomes. J. Cell Biol. **216**: 2167–2177.

Van den Burg, H.A., Harrison, S.J., Joosten, M.H.A.J., Vervoort, J., and de Wit, P.J.G.M. (2006). *Cladosporium fulvum* Avr4 protects fungal cell walls against hydrolysis by plant chitinases accumulating during infection. Mol. Plant-Microbe Interact. **19**: 1420–1430.

Van Den Burg, H.A., Spronk, C.A.E.M., Boeren, S., Kennedy, M.A., Vissers, J.P.C., Vuister, G.W., De Wit, P.J.G.M., and Vervoort, J. (2004). Binding of the AVR4 elicitor of *Cladosporium fulvum* to chitotriose units is facilitated by positive allosteric protein-protein interactions: The chitin-binding site of AVR4 represents a novel binding site on the folding scaffold shared between the invertebrate and the plant chitin-binding domain. J. Biol. Chem. **279**: 16786–16796.

van den Burg, H.A., Tsitsigiannis, D.I., Rowland, O., Lo, J., Rallapalli, G., MacLean, D., Takken, F.L.W., and Jones, J.D.G. (2008). The F-Box protein ACRE189/ACIF1 regulates cell death and defense responses activated during pathogen recognition in tobacco and tomato. Plant Cell **20**: 697–719.

Van den Burg, H.A., Westerink, N., Francoijs, K.J., Roth, R., Woestenenk, E., Boeren, S., De Wit,

P.J.G.M., Joosten, M.H.A.J., and Vervoort, J. (2003). Natural disulfide bond-disrupted mutants of AVR4 of the tomato pathogen *Cladosporium fulvum* are sensitive to proteolysis, circumvent Cf-4-mediated resistance, but retain their chitin binding ability. J. Biol. Chem. **278**: 27340–27346.

Burow, M. and Halkier, B.A. (2017). How does a plant orchestrate defense in time and space? Using glucosinolates in Arabidopsis as case study. Curr. Opin. Plant Biol. **38**: 142–147.

Burr, C.A., Leslie, M.E., Orlowski, S.K., Chen, I., Wright, C.E., Daniels, M.J., and Liljegren, S.J. (2011). CASTAWAY, a membrane-associated receptor-like kinase, inhibits organ abscission in Arabidopsis. Plant Physiol. **156**: 1837–1850.

Büschges, R., Hollricher, K., Panstruga, R., Simons, G., Wolter, M., Frijters, A., van Daelen, R., van der Lee, T., Diergaarde, P., Groenendijk, J., Töpsch, S., Vos, P., Salamini, F., and Schulze-Lefert, P. (1997). The barley *Mlo* gene: a novel control element of plant pathogen resistance. Cell **88**: 695–705.

Cai, H., Yu, S., Menon, S., Cai, Y., Lazarova, D., Fu, C., Reinisch, K., Hay, J.C., and Ferro-Novick, S. (2007). TRAPPI tethers COPII vesicles by binding the coat subunit Sec23. Nature **445**: 941–944.

Cai, Q., Cai, Q., Qiao, L., Wang, M., He, B., Lin, F., Palmquist, J., Huang, H., and Jin, H. (2018). Plants send small RNAs in extracellular vesicles to fungal pathogen to silence virulence genes. Science **360**: 1126-1129.

Campe, R., Langenbach, C., Leissing, F., Popescu, G. V., Popescu, S.C., Goellner, K., Beckers, G.J.M., and Conrath, U. (2016). ABC transporter PEN3/PDR8/ABCG36 interacts with calmodulin that, like PEN3, is required for Arabidopsis nonhost resistance. New Phytol. **209**: 294–306.

Cao, Y., Liang, Y., Tanaka, K., Nguyen, C.T., Jedrzejczak, R.P., Joachimiak, A., and Stacey, G. (2014). The kinase LYK5 is a major chitin receptor in Arabidopsis and forms a chitin-induced complex with related kinase CERK1. Elife. 03766

Cao, Y., Tang, X., Giovannoni, J., Xiao, F., and Liu, Y. (2012). Functional characterization of a tomato *COBRA*-like gene functioning in fruit development and ripening. BMC Plant Biol. **12**: 211

Carter, C. (2004). The vegetative vacuole proteome of *Arabidopsis thaliana* reveals predicted and unexpected proteins. Plant Cell **16**: 3285–3303.

Century, K.S., Shapiro, A.D., Repetti, P.P., Dahlbeck, D., Holub, E., and Staskawicz, B.J. (1997). NDR1, a pathogen-induced component required for Arabidopsis disease resistance. Science. **278**: 1963-1965.

Cesari, S., Bernoux, M., Moncuquet, P., Kroj, T., and Dodds, P.N. (2014). A novel conserved mechanism for plant NLR protein pairs: the "integrated decoy" hypothesis. Front. Plant Sci. **5**: 1–11.

Chaparro-Garcia, A., Schwizer, S., Sklenar, J., Yoshida, K., Petre, B., Bos, J.I.B., Schornack, S., Jones, A.M.E., Bozkurt, T.O., and Kamoun, S. (2015). *Phytophthora infestans* RXLR-WY effector AVR3a associates with dynamin-related protein 2 required for endocytosis of the plant pattern recognition receptor FLS2. PLoS One **10**: 1–27.

Chatre, L., Brandizzi, F., Hocquellet, A., Hawes, C., and Moreau, P. (2005). Sec22 and Memb11 are v-SNAREs of the anterograde endoplasmic reticulum-Golgi pathway in tobacco leaf epidermal cells. Plant Physiol. **139**: 1244–1254.

Chen, N., Hsiang, T., and Goodwin, P.H. (2003). Use of green fluorescent protein to quantify the growth of Colletotrichum during infection of tobacco. J. Microbiol. Methods **53**: 113–122.

Chen, X.-Y., Liu, L., Lee, E., Han, X., Rim, Y., Chu, H., Kim, S.-W., Sack, F., and Kim, J.-Y. (2009). The Arabidopsis callose synthase gene *GSL8* is required for cytokinesis and cell patterning. Plant

Physiol. **150**: 105–113.

Chinchilla, D., Shan, L., He, P., de Vries, S., and Kemmerling, B. (2009). One for all: the receptor-associated kinase BAK1. Trends Plant Sci. **14**: 535-41.

Chinchilla, D., Zipfel, C., Robatzek, S., Kemmerling, B., Nürnberger, T., Jones, J.D.G., Felix, G., and Boller, T. (2007). A flagellin-induced complex of the receptor FLS2 and BAK1 initiates plant defence. Nature. **448**: 467-500.

Choi, H., Larsen, B., Lin, Z., Breitkreutz, A., Fermin, D., Qin, Z.S., and Tyers, M. (2011). SAINT: probabilistic scoring of affinity purification-mass spectrometry data. Nature Methods. **8**: 70–73.

Choi, H.W. and Klessig, D.F. (2016). DAMPs, MAMPs, and NAMPs in plant innate immunity. BMC Plant Biol. **1**: 232

Choi, S.W., Tamaki, T., Ebine, K., Uemura, T., Ueda, T., and Nakano, A. (2013). RABA members act in distinct steps of subcellular trafficking of the FLAGELLIN SENSING2 receptor. Plant Cell **25**: 1174–1187.

Clay, N.K., Adio, A.M., Denoux, C., Jander, G., and Ausubel, F.M. (2009). Glucosinolate metabolites required for an Arabidopsis innate immune response. Science **323**: 95–101.

Collier, S.M., Hamel, L.-P., and Moffett, P. (2011). Cell death mediated by the N-terminal domains of a unique and highly conserved class of NB-LRR protein. Mol. Plant-Microbe Interact. **24**: 918–931.

Collings, D.A., Gebbie, L.K., Howles, P.A., Hurley, U.A., Birch, R.J., Cork, A.H., Hocart, C.H., Arioli, T., and Williamson, R.E. (2008). Arabidopsis dynamin-like protein DRP1A: A null mutant with widespread defects in endocytosis, cellulose synthesis, cytokinesis, and cell expansion. J. Exp. Bot. **2**: 361-76.

Collins, N.C., Thordal-Christensen, H., Lipka, V., Bau, S., Kombrink, E., Qiu, J.L., Hückelhoven, R., Steins, M., Freialdenhoven, A., Somerville, S.C., and Schulze-Lefert, P. (2003). SNARE-protein-mediated disease resistance at the plant cell wall. Nature **425**: 973–977.

Consonni, C., Humphry, M.E., Hartmann, H.A., Livaja, M., Durner, J., Westphal, L., Vogel, J., Lipka, V., Kemmerling, B., Schulze-Lefert, P., Somerville, S.C., and Panstruga, R. (2006). Conserved requirement for a plant host cell protein in powdery mildew pathogenesis. Nat. Genet. **38**: 716–720.

Cook, D.E., Mesarich, C.H., and Thomma, B.P.H.J. (2015). Understanding plant immunity as a surveillance system to detect invasion. Annu. Rev. Phytopathol. **53**: 541-63.

Crowell, E.F., Bischoff, V., Desprez, T., Rolland, A., Stierhof, Y.-D., Schumacher, K., Gonneau, M., Hofte, H., and Vernhettes, S. (2009). Pausing of Golgi bodies on microtubules regulates secretion of cellulose synthase complexes in Arabidopsis. Plant Cell **21**: 1141–1154.

Cui, F., Wu, H., Safronov, O., Zhang, P., Kumar, R., Kollist, H., Salojärvi, J., Panstruga, R., and Overmyer, K. (2018). Arabidopsis MLO2 is a negative regulator of sensitivity to extracellular reactive oxygen species. Plant Cell Environ. **41**: 782–796.

Cui, X., Lu, F., Li, Y., Xue, Y., Kang, Y., Zhang, S., Qiu, Q., Cui, X., Zheng, S., Liu, B., Xu, X., and Cao, X. (2013). Ubiquitin-specific proteases UBP12 and UBP13 act in circadian clock and photoperiodic flowering regulation in Arabidopsis. Plant Physiol. **162**: 897–906.

Cui, Y., Zhao, Q., Gao, C., Ding, Y., Zeng, Y., Ueda, T., Nakano, A., and Jiang, L. (2014a). Activation of the Rab7 GTPase by the MON1-CCZ1 complex is essential for PVC-to-vacuole trafficking and plant growth in Arabidopsis. Plant Cell **26**: 2080–2097.

Daniel, B., Pavkov-Keller, T., Steiner, B., Dordic, A., Gutmann, A., Nidetzky, B., Sensen, C.W., Van

Der Graaff, E., Wallner, S., Gruber, K., and Macheroux, P. (2015). Oxidation of monolignols by members of the berberine bridge enzyme family suggests a role in plant cell wall metabolism. J. Biol. Chem. **290**: 18770–18781.

Daskalov, A., Habenstein, B., Sabaté, R., Berbon, M., Martinez, D., Chaignepain, S., Coulary-Salin, B., Hofmann, K., Loquet, A., and Saupe, S.J. (2016). Identification of a novel cell death-inducing domain reveals that fungal amyloid-controlled programmed cell death is related to necroptosis. Proc. Natl. Acad. Sci. **113**: 2720–2725.

Dean, R., Van Kan, J.A.L., Pretorius, Z.A., Hammond-Kosack, K.E., Di Pietro, A., Spanu, P.D., Rudd, J.J., Dickman, M., Kahmann, R., Ellis, J., and Foster, G.D. (2012). The Top 10 fungal pathogens in molecular plant pathology. Mol. Plant Pathol. **4**: 414-30

Denoux, C., Galletti, R., Mammarella, N., Gopalan, S., Werck, D., De Lorenzo, G., Ferrari, S., Ausubel, F.M., and Dewdney, J. (2008). Activation of defense response pathways by OGs and Flg22 elicitors in Arabidopsis seedlings. Mol. Plant. **3**: 423-45

Dettmer, J., Hong-Hermesdorf, A., Stierhof, Y.-D., and Schumacher, K. (2006). Vacuolar H+-ATPase activity is required for endocytic and secretory trafficking in Arabidopsis. Plant Cell **18**: 715–730.

Dittgen, J., Sa, C., Hou, B., Molina, A., Schulze-lefert, P., Lipka, V., Somerville, S., Stein, M., Dittgen, J., Sánchez-Rodríguez, C., Hou, B., Molina, A., Schulze-lefert, P., Lipka, V., and Somerville, S. (2006). Arabidopsis PEN3/PDR8, an ATP binding cassette transporter, contributes to nonhost resistance to inappropriate pathogens that enter by direct penetration. Plant Cell **18**: 731–746.

Dixon, M.S., Jones, D.A., Keddie, J.S., Thomas, C.M., Harrison, K., and Jones, J.D.G. (1996). The tomato *Cf-2* disease resistance locus comprises two functional genes encoding leucine-rich repeat proteins. Cell **84**: 451–459.

Van der Does, D., Boutrot, F., Engelsdorf, T., Rhodes, J., McKenna, J., Vernhettes, S., Koevoets, I., Tintor, N., Veerabagu, M., Miedes, E., Segonzac, C., Roux, M., Breda, A., Hardtke, C., Molina, A., Rep, M., Testering, C., Mouille, G., Höfte, H., Hamann, T., Zipfel, C. (2017). The Arabidopsis leucine-rich repeat receptor kinase MIK2/LRR-KISS connects cell wall integrity sensing, root growth and response to abiotic and biotic stresses. PLoS Genet. **13**: 1–27.

Domazakis, E., Wouters, D., Visser, R.G.F., Kamoun, S., Joosten, M.H.A.J., and Vleeshouwers, V.G.A.A. (2018). The ELR-SOBIR1 complex functions as a two-component receptor-like kinase to mount defense against *Phytophthora infestans*. Mol. Plant-Microbe Interact. **8**: 795–802.

Domínguez-Ferreras, A., Kiss-Papp, M., Jehle, A.K., Felix, G., and Chinchilla, D. (2015). An overdose of the arabidopsis coreceptor BRASSINOSTEROID INSENSITIVE1-ASSOCIATED RECEPTOR KINASE1 or its ectodomain causes autoimmunity in a SUPPRESSOR OF BIR1-1-dependent manner. Plant Physiol. **168**: 1106–1121.

Donaldson, J.G. and Jackson, C.L. (2000). Regulators and effectors of the ARF GTPases. Curr. Opin. Cell Biol. **12**: 475–482.

Dong, O.X., Tong, M., Bonardi, V., El Kasmi, F., Woloshen, V., Wünsch, L.K., Dangl, J.L., and Li, X. (2016). TNL-mediated immunity in Arabidopsis requires complex regulation of the redundant *ADR1* gene family. New Phytol. **210**: 960–973.

Dong, X., Hong, Z., Sivaramakrishnan, M., Mahfouz, M., and Verma, D.P.S. (2005). Callose synthase (CalS5) is required for exine formation during microgametogenesis and for pollen viability in Arabidopsis. Plant J. **42**: 315–328.

Downie, J.A. (2014). Legume nodulation. Curr. Biol. **24**: 184–190.

Drakakaki, G., Van De Ven, W., Pan, S., Miao, Y., Wang, J., Keinath, N.F., Weatherly, B., Jiang, L., Schumacher, K., Hicks, G., and Raikhel, N. (2012). Isolation and proteomic analysis of the SYP61 compartment reveal its role in exocytic trafficking in Arabidopsis. Cell Res. **22**: 413–424.

Du, J., Verzaux, E., Chaparro-Garcia, A., Bijsterbosch, G., Keizer, L.C.P., Zhou, J., Liebrand, T.W.H., Xie, C., Govers, F., Robatzek, S., Van Der Vossen, E.A.G., Jacobsen, E., Visser, R.G.F., Kamoun, S., and Vleeshouwers, V.G.A.A. (2015). Elicitin recognition confers enhanced resistance to *Phytophthora infestans* in potato. Nat. Plants **1**: 1–29.

Du, Y., Tejos, R., Beck, M., Himschoot, E., Li, H., Robatzek, S., Vanneste, S., and Friml, J. (2013). Salicylic acid interferes with clathrin-mediated endocytic protein trafficking. Proc. Natl. Acad. Sci. **110**: 7946-51.

Dubiella, U., Seybold, H., Durian, G., Komander, E., Lassig, R., Witte, C.-P., Schulze, W.X., and Romeis, T. (2013). Calcium-dependent protein kinase/NADPH oxidase activation circuit is required for rapid defense signal propagation. Proc. Natl. Acad. Sci. **110**: 8744–8749.

Ebine, K., Fujimoto, M., Okatani, Y., Nishiyama, T., Goh, T., Ito, E., Dainobu, T., Nishitani, A., Uemura, T., Sato, M.H., Thordal-Christensen, H., Tsutsumi, N., Nakano, A., and Ueda, T. (2011). A membrane trafficking pathway regulated by the plant-specific RAB GTPase ARA6. Nat. Cell Biol. **13**: 853–859.

Ebine, K., Miyakawa, N., Fujimoto, M., Uemura, T., Nakano, A., and Ueda, T. (2012). Endosomal trafficking pathway regulated by ARA6, a RAB5 GTPase unique to plants. Small GTPases. **3**: 23-7.

Ebine, K., Okatani, Y., Uemura, T., Goh, T., Shoda, K., Niihama, M., Morita, M.T., Spitzer, C., Otegui, M.S., Nakano, A., and Ueda, T. (2008). A SNARE complex unique to seed plants is required for protein storage vacuole biogenesis and seed development of Arabidopsis thaliana. Plant Cell **20**: 3006–3021.

Ederli, L., Madeo, L., Calderini, O., Gehring, C., Moretti, C., Buonaurio, R., Paolocci, F., and Pasqualini, S. (2011). The *Arabidopsis thaliana* cysteine-rich receptor-like kinase CRK20 modulates host responses to *Pseudomonas syringae* pv . *tomato* DC3000 infection. J. Plant Physiol. **168**: 1784–1794.

Eisenach, C., Chen, Z., Grefen, C., and Blatt, M.R. (2012). The trafficking protein SYP121 of Arabidopsis connects programmed stomatal closure and K^+ channel activity with vegetative growth. Plant J. **69**: 241–251.

Ellinger, D., Glöckner, A., Koch, J., Naumann, M., Stürtz, V., Schütt, K., Manisseri, C., Somerville, S.C., and Voigt, C. a. (2014). Interaction of the Arabidopsis GTPase RabA4c with its effector PMR4 results in complete penetration resistance to powdery mildew. Plant Cell **26**: 3185–200.

Ellinger, D., Naumann, M., Falter, C., Zwikowics, C., Jamrow, T., Manisseri, C., Somerville, S.C., and Voigt, C.A. (2013). Elevated early callose deposition results in complete penetration resistance to powdery mildew in Arabidopsis. Plant Physiol. **161**: 1433–1444.

Ellinger, D. and Voigt, C.A. (2014). Callose biosynthesis in arabidopsis with a focus on pathogen response: What we have learned within the last decade. Ann. Bot. **114**: 1349–1358.

Ellis, J.G. (2016). Integrated decoys and effector traps: How to catch a plant pathogen. BMC Biol. **14**: 14–16.

Elortza, F., Mohammed, S., Bunkenborg, J., Foster, L.J., Nühse, T.S., Brodbeck, U., Peck, S.C., and Jensen, O.N. (2006). Modification-specific proteomics of plasma membrane proteins: Identification and characterization of glycosylphosphatidylinositol-anchored proteins released upon phospholipase D treatment. J. Proteome Res. **5**: 935–943.

Endler, A. and Persson, S. (2011). Cellulose synthases and synthesis in Arabidopsis. Mol. Plant **4**: 199–211.

Engelhardt, S., Boevink, P.C., Armstrong, M.R., Ramos, M.B., Hein, I., and Birch, P.R.J. (2012). Relocalization of late blight resistance protein R3a to endosomal compartments is associated with effector recognition and required for the immune response. Plant Cell **24**: 5142–5158.

van Esse, H.P., Bolton, M.D., Stergiopoulos, I., de Wit, P.J.G.M., Thomma, B.P.H.J., Esse, H.P. Van, Bolton, M.D., Stergiopoulos, I., Wit, P.J.G.M. De, Thomma, B.P.H.J., van Esse, H.P., Bolton, M.D., Stergiopoulos, I., de Wit, P.J.G.M., and Thomma, B.P.H.J. (2007). The chitin-binding *Cladosporium fulvum* effector protein Avr4 is a virulence factor. Mol. Plant. Microbe. Interact. **20**: 1092–101.

Ewan, R., Pangestuti, R., Thornber, S., Craig, A., Carr, C., O'Donnell, L., Zhang, C., and Sadanandom, A. (2011). Deubiquitinating enzymes AtUBP12 and AtUBP13 and their tobacco homologue NtUBP12 are negative regulators of plant immunity. New Phytol. **191**: 92–106.

Farid, A., Malinovsky, F.G., Veit, C., Schoberer, J., Zipfel, C., and Strasser, R. (2013). Specialized Roles of the conserved subunit OST3/6 of the oligosaccharyltransferase complex in innate immunity and tolerance to abiotic stresses. Plant Physiol. **162**: 24–38.

Felix, G., Duran, J.D., Volko, S., and Boller, T. (1999). Plants have a sensitive perception system for the most conserved domain of bacterial flagellin. Plant J. **18**: 265–276.

Feraru, E., Feraru, M.I., Asaoka, R., Paciorek, T., De Rycke, R., Tanaka, H., Nakano, A., and Friml, J. (2012). BEX5/RabA1b Regulates *trans*-Golgi network-to-plasma membrane protein trafficking in Arabidopsis. Plant Cell **24**: 3074–3086.

Fernández-Chacón, R. and Südhof, T.C. (2000). Novel SCAMPs lacking NPF repeats: ubiquitous and synaptic vesicle-specific forms implicate SCAMPs in multiple membrane-trafficking functions. J. Neurosci. **20**: 7941–7950.

Foresti, O. and Denecke, J. (2008). Intermediate organelles of the plant secretory pathway: Identity and function. Traffic. **9**: 1599-612.

Fradin, E.F., Abd-El-Haliem, A., Masini, L., van den Berg, G.C.M., Joosten, M.H.A.J., and Thomma, B.P.H.J. (2011). Interfamily transfer of tomato *Ve1* Mediates Verticillium resistance in Arabidopsis. PLANT Physiol. **156**: 2255–2265.

Frei dit Frey, N., Mbengue, M., Kwaaitaal, M., Nitsch, L., Altenbach, D., Haweker, H., Lozano-Duran, R., Njo, M.F., Beeckman, T., Huettel, B., Borst, J.W., Panstruga, R., and Robatzek, S. (2012). plasma membrane calcium ATPases are important components of receptor-mediated signaling in plant immune responses and development. Plant Physiol. **159**: 798–809.

Frick, M., Bright, N.A., and Riento, K. (2007). Coassembly of Flotillins induces formation of membrane microdomains, membrane curvature, and vesicle budding. Curr. Biol. **17**: 1151–1156.

Fuchs, R., Kopischke, M., Klapprodt, C., Hause, G., Meyer, A.J., Schwarzländer, M., Fricker, M.D., and Lipka, V. (2015). Immobilized subpopulations of leaf epidermal mitochondria mediate PEN2-dependent pathogen entry control in Arabidopsis. Plant Cell **28**: 130-45.

Furman-Matarasso, N., Cohen, E., Du, Q., Chejanovsky, N., Hanania, U., and Avni, A. (1999). A point mutation in the ethylene-inducing xylanase elicitor inhibits the beta-1-4-endoxylanase activity but not the elicitation activity. Plant Physiol. **121**: 345-51.

Gamir, J., Darwiche, R., van't Hof, P., Choudhary, V., Stumpe, M., Schneiter, R., and Mauch, F. (2017). The sterol-binding activity of PATHOGENESIS-RELATED PROTEIN 1 reveals the mode of action of an antimicrobial protein. Plant J. **89**: 502-509.

Gao, C., Zhuang, X., Shen, J., and Jiang, L. (2017). Plant ESCRT complexes: moving beyond endosomal sorting. Trends Plant Sci. **22**: 986-998.

Gao, M., Wang, X., Wang, D., Xu, F., Ding, X., Zhang, Z., Bi, D., Cheng, Y.T., Chen, S., Li, X., and Zhang, Y. (2009). Regulation of cell death and innate immunity by two receptor-like kinases in Arabidopsis. Cell Host Microbe **6**: 34–44.

Garcia-Guzman, G. and Morales, E. (2007). Life-history strategies of plant pathogens: Distribution patterns and phylogenetic analysis. Ecology **88**: 589-96.

Gasson, M.J. (1980). Indicator technique for antimetabolic toxin production by phytopathogenic species of Pseudomonas. Appl. Environ. Microbiol. **39**: 25-9.

Geldner, N., Dénervaud-Tendon, V., Hyman, D.L., Mayer, U., Stierhof, Y.D., and Chory, J. (2009). Rapid, combinatorial analysis of membrane compartments in intact plants with a multicolor marker set. Plant J. **59**: 169–178.

Gendre, D., Jonsson, K., Boutté, Y., and Bhalerao, R.P. (2015). Journey to the cell surface—the central role of the *trans*-Golgi network in plants. Protoplasma **252**: 385–398.

Gilroy, E.M., Taylor, R.M., Hein, I., Boevink, P., Sadanandom, A., and Birch, P.R.J. (2011). CMPG1-dependent cell death follows perception of diverse pathogen elicitors at the host plasma membrane and is suppressed by *Phytophthora infestans* RXLR effector AVR3a. New Phytol. **190**: 653–666.

Glebov, O.O., Bright, N.A., and Nichols, B.J. (2006). Flotillin-1 defines a clathrin-independent endocytic pathway in mammalian cells. Nat. Cell. Biol. **8**: 46-54.

Goh, T., Uchida, W., Arakawa, S., Ito, E., Dainobu, T., Ebine, K., Takeuchi, M., Sato, K., Ueda, T., and Nakano, A. (2007). VPS9a, the common activator for two distinct types of Rab5 GTPases, Is essential for the development of *Arabidopsis thaliana*. Plant Cell **19**: 3504–3515.

Göhre, V., Spallek, T., Häweker, H., Mersmann, S., Mentzel, T., Boller, T., de Torres, M., Mansfield, J.W., and Robatzek, S. (2008). Plant pattern-recognition receptor FLS2 is directed for degradation by the bacterial ubiquitin ligase AvrPtoB. Curr. Biol. **18**: 1824–1832.

Greenberg, J.T., Silverman, F.P., and Liang, H. (2000). Uncoupling salicylic acid-dependent cell death and defense-related responses from disease resistance in the Arabidopsis mutant *acd5*. Genetics **156**: 341-50.

Grefen, C., Chen, Z., Honsbein, A., Donald, N., Hills, A., and Blatt, M.R. (2010). A novel motif essential for SNARE interaction with the K^+ channel KC1 and channel gating in Arabidopsis. Plant Cell **22**: 3076–3092.

Griffis, A.H.N., Groves, N.R., Zhou, X., and Meier, I. (2014). Nuclei in motion: movement and positioning of plant nuclei in development, signaling, symbiosis, and disease. Front. Plant Sci. **5**: 129.

Groen, A.J., Sancho-Andrés, G., Breckels, L.M., Gatto, L., Aniento, F., and Lilley, K.S. (2014). Identification of *trans*-Golgi network proteins in Arabidopsis thaliana root tissue. J. Proteome Res. **13**: 763–776.

Grosshans, B.L., Ortiz, D., and Novick, P. (2006). Rabs and their effectors: Achieving specificity in membrane traffic. Proc. Natl. Acad. Sci. **103**: 11821-7.

Gruner, K., Zeier, T., Aretz, C., and Zeier, J. (2018). A critical role for Arabidopsis MILDEW RESISTANCE LOCUS O2 in systemic acquired resistance. Plant J. **94**: 1064-1082.

Gu, Y. and Innes, R.W. (2012). The KEEP ON GOING protein of Arabidopsis regulates intracellular

protein trafficking and is degraded during fungal infection. Plant Cell. **24**: 4717-30.

Gubert, C.M. and Liljegren, S.J. (2014). HAESA and HAESA-LIKE2 activate organ abscission downstream of NEVERSHED and EVERSHED in Arabidopsis flowers. Plant Signal. Behav. **9**: e29115.

Gust, A.A. and Felix, G. (2014). Receptor like proteins associate with SOBIR1-type of adaptors to form bimolecular receptor kinases. Curr. Opin. Plant Biol. **21**: 104–111.

Hammond-Kosack, K.E. and Kanyuka, K. (2007). Resistance genes (R genes) in plants. Encycl. Life Sci.

Haney, C.H., Riely, B.K., Tricoli, D.M., Cook, D.R., Ehrhardt, D.W., and Long, S.R. (2011). Symbiotic rhizobia bacteria trigger a change in localization and dynamics of the *Medicago truncatula* receptor kinase LYK3. Plant Cell **23**: 2774–2787.

Häweker, H., Rips, S., Koiwa, H., Salomon, S., Saijo, Y., Chinchilla, D., Robatzek, S., and Von Schaewen, A. (2010). Pattern recognition receptors require N-glycosylation to mediate plant immunity. J. Biol. Chem. **285**: 4629–4636.

He, Q., McLellan, H., Boevink, P.C., Sadanandom, A., Xie, C., Birch, P.R.J., and Tian, Z. (2015). U-box E3 ubiquitin ligase PUB17 acts in the nucleus to promote specific immune pathways triggered by *Phytophthora infestans*. J. Exp. Bot. **66**: 3189–3199.

Heard, W., Sklenář, J., Tomé, D.F.A., Robatzek, S., and Jones, A.M.E. (2015). Identification of regulatory and cargo proteins of endosomal and secretory pathways in *Arabidopsis thaliana* by proteomic dissection. Mol. Cell. Proteomics **14**: 1796–813.

Heese, A., Hann, D.R., Gimenez-ibanez, S., Jones, A.M.E., He, K., Li, J., Schroeder, J.I., Peck, S.C., Rathjen, J.P., and Kinase, R. (2007). The receptor-like kinase SERK3/BAK1 is a central regulator of innate immunity in plants. Proc. Natl. Acad. Sci. **104**: 12217–12222.

Hegenauer, V., Fürst, U., Kaiser, B., Smoker, M., Zipfel, C., Felix, G., Stahl, M., and Albert, M. (2016). Detection of the plant parasite *Cuscuta reflexa* by a tomato cell surface receptor. Science **353**: 478–481.

Henderson, S.W., Wege, S., Qiu, J., Blackmore, D.H., Walker, A.R., Tyerman, S., Walker, R.R., and Gilliham, M. (2015). Grapevine and Arabidopsis cation-chloride cotransporters localise to the Golgi and *trans*-Golgi network and indirectly influence long-distance ion homeostasis and plant salt tolerance. Plant Physiol. **169**: 2215-29.

Heucken, N. and Ivanov, R. (2017). The retromer, sorting nexins and the plant endomembrane protein trafficking. J. Cell Sci. **131**.

Ho, C.M.K., Paciorek, T., Abrash, E., and Bergmann, D.C. (2016). Modulators of stomatal lineage signal transduction alter membrane contact sites and reveal specialization among ERECTA kinases. Dev. Cell **38**: 345–357.

Holsters, M., Silva, B., Van Vliet, F., Genetello, C., De Block, M., Dhaese, P., Depicker, A., Inzé, D., Engler, G., Villarroel, R., Van Montagu, M., and Schell, J. (1980). The functional organization of the nopaline *A. tumefaciens* plasmid pTiC58. Plasmid **3**: 212–230.

Honsbein, A., Sokolovski, S., Grefen, C., Campanoni, P., Paneque, M., Chen, Z., Johansson, I., and Blatt, M.R. (2009). A tripartite SNARE-K^+ channel complex mediates in channel-dependent K^+ nutrition in Arabidopsis. **21**: 2859–2877.

Van der Hoorn, R.A.L. (2001). Identification of distinct specificity determinants in resistance protein Cf-4 allows construction of a Cf-9 mutant that confers recognition of avirulence protein AVR4. Plant Cell

13: 273–285.

Huang, L., Chen, X.Y., Rim, Y., Han, X., Cho, W.K., Kim, S.W., and Kim, J.Y. (2009). Arabidopsis glucan synthase-like 10 functions in male gametogenesis. J. Plant Physiol. **166**: 344–352.

Husebye, H., Halaas, Ø., Stenmark, H., Tunheim, G., Sandanger, Ø., Bogen, B., Brech, A., Latz, E., and Espevik, T. (2006). Endocytic pathways regulate Toll-like receptor 4 signaling and link innate and adaptive immunity. EMBO J. **25**: 683–692.

Imkampe, J., Halter, T., Huang, S., Schulze, S., Mazzotta, S., Schmidt, N., Manstretta, R., Postel, S., Wierzba, M., Yang, Y., van Dongen W.M.A.M., Stahl, M., Zipfel, C., Goshe, M.B., Clouse, S., de Vries, S.C., Tax, F., Wang, X., Kemmerling, B. (2017). The Arabidopsis Leucine-rich repeat receptor kinase BIR3 negatively regulates BAK1 receptor complex formation and stabilizes BAK1. Plant Cell **29**: 2285-2303.

Inada, N., Betsuyaku, S., Shimada, T.L., Ebine, K., Ito, E., Kutsuna, N., Hasezawa, S., Takano, Y., Fukuda, H., Nakano, A., and Ueda, T. (2016). Modulation of plant RAB GTPase-mediated membrane trafficking pathway at the interface between plants and obligate biotrophic pathogens. Plant Cell Physiol. **57**: 1854–1864.

Ishiga, Y., Takeuchi, K., Taguchi, F., Inagaki, Y., Toyoda, K., Shiraishi, T., and Ichinose, Y. (2005). Defense responses of *Arabidopsis thaliana* inoculated with *Pseudomonas syringae* pv. *tabaci* wild type and defective mutants for flagellin (ΔfliC) and flagellin-glycosylation (Δorf1). J. Gen. Plant Pathol. **71**: 302–307.

Ito, E., Ebine, K., Choi, S., and Ichinose, S. (2018). Integration of two RAB5 groups during endosomal transport in plants. Elife e34064.

Ito, Y., Toyooka, K., Fujimoto, M., Ueda, T., Uemura, T., and Nakano, A. (2017). The *trans*-Golgi network and the Golgi stacks behave independently during regeneration after Brefeldin-A treatment in tobacco BY-2 cells. Plant Cell Physiol. **58**: 811–821.

Jacobs, A.K., Lipka, V., Burton, R.A., Panstruga, R., Strizhov, N., Schulze-Lefert, P., and Fincher, G.B. (2003). An Arabidopsis callose synthase, GSL5, is required for wound and papillary callose formation. Plant Cell **15**: 2503–2513.

Jarsch, I.K., Konrad, S.S.A., Stratil, T.F., Urbanus, S.L., Szymanski, W., Braun, P., Braun, K.-H., and Ott, T. (2014). Plasma membranes are subcompartmentalized into a plethora of coexisting and diverse microdomains in Arabidopsis and *Nicotiana benthamiana*. Plant Cell **26**: 1698–1711.

Jarsch, I.K. and Ott, T. (2011). Perspectives on remorin proteins, membrane rafts, and their role during plant–microbe interactions. Mol. Plant-Microbe Interact. **24**: 7–12.

Jia, T., Gao, C., Cui, Y., Wang, J., Ding, Y., Cai, Y., Ueda, T., and Nakano, A. (2013). ARA7 (Q69L) expression in transgenic Arabidopsis cells induces the formation of enlarged multivesicular bodies. J. Exp. Bot. **7**: 1–13.

Jiménez-Góngora, T., Kim, S.-K., Lozano-Durán, R., and Zipfel, C. (2015). Flg22-triggered immunity negatively regulates key BR biosynthetic genes. Front. Plant Sci. **6**: 981.

Jonge, R. De, Esse, H.P. Van, Maruthachalam, K., Bolton, M.D., and Santhanam, P. (2012). Tomato immune receptor Ve1 recognizes effector of multiple fungal pathogens uncovered by genome and RNA sequencing. Proc. Natl. Acad. Sci. **109**: 5110-5.

Joosten, M. and de Wit, P. (1999). The tomato-*Cladosporium fulvum* interaction: A versatile experimental system to study plant-pathogen interactions. Annu. Rev. Phytopathol. **37**: 335-367.

Joosten, M.H.A.J., Cozijnsen, T.J., and De Wit, P.J.G.M. (1994). Host resistance to a fungal tomato

pathogen lost by a single base-pair change in an avirulence gene. Nature. **367**: 384-6.

Jung, C.J., Hui Lee, M., Ki Min, M., and Hwang, I. (2011). Localization and trafficking of an isoform of the *At*PRA1 family to the Golgi apparatus depend on both N- and C-terminal sequence motifs. Traffic **12**: 185–200.

Kadota, Y., Sklenar, J., Derbyshire, P., Stransfeld, L., Asai, S., Ntoukakis, V., Jones, J.D., Shirasu, K., Menke, F., Jones, A., and Zipfel, C. (2014). Direct regulation of the NADPH oxidase RBOHD by the PRR-associated kinase BIK1 during plant immunity. Mol. Cell **54**: 43–55.

Kalde, M., Nuhse, T.S., Findlay, K., and Peck, S.C. (2007). The syntaxin SYP132 contributes to plant resistance against bacteria and secretion of pathogenesis-related protein 1. Proc. Natl. Acad. Sci. **104**: 11850–11855.

Kamoun, S., Furzer, O., Jones, J.D., Judelson, H.S, Ali, G.S., Dalio, R.J., Roy, S.G., Schena, L., Zambounis, A., Panabières, F., Cahill, D., Ruocco, M., Figueiredo, A., Chen, X.R., Hulvey, J., Stam, R., Lamour, K., Gijzen, M., Tyler, B.M., Grünwald, N.J., Mukhtar, M.S., Tomé, D.F., Tör, M., Van Den Ackerveken, G., McDowell, J., Daayf, F., Fry, W.E., Lindqvist-Kreuze, H., Meijer, H.J., Petre, B., Ristaino, J., Yoshida, K., Birch, P.R., Govers, F. (2015). The Top 10 oomycete pathogens in molecular plant pathology. Mol. Plant Pathol. **16**: 413-34.

El Kasmi, F., Chung, E.-H., Anderson, R.G., Li, J., Wan, L., Eitas, T.K., Gao, Z., and Dangl, J.L. (2017). Signaling from the plasma-membrane localized plant immune receptor RPM1 requires self-association of the full-length protein. Proc. Natl. Acad. Sci. **114**: 7385-7394.

El Kasmi, F. and Nishimura, M.T. (2016). Structural insights into plant NLR immune receptor function. Proc. Natl. Acad. Sci. **113**: 12619–12621.

Khaled, S. Ben, Postma, J., and Robatzek, S. (2015). A moving view: subcellular trafficking processes in pattern recognition receptor–triggered plant immunity. Annu. Rev. Phytopathol. **53**: 379–402.

Kim, D.S. and Hwang, B.K. (2012). The pepper *MLO* gene, *CaMLO2*, is involved in the susceptibility cell-death response and bacterial and oomycete proliferation. Plant J. **72**: 843–855.

Kim, H., Connell, R.O., Maekawa-yoshikawa, M., Uemura, T., Neumann, U., and Schulze-lefert, P. (2014). The powdery mildew resistance protein RPW8.2 is carried on VAMP721/722 vesicles to the extrahaustorial membrane of haustorial complexes. Plant J. **79**: 835–847.

Kim, M.C., Panstruga, R., Elliott, C., Möller, J., Devoto, A., Yoon, H.W., Park, H.C., Cho, M.J., and Schulze-Lefert, P. (2002). Calmodulin interacts with MLO protein to regulate defence against mildew in barley. Nature **416**: 447-51.

Kimura, S., Waszczak, C., Hunter, K., and Wrzaczek, M. (2017). Bound by fate: the role of reactive oxygen species in receptor-like kinase signaling. Plant Cell **29**: 638–654.

Kirchhelle, C., Chow, C.M., Foucart, C., Neto, H., Stierhof, Y.D., Kalde, M., Walton, C., Fricker, M., Smith, R.S., Jérusalem, A., Irani, N., and Moore, I. (2016). The specification of geometric edges by a plant Rab GTPase is an essential cell-patterning principle during organogenesis in Arabidopsis. Dev. Cell **36**: 386–400.

Kohler, A.C., Chen, L.-H., Hurlburt, N., Salvucci, A., Schwessinger, B., Fisher, A.J., and Stergiopoulos, I. (2016). Structural Analysis of an Avr4 effector ortholog offers insight into chitin binding and recognition by the Cf-4 receptor. Plant Cell **28**: 1945–1965.

Kohorn, B.D. and Kohorn, S.L. (2012). The cell wall-associated kinases, WAKs, as pectin receptors. Front. Plant Sci. **3**: 88.

Kuhn, H., Lorek, J., Kwaaitaal, M., Consonni, C., Becker, K., Micali, C., Ver Loren van Themaat, E.,

Bednarek, P., Raaymakers, T.M., Appiano, M., Bai, Y., Meldau, D., Baum, S., Conrath, U., Feussner, I., and Panstruga, R. (2017). Key components of different plant defense pathways are dispensable for powdery mildew resistance of the Arabidopsis *mlo2 mlo6 mlo12* triple mutant. Front. Plant Sci. **8**: 1–19.

Kumar, M. and Turner, S. (2015). Plant cellulose synthesis: CESA proteins crossing kingdoms. Phytochemistry **112**: 91-9.

Künzl, F., Früholz, S., Fäßler, F., Li, B., and Pimpl, P. (2016). Receptor-mediated sorting of soluble vacuolar proteins ends at the *trans*-Golgi network/early endosome. Nat. Plants **2**: 1–10.

Kusch, S. and Panstruga, R. (2017). *Mlo*-based resistance: an apparently universal "weapon" to defeat powdery mildew disease. Mol. Plant-Microbe Interact. **30**: 179–189.

Kwon, C., Neu, C., Pajonk, S., Yun, H.S., Lipka, U., Humphry, M., Bau, S., Straus, M., Kwaaitaal, M., Rampelt, H., Kasmi, F. El, Jürgens, G., Parker, J., Panstruga, R., Lipka, V., and Schulze-Lefert, P. (2008). Co-option of a default secretory pathway for plant immune responses. Nature **451**: 835–840.

Lacombe, S., Rougon-cardoso, A., Sherwood, E., Peeters, N., Dahlbeck, D., Esse, H.P. Van, Smoker, M., Rallapalli, G., Thomma, B.P.H.J., Staskawicz, B., Jones, J.D.G., and Zipfel, C. (2010). Interfamily transfer of a plant pattern-recognition receptor confers broad-spectrum bacterial resistance. Nat. Biotechnol. **28**: 365–370.

Lacomme, C. and Santa Cruz, S. (1999). Bax-induced cell death in tobacco is similar to the hypersensitive response. Proc. Natl. Acad. Sci. **96**: 7956–7961.

Lam, S.K., Siu, C.L., Hillmer, S., Jang, S., An, G., Robinson, D.G., and Jiang, L. (2007). Rice SCAMP1 defines clathrin-coated, *trans*-Golgi-located tubular-vesicular structures as an early endosome in tobacco BY-2 cells. Plant Cell **19**: 296–319.

LaMontagne, E.D. and Heese, A. (2017). *Trans*-Golgi network/early endosome: a central sorting station for cargo proteins in plant immunity. Curr. Opin. Plant Biol. **40**: 114–121.

Langhorst, M.F., Solis, G.P., Hannbeck, S., Plattner, H., and Stuermer, C.A.O. (2007). Linking membrane microdomains to the cytoskeleton: Regulation of the lateral mobility of reggie-1/flotillin-2 by interaction with actin. FEBS Lett. **581**: 4697–4703.

Lee, H.Y., Bowen, C.H., Popescu, G. V., Kang, H.-G., Kato, N., Ma, S., Dinesh-Kumar, S., Snyder, M., and Popescu, S.C. (2011). Arabidopsis RTNLB1 and RTNLB2 reticulon-like proteins regulate intracellular trafficking and activity of the FLS2 immune receptor. Plant Cell **23**: 3374-91.

Lemmon, M.A. and Schlessinger, J. (2010). Cell signaling by receptor tyrosine kinases. Cell **141**: 1117–1134.

Leshem, Y., Melamed-Book, N., Cagnac, O., Ronen, G., Nishri, Y., Solomon, M., Cohen, G., and Levine, A. (2006). Suppression of Arabidopsis vesicle-SNARE expression inhibited fusion of H_2O_2-containing vesicles with tonoplast and increased salt tolerance. Proc. Natl. Acad. Sci. **103**: 18008–18013.

Leslie, M.E., Lewis, M.W., Youn, J.-Y., Daniels, M.J., and Liljegren, S.J. (2010a). The EVERSHED receptor-like kinase modulates floral organ shedding in Arabidopsis. Development **137**: 467–476.

Lewis, J.D., Wan, J., Ford, R., Gong, Y., Fung, P., Nahal, H., Wang, P.W., Desveaux, D., and Guttman, D.S. (2012). Quantitative interactor screening with next-generation sequencing (QIS-seq) identifies Arabidopsis thaliana MLO2 as a target of the *Pseudomonas syringae* type III effector HopZ2. BMC Genomics **13**: 8.

Li, J., Zhao-Hui, C., Batoux, M., Nekrasov, V., Roux, M., Chinchilla, D., Zipfel, C., and Jones, J.D.G. (2009). Specific ER quality control components required for biogenesis of the plant innate immune receptor EFR. Proc. Natl. Acad. Sci. **106**: 15973–15978.

Li, R., Liu, P., Wan, Y., Chen, T., Wang, Q., Mettbach, U., Baluska, F., Samaj, J., Fang, X., Lucas, W.J., and Lin, J. (2012). A membrane microdomain-associated protein, Arabidopsis Flot1, is involved in a clathrin-independent endocytic pathway and is required for seedling development. Plant Cell **24**: 2105–2122.

Li, X., Kapos, P., and Zhang, Y. (2015). NLRs in plants. Curr. Opin. Immunol. **32**: 114–121.

Li, X. and Pan, S.Q. (2017). Agrobacterium delivers VirE2 protein into host cells via clathrin-mediated endocytosis. Sci. Adv. **3**: e1601528.

Li, X., Yang, Q., Tu, H., Lim, Z., and Pan, S.Q. (2014). Direct visualization of Agrobacterium-delivered VirE2 in recipient cells. Plant J. **77**: 487–495.

Li, Y.B., Rogers, S.W., Tse, Y.C., Lo, S.W., Sun, S.S.M., Jauh, G.Y., and Jiang, L. (2002). BP-80 and homologs are concentrated on post-Golgi, probable lytic prevacuolar compartments. Plant Cell Physiol. **43**: 726–742.

Liang, X., Ding, P., Lian, K., Wang, J., Ma, M., Li, L., Li, L., Li, M., Zhang, X., Chen, S., Zhang, Y., and Zhou, J.M. (2016). Arabidopsis heterotrimeric G proteins regulate immunity by directly coupling to the FLS2 receptor. Elife **5**: e13568.

Liebrand, T.W.H., van den Berg, G.C.M., Zhang, Z., Smit, P., Cordewener, J.H.G., America, A.H.P., Sklenar, J., Jones, A.M.E., Tameling, W.I.L., Robatzek, S., Thomma, B.P.H.J., and Joosten, M.H.A.J. (2013). Receptor-like kinase SOBIR1/EVR interacts with receptor-like proteins in plant immunity against fungal infection. Proc. Natl. Acad. Sci. **110**: 10010–10015.

Liebrand, T.W.H., van den Burg, H.A., and Joosten, M.H.A.J. (2014). Two for all: Receptor-associated kinases SOBIR1 and BAK1. Trends Plant Sci. **19**: 123–132.

Liebrand, T.W.H., Smit, P., Abd-el-haliem, A., Jonge, R. De, Cordewener, J.H.G., America, A.H.P., Sklenar, J., Jones, A.M.E., Robatzek, S., Thomma, B.P.H.J., Tameling, W.I.L., and Joosten, M.H.A.J. (2012). Endoplasmic reticulum-quality control chaperones facilitate the biogenesis of Cf receptor-like proteins involved in pathogen resistance of tomato. Plant Phys. **159**: 1819–1833.

Liljegren, S.J., Leslie, M.E., Darnielle, L., Lewis, M.W., Taylor, S.M., Luo, R., Geldner, N., Chory, J., Randazzo, P.A., Yanofsky, M.F., and Ecker, J.R. (2009). Regulation of membrane trafficking and organ separation by the NEVERSHED ARF-GAP protein. Development **136**: 1909–1918.

Lipka, V., Dittgen, J., Bednarek, P., Bhat, R., Wiermer, M., Stein, M., Landtag, J., Brandt, W., Rosahl, S., Scheel, D., Llorente, F., Molina, A., Parker, J., Somerville, S., and Schulze-Lefert, P. (2005). Pre- and postinvasion defenses both contribute to nonhost resistance in Arabidopsis. Science **310**: 1180–1183.

Lipka, V., Kwon, C., and Panstruga, R. (2007). SNARE-ware: The role of SNARE-domain proteins in plant biology. Annu. Rev. Cell Dev. Biol. **23**: 147–174.

Liu, J., Elmore, J.M., Lin, Z.J.D., and Coaker, G. (2011). A receptor-like cytoplasmic kinase phosphorylates the host target RIN4, leading to the activation of a plant innate immune receptor. Cell Host Microbe **9**: 137–146.

Liu, N., Hake, K., Wang, W., Zhao, T., Romeis, T., and Tang, D. (2017). CALCIUM-DEPENDENT PROTEIN KINASE5 associates with the truncated NLR protein TIR-NBS2 to contribute to *exo70B1*-mediated immunity. Plant Cell **29**: 746-759.

Liu, Y., Huang, X., Li, M., He, P., and Zhang, Y. (2016). Loss-of-function of Arabidopsis receptor-like kinase BIR1 activates cell death and defense responses mediated by BAK1 and SOBIR1. New Phytol. **212**: 637–645.

van Loon, L.C. (1975). Polyacrylamide disc electrophoresis of the soluble leaf proteins from Nicotiana tabacum var. “Samsun” and “Samsun NN”. IV. Similarity of qualitative changes of specific proteins after infection with different viruses and their relationship to acquired resistance. Virology. **67**: 566-75.

Van Loon, L.C. and Van Strien, E.A. (1999). The families of pathogenesis-related proteins, their activities, and comparative analysis of PR-1 type proteins. Physiol. Mol. Plant Pathol. **55**: 85-97.

López-Marqués, R.L., Poulsen, L.R., and Palmgren, M.G. (2012). A putative plant aminophospholipid flippase, the Arabidopsis p4 ATPase ALA1, localizes to the plasma membrane following association with a β-subunit. PLoS One **7**: 1–10.

Lozano-Durán, R., Bourdais, G., He, S.Y., and Robatzek, S. (2014). The bacterial effector HopM1 suppresses PAMP-triggered oxidative burst and stomatal immunity. New Phytol. **202**: 259–269.

Lu, D., Lin, W., Gao, X., Wu, S., Cheng, C., Avila, J., Heese, A., Devarenne, T.P., He, P., and Shan, L. (2011). Direct ubiquitination of pattern recognition receptor FLS2 attenuates plant innate immunity. Science **332**: 1439–1442.

Lu, X., Dittgen, J., Pi, M., Molina, A., and Schneider, B. (2015). Mutant allele-specific uncoupling of PENETRATION3 functions reveals engagement of the ATP-binding cassette transporter in distinct tryptophan metabolic pathways. Plant Phys. **168**: 814–827.

Lu, X., Tintor, N., Mentzel, T., Kombrink, E., Boller, T., Robatzek, S., Schulze-Lefert, P., and Saijo, Y. (2009). Uncoupling of sustained MAMP receptor signaling from early outputs in an Arabidopsis endoplasmic reticulum glucosidase II allele. Proc. Natl. Acad. Sci. **106**: 22522–22527.

Lu, Y.J., Schornack, S., Spallek, T., Geldner, N., Chory, J., Schellmann, S., Schumacher, K., Kamoun, S., and Robatzek, S. (2012). Patterns of plant subcellular responses to successful oomycete infections reveal differences in host cell reprogramming and endocytic trafficking. Cell. Microbiol. **14**: 682–697.

Luna, E., Pastor, V., Robert, J., Flors, V., Mauch-Mani, B., and Ton, J. (2011). Callose deposition: a multifaceted plant defense response. Mol. Plant-Microbe Interact. **24**: 183–193.

Lunn, D., Gaddipati, S.R., Tucker, G.A., and Lycett, G.W. (2013). Null mutants of individual RABA genes impact the proportion of different cell wall components in stem tissue of *Arabidopsis thaliana*. PLoS One **8**: 1–7.

Mackey, D., Holt, B.F., Wiig, A., and Dangl, J.L. (2002). RIN4 interacts with *Pseudomonas syringae* type III effector molecules and is required for RPM1-mediated resistance in *Arabidopsis*. Cell **108**: 743–754.

Malinovsky, F.G., Brodersen, P., Fiil, B.K., McKinney, L.V., Thorgrimsen, S., Beck, M., Nielsen, H.B., Pietra, S., Zipfel, C., Robatzek, S., Petersen, M., Hofius, D., and Mundy, J. (2010). Lazarus1, a DUF300 protein, contributes to programmed cell death associated with Arabidopsis acd11 and the hypersensitive response. PLoS One. **5**: e12586.

Mansfield, J., Genin, S., Magori, S., Citovsky, V., Sriariyanum, M., Ronald, P., Dow, M., Verdier, V., Beer, S. V., Machado, M.A., Toth, I., Salmond, G., and Foster, G.D. (2012). Top 10 plant pathogenic bacteria in molecular plant pathology. Mol. Plant Pathol. **13**: 614-29.

Mao, H., Nakamura, M., Viotti, C., and Grebe, M. (2016). A framework for lateral membrane trafficking and polar tethering of the PEN3 ATP-binding cassette transporter. Plant Physiol. **172**: 2245–2260.

Marmagne, A., Ferro, M., Meinnel, T., Bruley, C., Kuhn, L., Garin, J., Barbier-Brygoo, H., and Ephritikhine, G. (2007). A high content in lipid-modified peripheral proteins and integral receptor kinases features in the Arabidopsis plasma membrane proteome. Mol. Cell. Proteomics. **6**: 1980-96.

Martins, S., Dohmann, E.M.N., Cayrel, A., Johnson, A., Fischer, W., Pojer, F., Satiat-Jeunemaître, B., Jaillais, Y., Chory, J., Geldner, N., and Vert, G. (2015). Internalization and vacuolar targeting of the brassinosteroid hormone receptor BRI1 are regulated by ubiquitination. Nat. Commun. **6**: 6151.

Mayers, J.R., Hu, T., Wang, C., Càrdenas, J.J., Tan, Y., Pan, J., and Bednarek, S. (2017). SCD1 and SCD2 form a complex that functions with the Exocyst and RabE1 in exocytosis and cytokinesis. Plant Cell **29**: 2610-2625.

Mbengue, M., Bourdais, G., Gervasi, F., Beck, M., Zhou, J., and Spallek, T. (2016). Clathrin-dependent endocytosis is required for immunity mediated by pattern recognition receptor kinases. Proc. Natl. Acad. Sci. **27**: 11034-9.

Meister, M. and Tikkanen, R. (2014). Endocytic trafficking of membrane-bound cargo: A flotillin point of view. Membranes (Basel). **4**: 356–371.

Melotto, M. and Kunkel, B.N. (2013). Virulence strategies of plant pathogenic bacteria. The Prokaryotes. Springer, Berlin, Heidelberg..

Melotto, M., Underwood, W., Koczan, J., Nomura, K., and He, S.Y. (2006). Plant stomata function in innate immunity against bacterial invasion. Cell. **126**: 969-80.

Mesarich, C.H., Stergiopoulos, I., Beenen, H.G., Cordovez, V., Guo, Y., Karimi Jashni, M., Bradshaw, R.E., and de Wit, P.J.G.M. (2016). A conserved proline residue in Dothideomycete Avr4 effector proteins is required to trigger a Cf-4-dependent hypersensitive response. Mol. Plant Pathol. **17**: 84–95.

Meyer, D., Pajonk, S., Micali, C., Connell, R.O., and Schulze-lefert, P. (2009). Extracellular transport and integration of plant secretory proteins into pathogen-induced cell wall compartments. Plant J. **57**: 986–999.

Micali, C.O., Neumann, U., Grunewald, D., Panstruga, R., and Connell, R.O. (2011). Biogenesis of a specialized plant – fungal interface during host cell internalization of *Golovinomyces orontii* haustoria. Cell. Microbiol. **13**: 210–226.

Monaghan, J. and Zipfel, C. (2012). Plant pattern recognition receptor complexes at the plasma membrane. Curr. Opin. Plant Biol. **15**: 349–357.

Mondragon-Palomino, M. and Gaut, B.S. (2005). Gene conversion and the evolution of three leucine-rich repeat gene families in *Arabidopsis thaliana*. Mol. Biol. Evol. **22**: 2444–2456.

Mudgett, M.B. and Staskawicz, B.J. (1999). Characterization of the *Pseudomonas syringae* pv. *tomato* AvrRpt2 protein: Demonstration of secretion and processing during bacterial pathogenesis. Mol. Microbiol. **32**: 927-41.

Mukhtar, M.S., Carvunis, A.R., Dreze, M., Epple, P., Steinbrenner, J., Moore, J., Tasan, M., Galli, M., Hao, T., Nishimura, M.T., Pevzner, S.J., Donovan, S.E., Ghamsari, L., Santhanam, B., Romero, V., Poulin, M.M., Gebreab, F., Gutierrez, B.J., Tam, S., Monachello, D., Boxem, M., Harbort, C.J., McDonald, N., Gai, L., Chen, H., He, Y.; European Union Effectoromics Consortium, Vandenhaute, J., Roth, F.P., Hill, D.E., Ecker, J.R., Vidal, M., Beynon, J., Braun, P., Dangl, J.L. (2011). Independently evolved virulence effectors converge onto hubs in a plant immune system network. Science **333**: 596–601.

Muller, R., Bleckmann, A., and Simon, R. (2008). The receptor kinase CORYNE of Arabidopsis

transmits the stem cell-limiting signal CLAVATA3 independently of CLAVATA1. Plant Cell **20**: 934-46..

Nandety, R.S., Caplan, J.L., Cavanaugh, K., Perroud, B., Wroblewski, T., Michelmore, R.W., and Meyers, B.C. (2013). The role of TIR-NBS and TIR-X proteins in plant basal defense responses. Plant Physiol. **162**: 1459–1472.

Navarro, L., Zipfel, C., Rowland, O., Keller, I., Robatzek, S., Boller, T., and Jones, J.D.G. (2004). The transcriptional innate immune response to flg22. Interplay and Overlap with Avr gene-dependent defense responses and bacterial pathogenesis Plant Phys. **135**: 1113–1128.

Nekrasov, V., Li, J., Batoux, M., Roux, M., Chu, Z.H., Lacombe, S., Rougon, A., Bittel, P., Kiss-Papp, M., Chinchilla, D., van Esse, H.P,. Jorda, L., Schwessinger, B., Nicaise, V., Thomma, B.P., Molina, A., Jones, J.D., Zipfel, C. (2009). Control of the pattern-recognition receptor EFR by an ER protein complex in plant immunity. EMBO J. **28**: 3428–3438.

Nelson, B.K., Cai, X., and Nebenfu, A. (2007). A multicolored set of in vivo organelle markers for co-localization studies in Arabidopsis and other plants. Plant J. **51**: 1126–1136.

Nielsen, E., Cheung, A.Y., and Ueda, T. (2008). The regulatory RAB and ARF GTPases for vesicular trafficking. Plant Physiol. **147**: 1516–1526.

Nielsen, M.E., Feechan, A., Bohlenius, H., Ueda, T., and Thordal-Christensen, H. (2012). Arabidopsis ARF-GTP exchange factor, GNOM, mediates transport required for innate immunity and focal accumulation of syntaxin PEN1. Proc. Natl. Acad. Sci. **109**: 11443–11448.

Nielsen, M.E., Jürgens, G., and Thordal-Christensen, H. (2017). VPS9a activates the Rab5 GTPase ARA7 to confer distinct pre- and post-invasive plant innate immunity. Plant Cell **29**: 1927-1937.

Nielsen, M.E. and Thordal-Christensen, H. (2012). Recycling of Arabidopsis plasma membrane PEN1 syntaxin. Plant Signal. Behav. **7**: 1541–1543.

Nielsen, M.E. and Thordal-Christensen, H. (2013). Transcytosis shuts the door for an unwanted guest. Trends Plant Sci. **18**: 611–616.

Nishimura, K., Matsunami, E., Yoshida, S., Kohata, S., Yamauchi, J., Jisaka, M., Nagaya, T., Yokota, K., and Nakagawa, T. (2016). The tyrosine-sorting motif of the vacuolar sorting receptor VSR4 from *Arabidopsis thaliana*, which is involved in the interaction between VSR4 and AP1M2, μ1-adaptin type 2 of clathrin adaptor complex 1 subunits, participates in the post-Golgi sorting of VS. Biosci. Biotechnol. Biochem. **80**: 694–705.

Nishimura, M.T., Stein, M., Hou, B.H., Vogel, J.P., Edwards, H., and Somerville, S.C. (2003). Loss of a callose synthase results in salicylic acid-dependent disease resistance. Science **15**: 969-72.

Nobori, T., Velásquez, A.C., Wu, J., Kvitko, B.H., Kremer, J.M., Wang, Y., He, S.Y., and Tsuda, K. (2018). Transcriptome landscape of a bacterial pathogen under plant immunity. Proc. Natl. Acad. Sci. **115**: 3055-3064.

Nomura, K., DebRoy, S., Lee, Y.H., Pumplin, N., Jones, J., and He, S.Y. (2006). A bacterial virulence protein suppresses host innate immunity to cause plant disease. Science **313**: 220–223.

Nomura, K., Mecey, C., Lee, Y.-N., Imboden, L.A., Chang, J.H., and He, S.Y. (2011). Effector-triggered immunity blocks pathogen degradation of an immunity-associated vesicle traffic regulator in Arabidopsis. Proc. Natl. Acad. Sci. **108**: 10774–10779.

Oa, M.C.W., Consonni, C., Bednarek, P., Humphry, M., Francocci, F., Ferrari, S., Harzen, A., Ver, E., Themaat, L. Van, and Panstruga, R. (2010). Tryptophan-derived metabolites are required for antifungal defense in the Arabidopsis *mlo2* mutant. Plant Phys. **152**: 1544–1561.

Obudulu, O., Mähler, N., Skotare, T., Bygdell, J., Abreu, I.N., Ahnlund, M., Gandla, M.L., Petterle, A., Moritz, T., Hvidsten, T.R., Jönsson, L.J., Wingsle, G., Trygg, J., and Tuominen, H. (2018). A multi-omics approach reveals function of Secretory Carrier-Associated Membrane Proteins in wood formation of Populus trees. BMC Genomics **19**: 1–18.

Ortiz-Morea, F.A., Savatin, D. V., Dejonghe, W., Kumar, R., Luo, Y., Adamowski, M., Van den Begin, J., Dressano, K., Pereira de Oliveira, G., Zhao, X., Lu, Q., Madder, A., Friml, J., Scherer de Moura, D., and Russinova, E. (2016). Danger-associated peptide signaling in Arabidopsis requires clathrin. Proc. Natl. Acad. Sci. **113**: 11028–11033.

Otto, G.P. and Nichols, B.J. (2011). The roles of flotillin microdomains - endocytosis and beyond. J. Cell Sci. **124**: 3933–3940.

Paez Valencia, J., Goodman, K., and Otegui, M.S. (2016). Endocytosis and endosomal trafficking in Plants. Annu. Rev. Plant Biol. **67**: 309–335.

Pajonk, S., Kwon, C., Panstruga, R., Pajonk, S., Kwon, C., Clemens, N., Panstruga, R., and Schulze-lefert, P. (2008). Activity Determinants and Functional Specialization of Arabidopsis PEN1 syntaxin in innate immunity J. Biol. Chem. **283**: 26974-84.

Panstruga, R. (2005). Serpentine plant MLO proteins as entry portals for powdery mildew fungi. Biochem. Soc. Trans. **33**: 389–392.

Paredez, A.R., Somerville, C.R., and Ehrhardt, D.W. (2006). Visualization of cellulose synthase demonstrates functional association with microtubules. Science **312**: 1491–1495.

Park, E., Lee, H.-Y., Woo, J., Choi, D., and Dinesh-Kumar, S.P. (2017). Spatiotemporal monitoring of *Pseudomonas syringae* effectors via type III secretion using split fluorescent protein fragments. Plant Cell **29**: 1571-1584.

Peart, J.R., Lu, R., Sadanandom, A., Malcuit, I., Moffett, P., Brice, D.C., Schauser, L., Jaggard, D.A.W., Xiao, S., Coleman, M.J., Dow, M., Jones, J.D.G., Shirasu, K., and Baulcombe, D.C. (2002). Ubiquitin ligase-associated protein SGT1 is required for host and nonhost disease resistance in plants. Proc. Natl. Acad. Sci. **99**: 10865–10869.

Peart, J.R., Mestre, P., Lu, R., Malcuit, I., and Baulcombe, D.C. (2005). NRG1, a CC-NB-LRR protein, together with N, a TIR-NB-LRR protein, mediates resistance against tobacco mosaic virus. Curr. Biol. **15**: 968–973.

Pečenková, T., Pleskot, R., and Žárský, V. (2017). Subcellular localization of Arabidopsis pathogenesis-related 1 (PR1) protein. Int. J. Mol. Sci. **18**: 1–13.

Pfalz, M., Mikkelsen, M.D., Bednarek, P., Olsen, C.E., Halkier, B.A., and Kroymann, J. (2011). Metabolic engineering in *Nicotiana benthamiana* reveals key enzyme functions in Arabidopsis indole glucosinolate modification. Plant Cell **23**: 716–29.

Pfalz, M., Mukhaimar, M., Perreau, F., Kirk, J., Hansen, C.I.C., Olsen, C.E., Agerbirk, N., and Kroymann, J. (2016). Methyl transfer in glucosinolate biosynthesis mediated by indole glucosinolate *O*-methyltransferase 5. Plant Physiol. **172**: 2190–2203.

Pinheiro, H., Samalova, M., Geldner, N., Chory, J., Martinez, A., and Moore, I. (2009). Genetic evidence that the higher plant Rab-D1 and Rab-D2 GTPases exhibit distinct but overlapping interactions in the early secretory pathway. J. Cell Sci. **122**: 3749–58.

Plotnikova, J.M., Rahme, L.G., and Ausubel, F.M. (2000). Pathogenesis of the human opportunistic pathogen *Pseudomonas aeruginosa* PA14 in Arabidopsis. Plant Physiol. **124**: 1766–74.

Pomorski, T. and Menon, A.K. (2006). Lipid flippases and their biological functions. Cell. Mol. Life Sci.

63: 2908–2921.

Postma, J., Liebrand, T.W.H., Bi, G., Evrard, A., Bye, R.R., Mbengue, M., Kuhn, H., Joosten, M.H.A.J., and Robatzek, S. (2016). Avr4 promotes Cf-4 receptor-like protein association with the BAK1/SERK3 receptor-like kinase to initiate receptor endocytosis and plant immunity. New Phytol. **210**: 627-42.

Poulsen, L.R., Lopez-Marques, R.L., McDowell, S.C., Okkeri, J., Licht, D., Schulz, A., Pomorski, T., Harper, J.F., and Palmgren, M.G. (2008). The Arabidopsis P4-ATPase ALA3 localizes to the Golgi and requires a beta-subunit to function in lipid translocation and secretory vesicle formation. Plant Cell **20**: 658–676.

Prince, D.C., Rallapalli, G., Xu, D., Schoonbeek, H., Çevik, V., Asai, S., Kemen, E., Cruz-mireles, N., Kemen, A., Belhaj, K., Schornack, S., Kamoun, S., Holub, E.B., Halkier, B.A., and Jones, J.D.G. (2017). Albugo-imposed changes to tryptophan-derived antimicrobial metabolite biosynthesis may contribute to suppression of non-host resistance to *Phytophthora infestans* in *Arabidopsis thaliana*. BMC Biol. **15**: 1–22.

Qi, X. and Zheng, H. (2011). Arabidopsis TRAPPII is functionally linked to Rab-A, but not Rab-D in polar protein trafficking in *trans*-Golgi network. Plant Signal. Behav. **6**: 1679–1683.

Ranf, S., Gisch, N., Schäffer, M., Illig, T., Westphal, L., Knirel, Y.A., Sánchez-Carballo, P.M., Zähringer, U., Hückelhoven, R., Lee, J., and Scheel, D. (2015). A lectin S-domain receptor kinase mediates lipopolysaccharide sensing in *Arabidopsis thaliana*. Nat. Immunol. **16**: 246-33.

Rasmussen, M.W., Roux, M., Petersen, M., and Mundy, J. (2012). MAP kinase cascades in Arabidopsis innate immunity. Front. Plant Sci. **3**: 169.

Richter, S., Kientz, M., Brumm, S., Nielsen, M.E., Park, M., Gavidia, R., Krause, C., Voss, U., Beckmann, H., Mayer, U., Stierhof, Y.D., and Jürgens, G. (2014). Delivery of endocytosed proteins to the cell-division plane requires change of pathway from recycling to secretion. Elife: e02131.

Rivas, S. and Thomas, C.M. (2005). Molecular interactions between tomato and the leaf mold pathogen *Cladosporium fulvum*. Annu. Rev. Phytopathol. **43**: 395–436.

Robatzek, S., Chinchilla, D., and Boller, T. (2006). Ligand-induced endocytosis of the pattern recognition receptor FLS2 in Arabidopsis. Genes Dev. **20**: 537–542.

Robinson, D.G. and Neuhaus, J.M. (2016). Receptor-mediated sorting of soluble vacuolar proteins: Myths, facts, and a new model. J. Exp. Bot. **67**: 4435–4449.

Rojo, E. and Denecke, J. (2008). What is moving in the secretory pathway of plants? Plant Phys. **147**: 1493-503.

Romeis, T., Ludwig, A.A., Martin, R., and Jones, J.D. (2001). Calcium-dependent protein kinases play an essential role in a plant defence response. EMBO J. **20**: 5556–5567.

Ron, M. (2004). The receptor for the fungal elicitor ethylene-inducing xylanase is a member of a resistance-like gene family in tomato. Plant Cell **16**: 1604-15.

Rosado, B.H.P., Almeida, L.C., Alves, L.F., Lambais, M.R., and Oliveira, R.S. (2018). The importance of phyllosphere on plant functional ecology: A phyllo trait manifesto. New Phytol. **219**: 1145-1149.

Roth, C., Lüdke, D., Klenke, M., Quathamer, A., Valerius, O., Braus, G.H., and Wiermer, M. (2017). The truncated NLR protein TIR-NBS13 is a MOS6/IMPORTIN-α3 interaction partner required for plant immunity. Plant J. **92**: 808-821.

Roudier, F. (2002). The COBRA family of putative GPI-anchored proteins in Arabidopsis. a new fellowship in expansion. Plant Physiol. **130**: 538–548.

Roux, M., Schwessinger, B., Albrecht, C., Chinchilla, D., Jones, A., Holton, N., Malinovsky, F.G., Tör, M., de Vries, S., and Zipfel, C. (2011). The *Arabidopsis* leucine-rich repeat receptor–like kinases BAK1/SERK3 and BKK1/SERK4 are required for innate immunity to hemibiotrophic and biotrophic pathogens. Plant Cell **23**: 2440–2455.

Russinova, E. (2004). Heterodimerization and endocytosis of arabidopsis brassinosteroid receptors BRI1 and *At*SERK3 (BAK1). Plant Cell **16**: 3216–3229.

Rutter, B.D. and Innes, R.W. (2017). Extracellular vesicles isolated from the leaf apoplast carry stress-response proteins. Plant Physiol. **173**: 728–741.

Saint-Jean, B., Seveno-Carpentier, E., Alcon, C., Neuhaus, J.-M., and Paris, N. (2010). The cytosolic tail dipeptide Ile-Met of the pea receptor BP80 is required for recycling from the prevacuole and for endocytosis. Plant Cell **22**: 2825–2837.

Saito, C. and Ueda, T. (2009). Functions of RAB and SNARE proteins in plant life. Int. Rev. Cell Mol. Biol. **274**: 183-233.

Sakurai, H.T., Inoue, T., Nakano, A., and Ueda, T. (2016). ENDOSOMAL RAB EFFECTOR WITH PX-DOMAIN, an Interacting Partner of RAB5 GTPases, regulates membrane trafficking to protein storage vacuoles in Arabidopsis. Plant Cell **28**: 1490–1503.

Sánchez-Rodríguez, C., Shi, Y., Kesten, C., Zhang, D., Sancho-Andrés, G., Ivakov, A., Lampugnani, E.R., Sklodowski, K., Fujimoto, M., Nakano, A., Bacic, A., Wallace, I.S., Ueda, T., Van Damme, D., Zhou, Y., and Persson, S. (2018). The cellulose synthases are cargo of the TPLATE adaptor complex. Mol. Plant **11**: 346–349.

Sappl, P.G., Carroll, A.J., Clifton, R., Lister, R., Whelan, J., Harvey Millar, A., and Singh, K.B. (2009). The Arabidopsis glutathione transferase gene family displays complex stress regulation and co-silencing multiple genes results in altered metabolic sensitivity to oxidative stress. Plant J. **58**: 53–68.

Sarris, P.F., Cevik, V., Dagdas, G., Jones, J.D.G., and Krasileva, K. V. (2016). Comparative analysis of plant immune receptor architectures uncovers host proteins likely targeted by pathogens. BMC Biol. **14**: 8.

Saur, I.M.L., Kadota, Y., Sklenar, J., Holton, N.J., Smakowska, E., Belkhadir, Y., Zipfel, C., and Rathjen, J.P. (2016). *Nb*CSPR underlies age-dependent immune responses to bacterial cold shock protein in *Nicotiana benthamiana*. Proc. Natl. Acad. Sci. **113**: 3389–3394.

Scheuring, D., Viotti, C., Kruger, F., Kunzl, F., Sturm, S., Bubeck, J., Hillmer, S., Frigerio, L., Robinson, D.G., Pimpl, P., and Schumacher, K. (2011). Multivesicular bodies mature from the *trans*-Golgi network/early endosome in Arabidopsis. Plant Cell Online **23**: 3463–3481.

Schindelman, G., Morikami, A., Jung, J., Baskin, T.I., Carpita, N.C., Derbyshire, P., McCann, M.C., and Benfey, P.N. (2001). *COBRA* encodes a putative GPI-anchored protein, which is polarly localized and necessary for oriented cell expansion in Arabidopsis. Genes Dev. **15**: 1115–1127.

Schwessinger, B., Roux, M., Kadota, Y., Ntoukakis, V., Sklenar, J., Jones, A., and Zipfel, C. (2011). Phosphorylation-dependent differential regulation of plant growth, cell death, and innate immunity by the regulatory receptor-like kinase BAK1. PLoS Genet. **7**: 1–32.

Selin, C., Kievit, T.R. De, Belmonte, M.F., Fernando, W.G.D., and Monaghan, J. (2016). Elucidating the role of effectors in plant-fungal interactions: progress and challenges. Front. Microbiol. **7**: 1–21.

Serrano, M., Coluccia, F., Torres, M., L'Haridon, F., and Métraux, J.-P. (2014). The cuticle and plant defense to pathogens. Front. Plant Sci. **5**: 274.

Sewelam, N., Kazan, K., and Schenk, P.M. (2016). Global plant stress signaling: reactive oxygen species at the cross-road. Front. Plant Sci. **7**: 1–21.

Sharfman, M., Bar, M., Ehrlich, M., Schuster, S., Melech-Bonfil, S., Ezer, R., Sessa, G., and Avni, A. (2011). Endosomal signaling of the tomato leucine-rich repeat receptor-like protein LeEix2. Plant J. **68**: 413–423.

Sharma, Y.K., Leon, J., Raskin, I., and Davis, K.R. (1996). Ozone-induced responses in *Arabidopsis thaliana*: The role of salicylic acid in the accumulation of defense-related transcripts and induced resistance. Proc. Natl. Acad. Sci. **93**: 5099–5104.

Singh, M.K., Krüger, F., Beckmann, H., Brumm, S., Vermeer, J.E.M., Munnik, T., Mayer, U., Stierhof, Y.D., Grefen, C., Schumacher, K., and Jürgens, G. (2014). Protein delivery to vacuole requires SAND protein-dependent Rab GTPase conversion for MVB-vacuole fusion. Curr. Biol. **24**: 1383–1389.

Smith, J.M., Salamango, D.J., Leslie, M.E., Collins, C.A., and Heese, A. (2014). Sensitivity to flg22 is modulated by ligand-induced degradation and *de novo* synthesis of the endogenous flagellin-receptor FLAGELLIN-SENSING2. Plant Physiol. **164**: 440–454.

Somssich, M., Bleckmann, A., and Simon, R. (2016). Shared and distinct functions of the pseudokinase CORYNE (CRN) in shoot and root stem cell maintenance of Arabidopsis. J. Exp. Bot. **67**: 4901–4915.

Song, W.-Y., Choi, K.S., Kim, D.Y., Geisler, M., Park, J., Vincenzetti, V., Schellenberg, M., Kim, S.H., Lim, Y.P., Noh, E.W., Lee, Y., and Martinoia, E. (2010). Arabidopsis PCR2 is a zinc exporter involved in both zinc extrusion and long-distance zinc transport. Plant Cell **22**: 2237–2252.

Song, W.Y., Hörtensteiner, S., Tomioka, R., Lee, Y., and Martinoia, E. (2011). Common functions or only phylogenetically related? The large family of PLAC8 motif-containing/PCR genes. Mol. Cells **31**: 1–7.

Sorek, N., Sorek, H., Kijac, A., Szemenyei, H.J., Bauer, S., Hématy, K., Wemmer, D.E., and Somerville, C.R. (2014). The Arabidopsis COBRA protein facilitates cellulose crystallization at the plasma membrane. J. Biol. Chem. **289**: 34911–34920.

Spallek, T., Beck, M., Ben Khaled, S., Salomon, S., Bourdais, G., Schellmann, S., and Robatzek, S. (2013). ESCRT-I mediates FLS2 endosomal sorting and plant immunity. PLoS Genet. **9**: e1004035.

Spanò, S. and Galán, J.E. (2017). Taking control: Hijacking of Rab GTPases by intracellular bacterial pathogens. Small GTPases **1248**: 1–10.

Sparks, J.A., Kwon, T., Renna, L., Liao, F., Brandizzi, F., and Blancaflor, E.B. (2016). HLB1 is a tetratricopeptide repeat domain-containing protein that operates at the intersection of the exocytic and endocytic pathways at the TGN/EE in Arabidopsis. Plant Cell **28**: 746–769.

Speth, E.B., Imboden, L., Hauck, P., and He, S.Y. (2009). Subcellular localization and functional analysis of the Arabidopsis GTPase RabE. Plant Physiol. **149**: 1824–1837.

Srivastava, R., Deng, Y., Shah, S., Rao, A.G., and Howell, S.H. (2013). BINDING PROTEIN is a master regulator of the endoplasmic reticulum stress sensor/transducer bZIP28 in Arabidopsis. Plant Cell **25**: 1416–1429.

Stahl, E., Bellwon, P., Huber, S., Schlaeppi, K., and Bernsdorff, F. (2016). Regulatory and functional aspects of indolic metabolism in plant systemic acquired resistance. Mol. Plant **9**: 662-681.

Stefano, G., Renna, L., Lai, Y., Slabaugh, E., Mannino, N., Buono, R.A., Otegui, M.S., and Brandizzi, F. (2015). ER network homeostasis is critical for plant endosome streaming and endocytosis. Cell Discov. **17**: 15033.

Stefano, G., Renna, L., Wormsbaecher, C., Gamble, J., Zienkiewicz, K., and Brandizzi, F. (2018). plant endocytosis requires the ER membrane-anchored proteins VAP27-1 and VAP27-3. Cell Rep. **23**: 2299–2307.

Stein, M., Dittgen, J., Sánchez-Rodríguez, C., Hou, B.-H., Molina, A., Schulze-Lefert, P., Lipka, V., and Somerville, S. (2006). Arabidopsis PEN3/PDR8, an ATP binding cassette transporter, contributes to nonhost resistance to inappropriate pathogens that enter by direct penetration. Plant Cell **18**: 731–746.

Stein, M.P., Müller, M.P., and Wandinger-Ness, A. (2012). Bacterial pathogens commandeer Rab GTPases to establish intracellular niches. Traffic. **13**: 1565-88.

Stergiopoulos, I., van den Burg, H.A., Okmen, B., Beenen, H.G., van Liere, S., Kema, G.H.J., and de Wit, P.J.G.M. (2010). Tomato Cf resistance proteins mediate recognition of cognate homologous effectors from fungi pathogenic on dicots and monocots. Proc. Natl. Acad. Sci. **107**: 7610–7615.

Stergiopoulos, I. and de Wit, P.J.G.M. (2009). Fungal Effector Proteins. Annu. Rev. Phytopathol. **47**: 233–263.

Stotz, H.U., Mitrousia, G.K., de Wit, P.J.G.M., and Fitt, B.D.L. (2014). Effector-triggered defence against apoplastic fungal pathogens. Trends Plant Sci. **19**: 491–500.

Stulemeijer, I.J.E., Stratmann, J.W., and Joosten, M.H.A.J. (2007). Tomato mitogen-activated protein kinases *Le*MPK1, *Le*MPK2, and *Le*MPK3 are activated during the Cf-4/Avr4-induced hypersensitive response and have distinct phosphorylation specificities. Plant Physiol. **144**: 1481–1494.

Szabo, L.J. and Bushnell, W.R. (2001). Hidden robbers: the role of fungal haustoria in parasitism of plants. Proc. Natl. Acad. Sci. **98**: 7654–5.

Szponarski, W., Sommerer, N., Boyer, J.C., Rossignol, M., and Gibrat, R. (2004). Large-scale characterization of integral proteins from Arabidopsis vacuolar membrane by two-dimensional liquid chromatography. Proteomics **4**: 397–406.

Takken, F.L.W., Thomas, C.M., Joosten, M.H.A.J., Golstein, C., Westerink, N., Hille, J., Nijkamp, H.J.J., De Wit, P.J.G.M., and Jones, J.D.G. (1999). A second gene at the tomato *Cf-4* locus confers resistance to *Cladosporium fulvum* through recognition of a novel avirulence determinant. Plant J. **20**: 279–288.

Tameling, W.I.L. and Baulcombe, D.C. (2007). Physical association of the NB-LRR resistance protein Rx with a Ran GTPase-activating protein is required for extreme resistance to Potato virus X. Plant Cell **19**: 1682–1694.

Tanaka, H., Kitakura, S., De Rycke, R., De Groodt, R., and Friml, J. (2009). Fluorescence imaging-based screen identifies ARF GEF component of early endosomal trafficking. Curr. Biol. **19**: 391–397.

Tang, D. and Zhou, J.-M. (2016). PEPRs spice up plant immunity. EMBO J. **35**: 4-5.

Tateda, C., Zhang, Z., Greenberg, J.T., Tateda, C., Zhang, Z., and Greenberg, J.T. (2015). Linking pattern recognition and salicylic acid responses in Arabidopsis through ACCELERATED CELL DEATH6 and receptors.Plant Signal. Behav. **10**: e1010912.

Tenhaken, R. (2015). Cell wall remodeling under abiotic stress. Front. Plant Sci. **5**: 1–9.

Thomas, C.M., Jones, D. a, Parniske, M., Harrison, K., Balint-Kurti, P.J., Hatzixanthis, K., and Jones, J.D. (1997). Characterization of the tomato Cf-4 gene for resistance to *Cladosporium fulvum* identifies sequences that determine recognitional specificity in Cf-4 and Cf-9. Plant Cell **9**: 2209–2224.

Thomas, C.M., Tang, S., Hammond-Kosack, K., and Jones, J.D.G. (2000). Comparison of the hypersensitive response induced by the tomato *Cf-4* and *Cf-9* genes in *Nicotiana* spp. Mol. Plant-Microbe Interact. **13**: 465–469.

Thomma, B.P.H.J., Nürnberger, T., and Joosten, M.H.A.J. (2011). Of PAMPs and effectors: the blurred PTI-ETI dichotomy. Plant Cell **23**: 4–15.

Thul, P.J., Åkesson, L., Wiking, M., Mahdessian, D., Geladaki, A., Ait Blal, H., Alm, T., Asplund, A., Björk, L., Breckels, L.M., Bäckström, A., Danielsson, F., Fagerberg, L., Fall, J., Gatto, L., Gnann, C., Hober, S., Hjelmare, M., Johansson, F., Lee, S., Lindskog, C., Mulder, J., Mulvey, C.M., Nilsson, P., Oksvold, P., Rockberg, J., Schutten, R., Schwenk, J.M., Sivertsson, Å., Sjöstedt, E., Skogs, M., Stadler, C., Sullivan, D.P., Tegel, H., Winsnes, C., Zhang, C., Zwahlen, M., Mardinoglu, A., Pontén, F., von Feilitzen, K., Lilley, K.S., Uhlén, M., Lundberg, E. (2017). A subcellular map of the human proteome. Science **356**: 6340.

Töller, A., Brownfield, L., Neu, C., Twell, D., and Schulze-Lefert, P. (2008). Dual function of Arabidopsis glucan synthase-like genes GSL8 and GSL10 in male gametophyte development and plant growth. Plant J. **54**: 911–923.

Tsuda, K., Glazebrook, J., and Katagiri, F. (2008). The interplay between MAMP and SA signaling. Plant Signal. Behav. **3**: 359–361.

Ueda, T., Uemura, T., Sato, M.H., and Nakano, A. (2004). Functional differentiation of endosomes in Arabidopsis cells. Plant J. **40**: 783–789.

Ueda, T., Yamaguchi, M., Uchimiya, H., and Nakano, A. (2001). Ara6, a plant-unique novel type Rab GTPase, functions in the endocytic pathway of *Arabidopsis thaliana*. EMBO J. **20**: 4730–4741.

Uemura, T., Kim, H., Saito, C., Ebine, K., Ueda, T., Schulze-Lefert, P., and Nakano, A. (2012). Qa-SNAREs localized to the *trans*-Golgi network regulate multiple transport pathways and extracellular disease resistance in plants. Proc. Natl. Acad. Sci. **109**: 1784–1789.

Uemura, T., Suda, Y., Ueda, T., and Nakano, A. (2014). Dynamic behavior of the *trans*-golgi network in root tissues of Arabidopsis revealed by super-resolution live imaging. Plant Cell Physiol. **55**: 694–703.

Uemura, T., Ueda, T., Ohniwa, R.L., Nakano, A., Takeyasu, K., and Sato, M.H. (2004). Systematic analysis of SNARE molecules in Arabidopsis: dissection of the post-Golgi network in plant cells. Cell Struct. Funct. **29**: 49–65.

Underwood, W. (2012). The plant cell wall: a dynamic barrier against pathogen invasion. Front. Plant Sci. **3**: 1–6.

Underwood, W., Ryan, A., and Somerville, S.C. (2017). An Arabidopsis lipid flippase is required for timely recruitment of defenses to the host–pathogen interface at the plant cell surface. Mol. Plant **10**: 805–820.

Underwood, W. and Somerville, S.C. (2008). Focal accumulation of defences at sites of fungal pathogen attack. J. Exp. Bot. **59**: 3501–3508.

Underwood, W. and Somerville, S.C. (2013). Perception of conserved pathogen elicitors at the plasma membrane leads to relocalization of the Arabidopsis PEN3 transporter. Proc. Natl. Acad. Sci. U. S. A. **110**: 12492–12497.

Varet, A., Hause, B., Hause, G., Scheel, D., and Lee, J. (2003). The Arabidopsis NHL3 gene encodes a plasma membrane protein and its overexpression correlates with increased resistance to *Pseudomonas syringae* pv. *tomato* DC3000. Plant Physiol. **132**: 2023–2033.

Voigt, C.A. (2014). Callose-mediated resistance to pathogenic intruders in plant defense-related papillae. Front. Plant Sci. **5**: 1–7.

Vukašinović, N. and Žárský, V. (2016). Tethering Complexes in the Arabidopsis endomembrane system. Front. Cell Dev. Biol. **4**: 1–13.

Wang, D., Weaver, N.D., Kesarwani, M., and Dong, X. (2005). Induction of protein secretory pathway is required for systemic acquired resistance. Science **308**: 1036–1040.

Wang, F., Shang, Y., Fan, B., Yu, J.Q., and Chen, Z. (2014). Arabidopsis LIP5, a positive regulator of multivesicular body biogenesis, is a critical target of pathogen-responsive MAPK cascade in plant basal defense. PLoS Pathog. **10**: e1004243.

Wang, F., Yang, Y., Wang, Z., Zhou, J., Fan, B., and Chen, Z. (2015). A critical role of Lyst-interacting protein5, a positive regulator of multivesicular body biogenesis, in plant responses to heat and salt stresses. Plant Physiol. **169**: 497–511.

Wang, W., Devoto, A., Turner, J.G., and Xiao, S. (2007). Expression of the membrane-associated resistance protein RPW8 enhances basal defense against biotrophic pathogens. Mol. Plant-Microbe Interact. **20**: 966–976.

Wang, W., Zhang, Y., Wen, Y., Berkey, R., Ma, X., Pan, Z., Bendigeri, D., King, H., Zhang, Q., and Xiao, S. (2013). A comprehensive mutational analysis of the Arabidopsis resistance protein RPW8.2 reveals key amino acids for defense activation and protein targeting. Plant Cell **25**: 4242–61.

Wang, Y., Xu, Y., Sun, Y., Wang, H., Qi, J., Wan, B., Ye, W., Lin, Y., Shao, Y., Dong, S., Tyler, B.M., and Wang, Y. (2018). Leucine-rich repeat receptor-like gene screen reveals that Nicotiana RXEG1 regulates glycoside hydrolase 12 MAMP detection. Nat. Commun. **9**: 594.

Watanabe, S., Shimada, T.L., Hiruma, K., and Takano, Y. (2013). Pathogen infection trial increases the secretion of proteins localized in the endoplasmic reticulum body of arabidopsis. Plant Physiol. **163**: 659–664.

Wattelet-Boyer, V., Brocard, L., Jonsson, K., Esnay, N., Joubès, J., Domergue, F., Mongrand, S., Raikhel, N., Bhalerao, R.P., Moreau, P., and Boutté, Y. (2016). Enrichment of hydroxylated C24- and C26-acyl-chain sphingolipids mediates PIN2 apical sorting at *trans*-Golgi network subdomains. Nat. Commun. **7**: 12788.

Wei, C., Hsu, S., Deng, W., Wen, Y., and Huang, H. (2012). Plant innate immunity induced by flagellin suppresses the hypersensitive response in non-host plants elicited by *Pseudomonas syringae* pv . *averrhoi*. PLoS One **7**: e41056.

Weßling, R., Epple, P., Altmann, S., He, Y., Yang, L., Henz, S.R., McDonald, N., Wiley, K., Bader, K.C., Gläßer, C., Mukhtar, M.S., Haigis, S., Ghamsari, L., Stephens, A.E., Ecker, J.R., Vidal, M., Jones, J.D., Mayer, K.F., Ver Loren van Themaat, E., Weigel, D., Schulze-Lefert, P., Dangl, J.L., Panstruga, R., Braun, P. (2014). Convergent targeting of a common host protein-network by pathogen effectors from three kingdoms of life. Cell Host Microbe **16**: 364–375.

Whalen, M.C. (1991). Identification of *Pseudomonas syringae* pathogens of Arabidopsis and a bacterial locus determining avirulence on both Arabidopsis and soybean. Plant Cell **3**: 49-59.

Whisson, S.C., Boevink, P.C., Wang, S., and Birch, P.R. (2016). The cell biology of late blight disease. Curr. Opin. Microbiol. **34**: 127-135.

Williams, S.J., Sohn, K.H., Wan, L., Bernoux, M., Sarris, P.F., Segonzac, C., Ve, T., Ma, Y., Saucet, S.B., Ericsson, D.J., Casey, L.W., Lonhienne, T., Winzor, D.J., Zhang, X., Coerdt, A., Parker, J.E., Dodds, P.N., Kobe, B., Jones, J.D.G. (2014). Structural basis for assembly and function of a heterodimeric plant immune receptor. Science **344**: 299–303.

de Wit, P.J., van der Burgt, A., Ökmen, B., Stergiopoulos, I., Abd-Elsalam, K.A., Aerts, A.L., Bahkali, A.H., Beenen, H.G., Chettri, P., Cox, M.P., Datema, E., de Vries, R.P., Dhillon, B., Ganley, A.R., Griffiths, S.A., Guo, Y., Hamelin, R.C., Henrissat, B., Kabir, M.S., Jashni, M.K., Kema, G., Klaubauf, S., Lapidus, A., Levasseur, A., Lindquist, E., Mehrabi, R., Ohm, R.A., Owen, T.J., Salamov, A., Schwelm, A., Schijlen, E., Sun, H., van den Burg, H.A., van Ham, R.C., Zhang, S., Goodwin, S.B., Grigoriev, I.V., Collemare, J., Bradshaw, R.E. (2012). The genomes of the fungal plant pathogens *Cladosporium fulvum* and *Dothistroma septosporum* reveal adaptation to different hosts and lifestyles but also signatures of common ancestry. PLoS Genet. **8**: e100308.

Woollard, A.A. and Moore, I. (2008). The functions of Rab GTPases in plant membrane traffic. Curr. Opin. Plant Biol. **11**:610-9.

Wu, C.-H., Abd-El-Haliem, A., Bozkurt, T.O., Belhaj, K., Terauchi, R., Vossen, J.H., and Kamoun, S. (2017). NLR network mediates immunity to diverse plant pathogens. Proc. Natl. Acad. Sci.: **114**: 811.-8118.

Wu, C.-H., Derevnina, L., and Kamoun, S. (2018). Receptor networks underpin plant immunity. Science **360**: 1300–1301.

Wu, Y. and Zhou, J.M. (2013). Receptor-like kinases in plant innate immunity. J. Integr. Plant Biol. **55**: 1271–1286.

Wulff, B.B.H., Chakrabarti, A., and Jones, D.A. (2009). Recognitional specificity and evolution in the tomato–*Cladosporium fulvum* pathosystem. Mol. Plant-Microbe Interact. **22**: 1191–1202.

Wulff, B.B.H., Thomas, C.M., Parniske, M., and Jones, J.D.G. (2004). Genetic variation at the tomato *Cf-4*/*Cf-9* locus induced by EMS mutagenesis and intralocus recombination. Genetics **167**: 459–470.

Xiao, S., Calis, O., Patrick, E., Zhang, G., Charoenwattana, P., Muskett, P., Parker, J.E., and Turner, J.G. (2005). The atypical resistance gene, *RPW8*, recruits components of basal defence for powdery mildew resistance in Arabidopsis. Plant J. **42**: 95–110.

Xiao, S., Ellwood, S., Calis, O., Patrick, E., Li, T., Coleman, M., Turner, J.G., Xiao, S., Ellwood, S., Callis, O., Patrick, E., Li, T., Coleman, M., and Turner, J.G. (2001). Broad-spectrum mildew resistance in Arabidopsis mediated by RPW8. Science **291**: 118–120.

Xin, X.-F., Nomura, K., Underwood, W., and He, S.Y. (2013). Induction and suppression of PEN3 focal accumulation during *Pseudomonas syringae* pv. *tomato* DC3000 infection of Arabidopsis. Mol. plant-microbe Interact. **26**: 861–7.

Xu, J., Meng, J., Meng, X., Zhao, Y., Liu, J., Sun, T., Liu, Y., Wang, Q., and Zhang, S. (2016). Pathogen-responsive MPK3 and MPK6 reprogram the biosynthesis of indole glucosinolates and their derivatives in Arabidopsis immunity. Plant Cell **28**: 1144-62.

Xu, N., Luo, X., Li, W., Wang, Z., and Liu, J. (2017). The bacterial effector AvrB-induced RIN4 hyperphosphorylation is mediated by a receptor-like cytoplasmic kinase complex in *Arabidopsis*. Mol. Plant-Microbe Interact. **30**: 502–512.

Yamada, K., Yamashita-Yamada, M., Hirase, T., Fujiwara, T., Tsuda, K., Hiruma, K., and Saijo, Y. (2016). Danger peptide receptor signaling in plants ensures basal immunity upon pathogen-induced depletion of BAK1. Eur. Mol. Biol. Organ. J. **35**: 46–61.

Yang, C.W., Gonzalez-Lamothe, R., Ewan, R.A., Rowland, O., Yoshioka, H., Shenton, M., Ye, H., O'Donnell, E., Jones, J.D., and Sadanandom, A. (2006). The E3 ubiquitin ligase activity of arabidopsis PLANT U-BOX17 and its functional tobacco homolog ACRE276 are required for cell death and defense. Plant Cell **18**: 1084–1098.

Yeh, Y.-H., Panzeri, D., Kadota, Y., Huang, Y.-C., Huang, P.-Y., Tao, C.-N., Roux, M., Chien, H.-C., Chin, T.-C., Chu, P.-W., Zipfel, C., and Zimmerli, L. (2016). The Arabidopsis malectin-like/LRR-RLK IOS1 is critical for BAK1-dependent and BAK1-independent pattern-triggered immunity. Plant Cell **28**: 1701–21.

Yu, M., Liu, H., Dong, Z., Xiao, J., Su, B., Fan, L., Komis, G., Šamaj, J., Lin, J., and Li, R. (2017). The dynamics and endocytosis of Flot1 protein in response to flg22 in Arabidopsis. J. Plant Physiol. **215**: 73–84.

Zbierzak, A.M., Porfirova, S., Griebel, T., Melzer, M., Parker, J.E., and Dörmann, P. (2013). A TIR-NBS protein encoded by Arabidopsis Chilling Sensitive 1 (CHS1) limits chloroplast damage and cell death at low temperature. Plant J. **75**: 539–552.

Zelazny, E., Santambrogio, M., Pourcher, M., Chambrier, P., Berne-Dedieu, A., Fobis-Loisy, I., Miège, C., Jaillais, Y., and Gaude, T. (2013). Mechanisms governing the endosomal membrane recruitment of the core retromer in Arabidopsis. J. Biol. Chem. **288**: 8815–8825.

Zhang, L., Kars, I., Essenstam, B., Liebrand, T.W.H., Wagemakers, L., Elberse, J., Tagkalaki, P., Tjoitang, D., van den Ackerveken, G., and van Kan, J.A.L. (2014a). Fungal endopolygalacturonases are recognized as microbe-associated molecular patterns by the Arabidopsis receptor-like protein RESPONSIVENESS TO BOTRYTIS POLYGALACTURONASES1. Plant Physiol. **164**: 352–364.

Zhang, L., Zhang, H., Liu, P., Hao, H., Jin, J.B., and Lin, J. (2011a). Arabidopsis R-SNARE proteins VAMP721 and VAMP722 are required for cell plate formation. PLoS One **6**.

Zhang, X. and Oppenheimer, D.G. (2009). Irregular Trichome Branch 2 (ITB2) encodes a putative aminophospholipid translocase that regulates trichome branch elongation in Arabidopsis. Plant J. **60**: 195–206.

Zhang, X., Zhao, H., Gao, S., Wang, W.C., Katiyar-Agarwal, S., Huang, H. Da, Raikhel, N., and Jin, H. (2011b). Arabidopsis Argonaute 2 regulates innate immunity via miRNA393*-mediated silencing of a Golgi-localized SNARE gene, MEMB12. Mol. Cell **42**: 356–366.

Zhang, Y., Nikolovski, N., Sorieul, M., Vellosillo, T., McFarlane, H.E., Dupree, R., Kesten, C., Schneider, R., Driemeier, C., Lathe, R., Lampugnani, E., Yu, X., Ivakov, A., Doblin, M.S, Mortimer, J.C., Brown, S.P., Persson, S., Dupree, P. (2016). Golgi-localized STELLO proteins regulate the assembly and trafficking of cellulose synthase complexes in Arabidopsis. Nat. Commun. **7**: 11656.

Zhang, Y., Wang, Y., Liu, J., Ding, Y., Wang, S., Zhang, X., Liu, Y., and Yang, S. (2017). Temperature-dependent autoimmunity mediated by chs1 requires its neighboring TNL gene SOC3. New Phytol. **213**: 1330–1345.

Zhang, Z., Lenk, A., Andersson, M.X., Gjetting, T., Pedersen, C., Nielsen, M.E., Newman, M.A., Hou, B.H., Somerville, S.C., and Thordal-Christensen, H. (2008). A lesion-mimic syntaxin double mutant in Arabidopsis reveals novel complexity of pathogen defense signaling. Mol. Plant. **1**: 510-27.

Zhang, Z., Shrestha, J., Tateda, C., and Greenberg, J.T. (2014b). Salicylic acid signaling controls the maturation and localization of the arabidopsis defense protein ACCELERATED CELL DEATH6. Mol. Plant **7**: 1365–1383.

Zhao, T., Rui, L., Li, J., Nishimura, M.T., Vogel, J.P., Liu, N., Liu, S., Zhao, Y., Dangl, J.L., and Tang, D. (2015). A truncated NLR Protein, TIR-NBS2, is required for activated defense responses in the *exo70B1* mutant. PLoS Genet. **11**. e1004945.

Zhong, Y. and Cheng, Z.M. (2016). A unique RPW8-encoding class of genes that originated in early land plants and evolved through domain fission, fusion, and duplication. Sci. Rep. **6**: 1–13.

Zhu, B., Gao, H., Xu, G., Wu, D., Song, S., Jiang, H., Zhu, S., Qi, T., and Xie, D. (2017). Arabidopsis ALA1 and ALA2 mediate RNAi-based antiviral immunity. Front. Plant Sci. **8**: 1–9.

Zipfel, C., Robatzek, S., Navarro, L., Oakeley, E.J., Jones, J.D.G., Felix, G., and Boller, T. (2004). Bacterial disease resistance in Arabidopsis through flagellin perception. Nature **428**: 764–767.

Zouhar, J., Rojo, E., and Bassham, D.C. (2009). *At*VPS45 is a positive regulator of the SYP41/SYP61/VTI12 SNARE complex involved in trafficking of vacuolar cargo. Plant Physiol. **149**: 1668–1678.